A geochemical study of processes in granulite facies migmatites from Prydz Bay, eastern Antarctica.

Gordon Richard Watt

A thesis submitted for the degree of Doctor of Philosophy.

University of Edinburgh
1993.

To my family, for all their encouragement.

Abstract

Partial melting has been proposed as a mechanism for producing the low aH_2O conditions characteristic of granulites, but the extent to which melts produced by water-undersaturated partial melting can be removed from granulite-facies migmatite complexes is less well understood. Three leucogneiss suites produced by water-undersaturated partial melting under high temperature, moderate pressure (6Kbar, 860°C), granulite-facies conditions have been distinguished on the basis of geochemistry and petrography. Type 1 Leucogneisses from the Brattstrand Bluffs coastline, eastern Antarctica, have near minimum-melt major element compositions (high SiO_2, low Fe_2O_3, MgO) low Zr, Th and LREE concentrations, positive Eu anomalies and limited entrained residual material, suggesting efficient segregation of small melt volumes before equilibration with the source. The limited dissolution of accessory phases in water-undersaturated melts has led to a concentration of monazite and zircon and high LREE concentrations in melanosomes. Melting depleted the plagioclase component of the metapelite source rocks almost completely, producing melts with high Eu concentrations. Granitic melts formed under vapour-present conditions are unlikely to show such extreme LREE and HREE depletion or positive Eu anomalies, even at high degrees of partial melting. Type 2 Leucogneisses have high Fe_2O_3, MgO and TiO_2 contents and were formed at higher degrees of melting than the Type 1 Leucogneisses. Consequently they were more viscous, less extractable and more likely to entrain restitic and peritectic phases as the metapelitic source rocks lost their coherence. Type 3 Leucogneisses have strongly enriched Zr, Th and LREE abundances, negative Eu anomalies and Zr/Zr^* and $LREE_t/LREE_t^*$ >1 resulting from preferential accessory phase entrainment. Melts acted as a transfer medium for H_2O, removing water from the site of melting into shear zones, allowing the preservation of anhydrous granulite-facies assemblages and preventing retrogression.

Acknowledgements.

First of all I would like to take this opportunity to thank Simon Harley for all his help, advice, encouragement, good humour when things weren't going too well, and for introducing me to *Himbergeist*. Simon and Ian Fitzsimons are thanked for providing the rationale, the background and the sample set which made this project possible after the diasppointments of the first year. Fitzy is especially thanked for all the advice and information I required on the field settings of the lithologies studied, and for leaving a little work to be done on the Brattstrand Bluffs migmatites for future generations.

Without the assistance of the staff at Edinburgh this thesis would have been much thinner. Stuart Kearns, Pete Hill, John Craven and Richard Hinton are thanked for sharing their electron and ion microprobe expertise, coffee, chocolate biscuits, offices and deeply held prejudices against Australians, the Welsh, Scotsmen, Scottish football, Microsoft Windows and software written by anyone but themselves. Thanks also to Godfrey Fitton and Dodie James for all their help during the XRF analysis, David Walker for showing me the C.L and S.E.M., and to Jane Foster and Mike Hall for all my thin sections. I am very grateful to Diana Baty and Yvonne Cooper for the help they gave me with draughting and photography, and especially to Yvonne for all the photographic tips she has kindly given me. Without the help of Shane, Ian Chisholm and Cliff Ford I would very probably have resorted to typing and hand draughting this thesis, so thanks for all your patient assistance and willing trouble-shooting. I would like to thank Nic Odling for sharing over 2000 cups of tea and coffee over the last four years, for keeping me sane while I extended my geological frontiers to the mantle, and for telling me the story about his daughter flushing his thesis down the toilet... Ta' very much also to all the secretarial staff in the Department. Special mention must be made of Nikki, who has, despite the obvious hardship and personal danger, kept the grim news from battle-torn Tranent coming in.

While Edinburgh is a fine place, I owe a great deal to the many people who have dragged me away from my work to foreign (and not so foreign) shores, and to those who've made my geological travels exciting, enlightening and fun. In (vaguely) chronological order I would like to take this opportunity to thank; Bas Hensen, Russell Shaw, Gladys Warren, Stan Kwasik (the field-hand from Hell!), Ian Buick, Martin Hand, Greg Ferguson, Gresley and Gordon Wakelin-King, Richard Hillis and the Littlejohn Family in Australia, John Hunt for Iceland, Nick Walsh and everyone at R.H.B.N.C., Egham, Pentti Hollta in Finland, Damian Carrington for suggesting the wee trip to Spain, and, finally, thanks to Sally Brown for a wonderfully alcoholic six weeks in northern Greece.

Random inspiration to keep me going during my PhD has come in many forms. Without the following, the whole process would've been far less interesting: Susan Hopkin's chocolate orgasm, Enard Bay, the surgeons at the Western General in Glasgow, Sandra's enthusiasm, Nambarrie tea, Toni's chip shop, Johnny Dawes, The Scottish Malt Whisky Society, Bamburgh Beach, Wind Things ("thou shalt not covet thy neighbours toys"), Anya's tea-pot, Calvin & Hobbes, Adam Watson, Pachuko Cantina, Van Morrison, Port Ellen, Ritter Sport, Bowden Doors and A Dream of White Horses.

Finally, and most importantly, I would like to express my gratitude to all the people who I've been lucky enough to spend time with in the mountains and hills, in bothies and bars, on beaches and on the crags over the last few years. Many thanks to: Jamie Andrew, Ugly Bond, Sam Bone, Sally Brown, Steve Deykin, Karen Dobbie, Alan Dunmur, Jane Foster, Sandra Gadd, Debbie Greene, Susan Hopkin, Andy Hume, Dave Kirk, Jerry Lloyd, Al Matthewson, Andy Patience, Ned Pegler, Anya Reading, Colin Sanderson, Ian Sharp, J.T., Tiddles and Jaki Tout, for all the days out, nights in, sunsets, beers, routes parties, kindness and company they've shared with me over the last few years.

A Geochemical study of processes in granulite-facies migmatites from Prydz Bay, eastern Antarctica.

Title Page.	i
Declaration.	ii
Dedication.	iii
Abstract.	iv
Acknowledgements.	v
List of figures.	xi
List of tables.	xvi
List of abbreviations.	xvii

PART 1. INTRODUCTION.

Chapter 1. Introduction.

1.1. AIMS OF THIS STUDY.	2
1.2. GEOLOGICAL SETTING.	4
1.2.1. Eastern Antarctica.	4
1.2.2. Ingrid Christensen Coast.	6
1.2.3. The Brattstrand Bluffs Coastline.	7
1.3. METHODOLOGY.	9
1.4. NOMENCLATURE.	9
1.5. OUTLINE OF THE THESIS.	13

Chapter 2: Partial Melting in Granulite Terranes.

2.1 INTRODUCTION.	15
2.2. THE ROLE OF PARTIAL MELTING IN GRANULITE TERRANES.	16
2.2.1. Introduction.	16
2.2.2. Vapour-Absent melting and the generation of granulites.	17
2.2.3. Partial Melting in the system KFMASH; the Brattstrand Bluffs Coastline.	20
2.2.4. Amounts of melt-production under vapour-absent conditions.	24
2.3. EQUILIBRIUM & DISEQUILIBRIUM MELTING.	28
2.3.1. Introduction.	28
2.3.2. Basic Theory.	29

2.4. CHEMICAL AND MINERALOGICAL CHARACTERISTICS OF CRUSTAL MELTS. 32

2.4.1. Introduction. 32
2.4.2. Chemical & Mineralogical Characteristics. 32

2.5. MELT EXTRACTION IN MIGMATITES. 38

2.5.1. Introduction. 38
2.5.2. Melt fraction and extraction. 39
2.5.3. Melt Distribution. 41
2.5.4. Melt extraction mechanisms. 44
2.5.5. Recognition of small and large melt fraction magmas. 45

2.6. RESIDUAL PHASES IN GRANITIC MELTS. 46

2.6.1. Recognition of residue in granitic melts. 46
2.6.2. The role of restite in determining melt chemistry. 50

2.7. POST-MELTING PROCESSES. 54

PART 2. PETROGRAPHY AND GEOCHEMISTRY OF THE BRATTSTRAND BLUFFS MIGMATITES.

Chapter 3. Petrography of the Brattstrand Bluffs Leucogneisses.

3.1. INTRODUCTION & FIELD RELATIONS. 58

3.2. LEUCOGNEISS PETROGRAPHY. 59

3.2.1. Introduction. 59
3.2.2. Quartz, K-Feldspar and Plagioclase. 62
3.2.2.1. Quartz 62
3.2.2.2. K-Feldspar 62
3.2.2.3. Plagioclase. 64
3.2.3. Peraluminous & Mafic Phases. 64
3.2.3.1. Garnet. 64
3.2.3.2. Cordierite 67
3.2.3.3. Sillimanite 68
3.2.3.4. Biotite 70
3.2.3.5. Hercynitic Spinel. 70
3.2.4. Accessory Phases. 70
3.2.4.1. Ilmenite. 70
3.2.4.2. Monazite and Zircon. 72
3.2.4.3. Graphite. 74

Chapter 4. Geochemistry of the Prydz Bay Leucogneisses.

4.1. INTRODUCTION. 77

4.2. TYPE 1 LEUCOGNEISSES (LG1). 78

4.2.1. Major elements. 78
4.2.2. Trace elements. 83
4.2.3. Rare Earth Elements. 83

4.3. TYPE 2 LEUCOGNEISSES (LG2). 86

4.3.1. Major elements. 86
4.3.2. Trace Elements. 87
4.3.3. Rare Earth Elements. 87

4.4. TYPE 3 LEUCOGNEISSES (LG3). 88

4.4.1. Major elements. 88
4.4.2. Trace Elements. 89
4.4.3. Rare Earth Elements. 90

Chapter 5. Petrography and Geochemistry of the Country Rocks.

5.1. INTRODUCTION. 93

5.2. PETROGRAPHY. 95

5.2.1. Metapelitic gneisses. 95
5.2.2. Melanosomes. 96

5.3. GEOCHEMISTRY OF THE METAPELITIC GNEISSES (MPG). 99

5.3.1. Major Elements. 99
5.3.2. Trace Elements. 100
5.3.3. Rare-Earth Elements. 105

5.4. GEOCHEMISTRY OF THE MELANOSOMES. 106

Chapter 6. Mineral Chemistry.

6.1. INTRODUCTION. 109

6.2. TYPE 1 LEUCOGNEISSES. 110

6.2.1. K-feldspar. 110
6.2.2. Plagioclase. 112
6.2.3. Garnet. 112

6.3. TYPE 2 LEUCOGNEISSES. 116

6.3.1. K-feldspar. 116
6.3.2. Plagioclase. 116
6.3.3. Garnet. 117
6.3.4. Biotite. 118

6.4. MELANOSOMES. 119

6.4.1. K-feldspar. 119
6.4.2. Plagioclase. 120
6.4.3. Garnet. 120

6.5. METAPELITIC GNEISSES. 122

6.5.1. K-feldspar. 122
6.5.2. Plagioclase. 123
6.5.3. Garnet. 123

6.6. ACCESSORY PHASES. 124

6.6.1. Monazite. 124
6.6.2. Zircon. 127

PART 3. SUMMARY & CONCLUSIONS.

Chapter 7. Petrographic and geochemical constraints on processes involved during partial melting under-granulite facies conditions.

7.1. PETROGRAPHIC CONSTRAINTS ON THE MELTING PROCESS.

7.1.1. Introduction. 131
7.1.2. Type 1 Leucogneisses. 133
7.1.3. Type 2 Leucogneisses. 136
7.1.4. Type 3 Leucogneisses. 139
7.1.5. Metapelitic Gneisses. 140
7.1.6. Melanosomes. 140

7.2. MINERAL CHEMISTRY CONSTRAINTS. 143

7.2.1. Introduction. 144
7.2.2. K-Feldspar. 144
7.2.3. Plagioclase. 145
7.2.4. Garnet. 146

7.3. BULK ROCK GEOCHEMICAL CONSTRAINTS. 147

7.3.1. Type 1 Leucogneisses. 147
7.3.2. Type 2 Leucogneisses. 150
7.3.3. Metapelitic Gneisses. 157
7.3.4. Melanosome. 158

7.4. MODEL FOR MELT PRODUCTION AND EXTRACTION. 160

7.4.1. Estimates of Melt Water Content. 160
7.4.2. Evolution of Melt Water Content and Controls on Extraction. 161
7.4.3. Composition of Fluids dissolved in the melt. 163

Chapter 8. Accessory phase controls on trace element behaviour.

8.1. ACCESSORY PHASE BEHAVIOUR DURING ANATEXIS. 167

8.2. GEOCHEMICAL IMPORTANCE OF ACCESSORY PHASES IN THE PRYDZ BAY LEUCOGNEISSES. 171

8.2.1. Mass Balance. 171
8.2.2. Zirconium and Light Rare Earth Element saturation and implicationsfor disequilibrium melting. 178
8.2.3. Constraints on the origin of monazite. 182
8.2.3.1. Monazite cores. 183
8.2.3.2. Monazite Rims. 185

8.3. MONAZITE AND ZIRCON ENTRAINMENT MECHANISMS. 186

Chapter 9. Conclusions.

9.1. INTRODUCTION. 190

9.2. MELT EXTRACTION FROM THE LOWER CRUST AND THE PRODUCTION OF GRANULITE FACIES TERRANES. 190

9.3. ACCESSORY PHASE CONTROLS ON MELT CHEMISTRY. 192

9.4. POST MELTING PROCESSES. 195

References. 199

Appendices.

APPENDIX A. Bulk Rock Chemistry.
APPENDIX B. Chondrite Normalising Factors.
APPENDIX C. Major element mineral chemistry.
APPENDIX D. Trace element mineral chemistry.
APPENDIX E. Analytical Procedures.

List of Figures

CHAPTER 1.

Figure 1.1. Map showing the location of the Brattstrand Bluffs Coastline, Prydz Bay, Eastern Antarctica.
Figure 1.2. Interpreted P-T diagram for the Brattstrand Bluffs Coastline (after Fitzsimons, 1991).
Figure 1.3. Mafic migmatite from the Rauer Islands, eastern Antarctica, showing mesosome, melanosome and leucosome components. Melanosome forms a continuous margin between the mesosome and the leucosome, and also occurs as small, partially disaggregated clumps within the leucosome (photo from Tait, 1989).
Figure 1.4. Granite nomenclature (White, 1990, after Streckeisen, 1973).

CHAPTER 2.

Figure 2.1. Phase relations in the system Qtz-Ab-Or-H_2O at 2Kbar for the minimum melt composition Qtz-35%, Ab-39%, Or-26%. L = aluminosilicate liquid; V = supercritical H_2O vapour; CT = crystals. After Holtz & Johannes, (in press).
Figure 2.2. Liquidus curves (for a given H_2O content) and maximum H_2O solubility curves in the system Qtz-Ab-Or-H_2O.
Figure 2.3. AFM compatability diagrams for the system KFMASH for melt compositions (a) more magnesian than coexisting garnet and (b) less magnesian than coexisting garnet.
Figure 2.4. T-aH_2O pseudosection for an Fe-rich bulk composition undergoing prograde metamorphism leading to anatexis by incongruent melting of biotite (after Fitzsimons, 1991).
Figure 2.5. P-T diagram showing the water suturated solidus (bold curve), vapour absent melting and vapour absent subsolidus reactions for different aH_2O values (after Clemens & Vielzeuf, 1987).
Figure 2.6. Solidus curves in the system Qtz-Ab-Or-H_2O at 5 and 10kbar (after Clemens & Vielzeuf, 1987).
Figure 2.7. Melt volumes produced during melting of a typical pelitic composition as a function of source water content (after Clemens & Vielzeuf, 1987).
Figure 2.8. The geometry of an idealised melt-solid system.
Figure 2.9. Nomenclature of peraluminous igneous rocks based on the primary mineralogical assemblage (after Miller, 1985).
Figure 2.10. Modified AFM diagram (after White, 1990) showing metaluminous (1), peraluminous (2) and weakly peralmunious (3) fields.
Figure 2.11. P-T diagram showing the experimentally determined stability fields for various phases in a granitic melt (after Clemens & Wall, 1988).
Figure 2.12. Viscosity against melt fraction showing the large decrease in effective viscosity at melt fractions of approximately 30-50 % (after Wickham, 1987).
Figure 2.13. Surface energy relative to a dry grain edge plotted against dihedral angle (after Jurewicz & Watson, 1985).
Figure 2.14. Variation of equilibrium melt fraction with dihedral angle.

CHAPTER 3.

Fig. 3.1. Field photograph from Brattstrand Bluffs, showing well segregated deformed leucogneisses in migmatitic pelites. The leucogneisses form vein and sheet like leucocratic bodies up to 1.5 m. thick. They are not associated with mafic selvedges. Photo: I. C. W. Fitzsimons. Notebook - 25cm long.

Fig. 3.2. Banded Leucogneiss containing abundant garnet- (reddish-black) and cordierite- (dark blue) porphryoblasts up to 2 cm in diameter. Photo: I. C. W. Fitzsimons. Lens cap - 5cm diameter.

Fig. 3.3. Narrow (5cm wide) leucogneiss veins cross-cutting deformed migmatised metapelitic gneisses. Photo: I. C. W. Fitzsimons. Lens cap - 5cm diameter.

Fig. 3.4. Patch leucosome in migmatite showing several deformed garnet-rich restitic melanosome schlieren. Leucogneiss - metapelite contacts are gradational over several cm at the base of the photo. Photo: I. C. W. Fitzsimons. Hammer - 50cm long.

Fig. 3.5. Garnet-rich melanosome schlieren in leucogneiss. Note small patches of leucocratic felsic material scattered throughout the mafic patch. Photo: I. C. W. Fitzsimons. Lens cap - 5cm in diameter.

Fig. 3.6. Quartz - K-feldspar - Plagioclase ternary plot (QAP) showing Type 1, 2 and 3 Leucogneisses. Field boundaries from White, 1990.

Fig. 3.7. Photomicrograph of a large strained quartz porphroblast (centre) in a granoblastic quartzofeldspathic leucogneiss. XPL. Scale Bar - 3mm.

Fig. 3.8. Photomicrograph of a large cracked porphyroblast in a leucogneiss (centre) with partially resorbed margins. Fractures are infilled by twinned plagioclase (labelled). XPL. Scale bar - 3mm.

Fig. 3.9. Photomicrograph of a large, poikiloblastic Type II garnet containing rounded quartz inclusions. PPL. Scale bar - 3mm.

Fig. 3.10. Photomicrograph of large rounded garnet (centre-top) overgrown by a cordierite-quartz-sillimanite symplectite. Quartz forms small worms and vermicules radiating normal to the garnet margin. Sillimanite is coarser and partially resorbed. PPL. Scale bar - 1.5mm.

Fig. 3.11. Photomicrograph of a large simply twinned K-feldspar containing abundant inclusions of rounded quartz (white, pale-grey), biotite (moderate birefringence), ilmenite (black) and tiny sillimanite inclusions (labelled). XPL. Scale bar - 3mm.

Fig. 3.12. Granular subhedral plagioclase grains with intercumulus quartz (bright white - centre). XPL. Scale bar - 1.2mm.

Fig. 3.13. Fine grained sillimanite, biotite and ilmenite inclusions defining an early foliation in the core of a Type I Garnet. Note crowding of inclusions in core. PPL. Scale bar - 0.3mm.

Fig. 3.14. Large Type I Garnet (with core of crowded sillimanite inclusions) overgrown by skeletal Type II Garnet containing large rounded quartz blebs. Note small, subhedral garnets (centre left). PPL. Scale Bar - 3mm.

Fig. 3.15. Small subhedral Type II Garnet containing round quartz inclusions. PPL. Scale bar - 1.2mm.

Fig. 3.16. Small subhedral to euhedral Type III Garnets in a quartzofeldspathic Type 1 Leucogneiss. PPL. Scale bar - 3mm

Fig. 3.17. Photomicrograph of large cordierite (pale) containing abundant poikiloblastic hercynitic spinel (black) and sillimanite (high birefringence). Note that cordierite separates sillimanite and spinel). XPL. Scale bar - 3mm.

Fig. 3.18. Large prismatic sillimanite, embayed and rimmed by pinitised cordierite. XPL. Scale bar - 1.2mm.

Fig. 3.19. Large Type II Garnet containing several small quartz inclusions, wrapped by fine grained "schlieren" of fine-grained sillimanite. PPL. Scale bar - 3.5mm.

Fig. 3.20. Late, coarse-grained biotite flakes growing on margin of Type II Garnet (pale grey). Garnet contains several small rounded biotite inclusions. PPL. Scale bar - 0.3mm.
Fig. 3.21. Anhedral hercynitic spinel (black, centre) overgrowing rhombs of medium-grained and fine-grained sillimanite. PPL. Scale bar - 3mm.
Fig. 3.22. Back-scattered electron image of a composite monazite grain with a zoned core and an unzoned rim. Bright zones represent Th rich areas, while darker zones have higher LREE contents and low Th. The darkest areas in the core have ThO_2 contents of 8-9 wt%, while the bright rim contains over 20 wt % ThO_2. Note the cuspate embayments indicating partial resorption of the monazite cores.
Fig. 3.23. Large rounded monazite in K-feldspar. A subhedral overgrowth is visible at the top of the grain, and the margin between the core and rim is marked by a slight dusting. PPL. Scale bar - 0.3mm.
Fig. 3.24. Rounded monazite (with rim, left side of grain) in Type II Garnet. The rim shows enrichment of Th similar to that of most other monazite grains. PPL. Scale bar - 0.3mm.
Fig. 3.25. False colour cathodoluminescence image of a large rounded zircon (approximate diameter 200μm) showing th eabsence of any obvious magmatic overgrowth (c.w. Fig. 3.22).
Fig. 3.26. Small ragged flakes of graphite (opaque) in K-feldspar-rich leucosome. PPL. Scale bar - 0.3mm.

CHAPTER 4.

Figure 4.1. Major element Harker plots. This and all other graphs: LG1 - white triangles; LG2 - black triangles; LG3 - black diamonds.
Figure 4.2. Trace element Harker plots. Symbols as Figure 4.1.
Figure 4.3. Trace Element Harker plots. Symbols as Figure 4.1. Also shown are A/CNK and XMg vs SiO_2 plots.
Figure 4.4. Chondrite normalised REE plots for the Type 1 Leucogneisses.
Figure 4.5. A plot of Eu/Eu* against SiO_2 (wt%) for all leucogneiss types (Symbols as Figure 4.1.)
Figure 4.6. Chondrite Normalised plot for literature compositions (Table 4.1)
Figure 4.7. Chondrite normalised REE plots for Type 2 Leucogneisses.
Figure 4.8. Chondrite normalised REE plots for Type 3 Leucogneisses.

CHAPTER 5.

Fig. 5.1. Migmatitic containing abundant garnet-rich leucosome. Dark streaks are restitic garnet-sillimanite schlieren. This facies is gradational between MPG and Type II Leucogneiss. Photo - I. C. W. Fitzsimons. Lens cap - 50mm.
Fig. 5.2. Folded banded migmatitic metapelites. Melt proportions in this photograph exceed 50%, but leucogneiss sheets are relatively free of mesosome and melanosome material. Photo - I. C. W. Fitzsimons. Lens cap - 50mm.
Fig. 5.3. Migmatitic metapelitic gneisses cross cut by a cordierite-garnet rich melanosome "vein" up to 10 cm wide. Small patches of felsic or quartzofeldspathic material (pale) are visible in the centre of the vein. Photo - S. L. Harley. Lens cap - 50mm.

Figure 5.5. Major element Harker plots. This and all other graphs: MPG - solid circles: MEL - solid squares.
Figure 5.6. Trace Element Harker plots. Symbols as Fig. 5.5.
Figure 5.7. Trace element Harker plots. Also shown is XMg against SiO_2. Symbols as Fig. 5.5.
Figure 5.8. Trace Element Spidergram for Average Brattstrand Bluffs MPG vs Post Archaean Average Shale (PAAS).
Figure 5.9. REE curves for Average MPG and Average LG2.
Figure 5.10. Melanosome REE patterns.

CHAPTER 6.

Figure 6.1. X_{or}-X_{ab}-X_{an} diagram showing K-feldspar and plagioclase compositions for LG1, LG2, MPG and MEL.
Figure 6.2. Chondrite normalised REE patterns for K-Feldspar, plagioclase and biotite from Brattstrand Bluffs samples.
Figure 6.3. Chondrite normalised garnet REE patterns from Brattstrand Bluffs samples.
Figure 6.4. FeO against TiO_2 for biotite from LG2.
Figure 6.5.a. X_{prp} vs X_{alm} for garnets from Brattstrand Bluffs samples. Symbols: Type I Garnet; MEL - solid squares; MPG - solid black triangles. Type II Garnet; LG1 - open triangles; LG2 - shaded triangles; MPG, shaded circles.
Figure 6.5.b. X_{spess} vs X_{alm} for garnets from Brattstrand Bluffs samples. Symbols: Type I Garnet; MEL - solid squares; MPG - solid black triangles. Type II Garnet; LG1 - open triangles; LG2 - shaded triangles; MPG, shaded circles.
Figure 6.6.a. La/Nd against La+Ce+Nd for all monazite analyses.
Figure 6.6.b. La/Nd against La+Ce+Nd for all monazite analyses, showing lithologies. Symbols: Cores - solid, Rims - open. LG3 - triangles; MPG - circles; MEL - squares.
Figure 6.7. Ca+Th against La+Ce+Nd. Symbols as Figure 6.6.b.

CHAPTER 7.

Figure 7.1. A simple mass-balance linear unmixing calculation carried out to determine N (degree of melting) to produce melt X from source Z, leaving residue X. Silica values represent typical LG1 (X), MPG (Z) and MEL (Y) values.
Figure 7.2.a. Th (ppm) vs K (ppm) Symbols as Figure 4.1.
Figure 7.2.b. Zr (ppm) vs Sr (ppm) Symbols as Figure 4.1.
Figure 7.3. The geometry of restite unmmixing lines
Figure 7.4. Reaction topologies in KFMASH for melts with compositions (a) more Al-rich and (b) less Al-rich than the gt-crd tieline (After Fitzsimons, 1991).
Figure 7.5. Fe_2O_3 vs MgO inter-element plot showing a single phase mixing/unmixing line.
Figure 7.6.a. Th (ppm) vs Fe_2O_3 (wt%) plot showing bimodal pattern.
Figure 7.6.b. Zr (ppm) vs SiO_2, showing bimodal pattern.
Figure 7.7. Chondrite normalised REE plot showing the similarity between average LG2 and average MPG.

Figure 7.8. Chondrite normalised REE curves for average LG1 and MEL (sample IF/88/58). Note the relatively high LREE concentration of IF/88/58.
Figure 7.9. Graph showing Wt % H_2O against aH_2O (black squares, using the methods of Burnham (1976) and Clemens & Vielzeuf (1987). Also shown is wt% melt produced as a function of source H_2O content (white triangles) for a source containing 1.23 wt % H_2O (after Clemens & Vielzeuf, 1987).

CHAPTER 8.

Figure 8.1. Zr solubility in haplogranitic melt as a function of T, time and H_2O (after Watson, 1988).
Figure 8.2. Variation of LREE content in a peraluminous magma with fractionation (after Miller & Mittelfehldt, 1982).
Figure 8.3. Monazite dissolution as a function of P, T and grainsize (after Rapp & Watson, 1986).
Fig.8.4.. The results of mass balance calculations for 4 lithologies. Fig. 8.4.a - Type 1 Leucogneiss, garnet absent. Fig. 8.4.b. - Type 1 Leucogneiss containing 5 wt% garnet. Fig. 8.4.c - Type 3 Leucogneiss. Fig. 8.4.d - Quartz-absent Melanosome.
Figure 8.5. Plot of La (ppm) vs Th (ppm) for Type 1 and Type 3 Leucogneisses.
Figure 8.6. Plot of La (ppm) against Eu/Eu* for Type 1 and Type 3 Leucogneisses.
Fig. 8.7.a. Zr (observed) vs Zr* (the equilibrium concentration required to saturate a melt in Zr calculated using the equation of Watson, 1988).
Figure 8.9. Th vs Fe_2O_3 for the Brattstrand Bluffs Leucogneisses.
Figure 8.10.a. Zr vs Th vs Fe_2O_3 plot for Type 1, 2 and 3 Leucogneisses (Symbols as Figure 4.1.).
Figure 8.10.b. Interpreted summary of Figure 8.10.a.

List of Tables

Table 4.1. S-Type granitoid and pelitic migmatite leucosome compositions from the literature. REE patterns for selected samples are shown in Figure 4.6.

Table 4.2. Geochemical Summary of Type 1, 2 and 3 Leucogneisses.

Table 6.1. Monazite rim-core pair compositions from IF/88/147, and selected analyses from the literature.

Table 7.1. Migmatite-forming processes.

Table 7.2. Interpreted origins of individual phases in the Brattstrand Bluffs Leucogneisses.

Table 7.3. Distribution of phases in the Brattstrand Bluffs Leucogneisses.

Table 7.4. Interpreted origins of individual phases in the Brattstrand Bluffs Melanosomes.

Table 8.1 Modal and SIMS REE compositions used for mass balance calculations.

Table 8.2. Melt compositions in equilibrium with cores and rims.

Table 8.3. Monazite core and rim compositions from IF/88/147 used in the monazite-melt equilibrium calculations.

List of symbols and abbreviations.

Minerals, components and phases.

an	anorthite	**grs**	grossularite	**spess**	spessartine
ann	annite	**grt**	garnet	**spl**	spinel
ab	albite	**hcy**	hercynite	**uvr**	uvarovite
adr	andradite	**ilm**	ilmenite	**V**	volatile fluid
alm	almandine	**L, Liq**	silicate melt	**zir**	zircon
bi	biotite	**mon**	monazite		
cor	corundum	**prp**	pyrope		
crd	cordierite	**qtz**	quartz		
gr	graphite	**sil**	sillimanite		

Lithologies

LG1	Type 1 Leucogneisses
LG2	Type 2 Leucogneisses
LG3	Type 3 Leucogneisses
MPG	Metapelitic gneisses
MEL	Melanosomes

Standard chemical symbols are used for all chemical elements and mineral formulae.

θ	dihedral (wetting) angle
°C	degrees Celsius.
μm	micrometres
A/CNK	molecular $Al_2O_3/CaO+Na_2O+K_2O$
AFM	projection onto the plane Al_2O_3-FeO-MgO from qtz, sillimanite and K-feldspar
a_i	activity of component "i"
CL	cathodoluminescence
cm	centimetres
CMF	critical melt fraction
CT	crystals
D_2	deformation event 2.
EMF	equilibrium melt fraction.
Eu*	extrapolated Eu value (from Sm and Gd).
Eu/Eu*	measured Eu concentration divided by extrapolated Eu concentration.
f_i	fugacity of component "i"
HREE	heavy rare earth elements
IF/88/91	Sample 91 collected by I. C. W. Fitzsimons, 1988 field season.
K	degrees Kelvin.
k	kilo (1000).
KFASH	chemical system K_2O-FeO-Al_2O_3-SiO_2-H_2O.
KFMASH	chemical system K_2O-FeO-MgO-Al_2O_3-SiO_2-H_2O.
km	kilometres
KMASH	chemical system K_2O-MgO-Al_2O_3-SiO_2-H_2O.
LILE	large ion lithophile elements.
LREE	light rare earth elements
LREE*	amount of LREE (La-Gd) required to saturate a melt in monazite.
m	metres
M_1	metamorphic event 1
Ma	million years

mm	millimetres
P	pressure
PAAS	post Archaean average shale (Taylor & McClellan, 1985).
QAP	quartz-alkali feldspar-plagioclase ternary diagram
RCMP	rheologically critical melt proportion.
REE	rare earth elements
$REEi_{(n)}$	REEi normalised to chondrite.
SEM	scanning electron microprobe.
S_3	planar fabric (associated with D_3)
T	temperature
t	time
X_i^a	mole fraction of component "i" in phase "a" (superscript usually omitted).
X_{Mg}	molecular MgO/MgO+Fe2O3 (whole rock), MgO/MgO+FeO (mineral).
XRF	X-Ray fluorescence.
Zr*	amount of zirconium required to saturate a melt in zircon.

Disequilibrium melting

L	thickness of ideal permeable layer
d	channel spacing
W_o	melt velocity
$t_{(diff)}$	diffusion time
D_s	solid state diffusion coefficient
$t_{(advec)}$	advection time
P_e	Peclet number.

Monazite Saturation

D	(Na + K + 2Ca) / (Al.(Al + Si))
REE_i	melt content in ppm divided by atomic weight of REE "i"
REE_t	La/139.91 + Ce/140.12 + Pr/140.90 + Nd/144.24 + Sm/150.40 + Gd/157.25. (REE in ppm, denominator is atomic weight).
$XREE_iPO_4$	mole fraction of REE_iPO_4 in monazite.
γi	correction factor to account for non-ideal mixing in monazite.
W_i	Empirical factor derived for REE "i"

Part 1.

Introduction

Chapter 1

Introduction.

Chapter 1. Introduction.

1.1. AIMS OF THIS STUDY.

Granulite terranes are characterised by relatively anhydrous mineral assemblages which reflect low water-activities. Three principal mechanisms for this have been proposed. Low aH_2O conditions could be produced by flushing of a carbonic fluid of mantle or lower crustal derivation (Touret, 1971; Newton, 1990; Newton *et al*, 1980) or by loss of a melt fraction enriched in H_2O (e.g. Fyfe, 1973; Vielzeuf & Holloway, 1988; Bhattachyrya & Sen, 1986; Lamb & Valley, 1985). Both mechanisms should give rise to a desiccated lower crust and a net upwards transport of volatiles and various incompatible elements. The third mechanism proposed is the metamorphism of an already anhydrous protolith (Lamb & Valley, 1985).

Recent studies have shown that fluxing of either pervasive fluids or melts does not provide an adequate explanation for many of the petrographic or geochemical features observed in pelitic granulites on local, outcrop and sample scale. Furthermore, metamorphism of an anhydrous protolith does not explain the widespread occurrence of pelitic granulites which form by metamorphism of protoliths rich in hydrous micas. CO_2 rich fluid inclusions, once interpreted as trapped peak-metamorphic fluids (Touret, 1986), are now considered to represent post-metamorphic fluids in some cases and therefore cannot be unequivocally used as direct evidence for CO_2 flushing (Lamb *et al*, 1987). The close spatial link between high-grade metamorphism, partial-melting and granite batholiths (Sederholm, 1967; Brown & Fyfe, 1970; White & Chappell, 1977) led many workers to propose a model where the extraction of granitic material has left a refractory, anhydrous lower crust. Large scale melt extraction would leave the crust with a broadly residual chemistry. (Nesbitt, 1980; Tarney & Windley, 1977; McCarthy, 1976).

Only a few granulite terranes have a chemical and mineralogical composition consistent with the extraction of large melt volumes (Clemens, 1990; Vielzeuf *et al*, 1990). Many pelitic granulite terranes do however show evidence of partial melting, and localised dehydration (vapour absent) melting has been shown to be important in the prograde evolution of

granulite assemblages (Waters & Whales, 1984; Waters, 1988; Hensen & Warren, 1988). Melts produced by vapour absent melting in pelitic lithologies are water undersaturated and viscous, and are therefore unlikely to represent the precursors of high-level, crustally derived S-type granites common in many orogenic belts unless they scavenge considerable amounts of water as they migrate upwards. These melts are important, however, in the redistribution of volatiles and incompatible elements within high-grade terranes. One of the principal arguments against localised lowering of aH_2O and the production of granulite assemblages by partial melting is that small degree water-undersaturated melts cannot be extracted since they are relatively viscous. Instead, they should remain *in-situ* and produce retrograde rehydration as dissolved H_2O is expelled on crystallisation (Warren, 1983). Experimental work suggests efficient melt segregation can occur even at melt fractions below 5% if melts have very low water contents (Wickham, 1987; Jurewicz & Watson, 1985; Holtz & Barbey, 1991). The study of melt extraction and retention in granulite facies migmatitic rocks can provide much information on the redistribution of trace elements and volatiles in the lower crust (Rudnick & Presper, 1990). In particular, characteristics of melts produced by vapour absent partial melting of crustal rocks (low H_2O, high A/CNK, relatively high temperatures) have important implications for elements (especially Th, U, Zr) contained in accessory phases. These phases are not only useful in geochronology, but provide efficient geochemical and petrographic markers in tracing the fate of crustal material involved in anatexis. It is therefore essential that the role of melt/source segregation in determining melt chemistry is understood if we are to evaluate the nature of partial melting processes involved in granulite terranes.

This project represents a study of the petrology and geochemistry of a suite of melts previously deduced to have formed by dehydration melting under granulite facies conditions from the Prydz Bay area, eastern Antarctica (Fitzsimons 1991, Fitzsimons & Harley, 1991). The aims of the project are to answer questions related to the processes involved in partial melting in pelitic lithologies under lower- and middle-crustal conditions. Geochemical and petrological study has concentrated on the following questions.

(i) Do felsic segregations and veins in migmatitic pelitic granulites represent former melt, do they include combinations of former melt and restitic or peritectic material (e.g. Weber & Barbey, 1985), or can they themselves be considered restitic (i.e. have they lost a late-stage melt or hydrous fraction)? Can we see evidence for disequilibrium melting processes (Sawyer, 1991)?

(ii) How effective has melt-source segregation been?

(iii) What geochemical features are associated with dehydration melting and subsequent melt extraction/retention?

(iv) What post-melting processes have occurred?

1.2. GEOLOGICAL SETTING.

1.2.1. Eastern Antarctica.

The East Antarctic Shield is one of the most extensive areas of high grade Archaean and Proterozoic rocks in the world. It forms the greater part of the Antarctic continent and is separated geologically and geographically from West Antarctica by the 3500km long Transantarctic Mountains. While the geology of West Antarctica has been dominated by several tectonic terranes active throughout Phanerozoic times, the East Antarctic Shield was last affected by a major metamorphic event at *ca*500Ma. Crystalline gneisses are the most common lithology, with subordinate igneous intrusions and a locally exposed Permo-Triassic cover sequence. Metamorphic grade of the gneisses varies from greenschist to granulite. Granulite terranes are comprised largely of quartzofeldspathic gneisses, pyroxene granulites and mixed metasediments (Grew, 1980).

The East Antarctic Shield is not a single terrane with a unique record but an assembly of discrete terranes with widely different ages and geological histories (James & Tingey, 1983). This study is concerned with a portion of the East Antarctic Shield on the southern coast of Prydz Bay, the Brattstrand

Bluffs Coastline (Fig. 1.1). In this region of eastern Antarctica three Archaean cratons have been recognised, bounded by mobile belts consisting of both

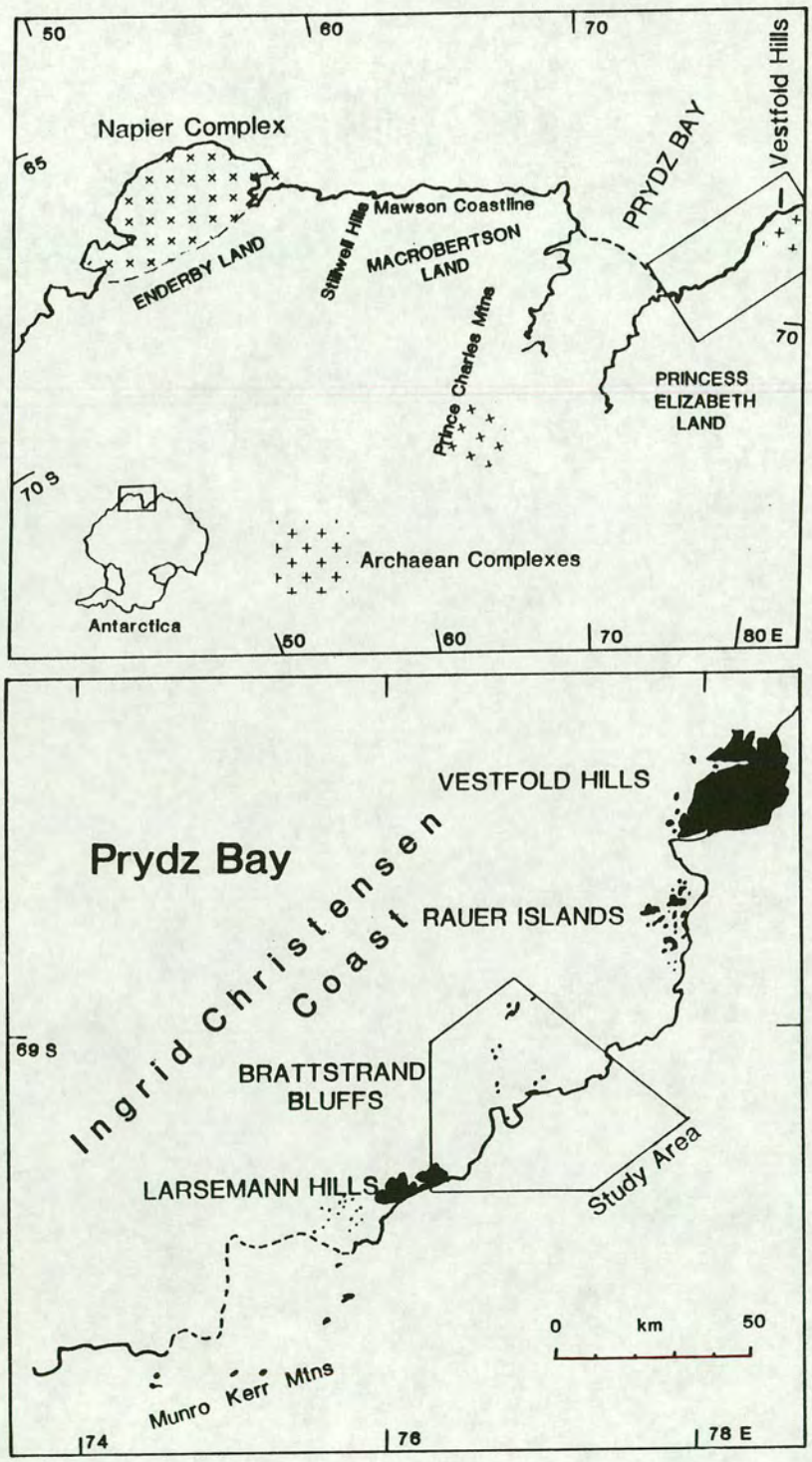

Figure 1.1. Map showing the location of the Brattstrand Bluffs Coastline, Prydz Bay, Eastern Antarctica. Solid areas - outcrop.

reworked Archaean material and voluminous new crust produced during Proterozoic times. Craton margins show only limited reworking (Clarke, 1988; Harley & Hensen, 1990; Sheraton *et al*, 1984). The oldest of the three Archaean cratons is the Napier Complex of Enderby Land (Sheraton *et al*, 1980; James & Tingey, 1983), a granulite terrane with regional mineral assemblages (sapphirine + quartz, osumilite in metapelites) indicative of unusually high temperatures of metamorphism (Ellis *et al*, 1980; Harley & Hensen, 1990; Sheraton *et al*, 1980). The southern Prince Charles Mountains and MacRobertson Land consist of granitic basement gneisses metamorphosed to amphibolite-facies and unconformably overlain by younger metasediments of lower-amphibolite to greenschist grade (Grew, 1980). The third main Archaean craton block recognised is the Vestfold Hills Block which lies at the eastern end of Princess Elizabeth Land, on the southern coast of Prydz Bay. This area is comprised dominantly of granulite-facies orthogneiss and paragneiss (Oliver *et al*, 1982; Sheraton *et al*, 1980). Ion probe dating of zircons (Black *et al*, 1990) indicates an age of *ca*2500Ma for this block. The Rauer Group, south of the Vestfold Hills block, consists of domains of Archaean basement and Proterozoic orthogneiss and paragneiss (Harley & Fitzsimons, 1991). Zircon ages from homogeneous tonalitic orthogneisses in the Rauers indicate two age components of 3300Ma and 2830Ma (Kinny and Black, 1990). Both these ages are considerably older than the Vestfold Block, suggesting that the Rauer Group does not simply consist of reworked Archaean material from the adjacent Vestfold Block, but is comprised of reworked material from a previously unrecognised Archaean terrane. Sapphirine bearing metapelites from metapelitic rocks in the Rauer Group yield P-T estimates for an early metamorphic event of 1000°C, 10-13 kbar (Harley & Fitzsimons, 1991).

The three major Archaean cratons are characterised by post metamorphic tholeiitic dykes and are separated by the extensive Late Proterozoic Complex which underwent metamorphism at *ca*1000ma and contains no undeformed Proterozoic dykes. A further metamorphic event at 500 Ma may have reached granulite facies in places (Harley, *pers. comm.*)

1.2.2. Ingrid Christensen Coast.

The Ingrid Christensen Coast is part of a large Proterozoic metamorphic terrane probably extending at least 2000km to the north and west (the Late Proterozoic Complex of Harley, 1988, Harley & Hensen, 1990). The terrane is comprised of a few areas of relatively continuous outcrop, including the extensive Rayner Complex which forms the southern boundary to the Napier Complex, the Northern Prince Charles Mountains, the Stillwell Hills and Mawson Coast areas of eastern MacRobertson Land and the aforementioned Ingrid Christensen Coast. The most extensive areas of outcrop of Proterozoic rocks on the southern coast of Prydz Bay occur in parts of the Rauer Group and perhaps in the Larsemann Hills, where a 500 Ma event may also occur. The Rauer Group is comprised of pyroxene-bearing felsic and mafic orthogneisses, with only minor paragneisses. These include composite orthogneisses (rafts of mafic granulite in tonalitic gneisses), felsic to intermediate orthogneisses retaining relict igneous characteristics and layered paragneiss successions containing metapelites, semipelites, calc-silicates and leucogneiss (Harley, 1987; Harley & Fitzsimons, 1991). In contrast, the Larsemann Hills are dominated by aluminous metapelites and garnet bearing felsic gneisses derived from psammites (Stuwe & Powell, 1989). In their regional subdivision of the Ingrid Christensen Coast, Stuwe & Powell (*op cit*) suggest that the Larsemann Hills type lithologies (Late Proterozoic Larsemann Series) form the bulk of the south coast of Prydz Bay from the Munro-Kerr Mountains in the south-west to the Rauer Group in the east. The extensive Prydz Bay metasedimentary succession may have been derived in part from the middle Proterozoic Rauer Group (Sheraton *et al*, 1984).

1.2.3. The Brattstrand Bluffs Coastline.

This project presents a detailed study of partial melting in metapelitic rocks from the Brattstrand Bluffs coastline, which lies between the Larsemann Hills area to the west and the Rauer Group to the east. The Brattstrand Bluffs coastline consists of granulite facies orthogneisses and migmatitic paragneisses (the latter being the focus of this study). The area underwent metamorphism during the 1000Ma event, experiencing estimated peak metamorphic conditions of 6 kbar, 860°C (Fig. 1.2).

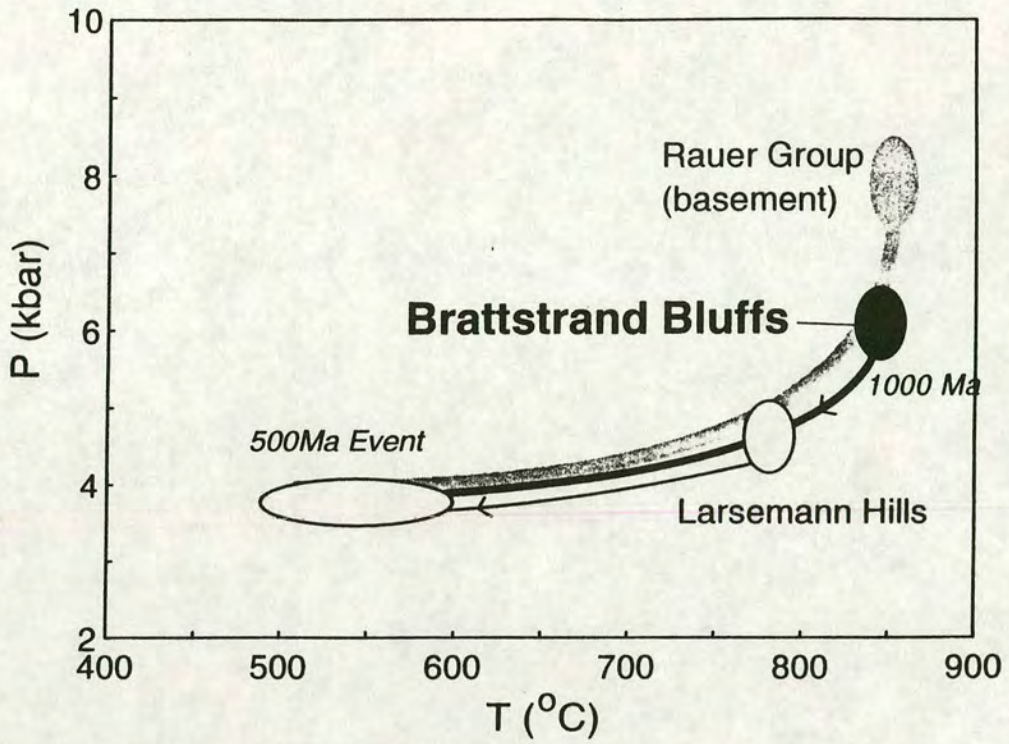

Figure 1.2. Interpreted P-T diagram for the Brattstrand Bluffs Coastline (after Fitzsimons, 1991).

Metamorphism produced an pervasive flat-lying foliation and extensive partial melting (Fitzsimons , 1991). The final stages of this metamorphism occurred in the absence of a free vapour phase (Harley & Fitzsimons, 1991; Fitzsimons & Harley, 1991). Peak metamorphic conditions were higher than those of the Larsemann Hills (4.5 kbar, 750°C) to the south-west (Stuwe & Powell, 1989) leading Fitzsimons (1991) to propose that the Brattstrand Bluffs area represents an interleaved basement and cover sequence from a lower crustal level than the straightforward cover succession of the Larsemann Hills. The stabilisation of garnet-sillimanite (Brattstrand Bluffs) relative to spinel-cordierite-quartz (Larsemann Hills) is consistent with this interpretation.

In the Brattstrand Bluffs area, peak metamorphism was followed by decompression and cooling to 3 kbar, 700°C, accompanied by the growth of spinel and cordierite (Fitzsimons & Harley, 1991). The clockwise P-T

evolution of the Brattstrand Bluffs coastline is proposed to indicate extensional collapse of thickened crust with increased heat-flow due to convective thinning of the mantle lithosphere (Fitzsimons, 1991; Harley & Fitzsimons, 1991).

1.3. METHODOLOGY.

The bulk of this thesis involves geochemical and petrographic study of a suite of samples collected from the Brattstrand Bluffs coastline. These samples were collected by Ian Fitzsimons as part of the 1987/1988 and 1991/1992 Australian National Antarctic Research Expeditions and are a small part of the extensive Antarctic Collection held at the Department of Geology & Geophysics at the University of Edinburgh. This detailed geochemical study is designed to follow on from the work of Fitzsimons (1991) which investigated the geological, structural and metamorphic history of the Brattstrands Bluffs coastline. Initial work involved the selection of a suite of representative leucogranites, metapelitic gneisses and migmatites and thin section identification of mineral assemblages. Detailed thin-section studies identified possible melt, source and restitic components. Selected leucogneiss, pelite and melanosome samples were analysed for whole rock chemistry using XRF (major and trace elements) and Atomic Emission spectroscopy (rare-earth elements). Mineral chemistry analyses were performed using electron-microprobe and ion-microprobe facilities at the University of Edinburgh. Detailed back-scattered electron (scanning electron microscope (SEM), electron microprobe) and cathodoluminescence imaging were carried out to determine the petrological importance of accessory phases. The petrographic and geochemical data was combined to enable petrogenetic modelling calculations and to determine the processes involved in crustal melting under granulite facies in the Brattstrand Bluffs area. Further details of these techniques are included in the appendices.

1.4. NOMENCLATURE.

Migmatite terminology has long been the subject of controversy. The term "migmatite" was coined by Sederholm in 1907 to describe a rock originating

from a mixture of metamorphic and igneous material. Despite the widely held view that most migmatites are formed by partial melting (Ashworth, 1985) subsequent definitions have attempted to give a non-genetic definition for both migmatite bodies and migmatite components. In this work, "migmatite" refers to a medium-grade to high-grade composite metamorphic rock consisting of two or more of the following components; "leucosome", "melanosome", "mesosome" and "paleosome" (Fig. 1.3).

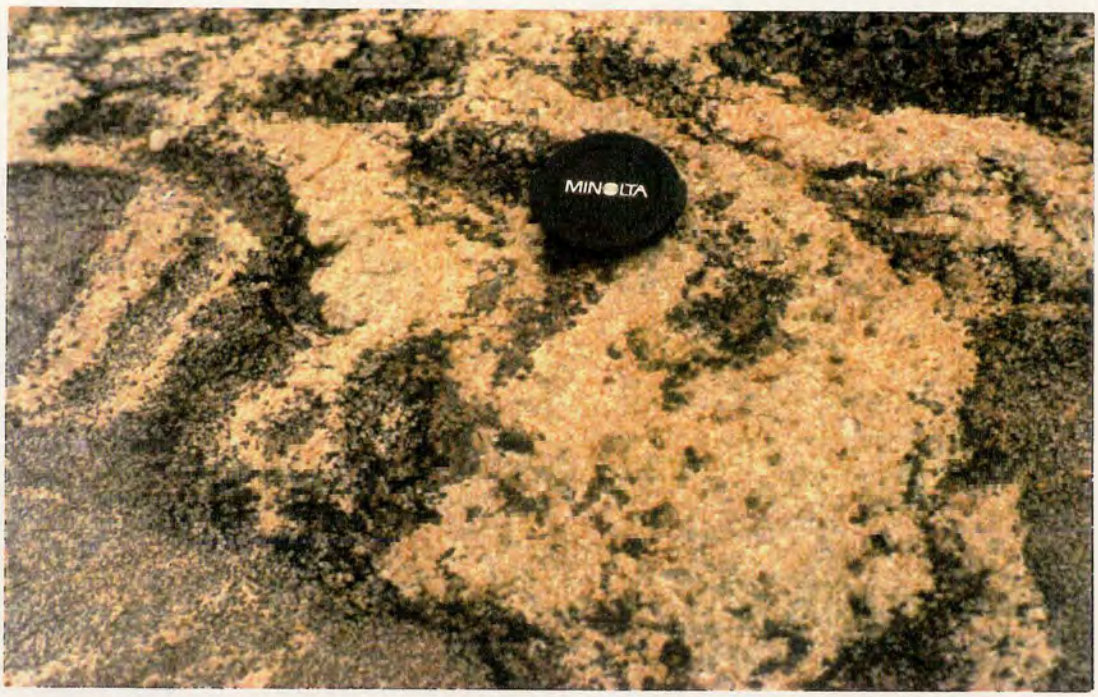

Figure 1.3. Mafic Migmatite from the Rauer Islands, eastern Antarctica, showing mesosome, melanosome and lecosome components. Melanosome forms a continuous margin between the mesosome and the leucosome, and also occurs as small, partially disaggregated clumps within the leucosome (photo from Tait, 1989).

The pale coloured, quartzofeldspathic or feldspathic portion of a migmatite of generally granitic (or aplitic, pegmatitic or plutonic) appearance is called leucosome. Melanosome is the term used to describe the melanocratic (dark) portion of a migmatite which is rich in mafic minerals and poor in quartzofeldspathic material. The term melt has not been used as a synonym for leucosome in this thesis. "Melt" refers to the granitic liquid produced by anatexis, while leucosome is used more broadly to describe the leucocratic portion of a migmatite containing non-melt components (e.g. peritectic or

residual phases). Restite refers to the geochemically immobile source rock or crystalline residuum left after removal of a melt component, and is used synonymously with melanosome. Chappell *et al* (1987) subdivide restite into primary (crystals residual from a melting episode) and secondary (crystals resulting from the recrystallisation of primary restite) restite types. In addition, in this work the term restite is used to describe crystals found in leucosome which did not crystalise directly from the melt. This category includes peritectic phases produced in the same reactions as the melt. The implications of this are considered in detail in Chapter 8 of this thesis. "Mesosome" and "paleosome" have been used to describe the metamorphic component of migmatites, intermediate in chemistry between melanosome and leucosome. Mesosome has no genetic implications, while palaeosome refers specifically to the portion of a migmatite unaffected by partial melting. Because of the difficulty in recognising true unmelted protoliths in migmatite terranes the term palaeosome has not been used in this thesis.

The term "granulite" is used for a rock formed under relatively high temperatures, moderate to high pressures and low water activities (granulite facies conditions) and characterised by an anhydrous mineral assemblage. The term granulite does not imply an equigranular, granoblastic rock as most of the lithologies in this study are gneissose (i.e. coarse-grained with a pervasive fabric on hand specimen scale). The term "leucogneiss" is therefore equivalent to a gneissic leucosome.

Granite nomenclature is typically complicated by the usage of the word granite for two purposes. "Granite" (*senso lato*) is used to describe coarse-grained igneous rocks comprised dominantly of quartz, plagioclase, K-feldspar and up to 30% mafic minerals. This usage (which is synonymous with the term "granitoid" as proposed by Streckeisen (1973)) includes alkali feldspar granites, true granites (*senso stricto*), monzogranites, granodiorites, tonalites and diorites (Fig. 1.4). True granites (according to the classification of White (1990)) are relatively rare in orogenic belts, but are the most important plutonic rock associated with many ore deposits. The granitoid

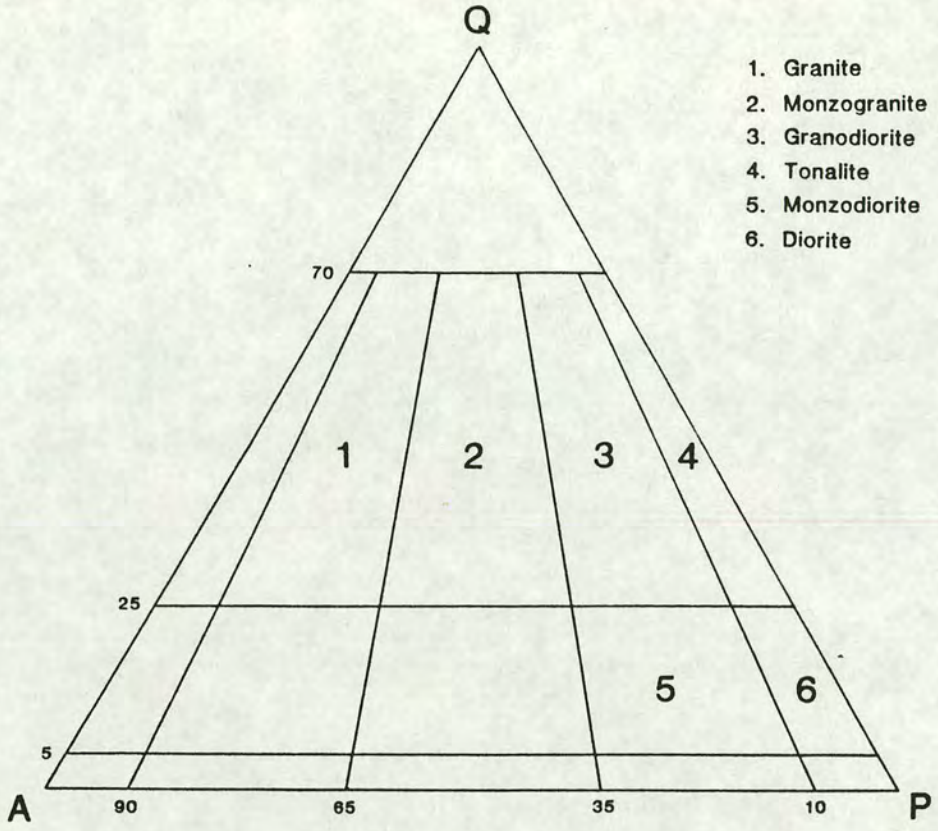

Figure 1.4. Granite nomenclature (White, 1990, after Streckeisen, 1973).

classification of Streckeisen (1973) has been modified by White (1990) by subdivision of the large granite (*s.s.*) field to include monzogranite, and by moving the division between diorites and more quartz rich granitoids from 20% to 25% SiO_2 to correspond more closely with geochemical definitions of diorite and andesite (White, *op cit*). White's mineralogical classification is the scheme adopted in this work.

Granitic rocks can be classified by geochemical, as well as mineralogical, criteria. Peraluminous granites have a molecular ratio Al_2O_3/Na_2O+K_2O+CaO (A/CNK) greater than 1. This means that they have excess aluminium over that required to produce feldspars, and contain a phase which contains the excess aluminium. Typical peraluminous minerals include cordierite, andalusite and garnet. Metaluminous granitic rocks, in contrast, have an excess of CaO, giving molecular Al_2O_3/Na_2O+K_2O+CaO ratios less than 1, but molecular Al_2O_3/Na_2O+K_2O ratios greater than 1.

Metaluminous granites are commonly referred to as "calc-alkaline" igneous rocks (Ragland, 1989). This purely descriptive classification leads to the more genetic subdivision of granites on the basis of their source lithology. Granites inferred to be derived from a sedimentary protolith are termed S-type granites while those derived from melting of an igneous precursor are termed I-type (Chappell & White, 1974). Since rocks which have been through a weathering cycle (sediments) will be depleted in Na and K relative to Al, granites derived from sedimentary sources (S-types) will typically be peraluminous (White, 1990). Because I-type granites can crystallise primary biotite (a slightly peraluminous mineral) White and Chappell (1977) proposed the division between S- and I-type granitoids should be at A/CNK=1.10 and not at A/CNK=1.0 . There is therefore no requirement for mildly peraluminous magmas to have been derived from sedimentary protoliths (e.g. Cawthorn & Brown, 1976).

1.5. OUTLINE OF THE THESIS.

The thesis is divided into three main parts. The first part provides an introduction to both the project and the study area (Chapter 1) and a synthesis of processes involved in partial melting under granulite facies conditions (Chapter 2). Part Two (Chapters 3-6) of the thesis contains the petrographic, whole rock- and mineral-geochemistry data from a suite of migmatitic granulites from the Brattstrand Bluffs coast. Chapters 3 and 4 consider the Prydz Bay leucogneisses while Chapter 5 reviews the pelitic country rocks and melanosomes. Chapter 6 is concerned with major and accessory phase mineral petrography and chemistry. Part Three (Chapters 7-9) utilises the data presented in the second part of the thesis to identify the important processes involved during partial melting in the study area. The role of restite entrainment and unmixing in controlling melt chemistry is considered and a model for melt extraction is developed in Chapter 7. The importance of accessory phases in influencing melt chemistry (Chapter 8) is considered, and Chapter 9 summarises the processes involved and the implications of these for partial melting and granite genesis in granulite terranes. The final chapter also compares the crustal melts from the Prydz Bay area with those from other anatectic complexes and suggests possibilities for further research arising from this project.

Chapter 2

Partial Melting in Granulite Terranes.

Chapter 2: Partial Melting in Granulite Terranes.

2.1 INTRODUCTION.

Most lithologies should melt under the P-T-aH_2O conditions of the lower crust (e.g. Clemens & Vielzeuf, 1987; Brown & Fyfe, 1970) and the common occurrence of migmatites in high-grade metamorphic terrains is often taken as evidence that melting does occur. Partial melting in the lower crust will have profound consequences on the nature of the continental crust. If partial melts are able to coalesce and rise up through the crust they provide an important mechanism of crustal differentiation, which will, with time, lead to a restitic lower crust (Clemens & Vielzeuf, 1987; Vielzeuf, 1990). Granulite terrains are generally considered as exposed sections of the lower crust. If these granulites do represent restitic material left after partial melting they should show some geochemical evidence for melt extraction (Thompson, 1990). Exposed lower crustal sections are dominantly comprised of silicic and mafic granulites which frequently do not exhibit the geochemical characteristics of a refractory residuum (Vielzeuf *et al*, 1990; Thompson, 1990). Even areas such as Calabria and Ivrea which exhibit the mineralogical charcteristics of residua do not show geochemical evidence (LILE depletion, positive Eu anomaly) for melt extraction (Kruhl, 1991; Vielzeuf *et al*, 1990). The restite model for the production of granitic melts requires that melt and residue are separated at an early stage and that the hot, dry, water-undersaturated melts ascend in the crust in a liquid state (Vielzeuf *et al*, 1990). Petrographic (Chappell *et al*, 1987; Scambos *et al*, 1986) and geochemical (Holtz, 1989; Holtz & Barbey, 1991; Patino-Douce & Johnston, 1991) evidence for the presence of restite and the importance of residual material in determining geochemistry in some granitoids suggests that efficient extraction of melt and residue at source does not always occur. Furthermore, the extraction of felsic melts from the lower crust (passive basification, Vielzeuf *et al*, 1990) should produce large volumes of mafic and ultramafic residue, "...for which no convenient hiding place within the continental crust has been found." (Arculus, 1988). This project aims to study the role of melt-residue segregation at the critical early stage (e.g. during migmatisation) to determine whether melts produced under granulite conditions could represent precursors to batholithic granitoids, whether the

efficient extraction of these melts was responsible for the production of granulite-facies conditions and whether the geochemistry of granulite terranes can be modelled in terms of melt extraction and retention or whether other processes (loss of late stage fluids, fluxing of a carbonic fluid species) are required to provide an adequate explanation.

The study of melt extraction from a granulite-facies migmatite terrane through melt chemistry and petrology requires an understanding of the mechanisms responsible for producing the melt, the evolution of the system during melting and the processes which affect melt and source after melt extraction. Melt reactions and the amount of melt produced are constrained by pressure, temperature, aH_2O and bulk composition, while the rate at which melting occurs may have important consequences for melt chemistry. The amount of melting, melt viscosity and the structural conditions under which melting takes place determine whether melt extraction can occur, or whether melt remains in the complex. As the melt migrates from the source region it may entrain and assimilate material, changing the bulk composition. Can this material (or the geochemical effects relating to entrainment) be recognised? Finally, what late-stage processes act upon melts and source lithologies - do retrogression and rehydration destroy granulite-grade assemblages if melts crystallise *in-situ* (e.g. Warren, 1987), and can relict melt textures be recognised after recrystallisation? The remainder of this chapter gives a summary of current ideas on melt production and extraction, the chemistry of peraluminous anatectic melts, the role of residual phases in crustal melts and post-crystallisation processes.

2.2. THE ROLE OF PARTIAL MELTING IN GRANULITE TERRANES.

2.2.1. Introduction.

Granulite terranes exhibit a diverse range of structural styles, a variety of geochemical signatures and petrological assemblages which reflect both pre-metamorphic history and metamorphic processes to varying extents, and are formed under a wide range of P and T conditions. Granulites

characteristically develop anhydrous mineral assemblages, stable only at low aH_2O; frequently (but not invariably) they exhibit geochemical patterns which indicate depletion in L.I.L. elements, and very often they are associated with varying degrees of partial melting and migmatisation. The minimum aH_2O required to produce melting, however, may be as low as 0.3 (Johannes & Holtz, 1990). Water activities this low have been frequently recorded in granulite terranes (e.g. Valley, 1986). The low aH_2O conditions of the lower crust have been the cause of considerable debate over the last decade. Most theories for the origins of granulite-facies assemblages involve the mass transfer of H_2O and/or CO_2. Processes invoked include widespread flooding of the crust by mantle derived CO_2 rich fluids, removal of H_2O by preferential concentration in siliceous partial melts and metamorphism of a dry protolith. Chapter 1 introduced the importance of melting and melt extraction in forming granulite terranes. This chapter aims to outline the role of anatexis in granulite complexes in more detail by studying the chemical and mineralogical characteristics of water-undersaturated partial melts derived from pelitic protoliths (including water contents), indicating the amounts of melt that can be generated during melting events in granulite complexes and outlining the metamorphic evolution and chemographic relationships in granulite-facies migmatites from the Brattstrand Bluffs coastline.

2.2.2. Vapour-Absent melting and the generation of granulites.

H_2O is preferentially partitioned into silicate melts over CO_2. Low aH_2O may therefore be related to the generation and subsequent removal of partial melts, or alternatively to the passage of originally dry magmas derived at deeper crustal levels (Essene, 1988). Local control of aH_2O by partial melting is commonly developed in many granulite terranes, including the Madras Charnockite (Bhattacharya & Sen, 1986), the granulite terrane to which the CO_2 dilution model has most successfully been applied.

Metamorphism can be considered as vapour-absent when there is no effective contact between a fluid phase and the minerals or melt in a lithology undergoing metamorphism. The products of vapour-absent melting are an anhydrous residuum and a water-undersaturated melt

(Clemens, 1990). If melt is not extracted then, on cooling, the end products of a vapour-absent melting event will be recrystallised melt and a rehydrated solid residuum. If some of the melt is extracted then more limited rehydration of the residuum will occur. In this work the terms water undersaturated partial melting and vapour-absent melting have been used in preference to the term dehydration melting. Although all three are synonymous, Clemens (*op cit*) suggests that the term dehydration melting should be avoided because of the implication that dehydration of micas liberates water which allows melting to ocur. Vapour-absent melting involves the breakdown of hydrous phases to anhydrous phases and instantaneous dissolution of the aqeous fluid into the melt. No free fluid phase is present at any time.

The role of vapour-absent melting in controlling metamorphic assemblages, aH_2O and melt production in pelitic lithologies has been recognised in many granulite terranes. Field and experimental data suggest that the incongruent breakdown of biotite is the most important melt producing reaction (Vielzeuf & Holloway, 1988; Le Breton & Thompson, 1988; Patino-Douce & Johnston, 1991), although the abundant Himalayan Leucogranites formed under conditions of high pressure and relatively low temperature are thought to have formed at least partially by the incongruent melting of muscovite (Harris & Inger, 1992; Le Fort *et al*, 1987; Vidal *et al*, 1982). Vapour absent melting involving biotite has been suggested for migmatisation and the origin of leucogranites in many areas, including the Arunta Complex (Warren & Hensen, 1989), Broken Hill (Powell & Downes, 1990; Phillips, 1980), Cooma (Ellis & Obata, 1992; White & Chappell, 1991) and the central Victorian magmatic province (Clemens & Wall, 1984) of Australia as well as the Madras example mentioned above.

In a prograde amphibolite-granulite transition zone in Namaqualand, South Africa, granulite and amphibolite-facies rocks are found interlayered in a series of metapelites (Waters, 1988; Waters and Whales, 1984). Iron-rich layers contain the granulite assemblage K-feldspar-garnet-cordierite while the more magnesian layers contain an amphibolite-facies assemblage of biotite-sillimanite-quartz. These contrasting assemblages could have co-existed at the same P-T conditions if aH_2O was lower in granulite layers. Waters & Whales (*op cit*) suggested that aH_2O was lowered in the Fe-rich

layers by partial melting via the vapour-absent vapour-absent melting reaction;

$$Bt + Sil + Qz = Grt + Kfs + Cd + Liq. \quad (2.1)$$

followed by melt extraction. This divariant reaction would occur at lower temperatures in rocks with a higher Fe content. A process such as this, operating on a scale of metres, implies a very localised control on aH_2O and indicates that the relatively anhydrous metamorphic conditions did not result from a pervasive flushing of CO_2 rich fluid.

Melts produced by vapour-absent melting under granulite-facies conditions are invariably water-undersaturated (Section 2.2.3). Water-saturated melts will only exist a few degrees above the solidus (until free water is dissolved in the melt) or as residual granitic melts shortly before crystallisation. The minimum water content is defined by the amount of water required to produce melting at a given P and T, while the maximum water content of a melt is defined by the maximum solubility of water in a melt of that composition at that P and T (Johannes & Holtz, 1990; Holtz & Johannes, *in press*). For water-saturated melts at a given P and T these values are identical, but they diverge with increasing temperature as melts become vapour-undersaturated (Fig. 2.1.). Figure 2.2. (after Holtz & Johannes, *op cit*) shows liquidus and maximum solubility curves in the haplogranitic system. Note the strong pressure and limited temperature dependence of maximum water solubility. A granitic melt produced at 5 kbar, 850°C has a maximum water solubility of approximately 10wt % H_2O, but could form if a minimum of approximately 2.5wt % H_2O was available. The relatively low amounts of water required to produce melts at high temperatures suggests that melting under granulite-facies conditions is a viable process, and that extraction of these melts could act as a dehydrating agent in the lower crust due to the relatively large amount of H_2O potentially soluble in granitic melts. Experimental work by Holtz *et al* (1992) has shown that the amount of water that can be dissolved in a haplogranitic melt depends on composition, with maximum solubilities in albite rich melts. This may have important implications for the extraction of Na-rich granitic melts, since increased solubility of water depolymerises silicate melts, making them less viscous and more easily extractable.

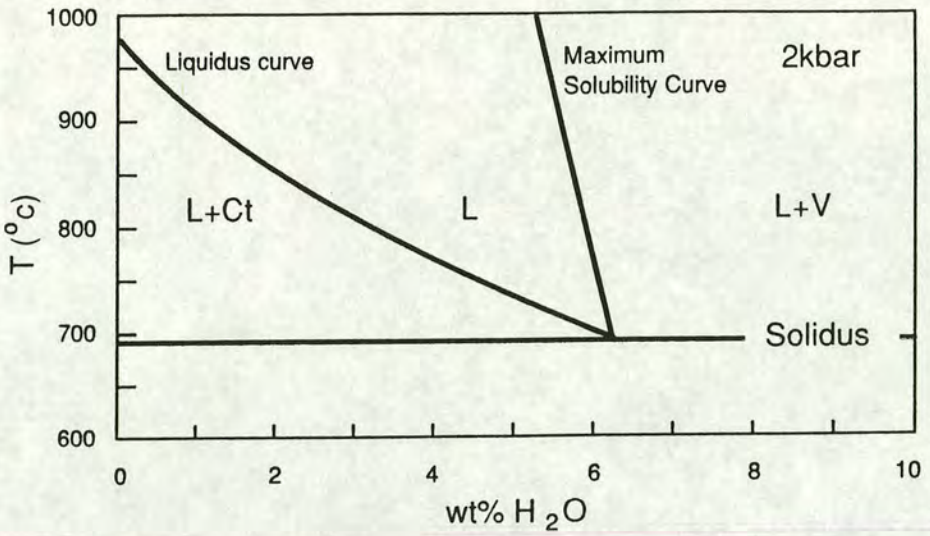

Figure 2.1. Phase relations in the system Qtz-Ab-Or-H_2O at 2Kbar for the minimum melt composition Qtz-35%, Ab-39%, Or-26%. L = aluminosilicate liquid; V = supercritical H2O vapour; CT = crystals. After Holtz & Johannes, (in press).

2.2.3. Partial Melting in the system KFMASH; the Brattstrand Bluffs Coastline.

A detailed study of the partial melting equilibria, pressure-temperature-fluid evolution and chemographic relations in the system KFMASH (K_2O-FeO-MgO-Al_2O_3-SiO_2-H_2O) was carried out by Fitzsimons (1991) as part of a PhD thesis at the University of Edinburgh. The following review of melting equilibria in the Brattstrand Bluffs metapelites has been included to provide a background for the geochemical study of partial melting which is the main aspect of this present work. For a more detailed evaluation of the metamorphic aspects of the melting equilibria the reader is referred to the above work.

Where melt production has been low in the Brattstrand Bluffs coastline, well-layerered pelitic gneisses commonly preserve reactants and products of the melting reactions adjacent to one another. Assemblages typically consist of garnet, cordierite, sillimanite, biotite, quartz and K-feldspar. Fitzsimons (1991) considered the partial melting relations in terms of reactions between these phases, with the addition of a volatile fluid and silicate melt, and

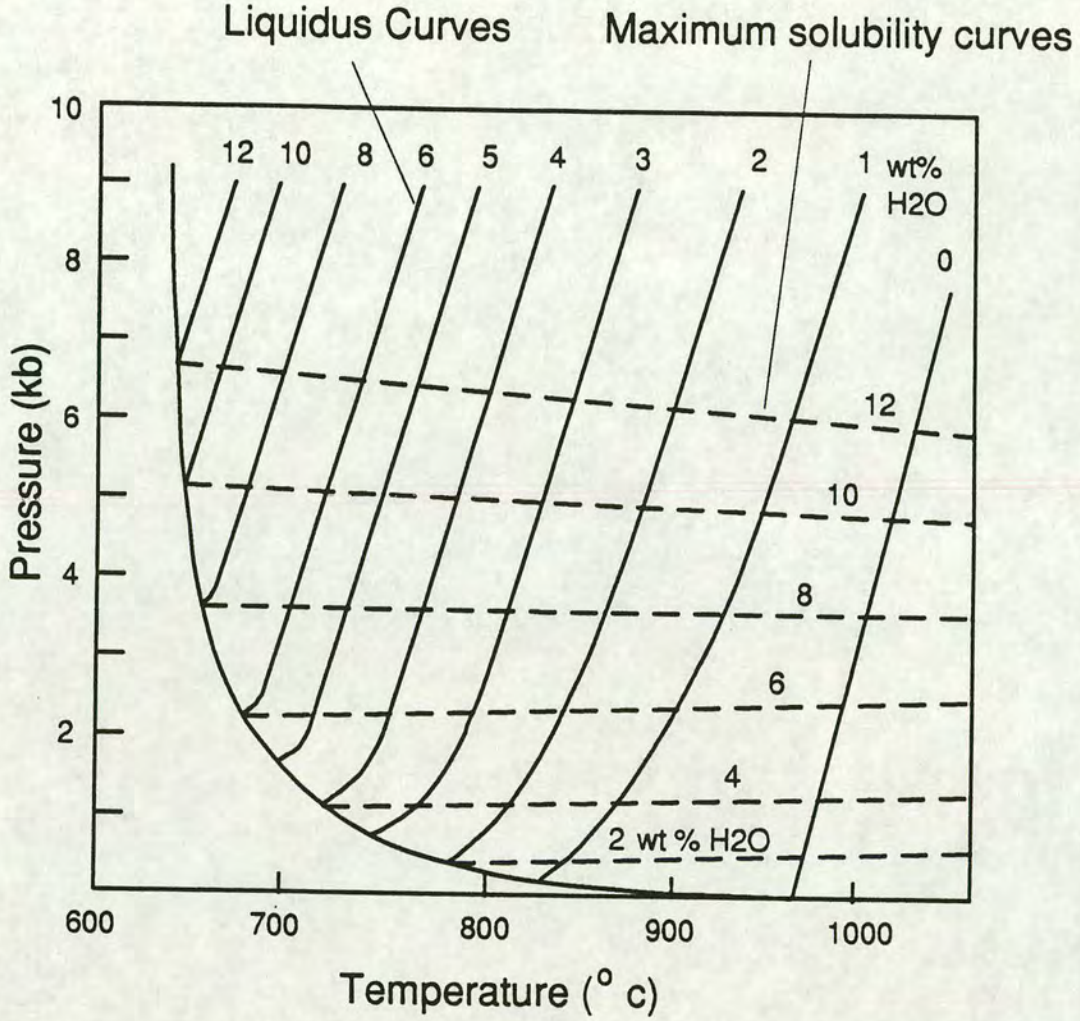

Figure 2.2. Liquidus curves (for a given H_2O content) and maximum H_2O solubility curves in the system Qtz-Ab-Or-H_2O.

constructed a simple P-T grid comprised of eight univariant reactions. Figure 2.3.a shows AFM compatability relations in the KFMASH system for a melt composition more magnesian than co-existing garnet (Clemens & Wall, 1981; Ellis, 1986), while Figure 2.3.b displays the same information for the less aluminous (although still peraluminous (c.f. Ellis, 1986; Vielzeuf & Holloway, 1988) melt composition of Grant (1985). Vapour-saturated eutectic melting at the solidus producing the less aluminous melt of Grant (*op cit*) would generate melts with slightly higher water contents than the melt composition of Ellis (1986) since it involves the breakdown of biotite rather than sillimanite.

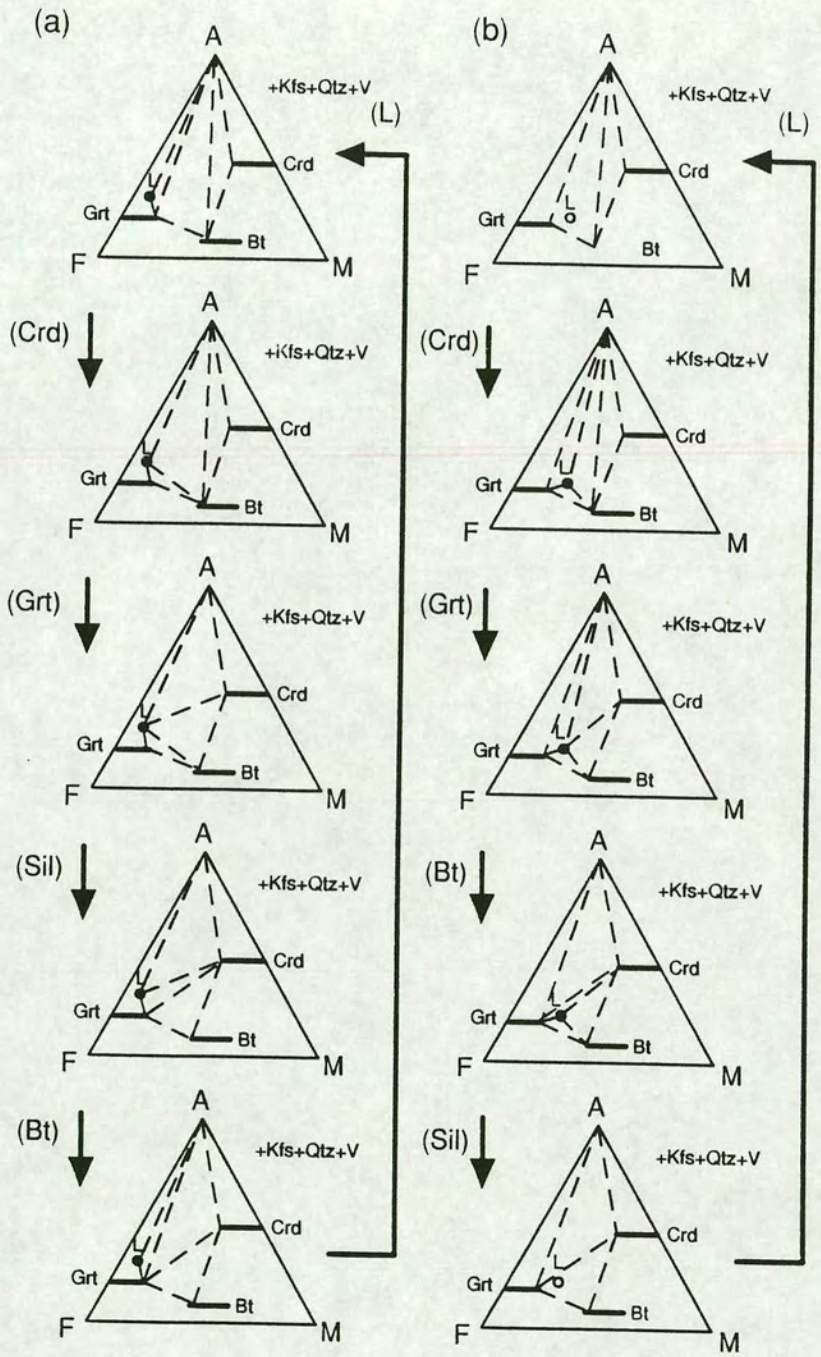

Figure 2.3. AFM compatability diagrams for the system KFMASH for melt compositions (a) less magnesian than coexisting garnet and (b) more magnesian than coexisting garnet. Arrows represent reactions encountered clockwise around the corresponding Schreinemacher's bundle.

Divariant equilibria are responsible for the assemblages formed in most metamorphic rocks (e.g Grant, 1985; Hensen & Harley, 1990). In the system KFMASH, each univariant reaction has a set of divariant reactions associated with it, each with another phase absent. By combining an isobaric univariant T-aH_2O section with divariant bands in the KFMASH system (derived from KFASH and KMASH univariant end-member systems assuming the dominant compositional change along univariant KFMASH reactions involves Fe and Mg exchange) Fitzsimons (1991) constructed a T-aH_2O pseudosection for an Fe-rich bulk composition (Figure 2.4) undergoing prograde metamorphism leading to anatexis by incongruent melting of biotite via several intermediate reactions.

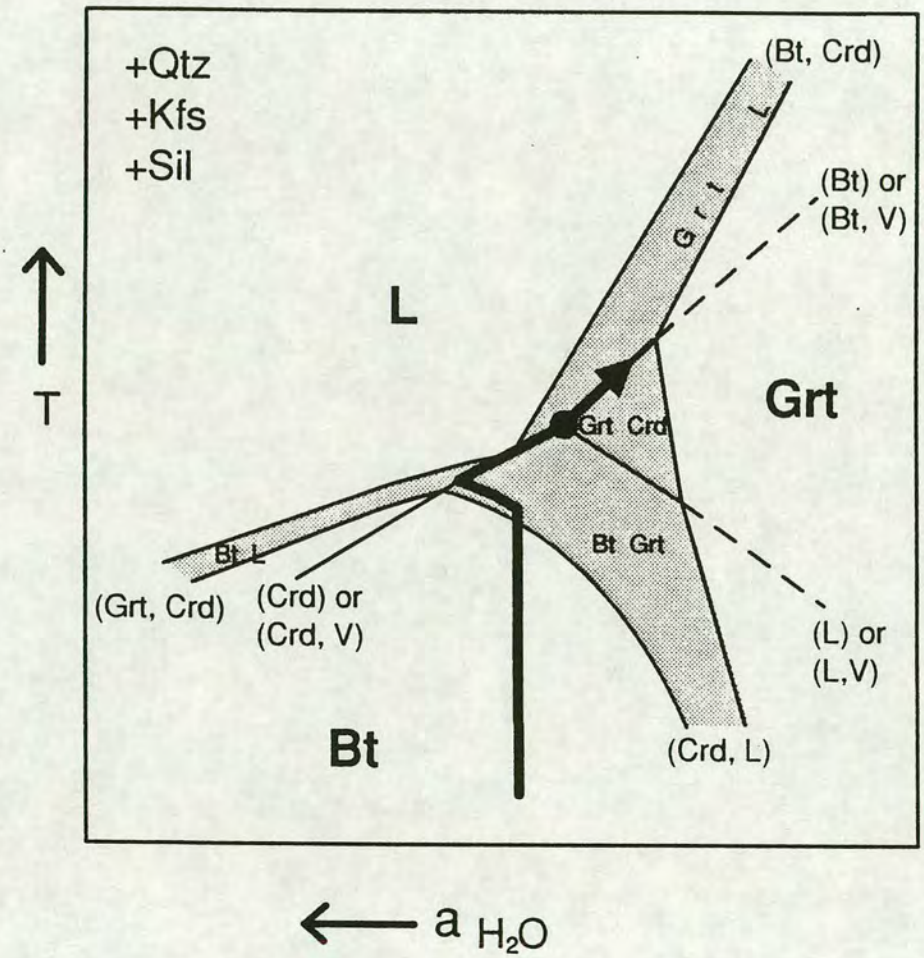

Figure 2.4. T-aH_2O pseudosection for an Fe-rich bulk composition undergoing prograde metamorphism leading to anatexis by incongruent melting of biotite (after Fitzsimons, 1991).

With increasing temperature, early garnet grows and aH_2O increases along the (Crd, L) divariant reaction until the assemblage begins to melt at the (Crd) univariant reaction;

$$Grt_{(1)} + Bi + Sill + Qtz + Kfs + Vap = L \qquad (2.2)$$

buffering aH_2O to lower values (as both free vapour and vapour from the biotite is partitioned into the melt) until all the vapour is consumed. At this point melting continues via the (Crd, V) divariant reaction (forming a second generation of garnet) until the vapour-absent invariant point (V) is intersected where cordierite begins to form by incongruent melting of biotite in Reaction 2.1 above. Once all the biotite is consumed an increase in temperature causes the aH_2O to decrease further as eutectic melting of the grt-sill-crd-qtz-kfs assemblage continues. Only small melt fractions are likely to be produced by partial melting of such a refractory assemblage at typical lower-crustal temperatures (Grant, 1985).

2.2.4. Amounts of melt-production under vapour-absent conditions.

The small amount of free fluid present in pores in the lower continental crust (<0.05wt % H_2O - Clemens & Vielzeuf, 1987) means that fluid-present melting only occurs for a few degrees above the solidus and melt rapidly becomes water-undersaturated. Water-undersaturated magmas are the normal product of crustal anatexis (Wylie, 1977; Ashworth, 1985; Le Breton & Thompson, 1988; Clemens & Vielzeuf, 1987). Figure 2.5 shows the relationship between the P-T curves of a simple subsolidus vapour-absent reaction, the water-saturated solidus and the vapour-absent melting reaction. The vapour-absent curve represents the P-T locii along which the invariant point *I* evolves as aH_2O is lowered (Clemens & Vielzuef, *op cit*). Along this curve a hydrous mineral (typically biotite, muscovite or amphibole) will breakdown to an anhydrous assemblage and a water-undersaturated melt (Patino-Douce & Johnston, 1991). The amount of melt which can be produced as a function of vapour-absent melting reactions is a function of the modal composition of the source. Using estimates of typical shale compositions and water contents, experimental work by Clemens & Vielzeuf (1987) in the system Qtz-Ab-Or-H_2O allowed them to calculate the solidus

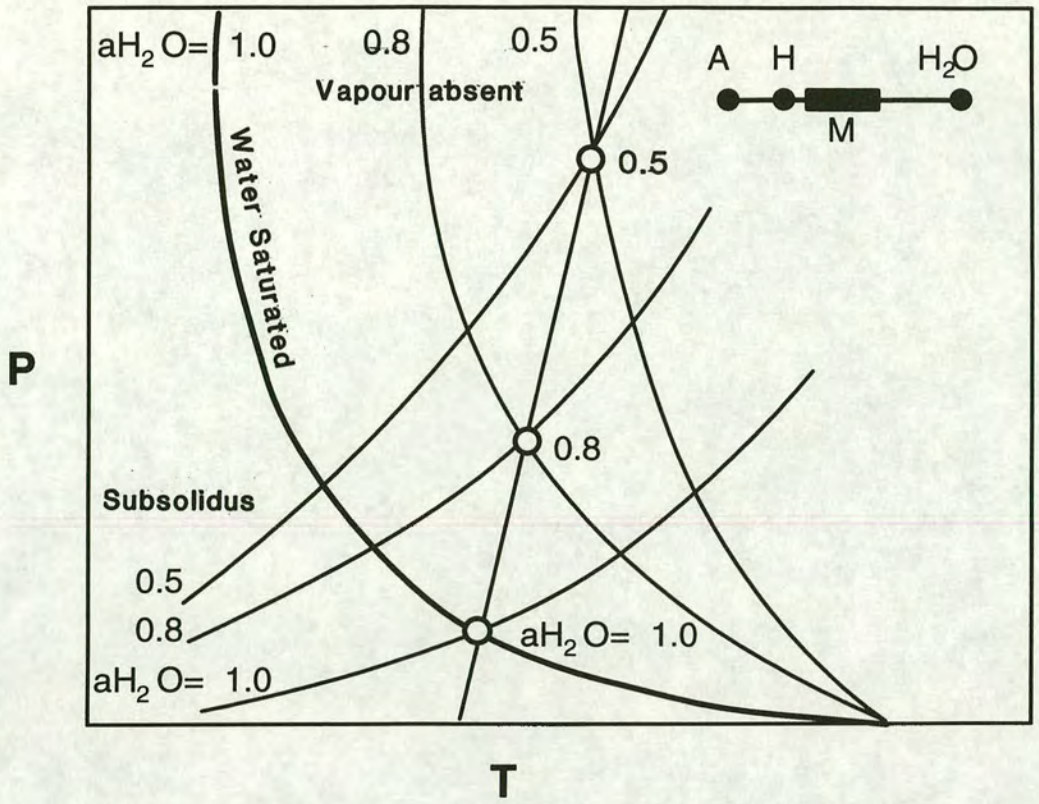

Figure 2.5. P-T diagram showing the water saturated solidus (bold curve), water-undersaturated melting and vapour absent subsolidus reactions for different aH_2O values (after Clemens & Vielzeuf, 1987). A - Anhydrous Phase: H - Hydrous phase: M - Melt.

for various aH_2O values. The results of this calculation are shown in Figure 2.6. If aH_2O is known the mole fraction of H_2O in the melt can be calculated from the relationship;

$$a_{H_2O} = k\left(X_{H_2O}^{melt}\right)^2 \qquad (2.3)$$

(Burnham, 1986) where k represents an experimentally derived empirical constant. If the melt is produced by a vapour-absent reaction the amount of melting (in wt %) is constrained by the hydrous mineral content of the source, e.g.

$$\text{wt \% melt} = 100 \times \left(\frac{H_2O \text{ content of source rock}}{H_2O \text{ content of melt formed}}\right) \qquad (2.4)$$

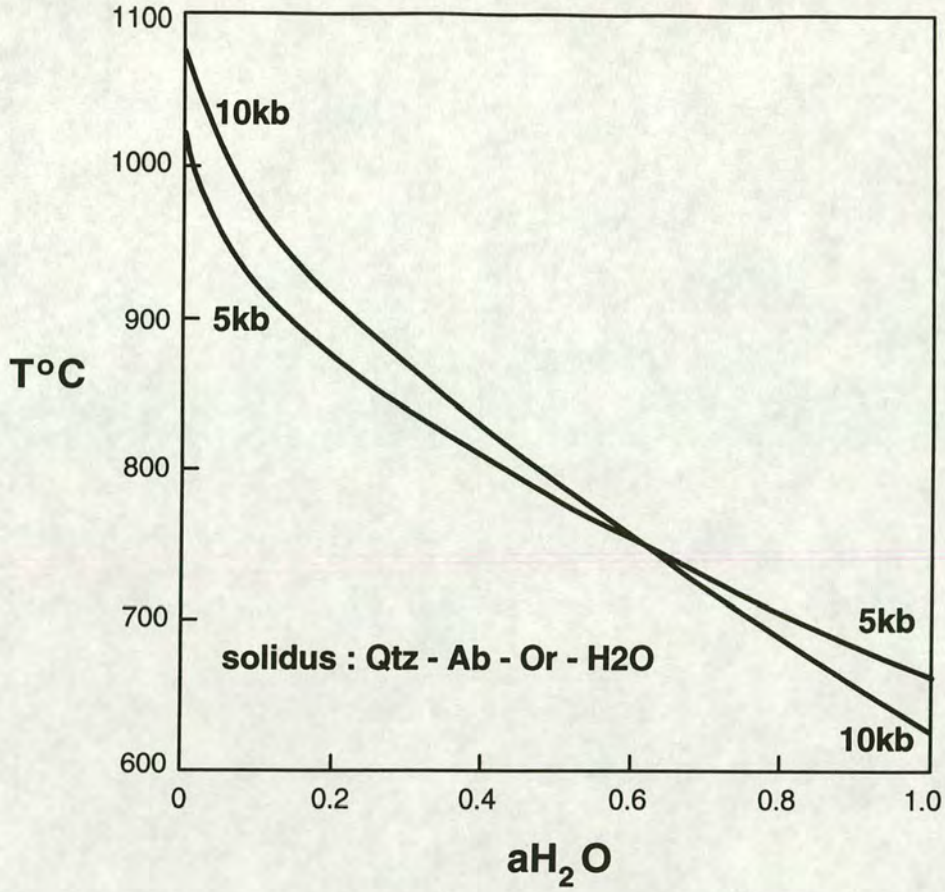

Figure 2.6. Solidus curves in the system Qtz-Ab-Or-H_2O at 5 and 10kbar (after Clemens & Vielzeuf, 1987).

(Clemens & Vielzeuf, 1987). Patino-Douce & Johnston (1991) suggested that the amount of melt produced is not solely a function of the modal concentration of hydrous phases, and that the degree to which the modal concentration of all phases approaches the stoichiometric proportions required for the melting reaction is important. The above authors calculated two "optimum bulk compositions" (one for their melt composition (L1) and one for that of a melt produced experimentally by Vielzeuf & Holloway (1988) (VH875). These optimum bulk compositions represent the bulk composition and modal mineralogy which would produce the maximum amount of a given melt at a give P-T and aH_2O. The modal compositions of these hypothetical fertile lithologies are given below, and approximate to impure greywackes or immature volcanoclastic sediments rather than true pelitic rocks.

41% bi, 23% plg, 31% qz, 6% als (L1, Patino-Douce & Johnston (1991))
36% bi, 21% plg, 34% qz, 9% als (VH875, Vielzeuf & Holloway (1988))

True pelites would yield much less than the 70% melt produced from these compositions, due mainly to low plagioclase and excess biotite and aluminosilicate. The melt volumes produced as a function of water content of the source rock are shown in Figure 2.7 (Clemens & Vielzeuf, 1987).

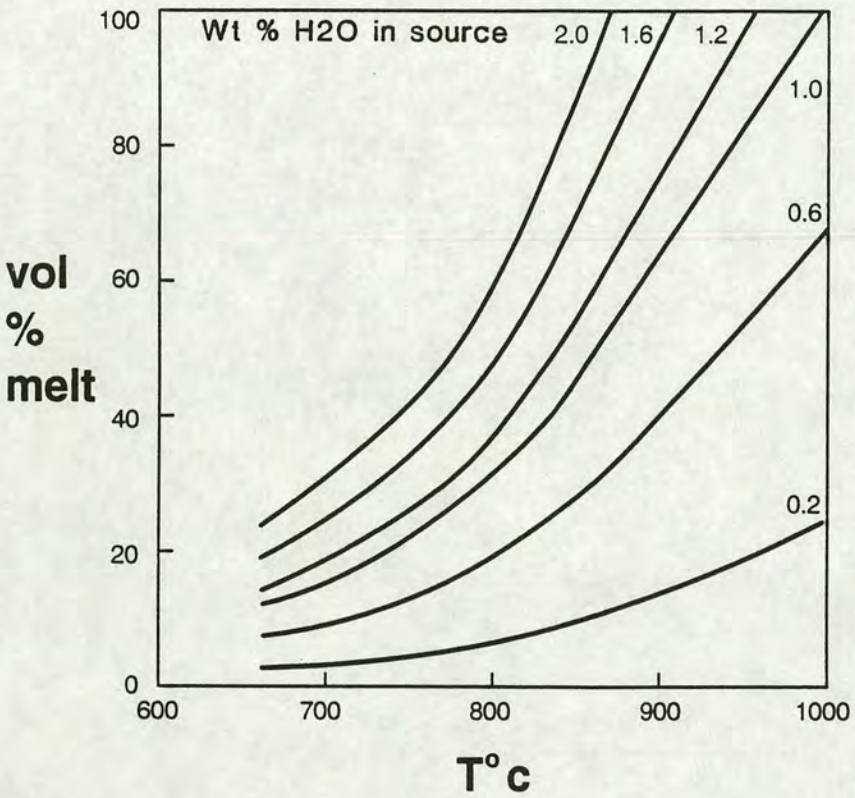

Figure 2.7. Melt volumes produced during melting of a typical pelitic composition as a function of source water content (after Clemens & Vielzeuf, 1987).

Experimental work (Le Breton & Thompson, 1988; Harris & Inger, 1992) has shown that metapelites will undergo two stages of vapour-absent melting as muscovite and then biotite react, over a temperature interval of approximately 100°c. At temperatures of 850°C and 5 kbar, melt proportions of 43-50 volume % were obtained experimentally from pelitic lithologies (Clemens & Vielzeuf, 1987), assuming vapour-absent melting of muscovite occurs at 665°C and biotite at 850°C (both at 5 kbar). Clemens & Vielzeuf (*op cit*) also showed that the contribution of the muscovite melting reaction is minor compared to the large volumes of melt which are produced as a result of the incongruent melting of biotite (see also Patino-Douce & Johnston, 1991). Large melt volumes can be generated under vapour-absent conditions

as long as temperatures are high enough. The production of water-undersaturated melt proportions of 45-55% can occur over a relatively small temperature interval (850-875°c) due to the breakdown of the assemblage biotite-sillimanite-plagioclase-quartz (Vielzeuf & Holloway, 1988). Water-undersaturated melts will not intersect the solidus on ascent because of the positive $\delta P/\delta T$ slope of vapour-absent melting reactions (Le Breton & Thompson, 1988; Clemens & Vielzeuf, 1987; Holtz & Johannes, *in press*), making them more likely precursors for S-Type granite batholiths than melts formed under water-saturated conditions. Vapour-saturated melting reactions have negative $\delta P/\delta T$ slopes and melts formed under these conditions will be unable to ascend significant distances in the crust before they intersect the solidus.

2.3. EQUILIBRIUM & DISEQUILIBRIUM MELTING.

2.3.1. Introduction.

When melting occurs in a solid polyphase aggregate it initiates at grain boundaries. The first increment of melt is only in equilibrium with the solid grain edge it is in contact with (Sawyer, 1991). Equilibrium melting (e.g. Wood & Fraser, 1977; Allegre & Minster, 1978; Barbey *et al*, 1989) only occurs if the melt is in chemical equilibrium with the whole of the solid body before extraction (Ashworth and Brown, 1990). If melt production and extraction rates are rapid then equilibration between liquid and restite phases may not be achieved. Chemical equilibration between the melt and the whole body of the solid occurs when;

(i) Components diffuse through the solid and into the melt (in the case of elements whose concentration in the melt is controlled by distribution cofficients).

(ii) Phases dissolve in or are precipitated from the melt (in the case of elements which are essential structural components of the dissolving phase).

If insufficient time is avaliable for these processes to go to completion before melt extraction occurs, then the melts generated will have disequilibrium compositions. Disequilibrium melting can occur if the temperature exceeds the solidus before melting begins. This may be the case when H_2O infiltrates dry rocks above the water-saturated solidus, or when reactant grains are not in mutual contact. Incongruent melting reactions (e.g. biotite dehydration reactions) require temperature oversteps of tens of degrees to nucleate new phases (Rubie & Brearley, 1990). Only small amounts of melt can be produced until these incongruent phases are produced.

Two important processes compete in partial melting to determine whether equilibrium or disequilibrium melting occurs.

(i) Transport of a chemical species by the melt.
(ii) Diffusion of that chemical species in the solid.

To maintain equilibrium, the time taken for a species to diffuse between melt channels (or veins, patches etc) must be short compared with the time taken for it to be removed from the system as the melt is extracted (Spiegelmann & Kenyon, 1992).

2.3.2. Basic Theory.

Consider a layer of an ideal permeable medium of depth L, consisting of a network of uniformly spaced melt channels of d spacing. The time taken for a species to diffuse through the solid medium over distance d must be shorter than the time taken for the melt to advect across distance L with melt velocity W_o for equilibrium melting to occur (Fig. 2.8).

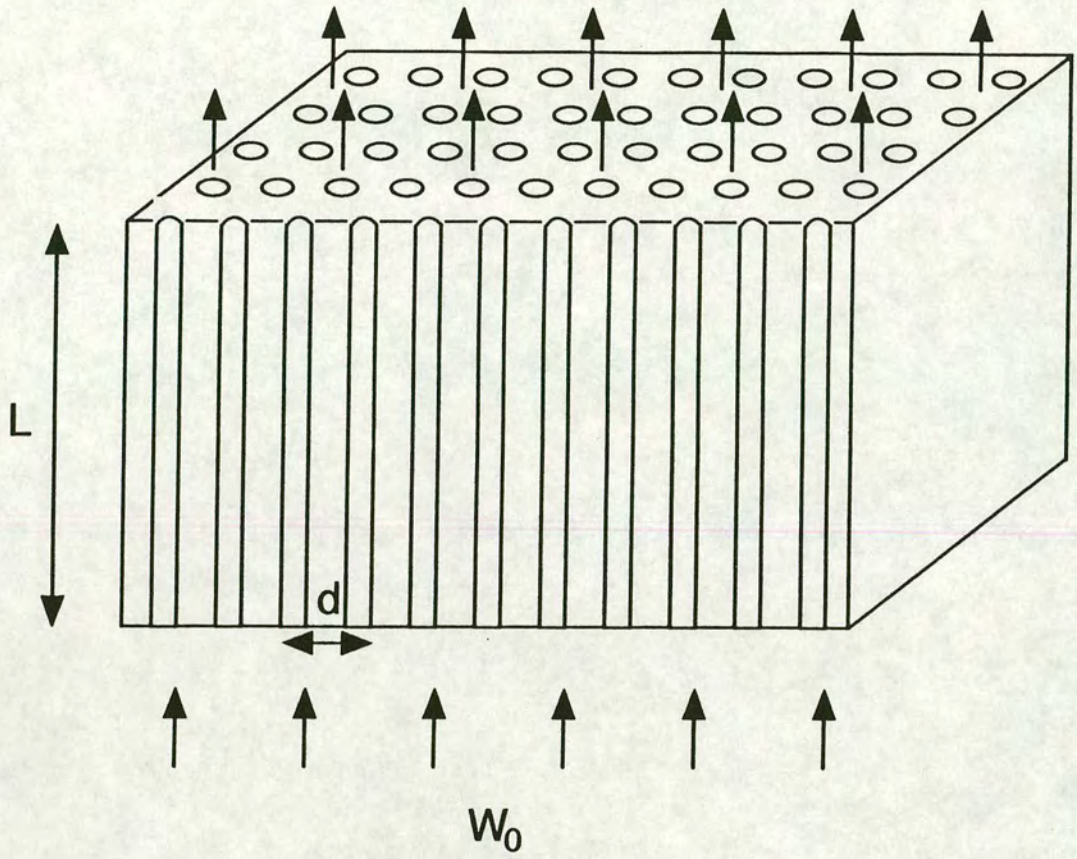

Figure 2.8. The geometry of an idealised melt-solid system.

The time taken to diffuse between melt channels is

$$t_{(diff)} = \frac{d^2}{D_s} \tag{2.5}$$

where D_s = solid state diffusion coefficient.

The time taken for melt advection is

$$t_{(advec)} = \frac{L}{W_o} \tag{2.6}$$

where W_o = melt velocity.

(note for migmatites where melt is not being extracted, or is migrating slowly, W_o will be small and advection times large).
The ratio of these two times is the Peclet number (Pe).

$$P_e = \frac{W_o d^2}{D_s L} \qquad (2.7)$$

If Pe << 10, diffusion dominates and equilibriation is rapid.
If Pe >> 10 advection dominates and disequilibrium occurs.

Disequilibrium conditions are favoured by rapid melt velocities. Melt extraction will be most rapid when melts are non-viscous (i.e. under water-saturated conditions) or during deformation). Melting under water-undersaturated conditions should theoretically therefore produce equilibrium melts, since advection times are large (Pe << 10).

In Equation 2.7 above, large Pe are favoured by large channel spacing (since diffusion times are much greater). Small changes in the distribution of melt can dramatically change the ability of the melt to remain in equilibrium with solid residue. Spiegelmann & Kenyon, (1992) show empirically that solid state diffusitivity must increase by four orders of magnitude for every order of magnitude increase in channel spacing if equilibrium is to be maintained. As melting proceeds in a migmatite system the melt may become ponded, thus increasing channel spacing and, consequently, giving rise to disequilibrium conditions.

In extreme disequilibrium melting (Allegre & Minster, 1978; Barbey *et al*, 1989; Ashworth & Brown, 1990), no fractionation occurs as a mineral dissolves into the melt. The mineral does not change composition as it melts, since the rate determining diffusion in the melt is much faster than in the solid reactants. Geochemically it is very difficult to distinguish this process from equilibrium melting coupled with mixture of restite with the melt, since both give rise to melt bulk compositions determined solely by the mode of the rock and individual mineral compositions. Furthermore, if equilibrium melting is followed by homogenisation of mineral chemistry then melt chemistry may be indistinguishable from the final products of

extreme disequilibrium melting. Because melt may not segregate from restite cleanly, recognition of equilibrium melt compositions can be very difficult (Sawyer, 1992).

2.4. CHEMICAL AND MINERALOGICAL CHARACTERISTICS OF CRUSTAL MELTS.

2.4.1. Introduction.

The origin of granites by partial melting was clearly demonstrated by the experimental work of Bowen & Tuttle (1950) and Tuttle & Bowen (1958), effectively ending the "granite controversy". They showed that crustal lithologies will melt at temperatures approximating those of high-grade metamorphism in the presence of excess H_2O. Melting of crustal lithologies can give rise to melts of granitic composition at temperatures as low as 680°C under vapour-saturated conditions (Wyllie, 1977). The lowest temperature (or minimum) melts which form are comprised dominantly of quartz and feldspar (Winkler, 1979). Subsequent work (e.g. Clemens, 1984; Wyllie, 1983; Wyllie, 1977) has shown that water-saturated liquids only exist for a few degrees above the solidus, and that water-undersaturated melts are the usual products of crustal anatexis. The remainder of this section aims to describe the chemical and mineralogical characteristics of crustally-derived aluminium-rich melts produced under vapour absent conditions.

2.4.2. Chemical & Mineralogical Characteristics.

Granites are coarse-grained igneous rocks comprised dominantly of quartz and feldspar, with subordinate mafic minerals which range in volume from 0% (haplogranite) to 30% (mafic granite) (White, 1990). Granites which have excess alumina present over that required to saturate the melt in feldspar will crystallise a mafic or aluminous phase which has a molecular $Al_2O_3/CaO+Na_2O+K_2O$ greater than 1.0 (White, 1990; Miller, 1985). These melts are termed peraluminous (Shand, 1927; White, 1990). Miller (1985)

erected a classification for granitic melts based upon primary mineralogy (Fig 2.9).

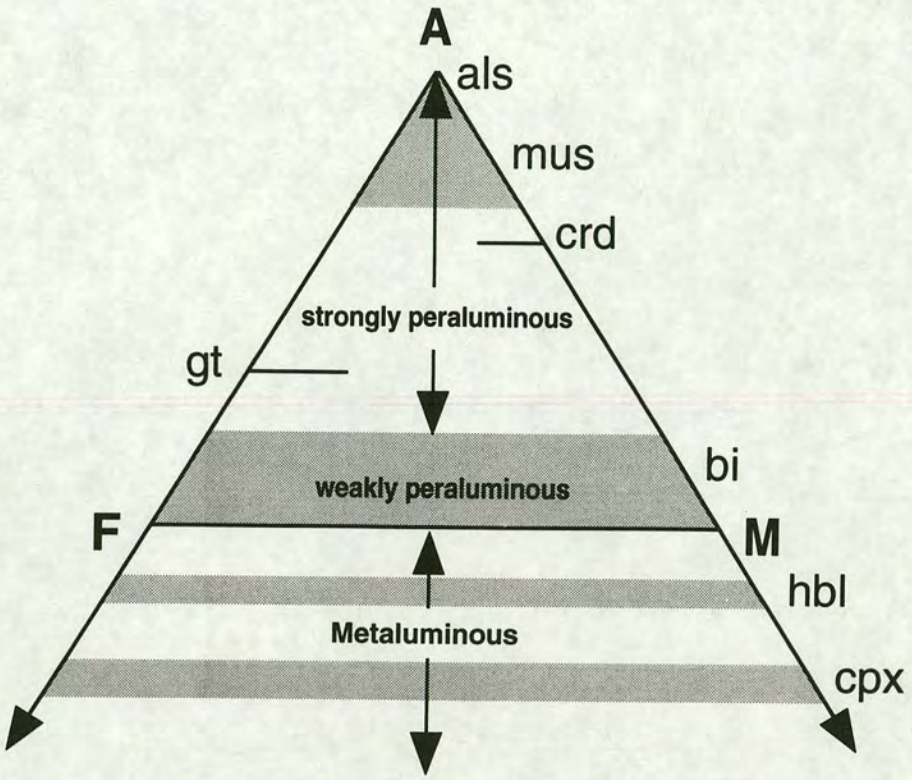

Figure 2.9. .Nomenclature of peraluminous igneous rocks based on the primary mineralogical assemblage (after Miller, 1985).

Weakly peraluminous liquids will crystallise biotite while strongly peraluminous magmas may precipitate muscovite, cordierite, garnet or an aluminosilicate phase (e.g. andalusite, Vernon & Collins, 1987) depending on the P-T and aH_2O conditions during magma ascent and crystallisation. Liquids with $Al_2O_3/CaO+Na_2O+K_2O < 1.0$ but $Al_2O_3/Na_2O+K_2O > 1.0$ have excess $CaO+Na_2O+K_2O$ caused by a surplus of Ca over that required to produce the anorthite component of plagioclase. This excess Ca forms hornblende, and hornblende bearing granites are termed metaluminous. Figure 2.10 shows the relationship between chemical composition and the mafic mineral precipitated by a melt (White, 1990). Metaluminous granites

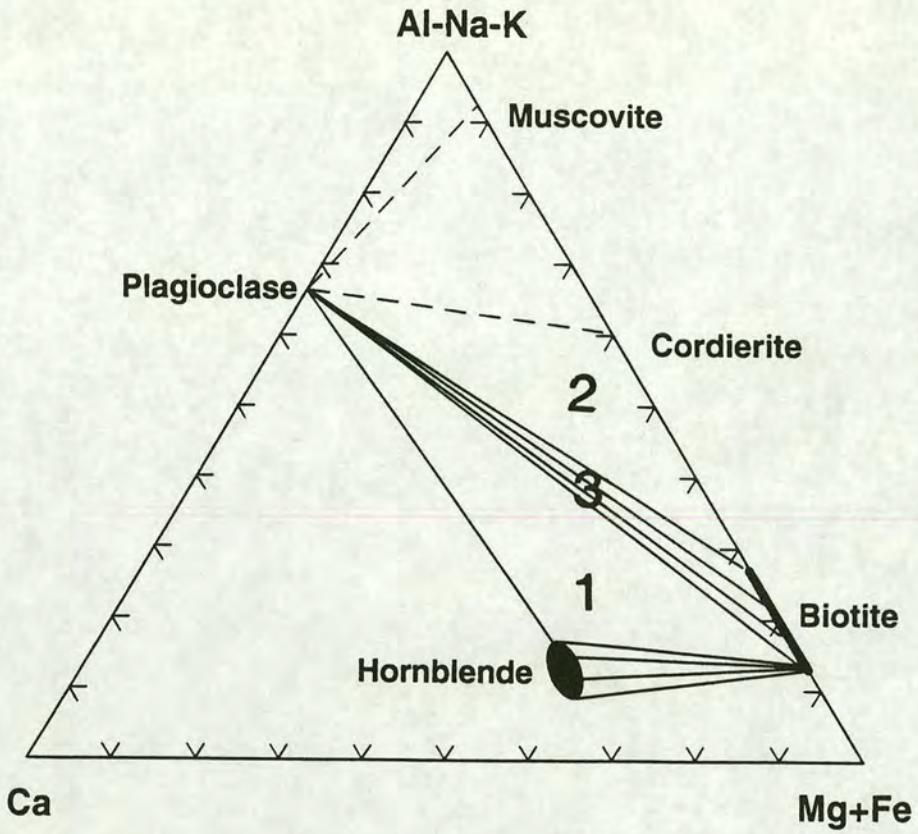

Figure 2.10. Modified AFM diagram (after White, 1990) showing metaluminous (1), peraluminous (2) and weakly peraluminous (3) fields.

will fall in field 1, while the bulk compositions of strongly peraluminous granites plot in field 2. Weakly peraluminous magmas (those crystallising biotite as their only mafic phase) will plot in field 3.

Many of the geochemical features of crustal melts can be ascribed to the nature of their source rocks. Miller (1985) suggested that typical S-Type granites (granites derived from sedimentary protoliths) will have low Na_2O (<3.2wt %), K_2O values of approximately 5.0wt %, high silica concentrations (SiO_2 > 65wt %) and molecular A/CNK > 1.10. The aluminium-rich, sodium- and calcium-poor nature of crustal melts reflects the chemistry of the protolith. Because the natural weathering cycle depletes calcium and sodium relative to aluminium, crustal rocks (including pelites, immature clastic sediments and volcanics) and melts derived from crustal sources will have molecular A/CNK greater than 1.0. This excess Al_2O_3 is manifested as peraluminous granites containing normative corundum. Crustally derived granitoids typically show a restricted range of SiO_2 values (70-75 wt %).

White (1990) ascribed this to the quartz-rich nature of the source rocks. Clemens & Wall (1988) suggested that the stability of cordierite in strongly peraluminous granites is enhanced at high $aSiO_2$ and that most granitoids are at or near the quartz-saturation boundary throughout their history. The effect of excess aluminium on melt phase relationships was examined experimentally by Holtz, Johannes & Pichavant (1992). Peraluminous compositions have the quartz-feldspar cotectic shifted towards more quartz-rich compositions (see also Holtz *et al*, 1991). Minimum melts in systems containing excess alumina are therefore slightly more quartz rich for both water-saturated and water-undersaturated melting. Holtz *et al* (1992) suggested that the higher quartz content of experimental melts in the presence of excess aluminium may explain in part the relatively high quartz content of some peraluminous crustal melts.

Crustal melts typically contain low concentrations of mafic minerals (Miller, 1985; White, 1990; Clemens & Wall, 1988, Puziewicz & Johannes, 1988). The amount of primary mafic minerals present in an anatectic melt is a function of the total Fe+Mg+Mn content of the melt, while the nature of the phases precipitating is determined by the contents of Al, Ca, Na and K as well as the P-T, aH_2O and fO_2 (White, 1990; Clemens & Wall, 1988; Chappell *et al*, 1987). Experimental work by Johannes & Holtz (1990) has shown that, at 5 kbar and temperatures up to 850°c, maximum FeO solubilities in peraluminous granitic melts reach only 2.0wt %, while MgO contents are lower (<0.5wt %). The maximum Al_2O_3 solubility in the same melts is equivalent to 5.5wt % normative corundum while Patino-Douce & Johnston (1991) recorded maximum Al_2O_3 solubilities equivalent to 2wt % corundum at 825°c and 4-5wt % corundum at 950-1000°C. At higher temperatures the solubilities of Fe and Mg in granitic melts are also enhanced. X_{Mg} is determined by the temperature of melting and the composition of the source (Clemens & Wall, 1988). At the temperatures typically encountered during crustal anatexis, melts derived from a typical pelite will be more magnesian than co-existing garnet, while at temperatures above approximately 900°C melts will be less magnesian than garnet (Clemens & Wall, 1981). Biotite is the most common ferromagnesian phase in granitic rocks, while cordierite is the most commonly described strongly peraluminous phase which occurs as a primary magmatic phase in crustally derived granites and volcanics. Cordierite is replaced by garnet at pressures higher than approximately 5-7

kbar for most pelitic bulk compositions (Green, 1976; Green & Ringwood, 1968). From Figure 2.11 it is clear that cordierite stability is enhanced at lower T and higher X_{H2O} relative to garnet.

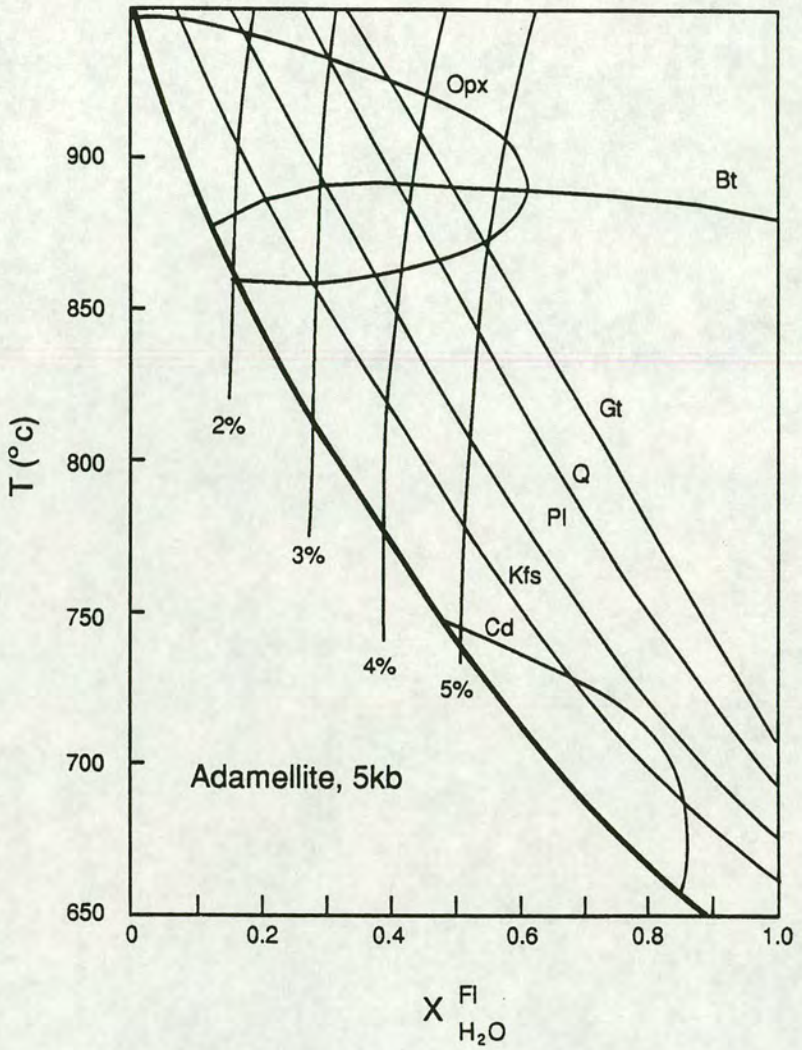

Figure 2.11. P-T diagram showing the experimentally determined stability fields for various phases in a granitic melt (after Clemens & Wall, 1988).

Garnet or cordierite may crystallise from rocks of a similar composition at the same pressure in the presence of excess sillimanite according to the reaction;

$$3(Mg,Fe)_2Al_4Si_5O_{18} = 2(Mg,Fe)_3Al_2Si_3O_{12} + 4Al_2SiO_5 + 5SiO_2 \qquad (2.8)$$
$$\text{Cd} \qquad\qquad \text{Gt} \qquad\qquad \text{Sill} \quad \text{Qtz}$$

(Clemens & Wall, 1988). This reaction has a shallow $\delta P/\delta T$ and is shifted to higher pressures by increasing X_{Mg}. Cordierite stability is therefore favoured

at low P, or at lower T, higher bulk X_{mg} and higher aH_2O in the presence of excess alumina.

The oxide and accessory phases of peraluminous melts are generally different to those of I-Type granitoids. Ca-rich accessory phases such as sphene and allanite are not found in melts derived from pelitic protoliths (due to high molecular A/CNK). Because these minerals typically host REE in granites a separate REE-bearing phase (monazite; $(Ce,La,Th)PO_4$) will form in low-Ca melts. Apatite is therefore relatively rare in peraluminous granites because the precipitation of monazite consumes any available P_2O_5 (White, 1990). Other accessory phases commonly found in peraluminous granites include zircon, ilmenite and magnetite. Ilmenite is more common in peraluminous melts because these are typically reduced. Fe^{3+} contents are low in S-Type granites and magnetite is generally absent.

When large-scale partial melting occurs in a migmatite terrane, melt compositions will migrate away from the granitic minimum unless the source rock has the granite minimum melt composition itself. Melts become more mafic and evolve from granitic to granodioritic compositions (Ashworth, 1985). Plagioclase becomes more calcic in higher temperature, more mafic melts (Ashworth, *op cit*). Exhaustion of one or more of the quartz, K-feldspar or plagioclase components will cause melt compositions to evolve away from the minimum melt composition, although experimental work by Wyllie (1977) indicated that not until two of these minerals have melted completely will melt compositions depart from the system Qtz-Ab-Or-H_2O. Once the temperatures of minimum melting have been exceeded, a wide variety of magmas can be produced by partial melting of a single lithology. The melt composition will be controlled by the source rock characteristics and the degree of melting, which is in turn controlled by the P-T and aH_2O conditions. Water undersaturation typically increases the K-feldspar component of the melt, while the solubility of Fe and Ca increases with increasing temperature and decreasing aH_2O (Holtz & Johannes, 1991; Johannes & Holtz, 1990). Harris & Inger (1992) outlined the major differences expected between vapour-saturated and vapour-undersaturated melts. Their work assumed that only small degrees of melting could occur under vapour-undersaturated conditions, while large degrees of melting require the

presence of a free fluid phase. Water-undersaturated melts produced by the incongruent melting of biotite in the reaction;

$$bi + sill + qtz + plag = grt + kfs + melt \quad (2.9)$$

or by Reaction 2.1 will produce a residue enriched in K-feldspar and garnet. At high temperatures complete melting of the K-feldspar component of the source may produce potassic melts. Eutectic liquids will not be produced at high degrees of melting since the plagioclase component will be consumed rapidly in many pelitic rocks. Since K-feldspar is produced as a peritectic phase during the vapour-absent melting of biotite, plagioclase or quartz are the most likely phase to be consumed during the high temperature melting required to produce non-minimum melts (Harris & Inger, 1992). At low degrees of partial melting liquids produced by vapour absent melting will be in equilibrium with residue which contains both plagioclase and alkali feldspar. This should lead to the production of melt with high Rb/Sr and low Sr and Ba contents. If garnet is a residual phase, then melts will be depleted in heavy rare-earth elements as well as LREE (which are retained in K-feldspar and plagioclase). Vapour-absent melts will contrast strongly with melts produced under vapour present conditions, which will have high Rb, Sr and Ba due to large degrees of melting which deplete the residue in feldspar. If large degrees of melting occur, however, under vapour-absent conditions at higher temperatures (>850°c) (e.g. Clemens & Vielzeuf, 1987; Vielzuef & Holloway, 1988) then depletion of the source in feldspar will also occur during vapour-absent melting. The depletion of Sr and Ba associated with small degrees of partial melting (because of the retention of K-feldspar and plagioclase in the residue) suggested by Harris & Inger (1992) would therefore not be diagnostic of vapour-absent melts.

2.5. MELT EXTRACTION IN MIGMATITES.

2.5.1. Introduction.

The extent that melts produced under lower-crustal conditions are extracted from the melting region has fundamental implications for the evolution of

the crust through time, the generation of batholithic complexes and the genesis of granulite-facies high grade-metamorphic rocks. If the melts are extracted from their source region, they may rise through the crust and become emplaced at higher structural levels, leading to a differentiation of the crust through time (e.g. Section 2.1., Vielzeuf *et al*, 1990). If water-bearing melts fail to segregate from the anatectic complex then the expulsion of dissolved H_2O on crystallisation will lead to retrogression (e.g. the pervasive formation of biotite after orthopyroxene-orthoclase in the Arunta Complex, central Australia; Warren and Hensen, 1989). Granitic melts (especially water-undersaturated granitic melts produced under granulite-grade conditions) are very viscous, and may only undergo limited segregation from their source (Shaw, 1972; Bottinga & Weil, 1972; McKenzie, 1985; Wickham, 1987). Factors influencing the efficiency of melt extraction include degree of melting, melt composition and viscosity, and conditions of deformation, which in turn are controlled by temperature, pressure and the availability of water. The remainder of this section will review the mechanisms for melt extraction from partially molten rocks at small and large degrees of melting and the petrographic, geochemical and genetic contrasts between large and small melt-fractions.

2.5.2. Melt fraction and extraction.

Initial melts produced during partial melting are concentrated at grain edges and corners. As melting proceeds melt volumes increase. Partially molten rocks with small melt contents have their gross rheological properties dominated by the mechanical properties of the solid grains (Wickham, 1987a; van der Molen & Paterson, 1979). As the melt volume increases the strength of the rock is lowered. At a certain melt fraction there is a rapid transition in behaviour from that of a solid with interstitial melt to that of a suspension with Newtonian fluid properties (Arzi, 1978; Ashworth & Brown, 1990; van der Molen & Paterson, 1979; McKenzie, 1985; Wickham, 1987a; Miller *et al*, 1988). This melt fraction was termed the Critical Melt Fraction (CMF) by van der Molen & Paterson (1979) and Wickham (1987a) and the Rheologically Critical Melt Percentage (RCMP) by Arzi (1978), Holtz (1989) and others. Estimates for the melt fraction required to produce the rapid decrease in viscosity associated with the change from solid to dense

suspension range from 20% (Arzi, 1978) to 50% (e.g. Wickham, 1987). Fig. 2.12 (after Wickham, *op cit*) shows the large drop in effective viscosity over a small increase in melt fraction and the range of values of the critical melt fraction (30-50%) adopted by most workers.

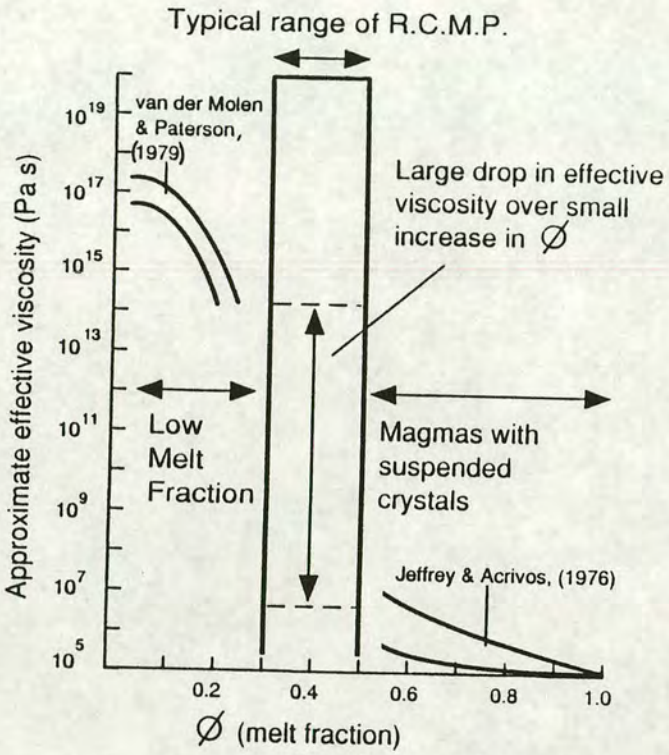

Figure 2.12. Viscosity v melt fraction showing the large degrease in effective viscosity at melt fractions of approximately 30-50 % (after Wickham, 1987).

Above the CMF there is little change in rheological behaviour over large increases in melt proportion. Granitic magmas containing less than 30-35% suspended material will therefore have similar viscosities to crystal free liquids (Wickham, 1987; Jeffrey & Acrivos, 1976). Van der Molen & Paterson (1979) state that the CMF will be approximately 30-35% irrespective of rocktype, and will be lowered slightly by small grain-size and grain-size heterogeneity.

Melts produced below the CMF may only segregate to a limited extent (Ashworth & Brown, 1990). Sawyer & Bedard (1991) suggest that extraction distances are short and melts are essentially retained in the complex. As melt volumes increase the CMF is exceeded and large volumes of granitic

material (containing entrained material) can be extracted. Segregation of residual melt during crystallisation may occur due to localised pressure differences or micro-settling (Sawyer & Bedard, 1991; Miller *et al*, 1988). Alternatively, if melts are retained in the complex then late-stage crystallisation may produce highly fractionated, low-viscosity water-saturated liquids which may form pegmatites (Ashworth & Brown, 1990; Wickham, 1987a). The distribution of melts in partially molten systems and the mechanisms by which this melt (especially at small melt fractions) can be moved from source are reviewed in the following sections.

2.5.3. Melt Distribution.

McKenzie (1985) stated that melt distributed in disconnected pockets cannot easily be removed from a crystalline network. The distribution of melt in partially molten systems is therefore clearly important in determining whether melt is extracted from a migmatite terrane. This is especially true when melt proportions are low such that melt must segregate from the solid matrix. Segregation is not required if melt volumes are high enough to exceed the CMF as the whole anatectic complex may begin to move.

The distribution of small degrees of melt among residual grains is controlled by the distribution of surface energy in the system (Watson, 1982; Jurewicz & Watson, 1985; McKenzie, 1985; Toramaru & Fujii, 1986). If crystal-melt interfacial energies are lower than crystal-crystal interfacial energies then melt will migrate along grain-edge intersections and along planar surfaces between grains to lower the free energy of the system. Melt will penetrate a specific distance along a grain boundary, forming a wetting angle (or dihedral angle - θ) whose value is determined by the balance of the interfacial energies (Jurewicz & Watson, 1985). Geometric analysis of the balance of forces at the melt-grain and grain-grain interfaces allows the calculation of the total interfacial energy for a range of values of θ. Figure 2.13 shows the result of these calculations. For wetting angles less than 60°, wet grain interfacial energies have a lower surface energy and are therefore more stable. Above 60° grain-grain rather than melt-grain boundaries are favoured (van Bargen & Waff, 1986; Watson, 1982; Jurewicz & Watson, 1985). The implication of this is that for values of $\theta<60°$ melt will percolate

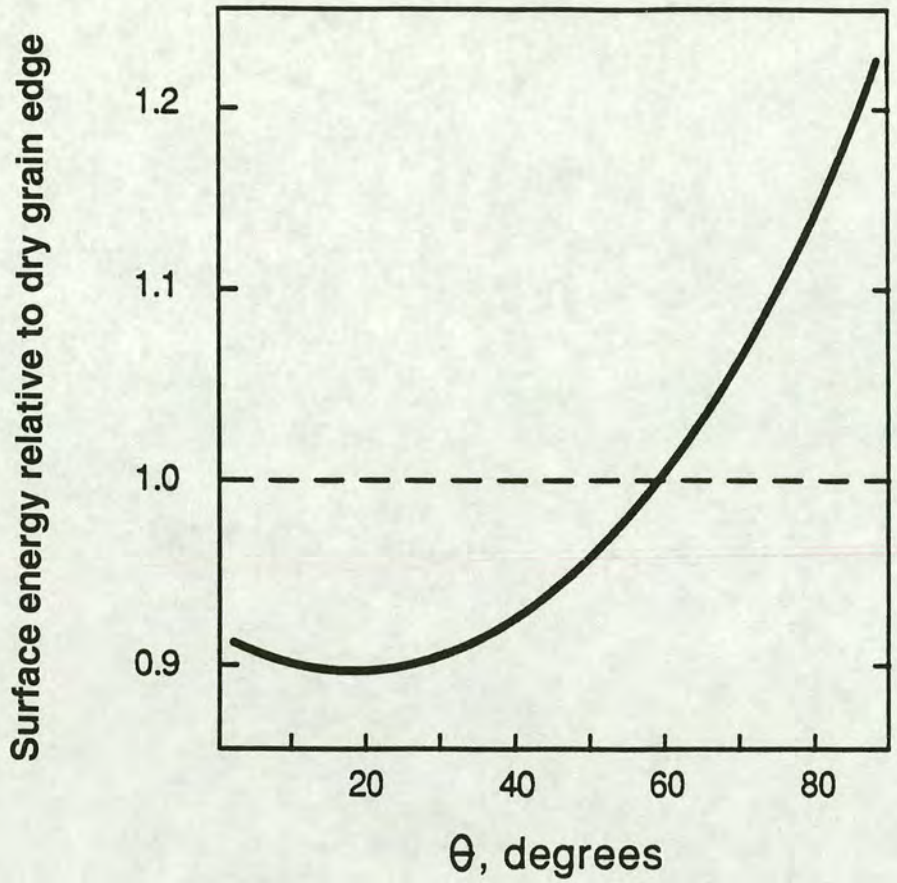

Figure 2.13. Surface energy relative to a dry grain edge plotted against dihedral angle (after Jurewicz & Watson, 1985).

along grain boundaries while wetting angles of $\theta>60°$ will cause melt to pool at grain corners. McKenzie (1985) states that wetting angles are commonly less than 60° for most silicate melts in a silicate matrix. In an experimental study of melt-grain distribution in the quartz-alkali feldspar-granitic melt Jurewicz & Watson (1985) recorded θ values of 44, 49 and 59 degrees for melt in contact with feldspar/feldspar, feldspar/quartz and quartz/quartz grains respectively. Pure dihedral angle considerations suggest that melt should be distributed along grain boundaries in this case. Jurewicz & Watson (*op cit*), however, noted that melt in the above experiments was distributed both along grain boundaries and in pools at grain corners. They explain this apparent discrepancy in terms of the equilibrium melt fraction (EMF). The EMF is the amount of melt present when a melt is distributed uniformly along grain edges with the minimum interfacial energy state, and varies for different θ. Figure 2.14 shows the relationship between melt percentage and wetting angle. For melt percentages less than the EMF (at a given θ) addition of melt would lower the interfacial energy; i.e. the system is undersaturated

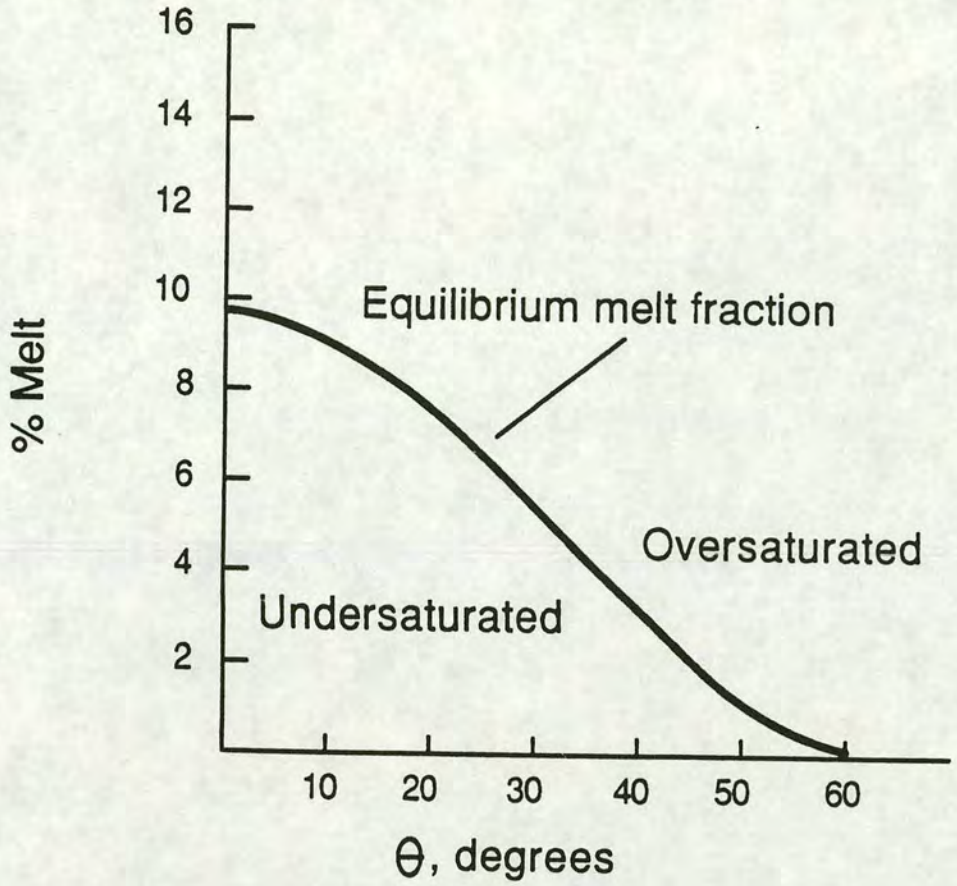

Figure 2.14. Variation of equilibrium melt fraction with dihedral angle.

in melt. The removal of melt from systems in the oversaturated region of the diagram would also lower the total interfacial energy until the EMF was reached. If melt fractions are above the EMF then excess melt is present and will tend to pool. Figure 2.14. shows that melt will pool at any melt fraction if wetting angles >60°. Three combinations of wetting angle and melt fraction are therefore possible (Jurewicz & Watson, 1985). If $\theta<60°$ and the melt fraction is lower than the EMF then melt will be distributed along grain boundaries in a uniform network of channels. If $\theta<60°$ and melt fractions exceed the EMF then melt will be distributed both along grain boundaries and in pools. At $\theta>60°$ no melt fraction is stable along grain boundaries and melt forms patches and pools. In most migmatite terranes, melt fractions will exceed the EMF (for $40°<\theta>60°$) and the distribution of melt will largely be determined by the distribution of small melt pools rather than by the formation of a grain boundary network. A critical melt volume will occur when these pools achieve inter-connectivity, allowing melt coalescence and homogenisation. Toramaru & Fujii (1986), using the analogy of randomly

distributed spheres in space, calculated this critical fraction to occur when 29% melt is present.

2.5.4. Melt Extraction Mechanisms.

Three main mechanisms (compaction, extensional fracturing and segregation during continuing deformation) have been suggested for the extraction of melt from partially molten aggregates (Wickham, 1987a). Compaction of partially molten rocks will expel intergranular liquid if the melt forms an interconnected network and a density difference exists between solid matrix and melt (McKenzie, 1985). Compaction is the only extraction mechanism which can occur if externally applied stress is absent. Because granitic melts are so viscous (relative to more basaltic compositions), extraction rates are low. Calculated extraction times are likely to be at least two orders of magnitude greater than those required for a melting episode, which typically last 10^3-10^4 years) (Mackenzie, 1985; Wickham, 1987a; Allibone & Norris, 1992). Granitic melt and matrix are therefore likely to undergo only limited segregation by compaction.

Melting reactions often involve a positive volume change at the site of melting (Clemens, 1984; Rubie & Brearley, 1990), and resultant high melt pressures may produce dilatant hydraulic fracturing, allowing ponding of small melt volumes (Rubie & Brearley *op cit*). Furthermore, the presence of melt localises deformation producing low pressure sites (e.g. boudin necks, shear-zones) into which melt will migrate (Sawyer, 1992; Allibone & Norris, 1992; Watt, 1992). Allibone & Norris (1992) have described leucogranites derived by low degree partial melting of pelites in the Taylor Valley of Victoria Land, Antarctica, where deformation-induced structures have allowed the coalescence of melt to form small microplutons (<50m in diameter). A close association between shear-zones and leucogranite emplacement was also noted by Sawyer & Bedard (1991). Goodman (1991) suggested that melting along shear-zones in the Scottish Dalradian was related to fluid influx and channelling. Melt fraction removal by deformation (e.g. filter-pressing; Wickham, 1987) or tectonic "kneading" (van der Molen & Paterson, 1979) may be efficient in terms of the amount of melt that can be extracted. Below the CMF, however, both shearing and segregative-

compactive filter-pressing require strain partitioning into the solid matrix, and are therefore slow processes. Over the duration of a melting event only a portion of the melt present may therefore be extracted.

2.5.5. Recognition of small and large melt fraction magmas.

Granitic melts produced at low degrees of partial melting are likely to be very different to those extracted above the RCMP. Liquids produced at low melt fractions will be emplaced close to the site of generation (Sawyer, 1991) and are likely to be at least partially retained in the anatectic complex. Limited melt-residuum separation distances are indicated by the close association of mafic selvedges with melts (, Mehnert, 1968; Sawyer, 1992; Wickham, 1987b). If melt extraction is enhanced by deformation, however, then even low-volume melts can migrate considerable distances. Wickham (1987a) estimates a maximum extraction distance for small-volume melts in the Pyrenees of 1000 metres. Small degree-partial melts are therefore not always spatially associated with restitic selvedges (*c.f.* Sawyer, 1992).

Melts produced at low degrees of melting are likely to be silica-rich (74-76% SiO_2) and close to minimum melt in composition (Wickham, 1987;). Powell & Downes (1990), however, described garnet-bearing small-volume leucosomes which were K-feldspar-rich but did not have minimum melt compositions. Although incongruent melting of biotite was responsible for melt generation, in this case the composition of the leucosome was suggested to be controlled by diffusion rather than segregation. Small melt proportion leucogranites may not therefore always have major element concentrations identical to those of minimum melt granites.

Because efficient segregation must occur to produce small melt fraction leucogranites these melts will be relatively free of restite minerals (Section 2.6). Trace elements concentrated in refractory major and accessory phases (Transition metals, rare-earths) will have low concentrations in migmatite leucosomes. Leucogranites are typically depleted in Mg, Fe, Ti, V, Ni, Cr, Co, Zn, Zr, Hf, Nb, Th and LREE (Wickham, 1987a; Sawyer, 1992; Holtz, 1989). While Holtz and Barbey (1991) noted that Zr and P_2O_5 concentrations in low melt fraction leucogranites were consistent with solubility data for zircon and apatite, Sawyer (1991, 1992) suggests that low-melt fraction leucosomes

are characterised by undersaturation in Zr due to rapid melting and extraction.

If the degree of melting is large (e.g. due to increasing temperature or influx of external H_2O - Holtz & Barbey, 1991; Wickham, 1987) melts will exhibit very different field relations, petrography and geochemistry. Larger volume melts may form discordant veins and sheets, and are unlikely to be spatially associated with melanosomes. If the RCMP is exceeded, the coherence of the anatectic complex may be lost, allowing melt and source rocks to ascend diapirically. The Cooma Granodiorite is perhaps an example of such a granite body (Flood & Vernon, 1978; Ellis & Obata, 1992). Melting in pelitic migmatites in the Cooma area was extensive enough to exceed the RCMP, allowing both the melt and the surrounding migmatite envelope to rise diapirically in the crust (Flood & Vernon, 1978).

Liquids produced by melting above the RCMP will contain abundant restitic and source rock material. Restite-rich granites will have compositions similar to the source rocks, but shifted slightly towards granitic minimum melt compositions (Holtz & Barbey, 1991). They will be more aluminous, richer in Fe_2O_3 and MgO and contain more unmelted refractory accessory phases than restite free granites, giving higher Zr and LREE concentrations. Entrainment of excess zircon and monazite may lead to oversaturation in the melt of Zr and LREE. LREE/LREE* and Zr/Zr* values greater than 1.0 may therefore be indicative of high degrees of melting (Section 2.3). Holtz & Barbey (1991) recorded melts with considerable restitic material which they ascribe to melting above the RCMP. These heterogeneous biotite- and cordierite-rich granites have much higher Fe, Mg, Zn, V, Sc, Cr, Ce and Zr than typical leucogranites, and contain monazites with corroded cores and euhedral overgrowths.

2.6. RESIDUAL PHASES IN GRANITIC MELTS.

2.6.1. Recognition of residue in granitic melts.

Any partial melting episode will produce a melt and a complementary residue. The residue will be enriched in refractory, insoluble phases while the melt will be enriched in easily fused components. The residue will also contain peritectic phases if melting occurred via incongruent reactions. Melts resulting from incongruent melting of a hydrous phase can contain five types of solid material:

(i) Phases crystallised from the melt.
(ii) Phases from the pre-melting parental lithologies (including phases which have equilibrated with the melt before extraction) i.e. true restite.
(iii) Peritectic phases formed as a consequence of incongruent melting reactions.
(iv) Xenolithic material entrained in the melt as it migrates from the source area.
(v) Enclaves of crystallised melts of different composition formed as a consequence of magma-mixing.

Fractionation or retention of these solids will alter melt chemistry to a greater or lesser extent. Phases of type (ii) have typically been the only phases considered as restite, whereas peritectic phases of type (iii) have usually been considered as melt-crystallisation products. In this work, however, peritectic phases (principally garnet and cordierite) are also considered as restite, because they are formed at the site of melting, they do not precipitate from the melt and their entrainment in the departing melt would change its bulk composition. Ellis & Obata (1992) state that concentrations of cordierite produced as a peritectic phase during the vapour-present incongruent breakdown of biotite represent cumulates of liquidus minerals. In fact, these cordierite rich leucosomes represent residual material (i.e. either restitic or crystallised material or both) after removal of a melt phase (e.g. White & Chappell, 1990). Leucosomes with anhydrous mineralogy and a lack of back-reaction with surrounding lithologies indicate that a hydrous portion of the melt formed during the incongruent melting of biotite may have been removed (Ellis & Obata, 1992). While melanosome may represent true residue after melt extraction, cordierite- (or garnet-) rich leucogneiss veins represent an accumulation of residual material and do not

correspond to true melt compositions. Instead they can be considered restitic after loss of a slightly more hydrous melt phase.

Most phases found in mid-crustal lithologies can exist as restite (Hanson, 1978). Typical restite phases produced by, or remaining after, anatexis of a metasedimentary protolith include quartz, garnet, cordierite, biotite, kyanite, sillimanite, hercynitic spinel, calcic plagioclase, K-feldspar, orthopyroxene, ilmenite, zircon, monazite and apatite (Wall *et al*, 1987; Miller, 1985; Patino-Douce & Johnston, 1991). Experimental work by Green (1976) showed that cordierite, plagioclase, K-feldspar, quartz, biotite and sillimanite comprise the residue at low pressures, and almandine garnet is stabilised at pressures greater than 7 kbar. If restitic material can be removed from the area of partial melting (e.g. the restite-unmixing model of White & Chappell, 1977; Chappell, White & Wyborn, 1987 and see next section) then these phases are all likely to exist as restitic material in granitic rocks. The presence or absence of individual restite phases can give useful information on the nature and depth of the source area. Cordierite (without the presence of garnet) is diagnostic of melting region pressures less than 6 kbar, while almandine rich garnets indicate melt production depths of >25Km (Green & Ringwood, 1968) if the melts have a typical X_{Mg}.

Material of restitic origin in granitoids can consist of single grains (through efficient disaggregation), monominerallic or polyminerallic clots or composite xenoliths, inclusions or enclaves (Wall *et al*, 1987; Vernon, 1983). Restite in the Center Pond Pluton, California (a granitoid suite whose chemistry is controlled strongly by the presence of entrained residual material) occurs as small, partially disaggregated clots and grains. Individual restitic crystals may exhibit euhedral overgrowths on anhedral, embayed cores (e.g. reversely zoned cordierites with well developed euhedral faces (Flood & Shaw, 1975). Garnet and cordierite are phases commonly interpreted as restite (Wall *et al*, 1987; Holtz & Barbey, 1991; Burnham, 1992; Fitzsimons & Harley, 1991; Maillet & Clarke, 1985; Scambos, 1986). One characteristic feature is the presence of fine, aligned sillimanite inclusion trails in the core of these phases, often overgrown by a clear, inclusion free rim. Garnet also often contains larger, ovoid inclusions of quartz. At pressures less than 5-7 kbar garnet is replaced by cordierite

(Harris, *pers comm*). Cordierite forms as a peritectic phase in both the the vapour present biotite melting reaction

$$Bi + Als + Kfs + Qz + V = Crd + L \qquad (2.10)$$

(e.g. Ellis & Obata, 1992) and as the low pressure stable ferromagnesian phase in the vapour absent dehydration melting of biotite at higher temperatures (e.g. Reaction 2.1)
Textures diagnostic of a restite origin in enclaves and mineral aggregates include;

(1) Granoblastic grain shapes.
(2) Foliated fabrics.
(3) High temperature refractory mineral assemblages, usually equilibrated at depths greater than those of emplacement.

(Wall *et al*, 1987). Restitic garnets are compositionally distinctive, but often rare in granites (Phillips *et al*, 1982). Almandine-rich compositions typical of metamorphic conditions contrast with Mn-enriched small euhedral garnets thought to have precipitated from melts (Miller & Stoddard, 1981; Stone, 1988; Harrison, 1988). Restitic garnet may have abundant inclusions and Fe+Mn enriched rims suggesting growth with falling temperature (Stone, 1988) while garnet and cordierite with few inclusions and euhedral grain shapes are likely to represent phases precipitated directly from the melt, rather than entrained material, since, as noted above, they are the normal crystallisation products of strongly peraluminous melts. Note that peritectic garnet and cordierite can also form euhedral, inclusion free grains and may therefore be difficult to distinguish from those precipiated from a melt. Harris (*pers comm*) notes strong compositional differences between sub-solidus garnet and garnets crystallised from a peraluminous granitic melt. While there is no difference in composition between garnets in kyanite grade assemblages which have remained unmelted and garnet from migmatitic sillimanite gneisses which have (suggesting disequilibrium melting), garnets hosted in the leucosomes have a very different composition. They are spessartine rich (17 mol. % spessartine) and are strongly enriched in Zr and Y (see also du Bray, 1988) relative to non-melt-precipitated garnets. Small euhedral Mn-rich garnets (35-52 mol. % spessartine) have also been recorded

in the Cairngorm granite, Scotland (Harrison, 1988). Again these garnets are Y-enriched. It may therefore be possible to distinguish restitic and magmatic garnet using trace element compositions, and hence to determine the extent of garnet entrainment.

Calcium-rich plagioclase commonly develops early in the granite-crystallisation sequence. White & Chappell (1977) suggest that the presence of complexly or patchily zoned and twinned Ca-rich plagioclase cores are diagnostic of a restitic origin. Restitic melanosomes from some migmatites, however, contain plagioclase which does not exhibit complex zoning patterns (Wall *et al*, 1987). Although Burnham (1992) notes that plagioclase core compositions remain almost constant throughout a suite of granioids (while restite unmixing has occurred), in the Center Pond Pluton, plagioclase is zoned due to partial re-equilibration with melt during ascent (Scambos, 1986). Plagioclase cores are still Ca-rich, however, consistent with an entrainment mechanism. Chappell, White and Wyborn (1987) suggest that individual plagioclases represent the bulk of the residual material in some granites. The processes controlling plagioclase evolution during entrainment are still poorly understood.

Restitic quartz is characteristically partially resorbed at higher crustal levels. Quartz may be a restite phase in many S-type granitoids, but is difficult to identify. In volcanics it often forms corroded xenocrysts (Burnham, 1992; Wall, *et al*, 1987). Many granites (especially those derived from metasedimentary rocks) contain old, crustally recycled refractory zircons. Other accessory phases (e.g. monazite and xenotime) exhibit similar behaviour (Montel *et al*, 1992; Copeland *et al*, 1987; Watt & Harley, *in press*). The behaviour of accessory phases in crustal melts produced under granulite conditions is treated more fully in Chapter 8.

2.6.2. The role of restite in determining melt chemistry.

Although restitic material had been recognised in granites and erupted volcanics earlier (Presnall & Bateman, 1973; Zeck, 1970) the hypothesis that the progressive unmixing of residual source material from minimum-melt composition granitic magmas may be the dominant control on granite

geochemistry was first suggested by White & Chappell (1977) (see also Chappell *et al* (1987) and references therein). The premise of the restite unmixing model is that a crustal fusion event will produce a whole suite of melts containing varying amounts of residual material. At one end of the spectrum is restite free minimum-melt, while the other extreme is represented by refractory residual material from which the maximum amount of melt has been removed. Between these extremes an apparent fractionation trend exists, carrying the signature of entrained material superimposed on minimum melt chemistry (White & Chappell, 1977; Chappell, White & Wyborn, 1987; Barbero & Villaseca, 1992, Scambos *et al*, 1986). The bulk chemistry of all these materials should lie along an "unmixing line" (White & Chappell, 1977; Chappell *et al*, 1987) which may be smeared out by the effects of melt fractionation, or by source heterogeneity (Holtz, 1991; Burnham, 1992).

The role of restite in determining melt chemistry has been hotly debated. Patino-Douce & Johnston (1991) suggest that restite separation or entrainment must be important in controlling the geochemical variation within and between granitoid suites because minimum-melt compositions are so restricted. They argue that restite fractionation is the most important factor in granite evolution. Clemens & Wall (1984) identify compositionally distinctive residual garnet in ignimbrites from the Violet Town Volcanics in southeastern Australia, but suggest that low modal abundances (approximately 2 volume %) restrict the influence of this phase on the evolution of melt chemistry (see also Phillips *et al*, 1981). Other workers suggest that restite volumes in granitoid melts can be as great as 65% (Burnham, 1992; Barbero & Villaseca, 1992). In one suite of S-type granites from southeastern Australia (the Dalgety Suite) Burnham (1992) calculated residue volumes between 27% (in the most felsic members) to 65% in the most mafic members. Similarity between calculated liquidus plagioclase compositions and the cores of plagioclases throughout the suite led Burnham (*op cit*) to suggest that the bulk of the residue in the Dalgety Suite represented true restite from the source area. The trapped restite component in the Hercynian Layos Granite (Spain) is estimated at approximately 65% from petrographic (high modal cordierite concentrations, unzoned plagioclase of constant composition throughout the suite) and geochemical data (Barbero & Villaseca, 1992). One interesting feauture of high-restite

content granitoids is that actual melt proportions (if restite does reach 65%) may be at or below the RCMP (Chapter 2.4). It is difficult to envisage the diapiric uprise of such low melt volume crystal-rich mushes, despite field evidence. Certainly the Layos granite has remained within a granulite complex, and has therefore only migrated a short distance (Barbero & Villaseca, 1992). Other arguments against the restite unmixing model include the extraction of melt from lower crustal granulite regions without disturbance of mesoscopic layering and wholescale ascent of the melting zone (Vielzeuf & Holloway, 1988; Clemens, 1989), the absence of unequivocal restitic crystals and textures (Wall *et al*, 1987; Clemens & Wall, 1984; Vernon, 1983, 1984) and the presence of enclaves more probably of magma-mixing origin in some rocks previously described as restite-rich (Wall *et al, op cit*). Furthermore, the recognition that Rayleigh Fractionation can produce straight line variation diagrams (Wall, Clemens & Clarke, 1988) and that simple two end-member mixing can produce curved variation diagrams similar to those formed by plagioclase fractionation (Clemens, 1989) mean that simple linear trends on Harker diagrams cannot be interpreted as diagnostic of a single process.

Evolved granitic and volcanic suites are far removed from their source areas and can become modified by fractional crystallisation, wall rock assimilation, magma mingling and re-equilibration of restite to form "secondary restite" (Chappell *et al*, 1987). In the Arunta Complex, Collins & Vernon (1992) recognised a suite of granitic bodies whose geochemistry and petrography has been controlled not by source area, restite unmixing or fractionation, but solely by wall-rock assimilation. Cordierite-, garnet- and orthopyroxene-bearing granites occur in cordierite-, garnet- and orthopyroxene gneisses respectively. Cordierite rich granites have high MgO, Ni, Cr and Zn while garnet-bearing granites have higher Fe/Mg and orthopyroxene granitoids contain higher amounts of CaO. The implications of this are important. Collins & Vernon (*op cit*) suggest that a melt could attain either an S- or an I-type chemistry solely by xenolith digestion. One fundamental tenet of the restite unmixing model, however, is that inclusions and enclaves in granites that have evolved by unmixing do not resemble those of the surrounding rocks. While wall rock assimilation may be a major process in some granitoids, recognition of xenolith digestion is evidence neither for or against restite involvement in the evolution of the geochemistry of a granitic suite.

Although Wall *et al* (1987) suggest that restite incorporation and unmixing do not play a major role relative to processes such as fractionation, accumulation and magma-mixing in the chemical variation of most mid- to upper-crust granitoids and siliceous volcanics, restite entrainment is likely to be more important at depth, and near source (Clemens & Wall, 1984). The juxtaposition of source rocks and melts in migmatite terranes allows the extent to which restite entrainment affects melt chemistry to be ascertained more clearly, without overprinting by the processes common at higher crustal levels outlined above (Holtz & Barbey, 1991; Holtz, 1989).

Holtz (*op cit*) suggests melts with different characteristics should be produced above and below the CMF. If the degree of melting is large the CMF will be exceeded and the complex will rise as a crystal rich magma (using the definition of magma of White & Chappell, 1990). If melt volumes are small (due to lower temperatures or strongly water-undersaturated conditions) the source area remains coherent and melt is produced which is almost completely restite-free. Low degrees of melting do not favour the wholescale mobilisation and bouyant diapiric uprise of the melt and solid mixture postulated by the restite unmixing model. If restite unmixing does occur, then melts which contain little or no restite (especially accessory phases such as zircon and monazite) must have segregated perfectly from their source rocks (Holtz & Barbey, 1991). Because of the limited extraction distances (e.g. Wickham, 1987) and the viscous nature of water-undersaturated melts (e.g. Mackenzie, 1985) the attainment of perfect segregation seems unlikely. A more geologically reasonable hypothesis is that small volume melts are simply segregated efficiently from their source rocks and extracted with little restite entrainment (Wickham, 1987; Holtz, 1989; Sawyer, 1991).

Larger volume melts recognised by Holtz & Barbey (1991) in the Tourem Complex (which are thought to have been produced by an influx of water) contain significant proportions of residual material (notably biotite and cordierite). The increased degree of melting has led to the loss of coherence of parts of the complex and the diapiric uprise of the crystal-melt mixture. In an earlier paper, Holtz (1989) ascribed the entrainment of abundant restite to the water-undersaturated nature of the melts, melts with high viscosity being more likely to incorporate residual phases. Since large (up to 50%) melt

volumes (greater than RCMP) can be obtained by crustal anatexis in metasedimentary lithologies even under water-undersaturated conditions (Vielzeuf & Holloway, 1988, Chapter 2.2), wholescale diapiric movement of restite rich melt in the lower crust may be possible.

The inference of the model of Holtz & Barbey (1991) is that melting occurs as a two stage process (Wickham, 1987). Early small volume melts may be extracted without retaining any of the source, while later melts, formed under higher temperatures or conditions of greater aH_2O, entrain residual material. The evolution of melt chemistry in this case is not controlled by the progressive unmixing of restitic material (a theory which has been looked on by many authors (e.g. Wall *et al*, 1987) as physically unfeasible due to minimal density contrasts) but by the more geologically reasonable mechanism of progressive (or sequential) restite entrainment as melting proceeds. The role of restite entrainment and/or unmixing in determining the chemistry of melts in the Prydz Bay anatectic complex will be discussed in Chapter 9 of this thesis.

2.7. POST-MELTING PROCESSES.

The stabilisation of granulite-facies assemblages by partial melting requires that the hydrous vapour partitioned into the melt does not cause retrogression as the melt cools. The vapour must be removed from the complex in order to prevent the back-reaction of anhydrous mineral assemblages to hydrous phases. Expulsion of H_2O as melts crystallise is essentially the reverse of vapour-absent melting (Ashworth & Brown, 1990). As granitic liquids cool they become enriched in water until water saturation occurs at temperatures slightly above the solidus (Johannes & Holtz, 1990; Holtz & Johannes, in press). The release of these aqueous fluids to the surrounding lithologies as the melt crystallises may cause retrogression. Alternatively the low viscosity water-saturated melts may escape as pegmatites. Movement of large volumes of aqueous fluid generated by the solidification of partial melts has been suggested as the dominant retrogressive process in several granulite terranes, including the Inverian retrogressive event of the Scottish Lewisian (Cartwright, 1990) and the

regional biotite event of the Arunta Complex, central Australia (Warren & Hensen, 1989). In the Arunta Complex, biotite replaced orthopyroxene-K-feldspar in pelitic lithologies while widespread growth of late hornblende was recorded in mafic granulites.

Various mechanisms for preventing the release of aqueous fluids into the source rocks by crystallising melts have been proposed. These were summarised by Waters (1988), and can be grouped into two categories. Either fluids are retained in the complex and back-reaction is impeded, or the fluid is removed from the complex preventing back-reaction altogether. In the first of these groups, armouring of the anhydrous phase(s) by a melt crystallisation product would prevent back reaction. Waters (*op cit*) recorded narrow quartz rims on garnet and orthopyroxene and suggested that if sufficient amounts of melt crystallisation occured before water saturation in the melt anhydrous phases would not "see" the aqueous fluid. Other mechanisms proposed which would inhibit retrogression include kinetic effects which impair retrograde reactions (Rubie & Brearley, 1990), or dilution of the aqueous vapour phase by CO_2. An influx of CO_2 would effectively "freeze" melting reactions by lowering aH_2O (Janardhan *et al.*, 1982). Waters (1988) discounts this mechanism because of the lack of evidence for post peak carbonic fluid influx. CO_2 flushing before peak conditions were attained would simply prevent melting from occurring.

Removal of a melt phase containing water extracted from the granulite terrane would produce dessication, but this in itself does not explain the anhydrous mineralogy of most melts found in granulite-facies migmatites. Anhydrous leucosomes comprised of quartz, K-feldspar, plagioclase and cordierite were described by Ellis & Obata (1992). The cordierite was fresh and had not broken down to biotite+andalusite, suggesting that the leucosomes had not experienced vapour-saturation. Since even water-undersaturated granitic melts contain a little water (from the breakdown of hydrous phases), an aqueous fluid must have been removed before the solidus was reached. If so it must have been transported in a melt phase, meaning that for many granulite-facies migmatites the leucosomes will not represent true melt compositions. Instead they must be considered as slightly "restitic" after losing a small residual melt fraction. These final-stage melts will be water-saturated, mobile and may be extracted relatively easily along

shear zones and extensional fractures (Section 2.5), explaining the widespread occurrence of biotite bearing leucogneisses in shear zones (Sawyer, 1992; Sawyer & Bedard, 1991; Fitzsimons, 1991).

2.8. SUMMARY.

1. Vapour absent melting is an important process in granulites, and can lead to high % melts if temperatures are high enough.

2. Disequilibrium melting only depends on the **relative** rates of extraction vs melt production and equilibration with the solids of interest. Equilibration in major elements does not imply global equilibration as ESC elements may be controlled by accessory phase dissolution.

3. Extraction of melts (and therefore their chemistry) will depend on source rock mineralogy and chemistry, H_2O contents of the source rocks (η), % of melt produced and the extent to which the melts equilibrate with their source. The RCMP is important in that it represents the melt fraction at which the whole complex (or parts of it at least) becomes mobile. Below the RCMP melts may segregate efficiently if η is low and melt connectivity occurs. Dihedral angle considerations suggest connectivity in granitic systems can be attained, so the most important considerations for melt extration are the amount of melt produced, and whether melt segregation can occur over sufficient timescales to allow equilibrium melting for most elements.

4. The importance of source entrainment and the role of restite in determining bulk chemistry is open to question. If the granulitic portion of the lower crust is to be considered the restitic portion after extraction of a granitic melt, then the implication is that melts removed from the lower crust are restite free. While unmixing from granitic magmas is not now generally considered viable, the viscosity of water undersaturated magmas suggests that source entrainment into departing melts may occur.

Part 2.

Petrography and geochemistry of the Brattstrand Bluffs migmatites.

Chapter 3

Petrography of the Brattstrand Bluffs Leucogneisses.

Chapter 3. Petrography of the Brattstrand Bluffs Leucogneisses.

3.1. INTRODUCTION & FIELD RELATIONS.

Metapelitic gneisses in the Brattstrand Bluffs area exhibit field evidence for various degrees of migmatisation, melt extraction and retention. Three main migmatite components have been recognised. Banded garnet-rich metapelites comprise the mesosome (using the nomenclature of Ashworth (1985), while leucocratic quartzofeldspathic gneisses of broadly granitic composition (containing minor amounts of garnet, sillimanite, cordierite and biotite) form the leucosome portion. Quartz absent garnet-sillimanite-cordierite-biotite gneisses constitute the melanosome. Aluminous melanosome material occurs as sub-parallel layers in banded mesosome-leucosome-melanosome gneiss successions and as dykes (containing some felsic material) truncating compositional and migmatitic layering in metapelitic gneisses. Stromatic-, schollen-, schlieren- and folded-migmatite types (Mehnert, 1968) are all developed. A complete spectrum of textures exists between apparently unmigmatised metapelitic gneisses with well developed compositional layering of quartzofeldspathic- and aluminous-material, through stromatic migmatites with closely associated mesosome and leucosome components, to well segregated leucogneiss sheets containing little or no mesosome. Leucosome and leucogneiss proportions in the field reach a maximum volume of approximately 40%. Leucogneisses may be interlayered with aluminous garnet-cordierite-sillimanite rich melanosome bands or truncate compositional layering in layered metapelites. In low-strain areas discordant contacts between leucogneiss sheets and host metapelites are more common. Large leucogneiss bodies form sheets and pods up to 5m wide with strike-lengths of tens to hundreds of metres. Leucogneiss bodies are often found in steep shear zones within metapelitic gneisses. These leucosomes commonly contain abundant biotite and a little garnet.

The leucosomes of the Brattstrand Bluffs coastline migmatite complex consist of leucocratic quartzofeldspathic gneisses containing variable (although generally minor) amounts of mafic and aluminous material in rafts, schlieren

and as discrete grains (Figures 3.1.-3.4.). Total amounts of non-quartzofeldspathic material rarely exceed 25%. Schlieren are typically comprised of garnet, sillimanite and rare biotite, and range in size from a few grains (less than 2 cm) to tens of centimetres. While some of these pelitic enclaves have wispy, indistinct contacts with leucogneisses, rafts of aluminous material with sharp margins have been recorded. Garnet is the principal non quartzofeldspathic phase found in the leucogneisses. It occurs as large individual grains up to 5cm in diameter, in trains of several grains aligned parallel to foliation, in schlieren with broadly pelitic composition (garnet-cordierite-sillimanite-biotite-quartz) (Fig. 3.5.) and in coarse inclusions with abundant cordierite. Individual cordierite crystals are much rarer than discrete garnet grains in leucogneiss sheets. Cordierite-rich enclaves have similar mineralogy to the melanosomes described above. The aim of the remainder of this Chapter is to fully describe the petrography of the leucogneiss suite. The geochemistry of the leucogneisses is summarised in Chapter 4, while Chapter 5 details the petrography and geochemistry of the migmatitic metapelitic gneisses and aluminous melanosomes.

3.2. LEUCOGNEISS PETROGRAPHY.

3.2.1. Introduction.

The leucosomes are leucocratic gneisses comprised dominantly of quartz, K-feldspar and plagioclase . They contain variable amounts (though typically less than 10%) of almandine garnet, sillimanite, cordierite, hercynitic spinel, ilmenite and accessory phases (zircon and monazite). The majority of leucogneisses contain little mafic or peraluminous material, or only garnet. A complete spectrum exists, however, from leucogneisses which are free of mafic, peraluminous or accessory phases (comprised almost entirely of quartz and two feldspars) to quartzofeldspathic garnet-biotite-cordierite rich gneisses containing up to 25% garnet, biotite and cordierite and traces of ilmenite, hercynitic spinel, zircon and monazite. Accessory phases are most abundant in samples with highest garnet and cordierite contents. Modally they classify as quartz-rich granites, monzogranites and alkali granites on a Q-A-P Streckeisen type plot. (Fig. 3.6.).

Plate 1.

Fig. 3.1. Field photograph from Brattstrand Bluffs, showing well segregated deformed leucogneisses in migmatitic pelites. The leucogneisses form vein and sheet like leucocratic bodies up to 1.5 m. thick. They are not associated with mafic selvedges. Photo: I. C. W. Fitzsimons. Notebook - 25cm long.

Fig. 3.2. Banded Leucogneiss containing abundant garnet- (reddish-black) and cordierite- (dark blue) porphryoblasts up to 2 cm in diameter. Photo: I. C. W. Fitzsimons. Lens cap - 5cm diameter.

Fig. 3.3. Narrow (5cm wide) leucogneiss veins cross-cutting deformed migmatised metapelitic gneisses. Photo: I. C. W. Fitzsimons. Lens cap - 5cm diameter.

Fig. 3.4. Patch leucosome in migmatite showing several deformed garnet-rich restitic melanosome schlieren. Leucogneiss - metapelite contacts are gradational over several cm at the base of the photo. Photo: I. C. W. Fitzsimons. Hammer - 50cm long.


Fig. 3.1


Fig. 3.2


Fig. 3.3


Fig. 3.4

Plate 2.

Fig. 3.5. Garnet-rich melanosome schlieren in leucogneiss. Note small patches of leucocratic felsic material scattered throughout the mafic patch. Photo: I. C. W. Fitzsimons. Lens cap - 5cm in diameter.

Fig. 3.6. Quartz - K-feldspar - Plagioclase ternary plot (QAP) showing Type 1, 2 and 3 Leucogneisses. Field boundaries from White, 1990.

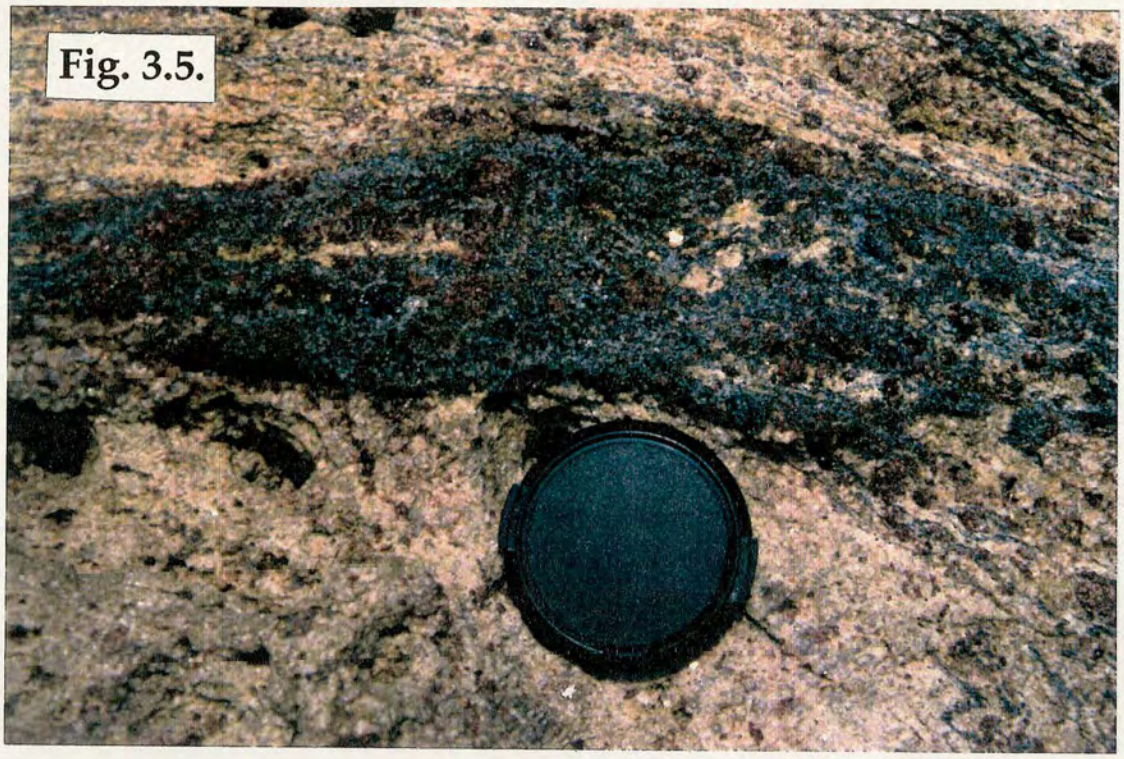
Fig. 3.5.

Fig. 3.6.

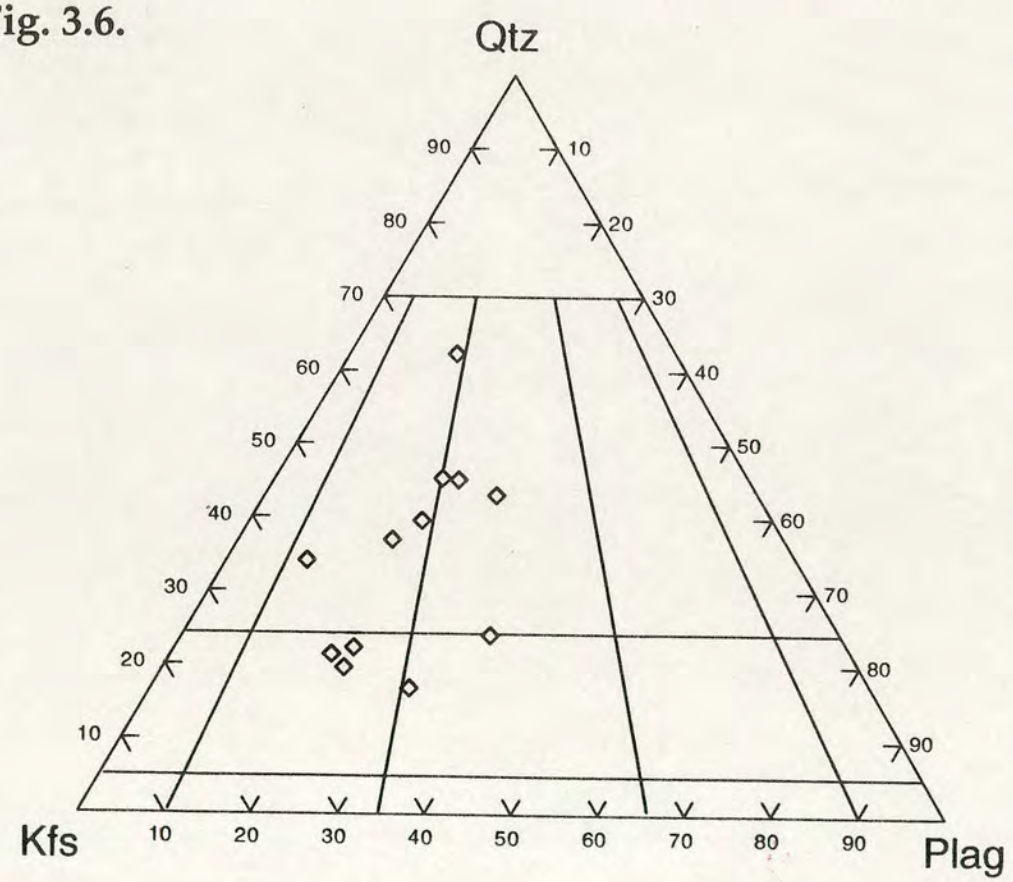
Qtz
90
10
80
20
70
30
60
40
50
50
40
60
30
70
20
80
10
90
Kfs
10
20
30
40
50
60
70
80
90
Plag

3.2.2. Quartz, K-Feldspar and Plagioclase.

3.2.2.1. Quartz

Quartz is the most abundant phase in nearly all the Brattstrand Bluffs Leucogneisses. It occurs most frequently as medium- to coarse-grained (often >3mm), anhedral xenoblastic grains intergrown with plagioclase, K-feldspar and, more rarely, cordierite, and more rarely as large rounded strained grains (Fig. 3.7.). These large grains often appear cracked and in one sample (IF/88/61) these cracks are filled by veins of plagioclase (Fig. 3.8.). Quartz is also commonly found as inclusions (up to 1mm in diameter) in garnet. These inclusions are rounded to ovoid in shape and are usually concentrated at the margins of the garnet grains (Fig. 3.9.). In some garnets these quartz inclusions may comprise more than half the garnet volume, making the garnet grains appear skeletal and anhedral in thin section.

Fine intricate symplectic intergrowths of quartz and cordierite are common as coronas on large garnets (with rounded quartz inclusions on their margins). Quartz in these coronas is vermicular and forms worms and ribbons up to 10mm long radiating outwards normal to the garnet margin (Fig. 3.10.). Quartz is also often found in granophyric intergrowths with K-feldspar in small (<2mm) rounded grains and and as very small (<0.1mm) rounded inclusions in the cores of large K-feldspar crystals.

3.2.2.2. K-Feldspar

The Prydz Bay Leucogneisses contain up to 30% K-feldspar. This K-feldspar is typically coarser grained than either quartz or plagioclase, forming anhedral grains up to 10mm in diameter. It is typically perthitic, containing small stringlets of more sodic material up to 20μm wide. Patches of finer grained, polygonal K-feldspar grains suggest recrystallisation. These patches often also contain polygonal plagioclase. Granophyric intergrowths comprised of single K-feldspar crystals (up to 2mm in diameter) containing numerous aligned quartz rhombs are common. Larger K-feldspar grains contain rare small (<200μm) rounded quartz inclusions, and one grain has

Plate 3.

Fig. 3.7. Photomicrograph of a large strained quartz porphroblast (centre) in a granoblastic quartzofeldspathic leucogneiss. XPL. Scale Bar - 3mm.

Fig. 3.8. Photomicrograph of a large cracked porphyroblast in a leucogneiss (centre) with partially resorbed margins. Fractures are infilled by twinned plagioclase (labelled). XPL. Scale bar - 3mm.

Fig. 3.9. Photomicrograph of a large, poikiloblastic Type II garnet containing rounded quartz inclusions. PPL. Scale bar - 3mm.

Fig. 3.10. Photomicrograph of large rounded garnet (centre-top) overgrown by a cordierite-quartz-sillimanite symplectite. Quartz forms small worms and vermicules radiating normal to the garnet margin. Sillimanite is coarser and partially resorbed. PPL. Scale bar - 1.5mm.

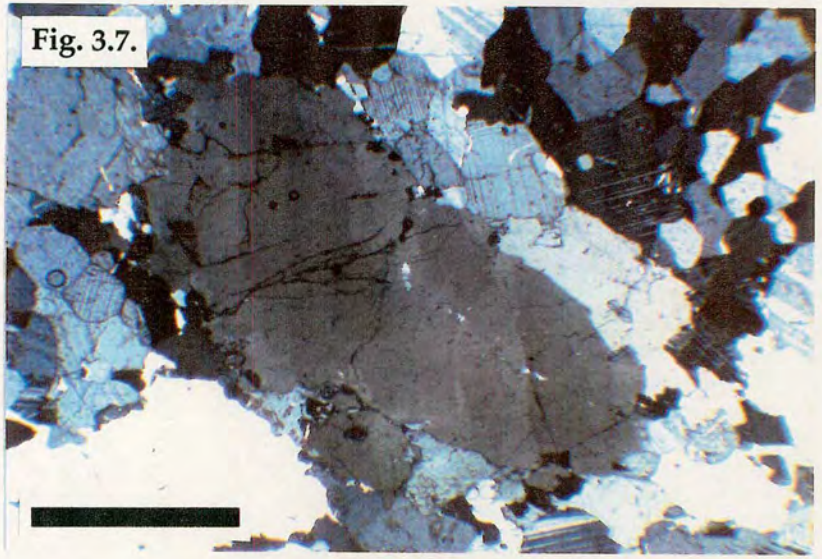
Fig. 3.7.

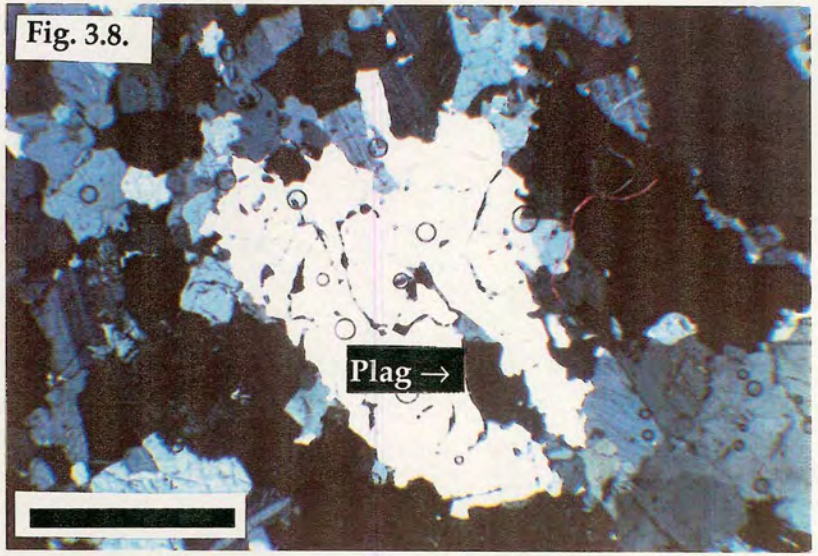

Fig. 3.8.

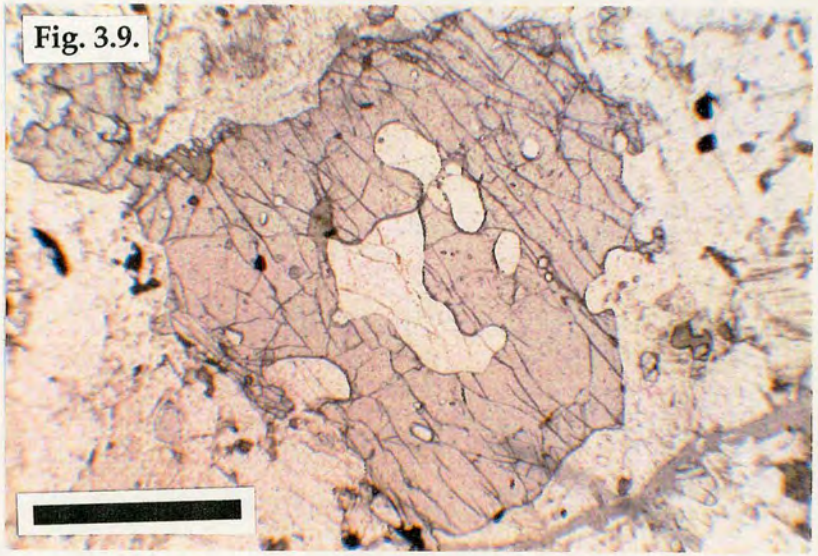
Fig. 3.9.

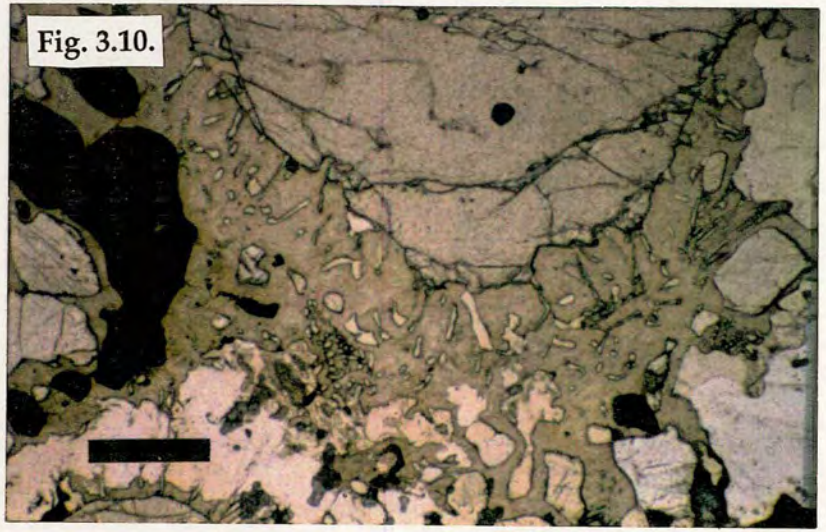
Fig. 3.10.

been noted which contains a cluster of tiny (<100μm) randomly oriented sillimanite needles in its core (Fig. 3.11.). An identical texture of abundant sillimanite inclusions concentrated in the cores of large garnets has also been witnessed. These are described in the garnet section below.

3.2.2.3. Plagioclase.

Plagioclase is typically less abundant than K-feldspar in the Brattstrand Bluffs Leucogneisses. Average modal abundances for plagioclase vary between 8 and 20%. Samples containing garnet appear to have slightly higher plagioclase contents. Two petrographically distinct plagioclase occurrences have been noted. Most plagioclase is anhedral, antiperthitic, generally finer grained than either quartz or K-feldspar and appears to have formed late in the crystallisation sequence. Often this plagioclase forms complex intergrowths with lobate garnet, or it may intrude cracks in large fractured quartz grains as described above. Rare subidiomorphic plagioclase grains have been noted in some samples. These form tablets reaching 1mm in length and occur as inclusions in K-feldspar, or as clusters of several grains surrounded by quartz and K-feldspar. Subhedral plagioclase grains appear to have formed earlier in the crystallisation sequence than the much more common anhedral plagioclase. In one sample a pseudo-cumulus texture comprised of subhedral-euhedral simply-twinned plagioclase grains with interstitial quartz in a garnet-cordierite rich leucogneiss has been noted (Fig. 3.12.)

3.2.3. Peraluminous & Mafic Phases.

3.2.3.1. Garnet.

Three petrographically distinct types of garnet porphyroblast have been recognised in the leucogneisses. Garnet (I) is coarse grained (up to 2cm long), anhedral and contains abundant flakes of fine grained biotite and sillimanite (<50μm) which define an early foliation (Fig. 3.13.). This foliation is often oblique to that of the surrounding quartzofeldspathic matrix. Other phases

Plate 4.

Fig. 3.11. Photmicrograph of a large simply twinned K-feldspar containing abundant inclusions of rounded quartz (white, pale-grey), biotite (moderate birefringence), ilmenite (black) and tiny sillimanite inclusions (labelled). XPL. Scale bar - 3mm.

Fig. 3.12. Granular subhedral plagioclase grains with intercumulus quartz (bright white - centre). XPL. Scale bar - 1.2mm.

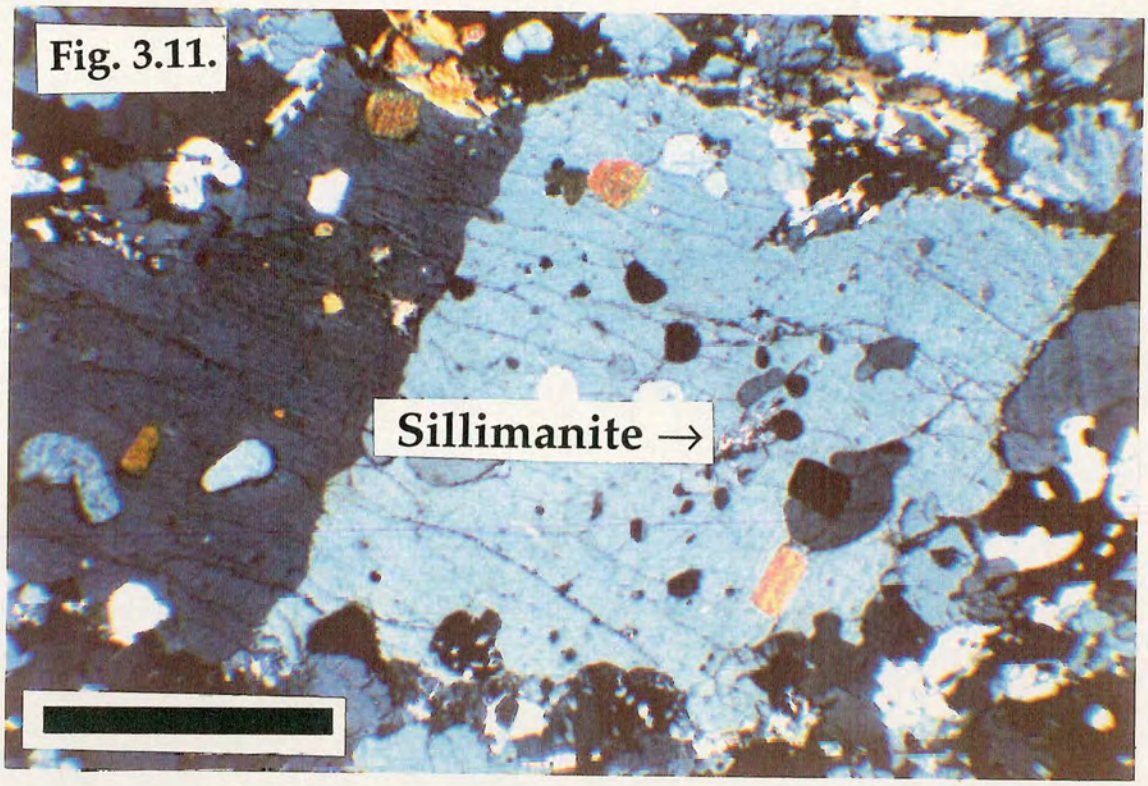
Fig. 3.11.
Sillimanite →

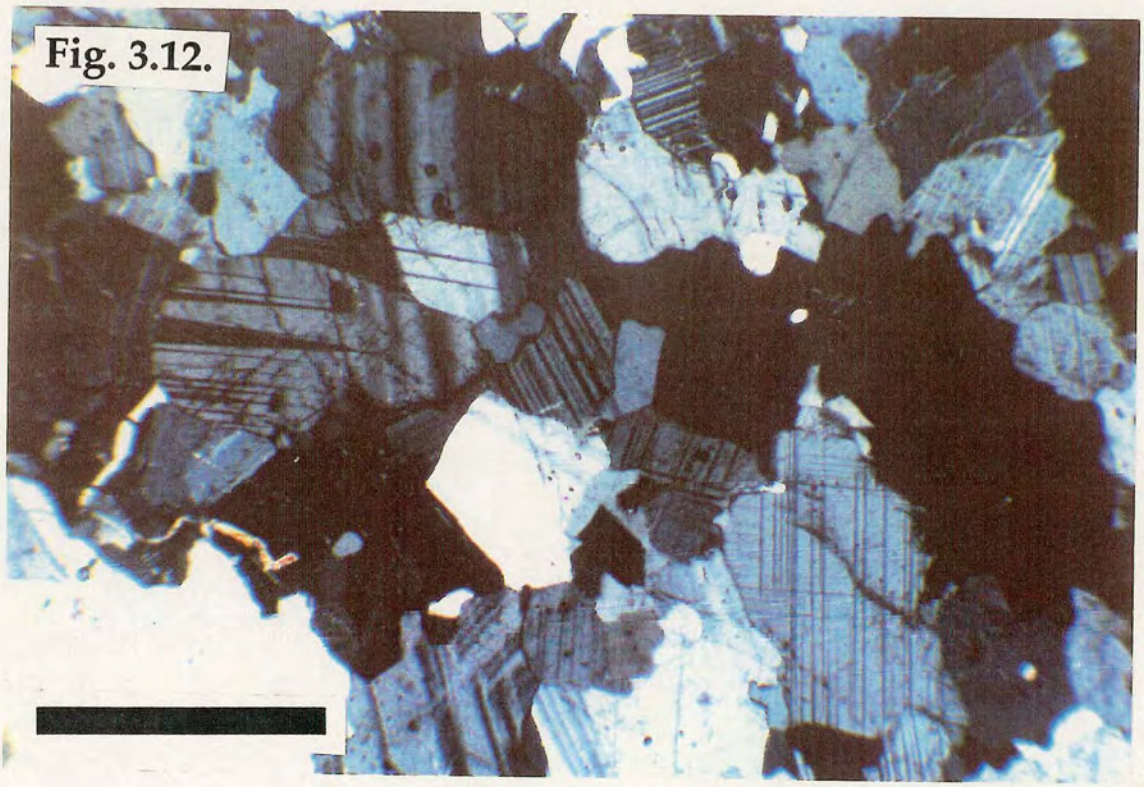
Fig. 3.12.

Plate 5.

Fig. 3.13. Fine grained sillimanite, biotite and ilmenite inclusions defining an early foliation in the core of a Type I Garnet. Note crowding of inclusions in core. PPL. Scale bar - 0.3mm.

Fig. 3.14. Large Type I Garnet (with core of crowded sillimanite inclusions) overgrown by skeletal Type II Garnet containing large rounded quartz blebs. Note small, subhedral garnets (centre left). PPL. Scale Bar - 3mm.

Fig. 3.15. Small subhedral Type II Garnet containing round quartz inclusions. PPL. Scale bar - 1.2mm.

Fig. 3.16. Small subhedral to euhedral Type III Garnets in a quartzofeldspathic Type 1 Leucogneiss. PPL. Scale bar - 3mm.

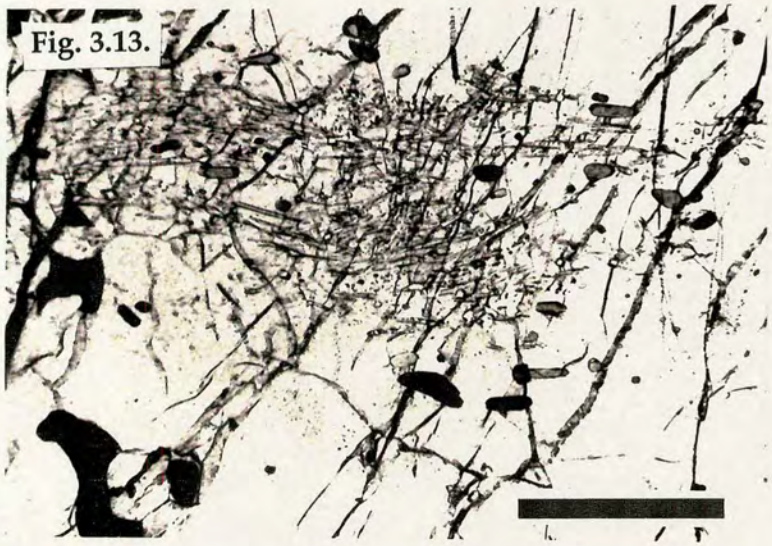

Fig. 3.13.

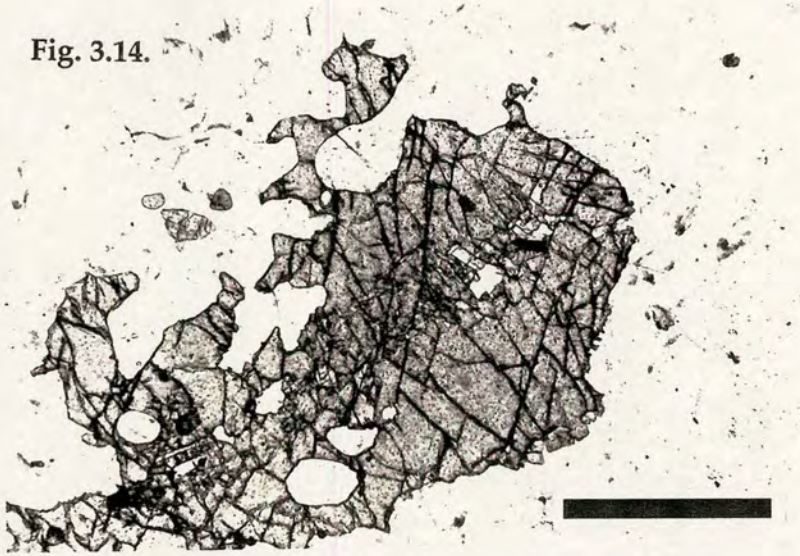

Fig. 3.14.

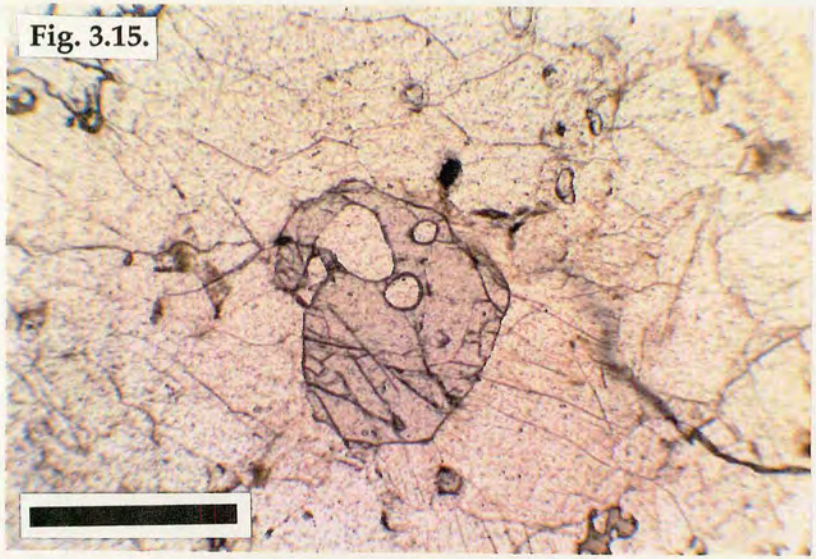

Fig. 3.15.

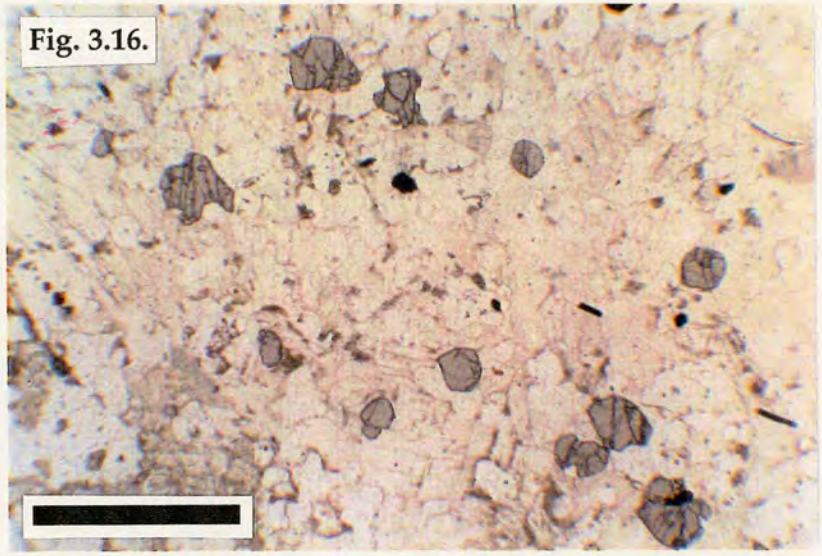

Fig. 3.16.

occurring as inclusions in these large garnets include small ilmenite grains and rare zircon. Garnet (I) is commonly found in narrow (<20cm) leucosome veinlets and is less abundant in larger leucogneiss bodies. Garnets with inclusion rich cores occasionally have inclusions crowded at their margins, where the garnet grain edge may truncate the foliation defined by fine sillimanite needles. Garnet (I) cores are often overgrown by inclusion free rims (or by rims which contain larger round or ovoid quartz inclusions only) (Fig. 3.14.).

The most abundant garnet type (Type II Garnet) in the Pryz Bay Leucogneisses is petrographically similar to the relatively inclusion free rims growing on Garnet (I). Garnet (II) occurs as large rounded, subhedral grains up to 30mm in diameter (Fig. 3.15) . Grain margins often appear resorbed, with lobate quartz intergrowths and large rounded quartz and, more rarely, K-feldspar inclusions. Often the abundance of inclusions is so great the garnet has a skeletal appearance. Garnet (II) occurs both as individual grains and in clusters of several garnets, often surrounded by sillimanite and, less frquently, by long laths of biotite. These grain clusters form trains several centimetres long and one grain wide aligned parallel to foliation.

The third type of garnet recorded in the leucogneisses forms small, idiomorphic, inclusion-free grains up to 1mm in diameter (Fig. 3.16.). These are much rarer that Type II Garnets (although as abundant as Type I Garnet) and have only been noted in three or four samples. They occur in samples which also contain Type II Garnet, but are more common in leucogneisses where mafic and peraluminous phases are scarce.

3.2.3.2. Cordierite

Cordierite abundances in the Brattstrand Bluffs Leucogneisses are lower than those of garnet. Garnet-rich samples contain the highest modal concentrations of cordierite. Several main cordierite types have been recognised. The most common occurrence is as subhedral to xenoblastic porphyroblasts commonly intergrown with quartz, both as subhedral to xenoblastic individual grains or clusters of grains (up to 1cm in diameter). Trains of cordierite are aligned parallel to foliation, similar to Type II Garnet.

Cordierite is also frequently recorded intergrown with quartz as rims around garnet. Quartz in these composite coronas is vermicular, while the cordierite ranges from fresh to completely pinitised. When not pinitised, cordierite is generally untwinned, although untwinned cordierite is also relatively common. Some larger, rounded, anhedral grains show deformation twins. These larger cordierite porphyroblasts occasionally contain tiny sillimanite inclusions in their cores, similar to those recorded in Type I Garnet. Narrow cordierite rims on spinel (separating spinel and sillimanite) and ilmenite, and rounded cordierite inclusions up to 0.2mm in diameter in Type II Garnet have also been noted (Fig. 3.17.).

Rare euhedral cordierite has been recorded in some samples, suggesting that there are at least two generations of cordierite are present. Euhedral cordierite forms small (<0.5mm long) equant crystals, and appears to have formed earlier than cordierite rims on garnet. Idiomorphic cordierite is much rarer than idiomorphic (Type III) garnet.

3.2.3.3. Sillimanite

Sillimanite is a very common phase in the leucogneisses, and occurs in several petrographic associations. Fine needles of sillimanite (<50μm long) defining an early foliation in Type I Garnet have already been described above. These are most often witnessed in the cores of Type I Garnets, but have been recorded at the margins of Type I Garnet, in the cores of large anhedral K-feldspar grains and more rarely in large rounded anhedral cordierite. The commonest occurence of sillimanite is as coarse prismatic grains up to 8mm in length, often rimmed by cordierite and intergrown with hercynitic spinel. Sillimanite is always separated from spinel by a rim of cordierite. Prismatic sillimanite grows parallel to the dominant foliation described by trains of garnet and cordierite. Large sillimanite crystals of this form often show resorbed margins, suggesting partial dissolution (Fig. 3.18). In garnet-poor leucogneisses sillimanite commonly occurs as individual grains, while leucogneisses containing more mafic or peraluminous material (garnet, biotite, cordierite) often contain monomineralic clumps or "schlieren" of sillimanite. Finer grained sillimanite schlieren comprised of many small

Plate 6.

Fig. 3.17. Photmicrograph of large cordierite (pale) containing abundant poikiloblastic hercynitic spinel (black) and sillimanite (high birefringence). Note that cordierite separates sillimanite and spinel). XPL. Scale bar - 3mm.

Fig. 3.18. Large prismatic sillimanite, embayed and rimmed by pinitised cordierite. XPL. Scale bar - 1.2mm.

Fig. 3.19. Large Type II Garnet containing several small quartz inclusions, wrapped by fine grained "schlieren" of fine-grained sillimanite. PPL. Scale bar - 3.5mm.

Fig. 3.20. Late, coarse-grained biotite flakes growing on margin of Type II Garnet (pale grey). Garnet contains several small rounded biotite inclusions. PPL. Scale bar - 0.3mm.

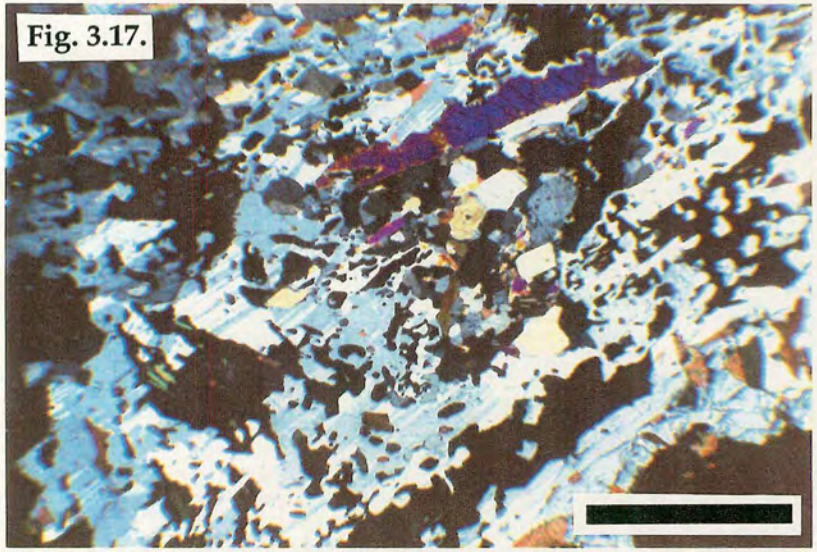
Fig. 3.17.

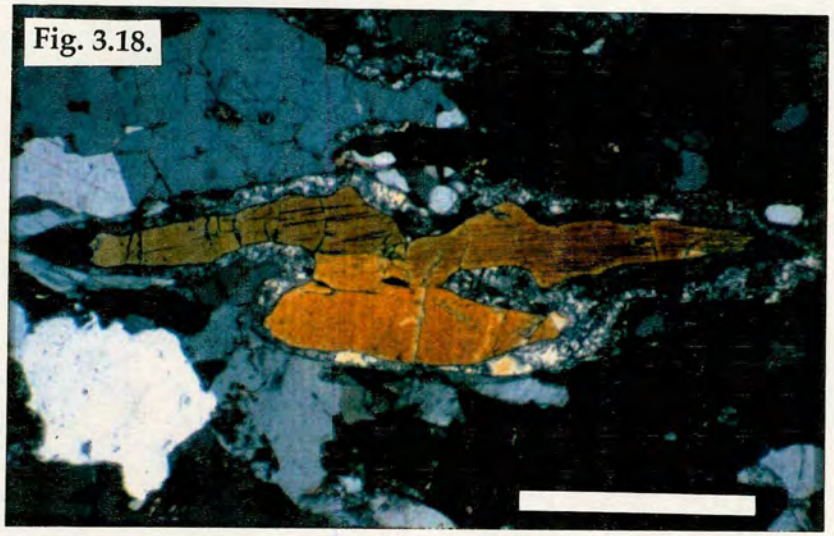
Fig. 3.18.

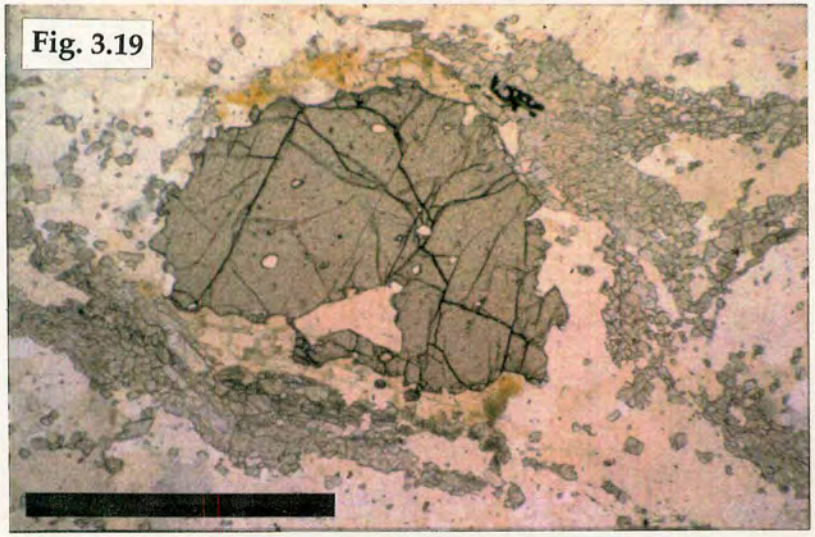
Fig. 3.19

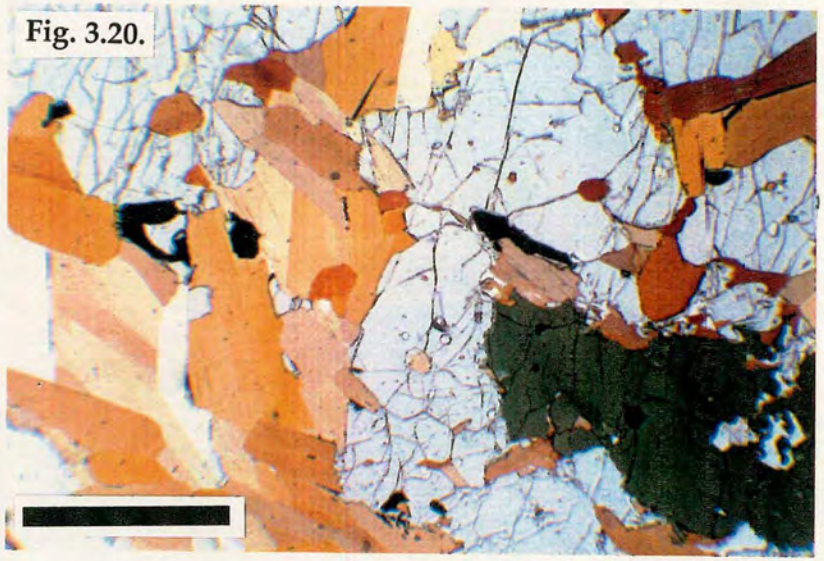
Fig. 3.20.

(<200μm) grains form parallel to foliation or as lens-shaped trains wrapping around large garnets (Fig. 3.19.).

3.2.3.4. Biotite

Biotite is less common than either garnet or cordierite in most leucogneisses, and rarely comprises more than 5-10 % of the rock. Two types of biotite have been recognised. Randomly oriented elongate biotite laths (up to 5mm long) around garnet are the most abundant. Biotite appears late, overprinting the general foliation (Fig. 3.20.). Small rounded biotite grains (often with rounded quartz) have been preserved in cores of Type I Garnet. The maximum size of these inclusions is approximately 100μm. Often these small rounded biotite inclusions in Type I Garnet are composite and contain a small amount of quartz. The foliation developed by these small biotite inclusions in early garnet cores is not as well defined as that exhibited by sillimanite.

3.2.3.5. Hercynitic Spinel.

Dark green hercynitic spinel is the most aluminous phase recorded in the Brattstrand Bluffs Leucogniesses. It appears to have formed very late, overprinting the foliation defined by prismatic sillimanite (Fig. 3.21). It is typically anhedral to xenoblastic, occurring as dispersed grains and in elongate, poikiloblastic patches rimmed by cordierite and intergrown with sillimanite and ilmenite. Spinel is most abundant in leucogneisses containing large amounts of cordierite and garnet, and is absent in the more quartzofeldspathic samples. Maximum modal concentrations of hercynite do not exceed 10% even in the most garnet-rich samples.

3.2.4. Accessory Phases.

3.2.4.1. Ilmenite.

Plate 7.

Fig. 3.21. Anhedral hercynitic spinel (black, centre) overgrowing rhombs of medium-grained and fine-grained sillimanite. PPL. Scale bar - 3mm.

Fig. 3.22. Back-scattered electron image of a composite monazite grain with a zoned core and an unzoned rim. Bright zones represent Th rich areas, while darker zones have higher LREE contents and low Th. The darkest areas in the core have ThO_2 contents of 8-9 wt%, while the bright rim contains over 20 wt % ThO_2. Note the cuspate embayments indicating partial resorption of the monazite cores.

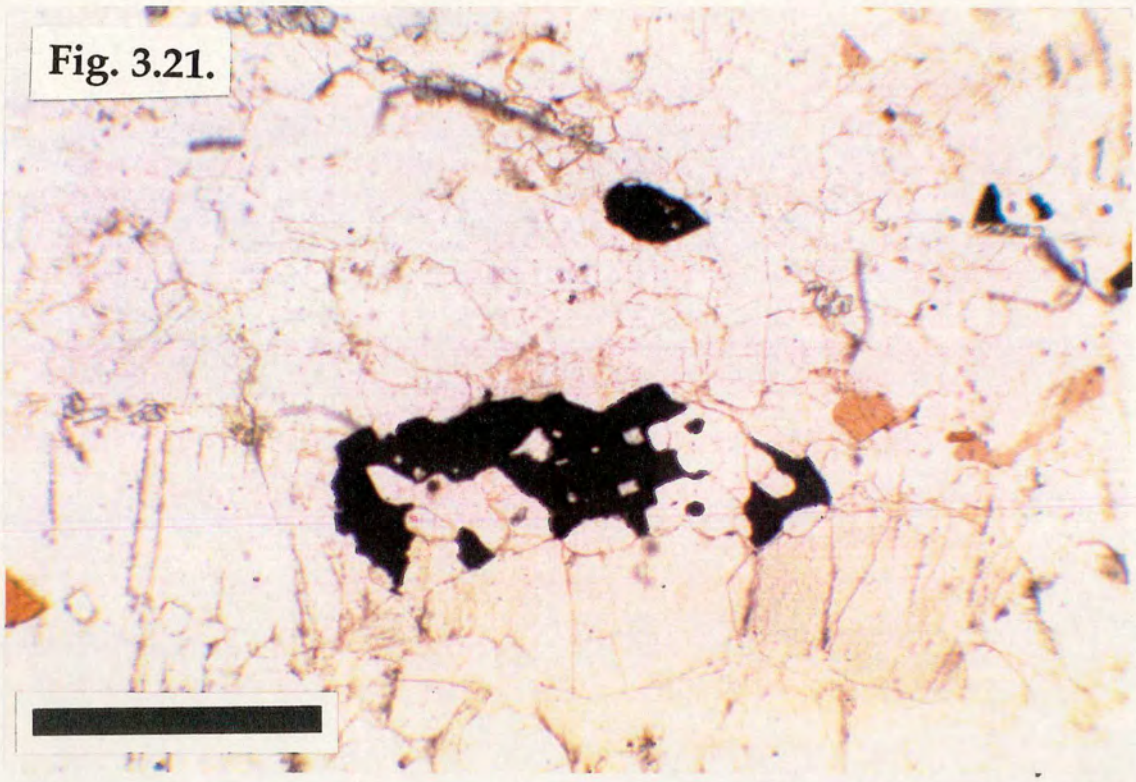

Fig. 3.22.

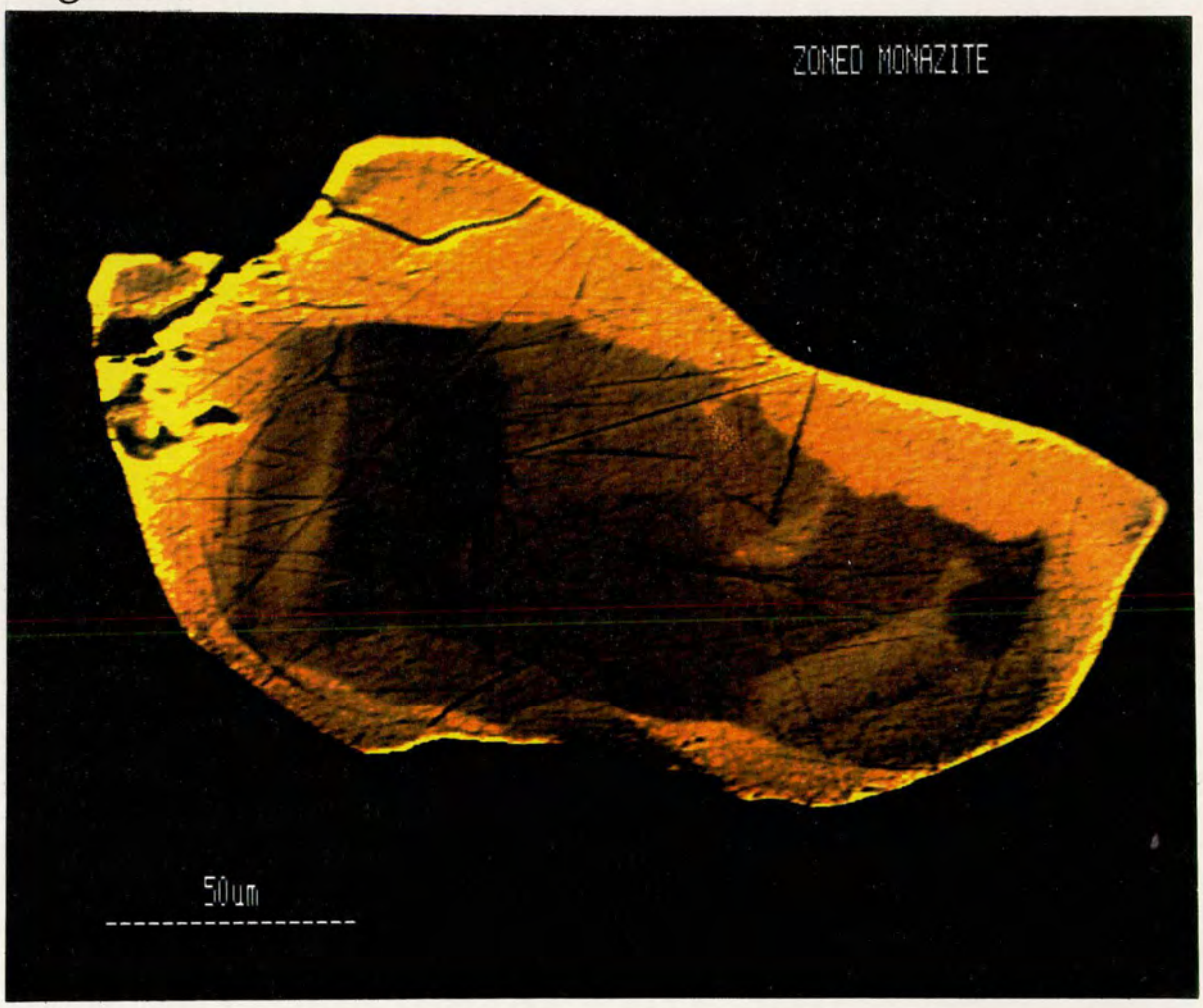

Ilmenite is the main oxide phase recorded in the leucogneisses. It is always anhedral, forming elongate skeletal grains up to 2mm long aligned parallel to foliation. Ilmenite typically occurs intergrown with hercynitic spinel, but also occurs frequently as anhedral inclusions in garnet along with rounded quartz grains and, occasionally, cordierite. Like spinel, it is most abundant in garnet- and cordierite-rich samples and only rarely occurs in garnet-poor or garnet-absent leucogneisses. Rare exsolution lamellae and flames of pyrrhotite (<20μm wide) in ilmenite have been recorded. No magnetite is present in any samples.

3.2.4.2. Monazite and Zircon.

Monazite and zircon are important accessory phases in many of the Brattstrand Bluffs Leucogneisses. No apatite has been recorded. Both monazite and zircon are more abundant in leucogneisses with high garnet and cordierite concentrations. While zircon and monazite may be almost absent in more quartzofeldspathic samples, twenty to thirty large monazite and zircon grains in a single thin-section is not unusual for more mafic leucogneisses. Monazite is more abundant than zircon in all samples. Both phases are commonly hosted in cordierite, quartz or K-feldspar. No monazite or zircon has been recorded in biotite, but small zircons have been recorded in Type I Garnet cores as part of the relict inclusion assemblage.

Zircon forms both elongate needles and more equant crystals, while monazite typically forms larger, rounded grains. Backscattered electron images obtained from both S.E.M. and Electron Microscope sources has identified strongly zoned and corroded monazite cores rimmed by clear magmatic overgrowths (Fig. 3.22.). Cores of monazite may reach 300 μm in diameter with subidiomorphic unzoned rims of varying width (<50μm) (Fig. 3.23.). Zoning varies from complex to almost euhedral, but may be truncated by overgrowths. Monazite rims may be as narrow as 10μm, but are always present. A large monazite with a well developed unzoned rim has been recorded as an inclusion in Type II garnet, suggesting that the monazite rims may have developed early in the crystallysation sequence (Fig. 3.24.).

Plate 8.

Fig. 3.23. Large rounded monazite in K-feldspar. A subhedral overgrowth is visible at the top of the grain, and the margin between the core and rim is marked by a slight dusting. PPL. Scale bar - 0.3mm.

Fig. 3.24. Rounded monazite (with rim, left side of grain) in Type II Garnet. The rim shows enrichment of Th similar to that of most other monazite grains. PPL. Scale bar - 0.3mm.

Fig. 3.25. False colour cathodoluminescence image of a large rounded zircon (approximate diameter 200μm) showing the absence of any obvious magmatic overgrowth (c.w. Fig. 3.22).

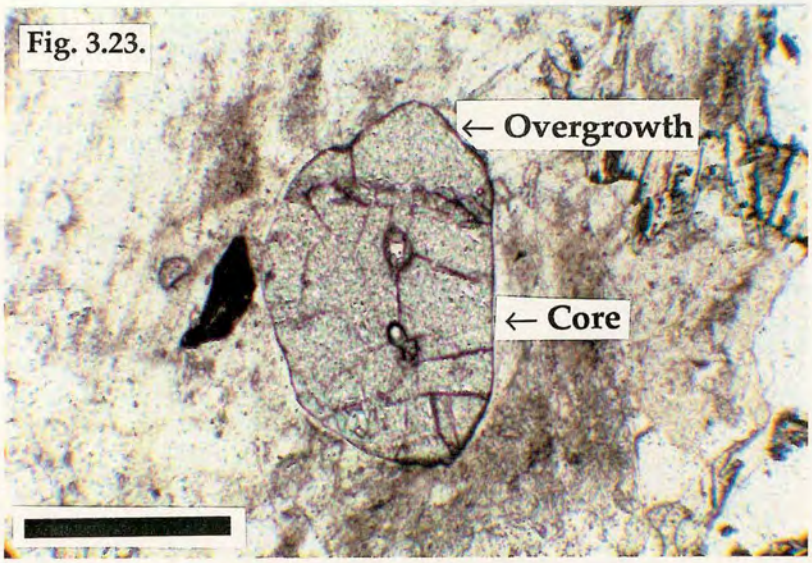
Fig. 3.23.
← Overgrowth
← Core

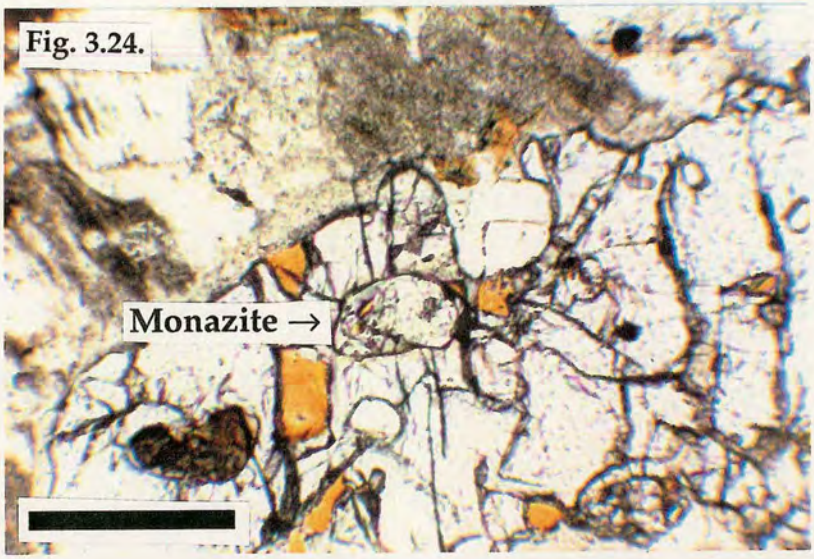
Fig. 3.24.
Monazite →

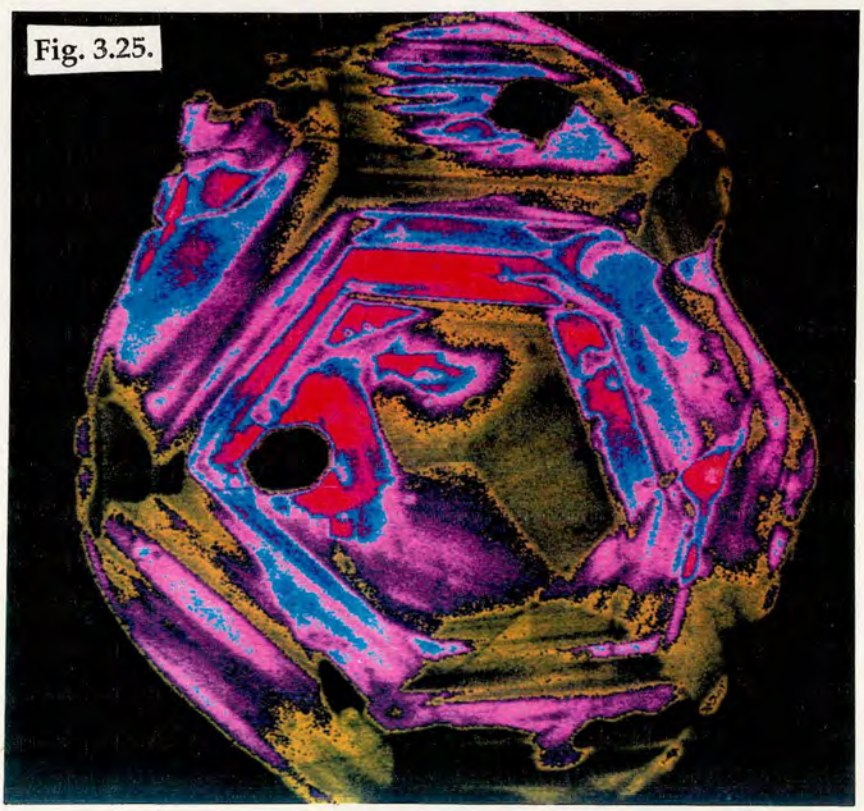
Fig. 3.25.

Backscatter S.E.M. and cathodoluminescence images show that zircons only rarely develop discrete overgrowths (Fig. 3.25.). More often they exhibit complex metamorphic and sector zoning patterns. Occasional small, euhedral zircon grains have been recorded with no zoning at all. These are commonly hosted in cordierite.

3.2.4.3. Graphite.

Rare graphite has been recorded in several leucogneiss samples. It forms easily recognisable clusters of opaque fibres and individual flakes up to 5mm long (although typically 1mm or less) with no preferred orientation. (Fig. 3.26.). These decussate graphite patches overprint foliation and are interpreted as having formed late in the petrogenetic evolution of the leucogneisses. Graphite is most common in quartzofeldspathic leucogneisses and do not show increased abundance in more garnetiferous or obviously peraluminous samples.

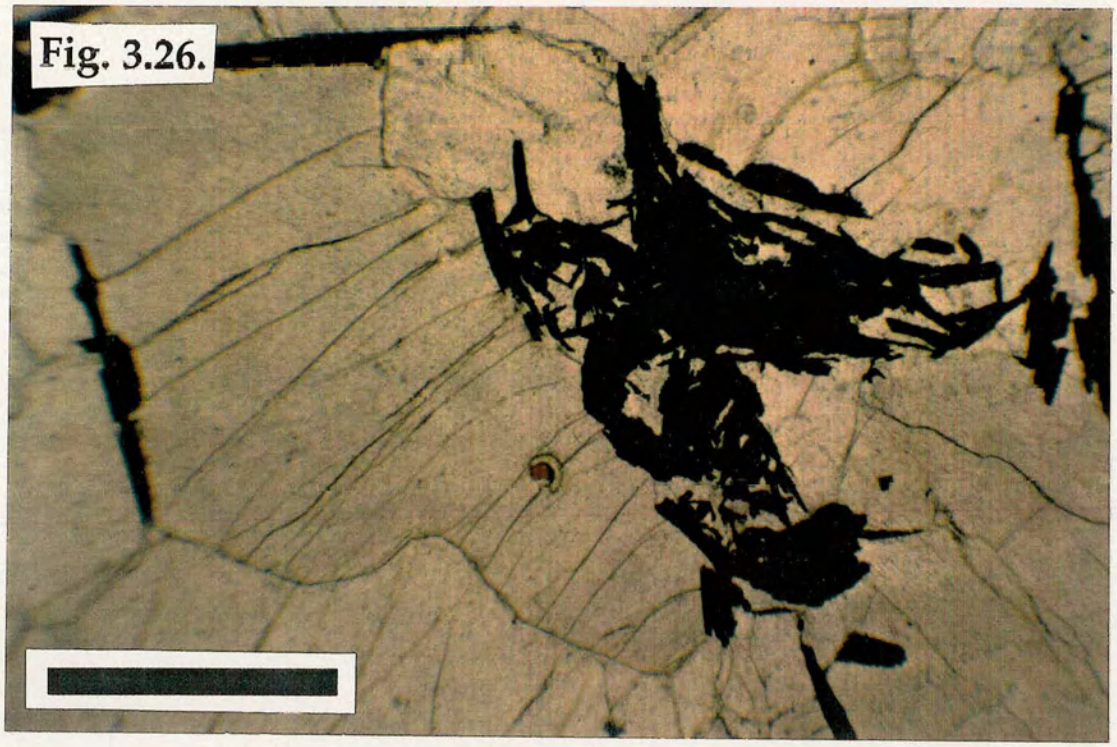

Plate 9.

Fig. 3.26. Small ragged flakes of graphite (opaque) in K-feldspar-rich leucosome. PPL. Scale bar - 0.3mm.

Chapter 4.

Geochemistry of the Prydz Bay Leucogneisses.

Chapter 4. Geochemistry of the Prydz Bay Leucogneisses.

4.1. INTRODUCTION.

The Prydz Bay Leucogneisses as a group have a chemistry characteristic of intra-crustal felsic melts derived from a metasedimentary source (Miller, 1985). They have restricted SiO_2 compositions (65-76 wt%), low Na_2O (<3.2 wt%) and K_2O values of approximately 5wt%. They are strongly corundum normative (up to 6wt%) and have molecular $Al_2O_3/CaO+Na_2O+K_2O$ (A/CNK) values greater than 1.10. These are typical of peraluminous S-Type granitoids as defined by Chappell & White (1974) (see also White, 1990).

Based on major, trace and rare-earth element data the leucogneisses have been subdivided into three geochemically distinct suites. Type 1 Leucogneisses (LG1) have high SiO_2 (>72wt%), low Al_2O_3, Fe_2O_3 and MgO. (Note: Fe_2O_3 is total Fe expressed as Fe_2O_3). They exhibit characteristic REE patterns, with low LREE and HREE totals, relatively unfractionated patterns and a positive Eu anomaly. The division between LG1 and Type 2 Leucogneisses was taken at approximately 72 wt% SiO_2 for convenience. LG2 leucogneisses have higher Al_2O_3, Fe_2O_3 and MgO, higher compatible (Ni, Cr, V), and incompatibe (Zr, Th) element concentrations and more melt-like REE patterns (moderately fractionated, negative Eu anomalies). Type 3 Leucogneisses have a major element chemistry intermediate between LG1 and LG2, but are markedly enriched in Zr, Th, and LREE, and have strongly fractionated (average $La_{(n)}/Yb_{(n)}$=147.6) REE patterns.

The remainder of this chapter will describe in more detail the chemistry of these leucogneisses, which have been interpreted as crustal melts formed under granulite facies conditions. The implications of the geochemistry of the leucogneisses for melt extraction in migmatite terranes will be considered in Part 3 of the thesis. Full bulk rock geochemical analyses are given in Appendix A.

4.2. TYPE 1 LEUCOGNEISSES (LG1).

4.2.1. Major elements.

Type 1 Leucogneisses have high SiO_2 contents (72.18 - 77.15 wt%). Al_2O_3 ranges from 12.37-15.64 wt% and shows a strong negative correlation with SiO_2 (Fig. 4.1a). Molecular A/CNK ratios range from mildy (A/CNK=1.03) to strongly (A/CNK=2.17) peraluminous (Fig 4.3g). Type 1 Leucogneisses have an average A/CNK value of 1.22 and can therefore be classified as S-Type granitoids. The peraluminous nature of LG1 samples is further reflected in the abundance of normative corundum (up to 8.4%). The Manaslu leucogranite (France-Lanord & Le Fort, 1988) (Table 4.1.) is a crustal melt with well constrained geochemistry which can be used for comparative purposes. Compared to the average Manaslu leucogranite the average LG1 is more siliceous, slightly enriched in K_2O and CaO, and much less sodic. $K_2O>Na_2O$ in almost all samples.

A typical feature of all leucogranites is their extremely low Fe_2O_3 and MgO content. LG1 leucogneisses have very low Fe_2O_3 (average=1.27wt%) and MgO (average=0.19wt%) concentrations. Both show a strong negative correlation with SiO_2 (Fig. 4.1.b and 4.1.c). Of the three leucogneiss suites LG1 leucogneisses have the lowest mafic component (Mg, Fe, Al) totals. Fe and Mg concentration are very similar to those of the Manaslu leucogranite. Whole rock XMg values ((MgO/40.32) / (MgO/40.32) + (Fe_2O_3/159.70) are variable (0.07-0.69) due to low Fe and Mg concentrations. LG1 leucogneisses have the lowest XMg values of the three leucogneiss suites (average = 0.25) (Fig 4.3.h), but the data show a very large scatter. Titanium values (average TiO_2 concentration = 0.09wt%) exhibit a similar pattern to Fe_2O_3 and MgO, with low totals and a strong negative correlation with SiO_2. MnO concentrations are also low (mean = 0.02wt%) consistent with typical leucogneiss compositions. The manganese enrichment associated with garnet bearing granitic rocks (e.g. du Bray, 1988) is not witnessed in LG1 leucogneisses.

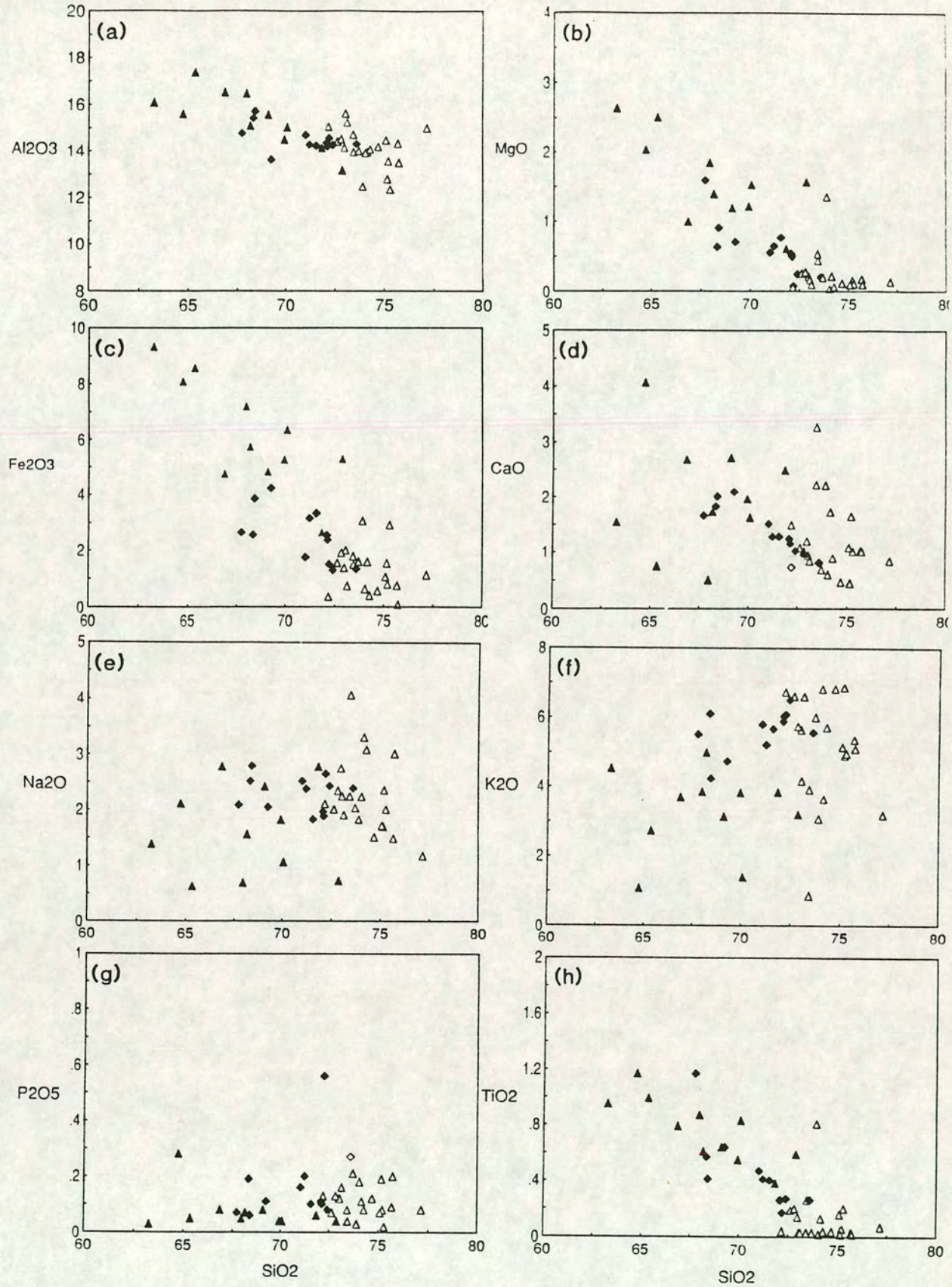

Figure 4.1. Major element Harker plots. This and all other graphs: LG1 - white triangles; LG2 - black triangles; LG3 - black diamonds.

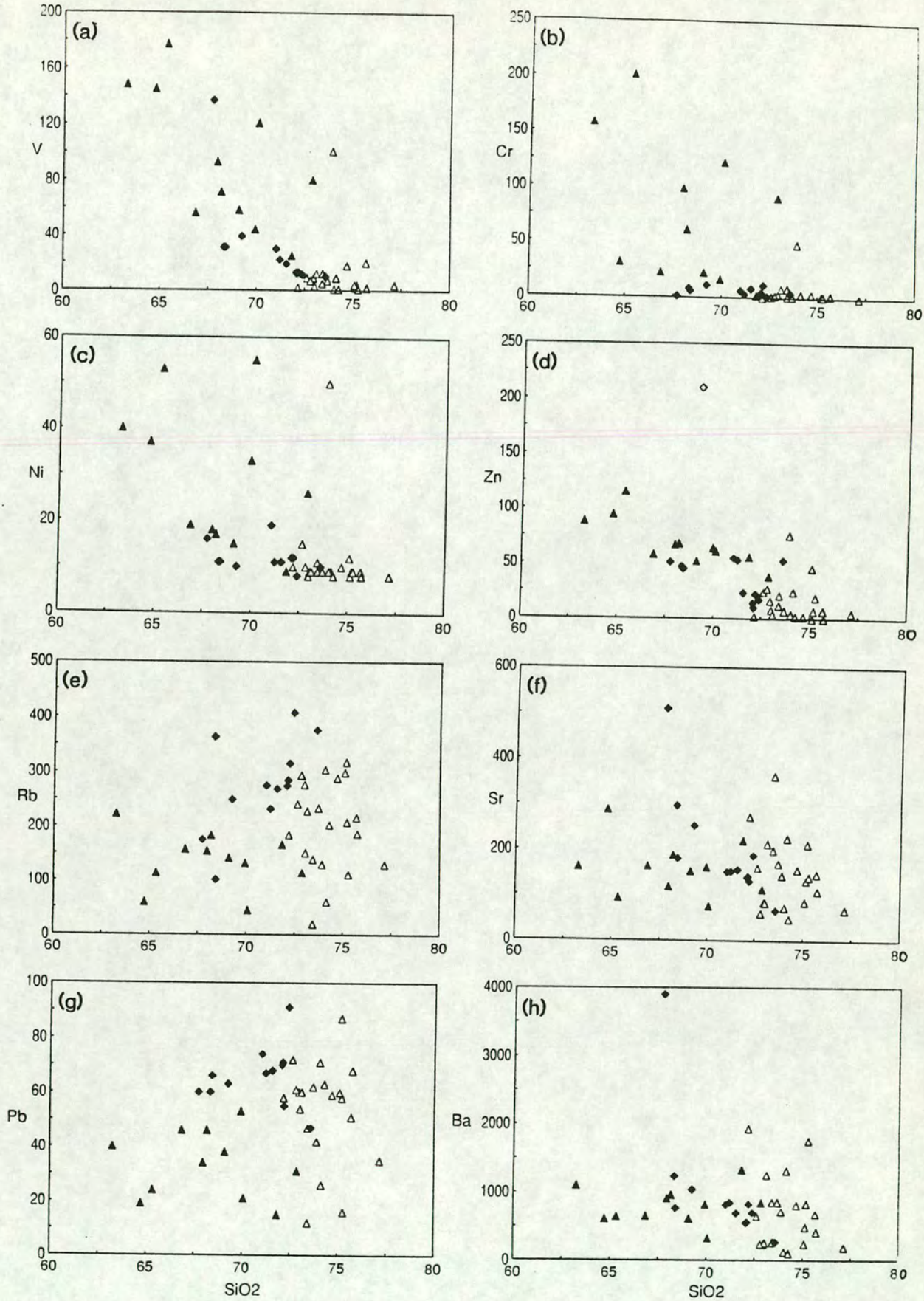

Figure 4.2. Trace element Harker plots. Symbols as Figure 4.1.

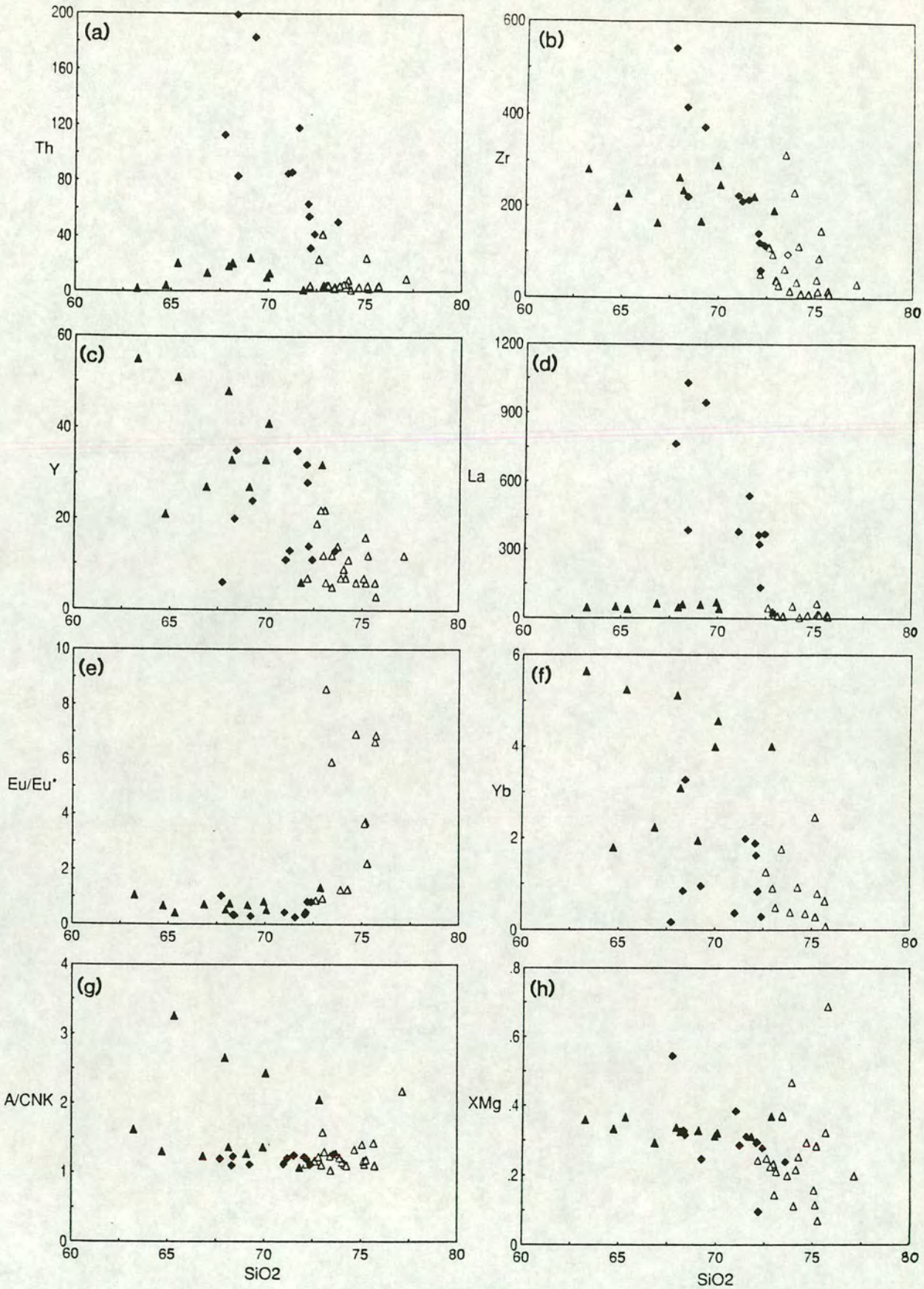

Figure 4.3. Trace Element Harker plots. Symbols as Figure 4.1. Also shown are A/CNK and XMg vs SiO_2 plots.

Fe2O3	0.83	0.59	0.13	-	1.33	2.17	1.47	1.11	0.15	1.54	2.48	0.16	0.21	0.00					
FeO	0.47	3.48	2.28	1.48	-	-	-	-	1.27	-	-	2.27	0.31	-	0.63	-	0.72	-	-
MnO	0.03	0.06	0.05	0.07	0.17	0.03	0.03	0.03	0.03	0.03	0.06	0.05	0.03	0.05	0.05	0.00	0.03	0.08	-
MgO	0.11	1.76	0.71	0.10	0.59	0.53	0.19	0.20	0.32	0.32	1.73	0.61	0.09	0.10	0.48	0.20	0.46	0.48	0.41
CaO	0.47	0.95	1.34	0.68	0.75	0.42	0.30	0.26	0.23	0.84	2.00	1.20	0.32	1.26	0.92	1.14	0.69	0.78	0.64
Na2O	4.05	1.49	2.69	3.99	4.03	2.81	2.84	3.34	4.21	3.27	3.10	2.58	3.64	3.84	3.86	4.37	2.52	5.19	2.82
K2O	4.56	3.73	4.42	4.20	3.42	2.84	5.93	4.79	3.80	5.13	1.74	4.60	4.24	2.94	4.59	3.88	5.50	1.82	5.82
TiO2	0.10	0.54	0.34	0.04	0.13	0.33	0.27	0.16	0.21	0.21	0.52	0.36	0.04	0.08	0.02	0.07	0.25	0.09	0.17
P2O5	0.13	0.13	0.15	0.05	0.14	0.28	0.14	0.46	-	-	-	0.17	0.21	0.14	0.06	0.16	0.23	0.13	0.22
LOI	-	-	-	-	0.66	2.84	0.73	1.68	-	0.77	0.51	1.15	1.10	-	0.50	-	-	1.00	0.92
Total	99.26	98.45	98.44	99.21	100.81	100.73	98.64	100.44	100.00	99.57	98.77	99.88	99.48	99.94	99.65	99.77	98.06	99.92	98.00
Co	96	-	-	-	-	-	-	-	-	41	-	-	-	36	-	-	-	-	68
Cr	-	56	17	-	-	-	-	-	-	2-11	-	13	<1	21	-	-	-	-	14
Ni	-	24	7	-	-	-	-	-	-	2-10	-	-	-	14	5	-	-	-	10
V	-	64	28	-	-	-	-	-	-	17 - 21	-	25	1	13	-	-	-	-	13
Sr	76	127	88	64	-	-	-	-	-	126	211	79	23	235	123	156	96	58	159
Rb	286	153	236	201	-	-	-	-	-	235	40	244	289	57	256	108	488	214	140
Ba	213	765	605	260	-	-	-	-	-	414	-	755	70	-	336	260	-	164	865
Th	6	22	12	4.6	-	-	-	-	-	-	4.07	15.6	4.4	2.5	55	1	19.6	16	-
Pb	-	35	24	-	-	-	-	-	-	-	-	25	25	-	62	-	-	47	-
U	8	4	6	0.71	-	-	-	-	-	-	1.41	5.8	2.8	0.8	11	-	-	6	-
Zr	-	-	-	-	-	-	-	-	-	-	135	183	31	77	136	24	80	15	81
Y	14.5	39	31	-	-	-	-	-	-	-	22	35	16	12	9	15	13	17	29
La	11.5	31	18	14	-	-	17.86	7.32	-	-	15.85	24	3	-	18	6.6	33.8	1.6	16.2
Ce	19	-	-	28	-	-	41.19	14.21	-	-	31.91	58	8	-	39	9.6	70.3	4.5	35.28
Nd	8	-	-	-	-	-	18.06	7.47	-	-	14.17	-	4	-	9	-	33.5	1.9	15.13
Sm	2	-	-	3.68	-	-	4.73	1.43	-	-	3.39	-	-	-	6	1.3	7.4	0.7	3.97
Eu	0.5	-	-	0.29	-	-	0.98	0.3	-	-	1.47	-	-	-	-	0.66	0.76	0.4	0.95
Gd	2	-	-	1.4	-	-	4.04	1.53	-	-	3.17	-	-	-	-	-	-	1.2	3.45
Dy	2.4	-	-	-	-	-	4.48	0.98	-	-	2.85	-	-	-	-	-	-	2.2	4.17
Er	1	-	-	-	-	-	3.02	0.28	-	-	1.57	-	-	-	-	-	-	-	2.72
Yb	1	-	-	1.4	-	-	2.93	0.21	-	-	1.65	-	-	-	-	1.13	1.05	0.6	2.69
Lu	0.14	-	-	0.22	-	-	0.48	0.03	-	-	0.32	-	-	-	-	-	0.11	-	0.49

A. Average Manaslu leucogranite (n=201). (France-Lanord & Le Fort, 1988).
B. Cooma Granodiorite (C1). (White & Chappell, 1988).
C. Average of 25 analyses of Strathbogie granites. (White & Chappell, 1988).
D. Biotite-muscovite-garnet granite (SW-7). (Mittelfehldt & Miller, 1983)
E. Garnet leucogneiss (L7G-1), New Hampshire. (Dougan, 1979).
F. Garnet leucogneiss (L3A-1), New Hampshire. (Dougan, 1979).
G. Cordierite granite (PH 101), Northern Portugal. (Holz, 1989).
H. Muscovite granite (PL39), Northern Portugal. (Holz, 1989).
I. Experimental melt composition (GB10, run 115). (Fyfe & Brown, 1970).
J. Model granite composition. (Debon & Le Fort, 1983).

K. Leucosome, pelitic migmatite. (Barbey et al, 1990)
L. Garnet cordierite granite, Strathbogie. (White, 1990)
M. Garnet granite, Strathbogie. (White, 1990)
N. Leucosome, pelitic migmatite, St Malo. (Weber et al, 1985)
O. Bi-poor leucogranite, Galway Pluton. (Coats & Wilson, 1971).
P. Barousse leucogranite, Pyrenees. (Harris et al, 1986).
Q. Cornish Type II granite. (Harris et al, 1986).
R. Garnet-tourmaline leucogranite (L121), Himalaya. (Searle & Fraser, 1986).
S. Felsic granite, Tourem Complex (PH509), Portugal. (Holtz & Barbey, 1991).

Table 4.1. S-Type Granitoid and pelitic migmatite leucosome compositions from the literature. REE patterns for selected samples are shown in Figure 4.6.

4.2.2. Trace elements.

Type 1 Leucogneisses have relatively low concentrations of most trace elements excepting those dominantly hosted by feldspar, reflecting their mineralogy. Transition elements (Ni, Cr, V, Sc, Cu and Zn) are uniformly low (typically less than 10ppm for each element) (Figs 4.2a-d). Rb/Sr values are typically high (max Rb/Sr = 4.9) reflecting the low plagioclase (and therefore Sr) content of the leucogneisses. Ba concentrations are variable, but typically range from 400-800ppm (Fig. 4.2h).

Type 1 Leucogneisses have restricted, low concentrations of Zr (average = 62ppm) (Fig. 4.3b) compared to both the other Prydz Bay Leucogneisses and to typical crustal melts (Table 4.1). Equilibrium melts derived by partial melting of pelitic source rocks containing sufficient Zr to saturate the melt in zircon generally contain around 200ppm Zr, much greater than that recorded in Type 1 Leucogneisses. U concentrations are uniformly low in all the leucogneiss types, while Th is more variable. Low Th/U values in Type 1 Leucogneisses reflect low Th concentrations (average Th = 6ppm).

4.2.3. Rare Earth Elements.

Type 1 Leucogneisses show moderately fractionated, slightly concave up rare-earth patterns (mean $La_{(n)}/Yb_{(n)}$=23.8, mean $Ce_{(n)}/Yb_{(n)}$=14.0; Fig. 4.4. Chondrite normalising factors are given in Appendix B. Absolute REE concentrations are the lowest of the three leucogneiss types. Type 1 Leucogneisses have Eu anomalies which vary from slightly negative (Eu/Eu*=0.88, one sample) to markedly positive (Eu/Eu*=8.56), but the majority of samples have a large positive Eu anomaly (mean Eu/Eu*=3.9). A plot of Eu/Eu* against SiO_2 (wt%) for all leucogneiss types (Fig 4.5.) shows a marked increase at approximately 72 wt% SiO_2, corresponding to the positive Eu anomaly characteristic of Type 1 Leucogneisses, which are the only samples which exhibit positive Eu anomalies. It is interesting to note that absolute Eu concentrations in Type 1 Leucogneisses are almost identical to those of the other leucogneiss suites while the size and shape of the Eu anomaly is very different.

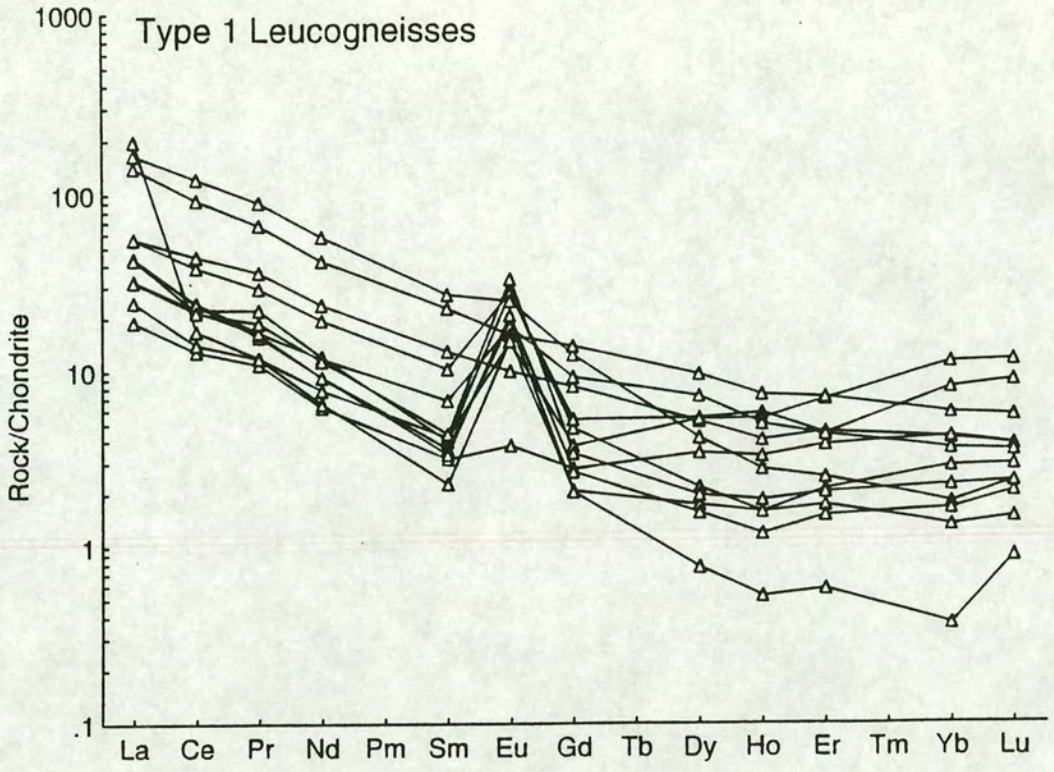

Figure 4.4. Chondrite normalised REE plots for the Type 1 Leucogneisses.

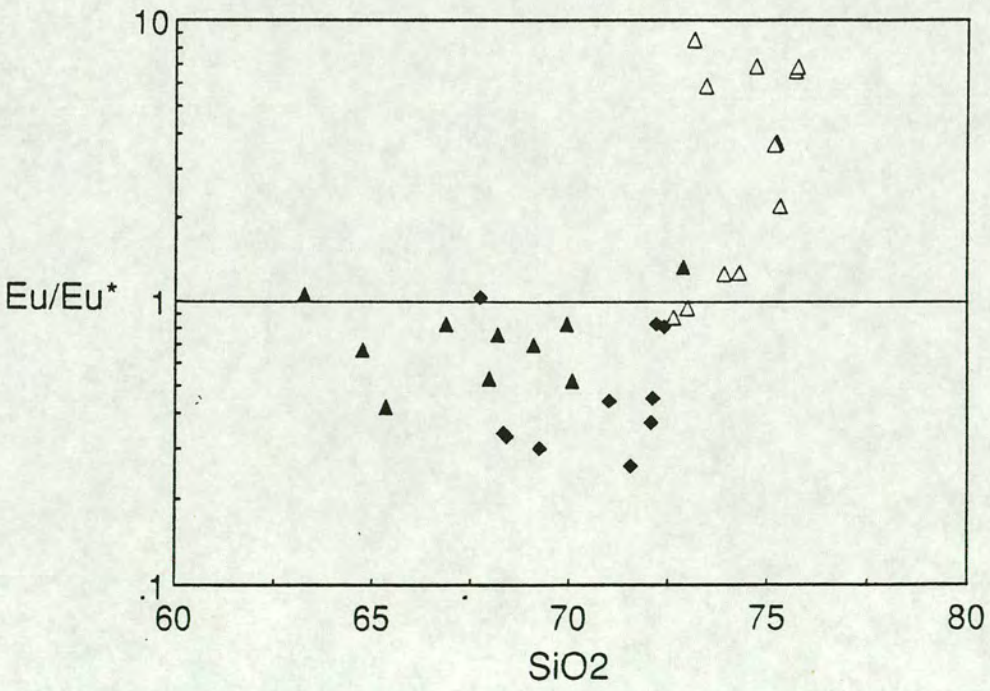

Figure 4.5. A plot of Eu/Eu* against SiO_2 (wt%) for all leucogneiss types (Symbols as Figure 4.1.)

Type 1 Leucogneisses have unusual REE patterns when compared to other crustal melts. Peraluminous granitic magmas generally exhibit moderately fractionated patterns with small to large negative Eu anomalies (e.g. Harris & Inger, 1992; Harris *et al*, 1986) (Fig 4.6.).

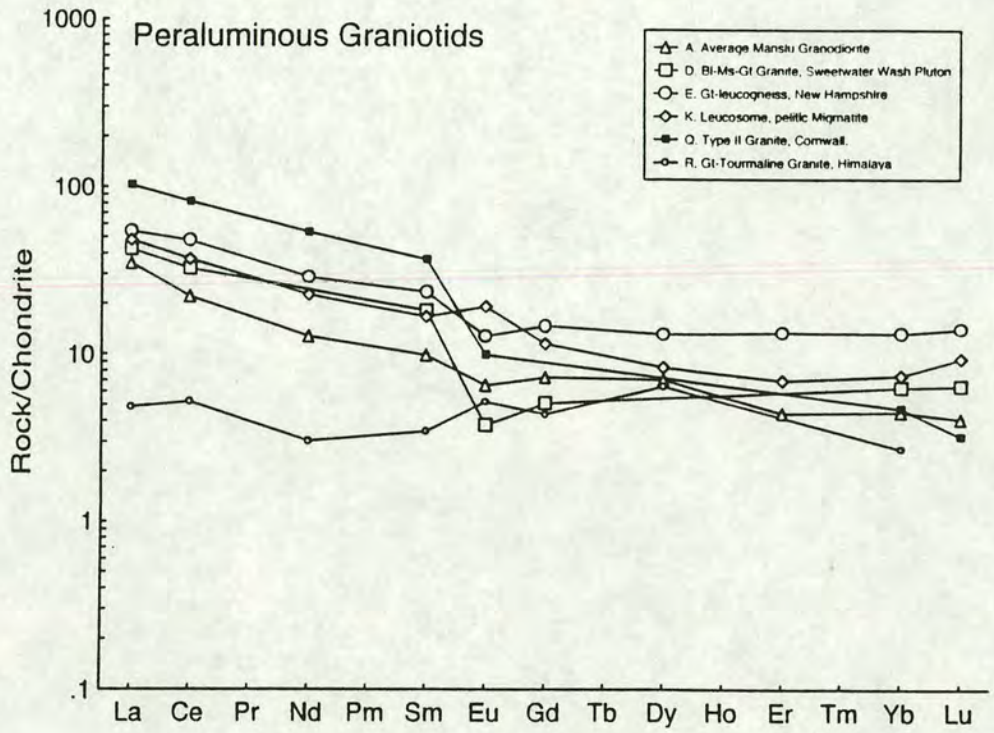

Figure 4.6. Chondrite Normalised plot for literature compositions (Table 4.1)

Absolute REE concentrations are typically higher in peraluminous granitoids from the literature. In addition, petrogenetic modelling calculations by Barbey *et al* (1989) and Harris & Inger (1992) indicate that equilibrium melts produced by melting of pelitic source rocks will have similar patterns to the majority of S-Type granite plutons. Migmatite complexes with leucosomes having concave-up, positive Eu anomaly REE patterns similar to those recorded here have been reported in the literature. Small-volume migmatite leucosomes of the Pena Negra Complex, Central Spain (F. Bea, *pers comm*), leucosomes of the Telohat Migmatites, Algeria (Barbey *et al*, 1989) and small-volume leucosomes in a suite of mafic migmatites from the Grenville Province of Quebec (Sawyer, 1991) exhibit equivalent REE patterns. In the Pena Negra complex, small-volume cordierite-bearing melts exhibit concave up, LREE depleted, positive Eu anomalies similar to LG1 whereas large-volume cordierite melts exhibit more typical crustal melt patterns. Both the

small volume Telohat leucosomes and the small-volume melts from the Grenville Province have been interpreted as disequilibrium melts produced under granulite facies conditions.

4.3. TYPE 2 LEUCOGNEISSES (LG2).

4.3.1. Major elements.

Type 2 Leucogneisses have the lowest SiO_2 contents of the three leucogneiss types (mean SiO_2 = 68.22 wt%), while Al_2O_3 values are the highest (max Al2O3 = 17.37 wt%). Al_2O_3 again shows a strong negative correlation with silica content (Fig. 4.1.a). Type 2 Leucogneisses are characteristically more peraluminous (maximum molecular A/CNK=3.26) and more mafic than either LG1 and LG3, and exhibit extremely high normative corundum concentrations (max=12.3%). Two A/CNK patterns can be determined in LG2 (Fig. 4.3.g). One group of Type 2 Leucogneisses has low (1.10-1.60) A/CNK values showing a slight negative trend when plotted against SiO_2, while a second association has much higher A/CNK values. CaO contents are higher than both LG1 and the average Manaslu Granite, while K_2O and Na_2O are both lower. Although $K_2O>Na_2O$ in all LG2 samples (as in LG1), $CaO>Na_2O$ in LG2 while $CaO<Na_2O$ in LG1. Mean Fe_2O_3 and MgO concentrations are approximately three times greater than those of Type 1 Leucogneisses. Both Fe_2O_3 and MgO show very strong negative correlations with SiO_2 content (Figs 4.1.b and 4.1.c). Fe and Mg contents are much higher than those of the Manaslu leucogranite, and of other typical crustal granites and pelitic migmatite leucosomes (Dougan, 1979; Holz, 1989; Weber, 1985). Fe and Mg are only soluble to a limited extent in peraluminous crustal melts (Clemens & Wall, 1988) so it is likely that these unusually high Fe_2O_3 and MgO contents in LG2 represent entrained mafic material rather than reflecting a more mafic liquid composition. The importance of this is considered in more detail in Chapter 7. Titanium concentrations are the highest of the three leucogneiss types and show a similar pattern to Fe and Mg (Fig. 4.1.h), with relatively high concentrations for crustal felsic melts (mean TiO_2=0.76wt%) and a clear negative correlation with SiO_2. MnO contents again are low.

4.3.2. Trace Elements.

Compared to LG1, Type 2 Leucogneisses have much higher concentrations of transition elements. Average Cr, V and Zn concentrations are up to ten times higher in LG2 than LG1, while Sc, Ni and Cu are also significantly enriched (Figs 4.2.a-d). Rb/Sr values are low (typically 0.8-1.2) reflecting lower absolute Rb abundances rather than increased Sr concentrations. Ba contents are variable but tend to be slightly lower than in Type 1 Leucogneisses (Fig. 4.2.h).

Type 2 Leucogneiss Zr concentrations are, on average, much higher than LG1 (mean Zr=227ppm) (Fig. 4.3.b). The average Zr content is very similar to that required to saturate a typical crustal melt in zirconium (Watson, 1987). Th concentrations are approximately twice as high in LG2 than in LG1 (average Th=12ppm). Y and Yb show very similar patterns to compatible transition elements such as Ni and V (Figs 4.3.c and 4.3.f). Concentrations of Y and Yb are the highest of the three leucogneiss suites.

4.3.3. Rare Earth Elements.

Type 2 Leucogneisses show REE patterns very similar to those of many S-Type granitoids and equilibrium crustal melts (e.g. Harris *et al*, 1986; France-Lanord & le Fort, 1988). REE curves are relatively flat, with mean $La_{(n)}/Yb_{(n)}=10.5$ (Fig. 4.7.). Absolute LREE and HREE abundances are higher than LG1, but still relatively low compared to Type 3 Leucogneisses. Eu anomalies vary from very slightly positive (Eu/Eu*=1.06) to strongly negative (Eu/Eu*=0.42). Most Type 2 Leucogneisses have a small negative Eu anomaly. The REE pattern of LG2 contrasts strongly with Type 1 Leucogneiss REE curves, but shows marked similarities with both typical high level crustal granites (Miller, 1985) and equilibrium melts (Harris & Inger, 1992). In addition LG2 melts exhibit REE very similar to the REE pattern exhibited by Post Archaean Average Shale (PAAS) and by pelitic gneisses from the Brattstrand Bluffs coastline (see Chapter 5).

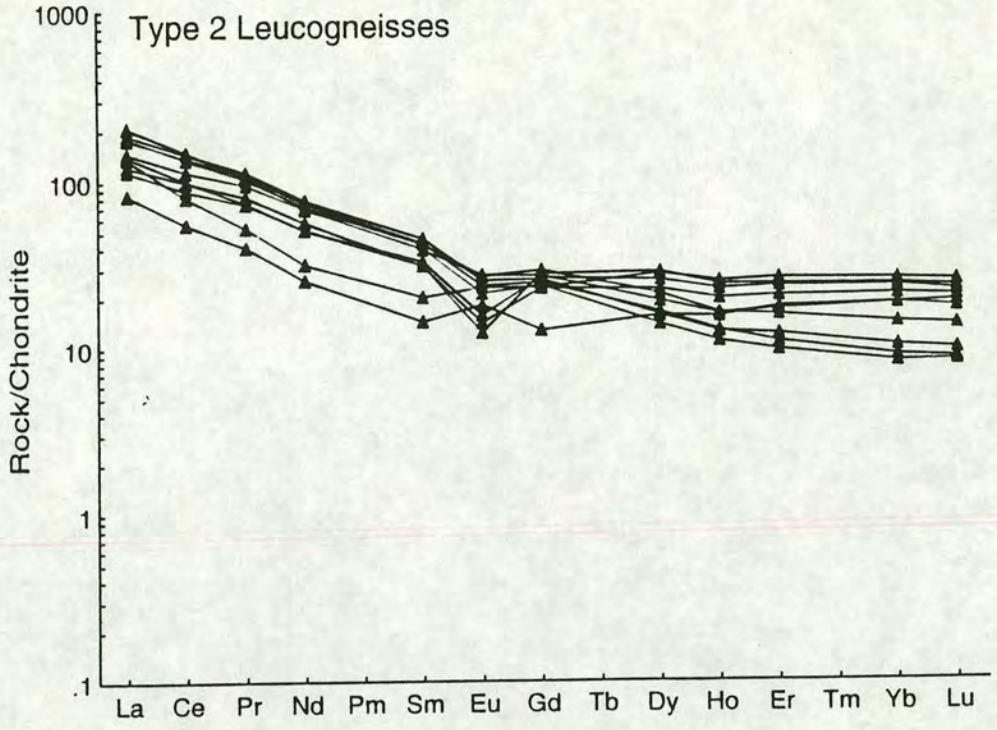

Figure 4.7. Chondrite normalised REE plots for Type 2 Leucogneisses.

4.4. TYPE 3 LEUCOGNEISSES (LG3).

4.4.1. Major elements.

Type 3 Leucogneisses have a chemistry intermediate between Type 1 and Type 2 Leucogneisses, with considerable overlap for all major elements. They are relatively siliceous, with SiO_2 contents which range from 67.72 to 73.58wt%. They have slightly higher Al_2O_3 contents than Type 1 Leucogneisses, and Al_2O_3 shows a slight negative correlation with SiO_2 (Fig. 4.1.a). They range from mildly to moderately peraluminous, with A/CNK showing the least variation of the three leucogneiss suites. Again they can be classified as S-Type granitoids using the classification of White and Chappell (1974) and White (1990). Alkali contents are similar to Type 1 Leucogneisses. $K_2O>Na_2O$, while CaO is low and shows a good positive correlation with SiO2 (Fig. 4.1.d). Compared to the Manaslu Granite Type 3 Leucogneisses are enriched in K_2O and depleted in Na_2O.

Type 3 leucogneisses have low Fe_2O_3 and MgO concentrations, although they are not as depleted with respect to these elements as Type 1 Leucogneisses. Average Fe_2O_3 (2.51wt%) and MgO (0.57wt%) values are fairly typical for leucogranitic crustal melts. Both show a good negative correlation with SiO_2 (Fig. 4.1.b and 4.1.c). Whole rock XMg values again are variable due to low MgO contents. Titanium values in Type 3 Leucogneisses are higher than Type 1 Leucogneisses (mean LG3 TiO_2=0.40wt%), and show a good negative correlation with SiO_2 (Fig. 4.1.h). MnO is almost absent in most samples.

4.4.2. Trace Elements.

Type 3 Leucogneisses have been distinguished from the other leucogneiss types on the basis of certain trace element and rare-earth element (Section 4.4.3.) characteristics. Concentrations of Th, Zr and the LREE are markedly enriched compared with Type 1 and Type 2 Leucogneisses. Other elements (notably the transition elements) have concentrations intermediate between Type 1 and Type 2 Leucogneisses. Ni, Cr and V concentrations are all low and have typical crustal melt concentrations (Fig. 4.2.a-c). Rb/Sr values are variable but typically >1.3 (max = 5.9). The absolute abundances of Sr and Rb are the highest of the three leucogneiss types. Ba concentrations are also higher in LG3 than LG1 and LG2, reflecting higher K_2O contents.
When Zr v's SiO_2 is plotted for all 3 leucogneiss types (Fig. 4.3.b) two clear trends are evident, converging on Type 1 leucogneisses at the high silica end of the diagram. Many Type 3 Leucogneisses have very high Zr contents (max Zr=542ppm), and Zr shows a remarkably strong negative correlation with SiO_2. Although Zr contents in LG3 are high, the mean Zr content of Type 3 Leucogneisses is slightly lower than that of LG2. The majority of Type 3 Leucogneisses, however, contain excess Zr over that required to saturate a felsic crustal melt due to the strong dependence of zircon solubility on melt bulk composition (Chapter 9). Similar converging trends are evident for Th and for the LREE (e.g. La). Th contents are exceedingly high compared with typical crustal melts. The maximum Th content (Fig. 4.3.a) of the Type 3 leucogneisses is 199ppm (over 30 times greater than the average LG1 Th content) whereas a typical peraluminous granitoid typically contains a maximum of 10ppm Th.

4.4.3. Rare Earth Elements.

Type 3 leucogneisses have very distinctive, steep REE patterns which contrast with the flatter curves of Type 2 Leucogneisses (Fig. 4.8).

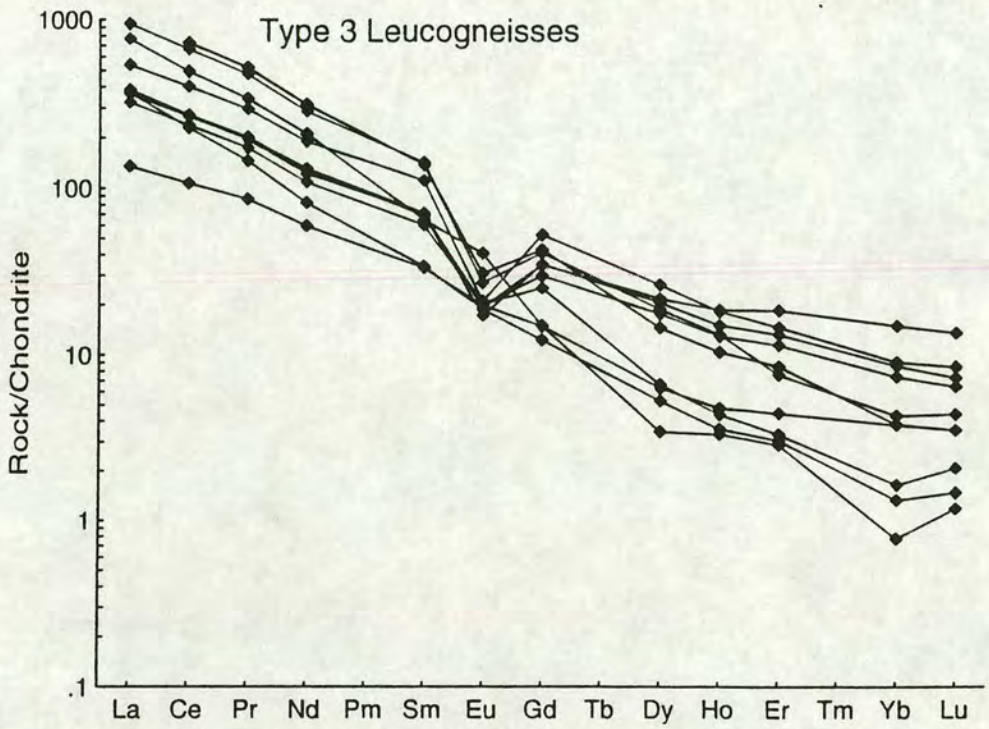

Figure 4.8. Chondrite normalised REE plots for Type 3 Leucogneisses.

Absolute LREE abundances are approximately ten times greater than LG1, giving rise to large $La_{(n)}/Yb_{(n)}$ values (average $La_{(n)}/Yb_{(n)}$= 147). Compared to typical crustal melt literature values, Type 3 Leucogneiss LREE concentrations are exceedingly high. Eu anomalies in Type 3 Leucogneisses are generally slightly negative, but range from almost zero (Eu/Eu*=1.03) to strongly negative (Eu/Eu*=0.26). Absolute Eu concentrations in Type 3 Leucogneisses (negative Eu anomaly) and Type 1 leucogneisses (strong positive Eu anomalies) are approximately equal, the difference in sign of the anomaly caused by the higher abundance of LREE and MREE in LG3. While LREE exhibit similar geochemical patterns to Zr and Th the HREE (e.g. Yb, Fig. 4.3.f) have patterns similar to those displayed by the transition elements and Y. HREE abundances are low (less than 10X chondrite normalised values) comparable with those of LG1.

4.5. SUMMARY.

The main geochemical features of the Brattstrand Bluffs leucogneisses are summarised in Table 4.2. below.

Table 4.2. Geochemical Summary of Type 1, 2 and 3 Leucogneisses.

	LG1	LG2	LG3
SiO_2 Values	>72.0 wt %	Broad range, <72wt %	Restricted c.w. LG2
A/CNK	varied, > or >> 1.1	2 trends with SiO_2	Near constant 1.1 - 1.2
Th content	Very low	Moderate	Range to very high
Zr content	Very low	Moderate	Range to very high
Transition elements	Very low	Moderate to high	Moderate
Ferromagnesian content	Very low	High	Low to moderate
LREE	Low	Moderate	Very high
Eu/Eu*	+ve	-ve to 1.0	-ve to 1.0
$La_{(n)}/Yb_{(n)}$	moderate	low	very high

Chapter 5

Petrography and Geochemistry of the Country Rocks.

Chapter 5. Petrography and Geochemistry of the Country Rocks.

5.1. INTRODUCTION.

The migmatites of the Brattstrand Bluffs coastline are dominated by metapelitic gneisses containing varying amounts of leucosome (referred to in this work as leucogneiss). Migmatitic features and structures developed have been described in Chapter 3 of this work, and more fully in Fitzsimons (1991).

Disrupted metapelitic migmatites with schollen, schlieren and leucosome components mineralogically and texturally similar to the leucosome, mesosome and melanosome components were interpreted by Fitzsimons (*op cit*) as evidence for poor extraction of leucosome. Larger leucogneiss bodies, with discordant contacts against adjacent metapelites probably have larger transport distances than small-scale, isolated stromatic leucosomes, which are interpreted to have migration distances of 1 metre or less. Discordant leucogneiss bodies, which may possibly be injected into the complex rather than locally derived, contain phases identical to those recorded in the mesosome and melanosome, and are clearly related to leucosome bodies within neighbouring stromatic mesosome. If they were not derived locally then they were formed by melting of very similar lithologies. Migration distances not exceeding 100m have been proposed by Fitzsimons, on the basis of similarities in mafic (especially cordierite and garnet) in leucogneisses with the surrounding host lithologies.

The mesosome (metapelitic) and melanosome (aluminous garnet- and cordierite-rich) components of the migmatites show evidence for variable degrees of leucosome (leucogneiss) segregation and retention (Figures 5.1.-5.4.). The spectrum of metapelite textures developed (ranging from stromatic banded migmatites comprised of millimetre thick layers of quartzofeldspathic and aluminous layers to leucosome-rich layers containing rafts and schlieren of mesosome) suggests that leucosome separation was not uniformly efficient. Aluminous melanosome occurs as schlieren in leucogneiss units, and as rarer discordant dykes cross-cutting layering in

Plate 10.

Fig. 5.1. Migmatite containing abundant garnet-rich leucosome. Dark streaks are restitic garnet-sillimanite schlieren. This facies is gradational between MPG and Type II Leucogneiss. Photo - I. C. W. Fitzsimons. Lens cap - 50mm.

Fig. 5.2. Folded banded migmatitic metapelites. Melt proportions in this photograph exceed 50%, but leucogneiss sheets are relatively free of mesosome and melanosome material. Photo - I. C. W. Fitzsimons. Lens cap - 50mm.

Fig. 5.3. Migmatitic metapelitic gneisses cross cut by a cordierite-garnet rich melanosome "vein" up to 10 cm wide. Small patches of felsic or quartzofeldspathic material (pale) are visible in the centre of the vein. Photo - S. L. Harley. Lens cap - 50mm.

Fig. 5.4. Close up of coarse grained garnet-cordierite vein shown in Fig. 5.3. Note small felsic patches between large cordierite (blue) and garnet (reddish-brown) grains. . Photo - S. L. Harley. Lens cap - 50mm.

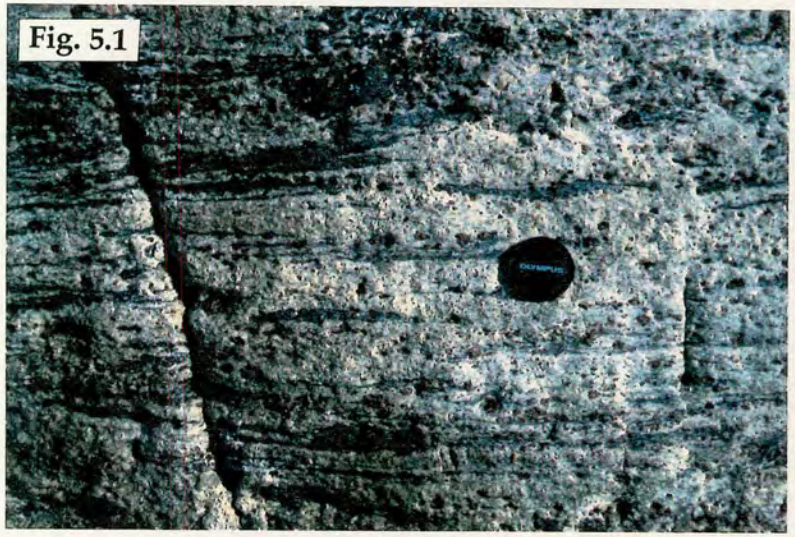
Fig. 5.1


Fig. 5.2

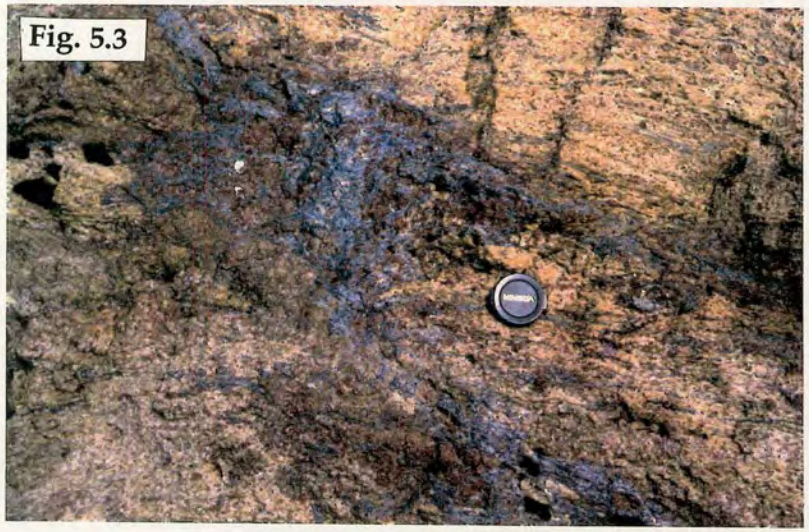
Fig. 5.3


Fig. 5.4

metapelites, similar to cordierite bearing aluminous veins described in the Cooma migmatite complex of southern Australia (White, 1990). Garnet-dominated and cordierite-dominated aluminous gneisses have both been recorded. Both melanosome types are coarse grained relative to metapelitic gneisses. Garnet-rich melanosome is often quartz-absent (or almost quartz-absent, see Section 5.2.2.), while cordierite-rich melanosome contains variable amounts of feldspar and quartz. A complete gradation from aluminous gneisses dominated by cordierite into leucosome containing only small amounts of aluminous material is observed in the field (Fitzsimons, *pers comm*).

The aim of this chapter is to describe the petrography and geochemistry of the metapelites and migmatites of the Brattstrand Bluffs migmatite complex. These data will be used in Chapter 7 to determine the presence or absence of mesosome and melanosome material in samples from the leucogneiss suite, since a knowledge of the petrography and geochemistry of the country rocks is essential if the role of the entrainment and/or unmixing of residual material is to be fully assessed.

5.2. PETROGRAPHY

5.2.1. Metapelitic gneisses

The metapelites of the Brattstrand Bluffs area consist of medium-coarse grained heterogeneous gneisses containing assemblages comprised of varying amounts of garnet, sillimanite, cordierite, quartz, K-feldspar, spinel, ilmenite and biotite. Accessory phases include monazite, zircon and graphite. For a more detailed description of the occurrence and petrography the reader is referred to Fitzsimons (1991), where the petrographic descriptions of evidence for melting reactions and P-T estimates of peak metamorphic conditions are given. Many of the phases, phase relations and textures recorded in the metapelites are similar to those witnessed in leucogneisses (especially the more mafic Type 2 Leucogneisses).

The majority of metapelitic gneisses are banded, and consist of quartz- and K-feldspar-rich bands alternating with more sillimanite-and garnet-rich layers. A pervasive foliation is defined by coarse, prismatic sillimanite, often intergrown with ilmenite and wrapping around garnets (up to 4cm in diameter), quartz and microperthitic K-feldspar. Quartz and K-feldspar in metapelitic samples are more uniform in size than in leucogneises. In all samples Plagioclase is much less abundant than K-feldspar, and is absent in many specimens.

Garnet is the most abundant mafic phase in MPG samples. Type I and Type II Garnets have been recorded and occur in almost equal amounts, in contrast with leucogneisses which principally contain Type II Garnet. Type I Garnets contain small sillimanite and rounded biotite inclusions (up to 100μm in diameter) aligned in trails oblique to dominant sillimanite foliation. These trails are occasionally folded, and only rarely extend to the edge of the garnet grain. Type I Garnet cores frequently have Type II Garnet overgrowths which contain rounded quartz inclusions. Type II Garnets without Type I cores are often extremely pokiloblastic and skeletal.

Cordierite often grows around garnets, forming partial halos which often contain sillimanite and dark green hercynitic spinel in fine-grained, intricate symplectites. These symplectic spl-crd intergrowths often contain resorbed sillimanite and/or garnet. Ilmenite is common, often showing straight grain boundaries against hercynite. Monazite and zircon are the dominant accessory phases. Monazite consists of elongate composite grains up to 300 μm long, comprised of a rounded and embayed core overgrown by a clear (slightly rounded) anhedral rim. Zircon is typically smaller, and two petrographic types have been distinguished. Most zircon occurs as rounded grains up to 100 μm in diameter, but several very small, spindle shaped needles have been recorded. These are more common in the leucogneisses. than the metapelites.

5.2.2. Melanosomes.

The migmatitite terrane of the Brattstrand Bluffs coastline is dominated by variably migmatised pelitic gneisses containing leucogneiss sheets, veins and

stringers. Restitic material, which appears to have undergone extensive removal of melt, comprises only a small component of the migmatite assemblage. This aluminous, magnesian and silica-depleted material is referred to here as melanosome (MEL) because it contains abundant mafic minerals (garnet, cordierite, spinel, biotite, ilmenite) and is depleted in K-Feldspar, plagioclase and quartz relative to the metapelitic gneisses. Strictly speaking the term melanosome refers to the dark, melanocratic portion of a migmatite rather than that part comprised of mafic minerals. Many of the melanosomes from the Brattstrand Bluffs area consist dominantly of garnet, spinel and biotite and can be referred to as melanosome (*senso stricto*). Aluminous lithologies comprised primarily of cordierite and sillimanite (which are therefore relatively leucocratic compared to the mesosome component) have, however, also been termed melanosome in this work. The lithological description *melanosome* has been used for both these lithologies because of their refractory mineralogy and not because they are interpreted to have formed as a result of the same processes, therefore avoiding genetic implications when referring to individual migmatite components.

Most Brattstrand Bluffs melanosomes are quartz-absent, and consist dominantly of coarse garnet, sillimanite, spinel and cordierite. Some are banded (e.g. IF/88/46) on a scale of 1-5 cm, and contain layers of sillimanite with spinel and ilmenite (and rare cordierite) alternating with more cordierite-rich bands. Garnet-rich bands containing cordierite, but no sillimanite, were recorded in the same sample. Garnet tends to be coarse, and finer grained sillimanite-cordierite-spinel matrix wraps around garnet porphyroblasts.

Most garnet found is large, with Type I Garnet cores common, crowded with acicular sillimanite needles aligned and oriented, sometimes folded. These Type I Garnet cores are typically overgrown by inclusion free Type II Garnet rims, forming composite grains up to 3-4 cm in diameter. Garnet is usually slightly elongated parallel to foliation, but sillimanite and small rounded biotite inclusions are generally oblique to the external foliation and often define small folds. Although inclusion-free rims on Type I Garnet are most frequent, sillimanite and fine biotite inclusion trails occasionally extend to grain margins. Type II garnet may have no inclusions, or may contain numerous rounded quartz and, more rarely, pinitised cordierite inclusions.

Small pools of plagioclase +K-feldspar±cordierite and rare small subhedral garnets (Type III garnet) in pressure shadows at ends of garnet have been recorded in IF/88/60 and IF/88/46a, and monominerallic cordierite clusters have been recorded with the same relationship to garnet. In several plag+kfs±crd pools an inclusion-free Type II garnets show development of euhedral crystal faces against plagioclase. In IF/91/178, faces of garnet against coarse prismatic sillimanite suggest that garnet grew after sillimanite.

Cordierite is very abundant in many melanosome samples. In more felsic specimens it may comprise 50-60 volume % of the rock, while garnet-rich melanosome samples contain 10-20 volume %. It occurs in a variety of textural settings. Large garnets in garnet-rich melanosome frequently have cordierite coronas up to 5mm wide, which in turn are surrounded by spinel-sillimanite-cordierite symplectites (e.g. IF/88/58, IF/88/60). These garnets are also commonly cracked, with cordierite (and sometimes microperthitic K-Feldspar) growing along the fractures (IF/88/46a). In more cordierite-rich samples, large rounded cordierite porphyroblasts (5-6mm), sometimes with small sillimanite grains concentrated at margins, are common. This suggests that sillimanite grew before cordierite. In the same samples (e.g. IF/91/360), these large cordierite porphyroblasts occur adjacent to sillimanite-spinel-cordierite intergrowths and polygonal multi-grain aggregates forming the majority of the matrix.

After garnet and cordierite, the most abundant phases in the Brattstrand Bluffs melanosomes are sillimanite and hercynitic spinel. Sillimanite (coarse, prismatic) schlieren wrapping around garnets (and sometimes extending into garnet rims (e.g. 88/58, 88/60)) define the dominant foliation. Acicular sillimanite inclusions in Type I Garnet cores are much finer grained than coarse matrix sillimanite. Coarse prismatic sillimanite with a small amount of anhedral, interstitial quartz has been recorded in IF/91/217, but coarse sillimanite more typically occurs either in monominerallic schlieren (forming clots up to 1mm long) or intergrown with spinel.

Spinel and sillimanite invariably rimmed by and separated from each other by cordierite (e.g. IF/91/178). Spinel is slightly less abundant than sillimanite, and is always found in elongate intergrowths with sillimanite

and cordierite. Ilmenite and biotite inclusions are common, and spinel appears to overgrow the sillimanite foliation in several samples.

Fitzsimons (1991) noted that melanosomes were quartz-absent. Although quartz is very rare, it has been recorded in some of the most mafic, aluminous samples and some (but not all) of the more felsic, cordierite-rich melanosomes often contain small amounts of quartz. IF/88/46a is one of the more aluminous garnet-rich melanosomes, and contains a composite grain comprised of several quartz crystals. This grain is adjacent to two large Type I Garnets with Type II overgrowths, and appears fractured and dissimilar to most quartz found in leucogneisses, which tends to be late and interstitial. Large K-Feldspar crystals containing tiny rounded quartz blebs as inclusions near rims were recorded in the garnet-rich melanosome IF/88/60, while cordierite from IF/88/46a contains similar small quartz inclusions. More cordierite-rich melanosomes such as IF/91/217 may have quartz-plagioclase pools in pressure shadows around garnet, or they may have no quartz or feldspar and consist only of cordierirte, sillimanite, spinel and garnet. Quartz in melanosomes is invariably associated with either large, microperthitic K-Feldspar and/or antiperthitic plagioclase. K-Feldspar tends to form large (up to 1mm long), anhedral grains elongate parallel to foliation, while plagioclase is most often found in small pressure shadow pools on garnet margins.

Monazite and zircon are very abundant in most melanosomes. Because of the abundance of cordierite they can easily be distinguished by their pleochroic haloes. Upwards of fifty monazite and zircon grains per single thin-section can easily be distinguished by eye in some samples. No apatite was recorded, even when samples were studied using cathodoluminescence.

5.3. GEOCHEMISTRY OF THE METAPELITIC GNEISSES (MPG).

5.3.1. Major Elements.

Metapelitic Gneisses (MPG) from Brattstrand Bluffs have variable SiO_2 contents ranging from 57.98 to 69.55 wt %. SiO_2 contents are typically higher

than those of PAAS (Post Archaean Average Shale - 62.8 wt %), while Al_2O_3 concentrations are, on average, lower (14.60 - 21.25 wt %) and show a strong negative correlation with SiO_2 (Figure 5.5). Molecular A/CNK values are variable and range from 1.36 to 4.40. Fe_2O_3 contents range from 5.98 to 11.18 wt%, while MgO contents are lower (1.39 - 3.71 wt %). Bulk rock X_{Mg} ((MgO/40.32) / (MgO/40.32) + (Fe_2O_3/159.70)) values vary from 0.21 to 0.46. Relative to PAAS the Brattstrand Bluffs Metapelitic gneisses are generally more iron-rich (PAAS Fe_2O_3 = 6.5 wt %) but have similar magnesium contents.

CaO concentrations are typically low (0.57 - 0.98) except for two samples (IF/88/146B and IF/88/147) which have CaO contents of 3.23 and 3.77 wt % respectively. Na_2O concentrations are generally higher (mean Na_2O = 1.58 wt %) with the samples listed above having the highest Na_2O contents. With the exception of samples 146B and 147, both Na_2O and CaO show a positive correlation with SiO_2. K_2O contents are variable, but show a similar positive correlation with SiO_2 except for the most silica-rich sample (IF/88/35). Samples 146B and 147 have the lowest K_2O contents recorded. The Brattstrand Bluffs metapelitic gneisses are depleted in CaO and slightly enriched in Na_2O relative to PAAS. TiO_2 contents show a strong negative correlation with SiO_2, and are typically lower than 1.0 wt %. Both P_2O_5 and MnO concentrations are very low.

Many of the more SiO_2-rich MPG have major-element chemistry similar to that of Type 2 Leucogneisses. Al_2O_3, MgO and Na_2O contents are almost identical in both lithologies, while CaO is higher in LG2 and Fe_2O_3 is higher in metapelitic gneisses. Molecular A/CNK values are higher in metapelitic gneisses. Relative to Type I Leucogneisses the metapelitic gneisses are enriched in Al_2O_3, Fe_2O_3, MgO and TiO_2 and depleted in CaO, Na_2O and K_2O.

5.3.2. Trace Elements.

Trace element concentrations for metapelitic gneisses from the Brattstrand Bluffs area are given in Appendix A, and the average MPG trace element concentration normalised to PAAS is shown in Figure 5.8. Cr, and Sc concentrations are slightly higher than typical shale values, while V and Ni

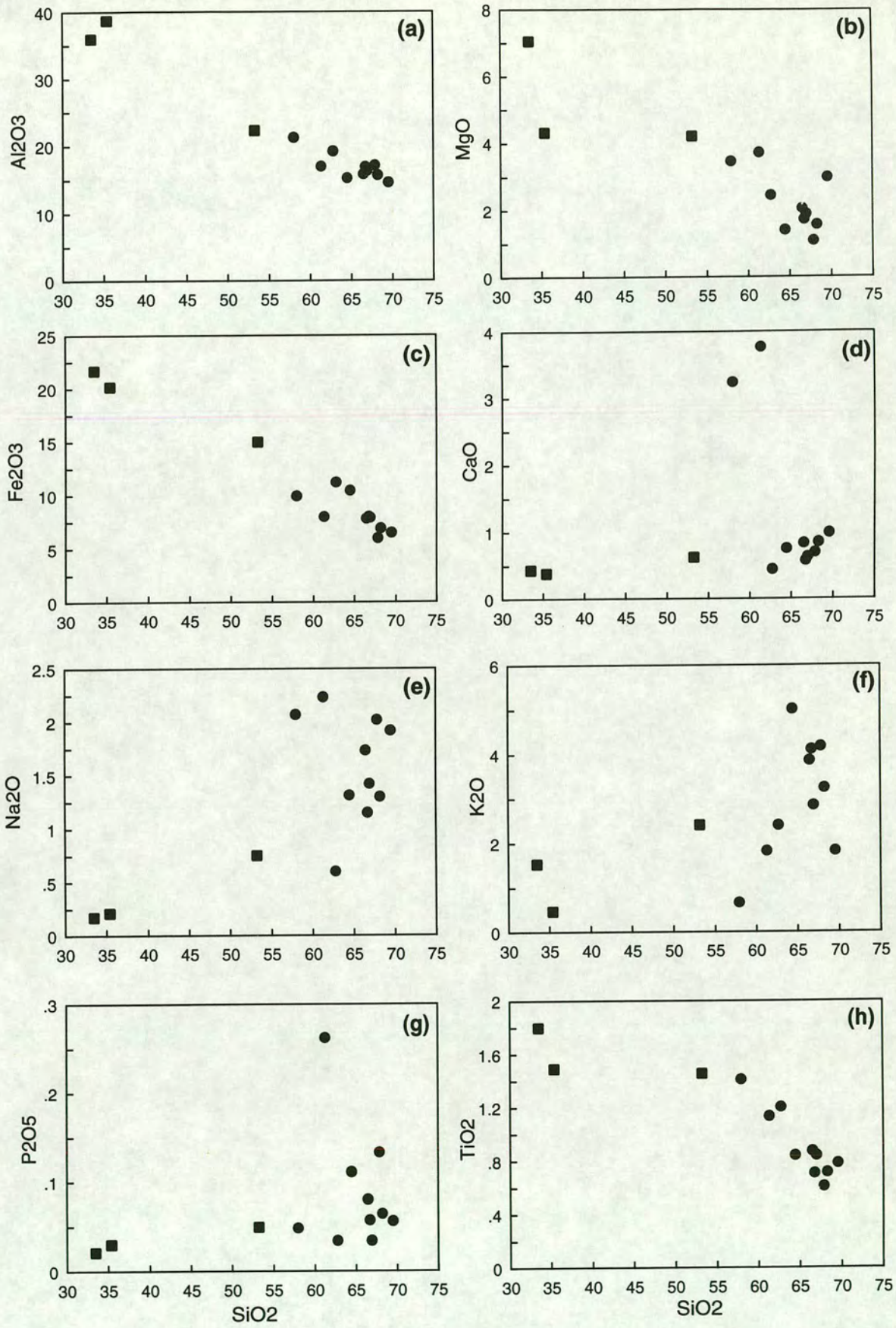

Figure 5.5. Major element Harker plots. This and all other graphs: MPG - solid circles; MEL - solid squares

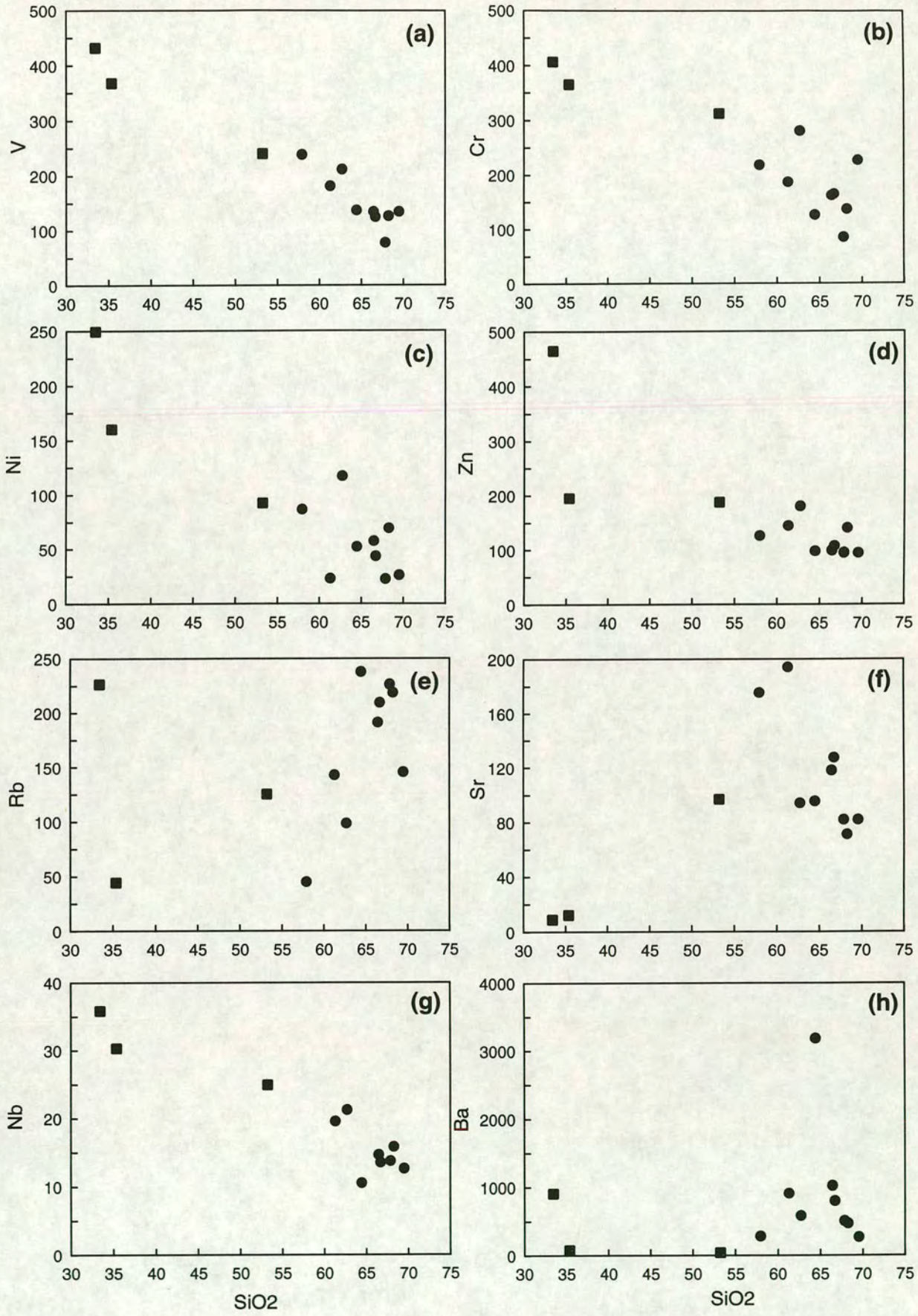

Figure 5.6. Trace element Harker plots. Symbols as Fig. 5.5.

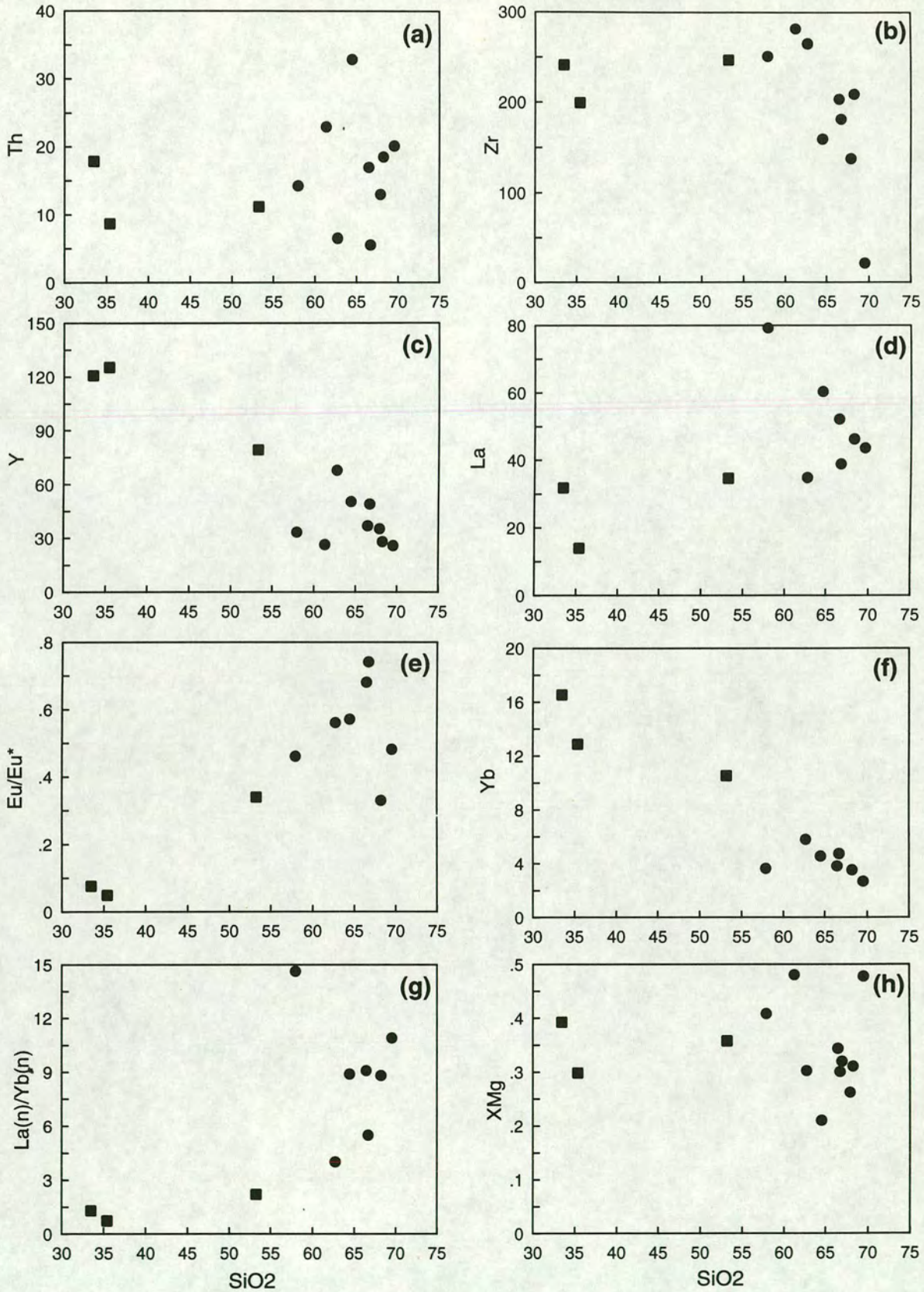

Figure 5.7. Trace element Harker plots. Also shown is XMg against SiO2. Symbols as Fig. 5.5.

concentrations are slightly lower (with the exception of high V concentrations in CaO-rich samples). V concentrations show a negative correlation with SiO_2.

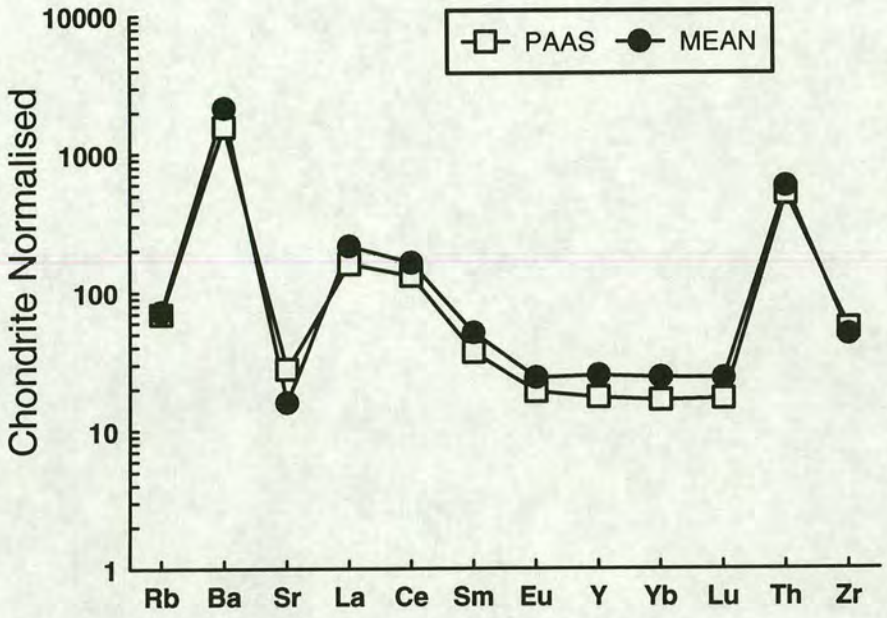

Figure 5.8. Trace Element Spidergram for Average Brattstrand Bluffs MPG vs Post Archaean Average Shale (PAAS).

Ba concentrations are variable, and range from 268 ppm to 1020 ppm. Rb and Sr contents show less variation. Rb/Sr values are typically greater than 1.0, and vary between 1.04 and 3.08 (with the exception of IF/88/146B and IF/88/147 which have higher Sr contents (>175ppm) and relatively low Rb concentrations (Rb/Sr = 0.26 and 0.74 respectively). The high Sr contents of these samples reflect high CaO values. Th contents are slightly enriched in the average MPG relative to PAAS, while Zr is marginally depleted. This may be due to the very low Zr content of IF/88/35 used in calculating the mean MPG Zr content (35ppm). If this is removed from the calculation, the average Zr concentration of the metapelitic gneisses is 210 ppm, identical to that of PAAS.

Trace element concentrations in metapelitic gneisses are similar to those of Type 2 Leucogneisses. Both are depleted in Sr and enriched in Ba and light and heavy rare-earth elements relative to PAAS (see below). The granulite-

facies metapelites show neither the marked depletion in LREE, Th and Zr exhibited by Type I Leucogneisses, nor the extreme enrichment in Th and LREE shown by the Type 3 Leucogneisses. Both Type I and Type 3 Leucogneisses are depleted in HREE relative to PAAS, while the metapelites show enrichment.

5.3.3. Rare-Earth Elements.

Metapelitic gneisses exhibit REE patterns and absolute LREE and HREE abundances very similar to those of the Type 2 Leucogneisses (Figure 5.9.). LREE portions of the curves are convex-up, while flat HREE distributions are most common. MPG have the least fractionated REE patterns of the lithologies studied (mean $La_{(n)}/Yb_{(n)} = 8.4$). Eu anomalies are moderately to strongly negative, and range from 0.33 to 0.74 (mean $Eu/Eu^* = 0.6$). Absolute Eu concentrations are slightly lower than in other suites. REE concentrations and patterns in MPG's are very similar to those of the average post-Archaean Australian shale (PAAS), with a slight enrichment of LREE in some samples (mean MPG $La_{(n)} = 145.1$ compared to mean PAAS $La_{(n)} = 115.2$).

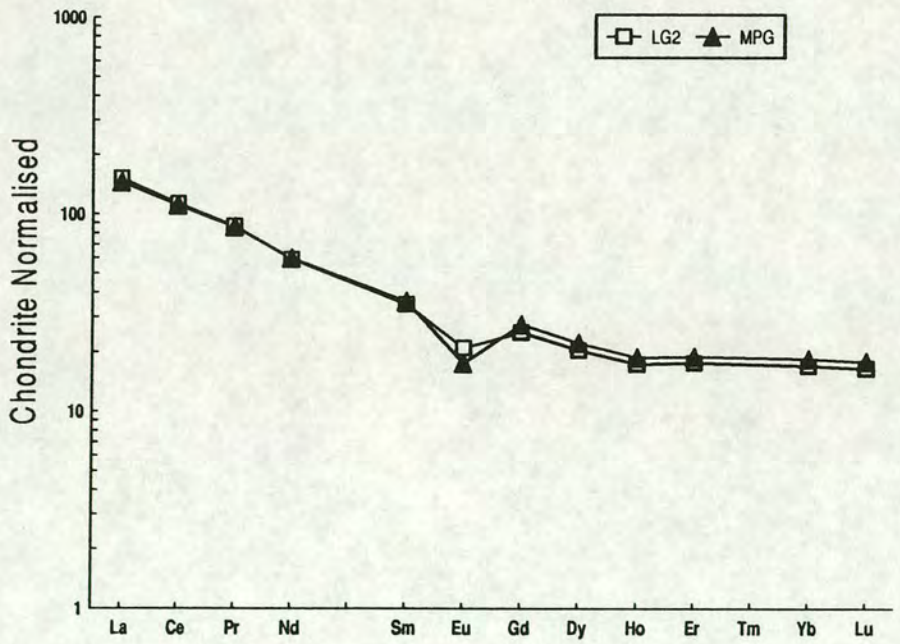

Figure 5.9. REE curves for Average MPG and Average LG2.

5.4. GEOCHEMISTRY OF THE MELANOSOMES.

Only a small amount of geochemical data has been collected from the Melanosomes of the Brattstrand Bluffs coastline. This is summarised in Appendix A. Petrographically melanosomes fall into two broad groups. Garnet-rich melanosomes are typically quartz-absent, and have assemblages dominated by large garnets, sillimanite, matrix cordierite and spinel-cordierite symplectites. Cordierite-rich melanosomes may be pegmatitic, slightly more felsic and often contain a little quartz. The more cordierite-rich samples show a gradation into coarse quartz-bearing granitic leucogneisses.

Samples IF/88/46A and IF/88/58 are garnet-rich melanosomes, and are characterised by extremely low SiO_2 contents (<36 wt % SiO_2), and very high Al_2O_3, Fe_2O_3, and MgO contents. Alumina contents are almost twice those of the more silica-rich metapelitic gneisses (35.90, 38.67 wt % Al_2O_3 in IF/88/46C and IF/88/58 respectively). CaO, Na_2O and K_2O contents are very low in garnet-rich melanosomes, with Na_2O values less than one-tenth of metapelitic gneisses concentrations. The combination of high Al_2O_3 and low CaO, Na_2O and K_2O gives extremely high molecular A/CNK values.

Garnet-rich melanosomes have extremely high transition-element concentrations relative to both metapelitic gneisses and leucogneisses. Cr and V contents are greater than 360ppm, while Ni and Zn contents are also enriched relative to metapelitic gneiss concentrations. High-field-strength elements (Zr, Th, U) are very similar to values from MPG samples. The slightly higher K-Feldspar content of IF/88/46C relative to IF/88/58 is evident in incompatible element concentrations. While both samples have extremely low Sr contents, (<15ppm), Ba and Rb are much higher in IF/88/46C than IF/88/58.

Melanosome REE patterns are very distinctive relative to metapelitic gneisses and leucogneisses (Figure 5.10.). Curves are generally flat (maximum La(n)/Yb(n) = 2.2), slightly concave-up at the LREE end and have large negative Eu anomalies (Eu/Eu* for IF/88/58 = 0.05). Absolute LREE concentrations are slightly lower than the metapelitic gneisses, but HREE abundances are higher and do not show any decrease from Gd to Lu in chondrite normalised plots. Overall, REE patterns in melanosomes are

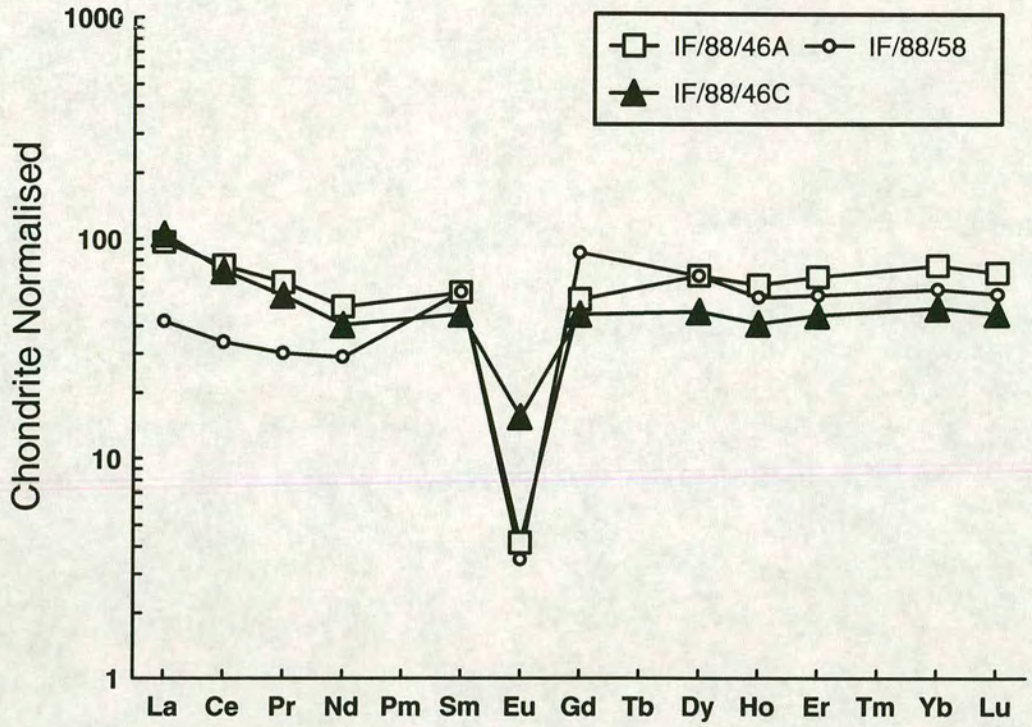

Figure 5.10. Melanosome REE patterns.

very similar to REE patterns shown by garnet. LREE abundances, however, are much higher even in garnet-rich (and often almost feldspar-absent) samples than in garnet analyses.

Chapter 6

Mineral Chemistry.

Chapter 6. Mineral Chemistry.

6.1. INTRODUCTION.

The assimilation of restitic or source rock phases in a melt during extraction will alter melt chemistry to some extent. The recognition of partially assimilated material is important if the processes involved in melt extraction in migmatite terranes are to be fully understood. It may be possible to identify restitic or entrained phases in melts on the basis of distinctive major- or trace-element compositions (see Section 2.6.1). Alternatively, restite and melt phases may have identical chemistry if melting is rapid and source material is unable to equilibrate before melt is extracted. This mechanism has been proposed to explain the lack of fractionation in plagioclase feldspar between melanosome and melt in some migmatites (e.g. the so-called "plagioclase problem"; see Ashworth, 1985). Mineral chemistry, combined with detailed textural analysis of entrained phases may therefore provide a powerful petrogenetic tool. This Chapter aims to describe the chemistry of major and accessory phases found in the melt and host lithologies in migmatites from the Brattstrand Bluffs area. The extent to which variations in mineral composition between lithologies and petrographic occurrences of individual phases can be used to determine melting processes is discussed in Chapters 7 and 8.

Major and trace element analyses of K-feldspar, plagioclase, garnet and biotite in Type 1 and Type 2 Leucogneiss, Melanosome and metapelitic gneiss specimens from the Brattstrand Bluffs coastline were determined by wavelength-dispersive electron-probe analysis (major elements) and secondary ion mass spectroscopy (trace and rare earth elements). Major element concentrations for monazite and zircon were also performed using wavelength-dispersive electron-probe analysis. Type 3 Leucogneisses have a major element chemistry which overlaps that of Type 1 and Type 2 Leucogneisses, but show enrichment of certain trace elements (principally LREE and Th). Since the principal geochemical distinction between Type 3 Leucogneisses and the other leucogneiss types is based on trace element concentrations, electron-probe analysis in LG3 samples was restricted to

accessory phases which contain the relevant trace elements in detectable amounts.

Full details of the instruments, operating conditions, analytical precision and acuracy and standards used, as well as representative anlyses of the phases above for each lithology, are given in Appendix C. For ease of comparison with the petrography and bulk-rock chemistry the mineral data (with the exception of accessory phases) is presented by lithology. Fitzsimons (1991) carried out a detailed electron-probe study of seventeen metapelite specimens from the Brattstrand Bluffs area. To avoid duplication of this work, only a limited amount of electron-probe analysis was performed on metapelite specimens; major element mineral chemistry was carried out for calibration of ion-probe work and some detailed accessory phase analysis was accomplished. Since the objective of the electron probe work was to determine whether source and residue phases entrained in a granitic melt can be recognised on the basis of major element chemistry the phase data of Fitzsimons (*op cit*) has been used for comparative purposes. The use of this data is acknowledged where relevant.

6.2. TYPE 1 LEUCOGNEISSES.

6.2.1. K-feldspar.

K-feldspar is the most abundant feldspar in all leucogneiss samples studied. Representative anlyses are given in Appendix C. A triangular X_{or}-X_{ab}-X_{an} plot for K-feldspar and plagioclase in leucogneiss, Melanosome and metapelitic gneiss specimens is shown in Figure 6.1. Calcium contents are low, ranging from 0.158 wt % CaO to 0.729 wt %. X_{an}^{kfs} is less than 0.04 in all specimens, and is highest in samples with high X_{ab}^{kfs}. X_{or}^{kfs} is typically in the range 0.73 to 0.84, and X_{ab}^{kfs} varies from 0.15 to 0.23. Na-rich spot analyses represent more sodic microperthite stringlets. There appears to be no difference in chemistry between large K-feldspar prophyroblasts with inclusions of quartz and/or sillimanite and smaller, anhedral, syn-S3 K-feldspar grains. FeO, MnO and MgO contents are negligible.

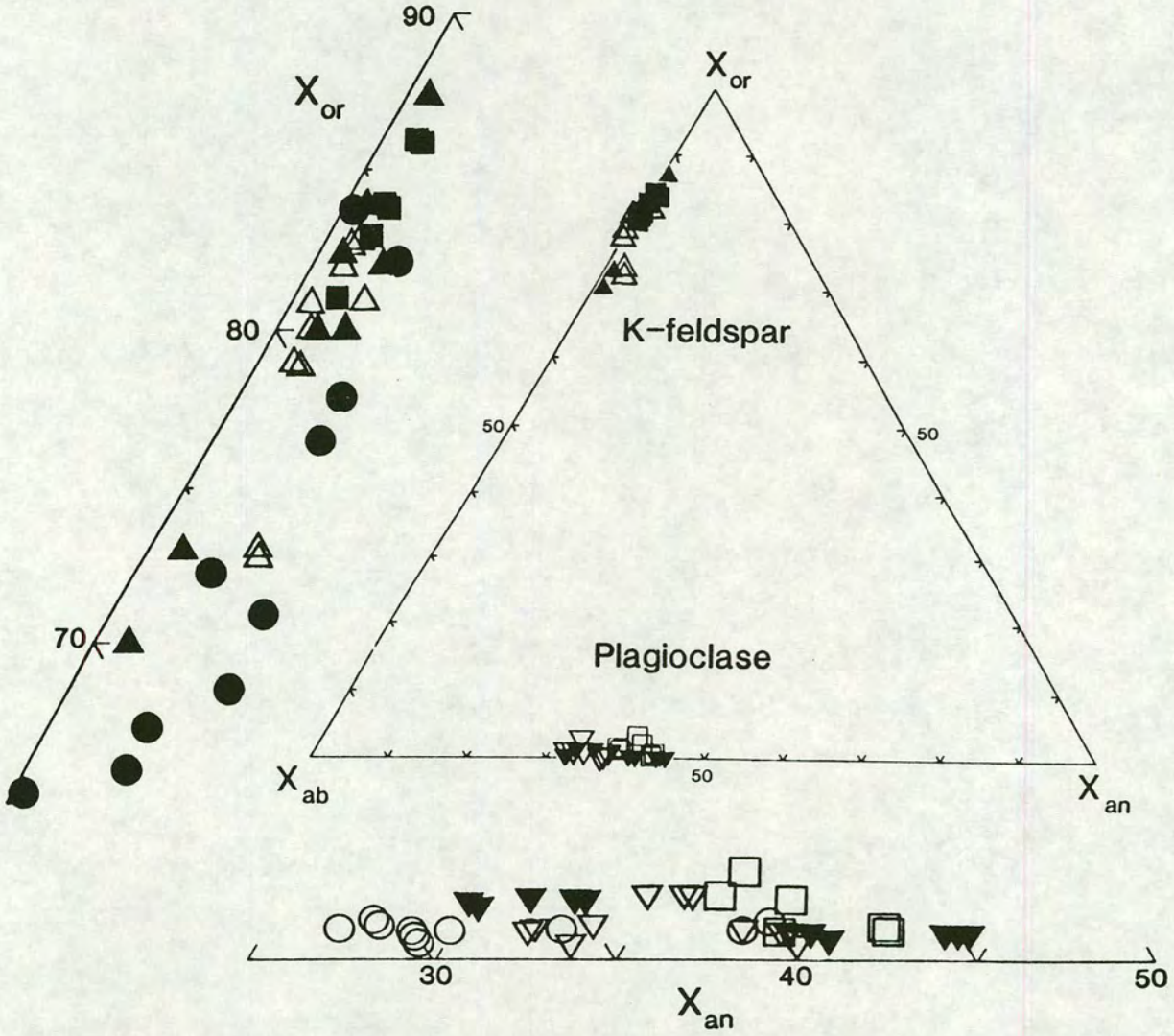

Figure 6.1. X_{or}-X_{ab}-X_{an} diagram showing K-feldspar and plagioclase compositions for LG1, LG2, MPG and MEL. Symbols:(a) Plagioclase; LG1 - open triangles; LG2 - filled triangles; MPG - open circles; MEL - open squares. (b) K-feldspar; LG1 - open triangles; LG2 - filled triangles; MPG - filled circles; MEL - filled squares.

Trace element concentrations for K-feldspar are given in Appendix D and REE curves are shown in Figure 6.2. REE distributions are typical for feldspars (e.g Gromet & Silver, 1978), with steeply fractionated LREE, large positive Eu anomalies and relatively flat HREE curves. Eu/Eu* values range from 20.3 to 63.6. A slight increase in the middle HREE (Ho, Er) relative to Gd was recorded in most samples. The only trace elements present in important quantities are Ba, Rb and Sr. Rb concentrations vary between 390 and 520 ppm and Rb/Sr values range from 1.6 to 3.7. Ba contents are relatively low (maximum Ba content = 1830 ppm).

6.2.2. Plagioclase.

Two main petrographic occurrences of plagioclase have been recorded in Type 1 Leucogneisses. Large, subhedral plagioclase grains are less abundant than later, anhedral, fine-grained plagioclase. Both petrographic types classify chemically as andesine. Plagioclase compositions are shown in Figure 6.1. X_{or}^{plag} is lower than 0.02 for almost all samples. X_{an}^{plag} varies from 0.32 to 0.40, and, while subidiomorphic plagioclase appears slightly more calcic than anhedral plagioclase, two chemically distinct plagioclase compositions are not evident.

Trace element concentrations in plagioclase are shown in Figure 6.2.e, and are tabulated in Appendix D. Plagioclase REE distributions are unusual, showing no positive Eu anomaly. Eu/Eu* values are less than 1.0. Chondrite-normalised LREE totals are higher than those of K-Feldspar in Type 1 Leucogneisses (mineral/chondrite values of 130-140 compared to 30-50), giving more steeply fractionated patterns. Plagioclase from Type 1 Leucogneisses, Type 2 Leucogneisses and metapelitic gneisses have similar REE curves with no positive Eu anomaly. LREE abundances in plagioclase from LG1 samples are lower than in plagioclase from other lithologies.

6.2.3. Garnet.

One major aspect of the electron microprobe study of garnet in the Brattstrand Bluffs migmatites was to establish whether restitic, peritectic and

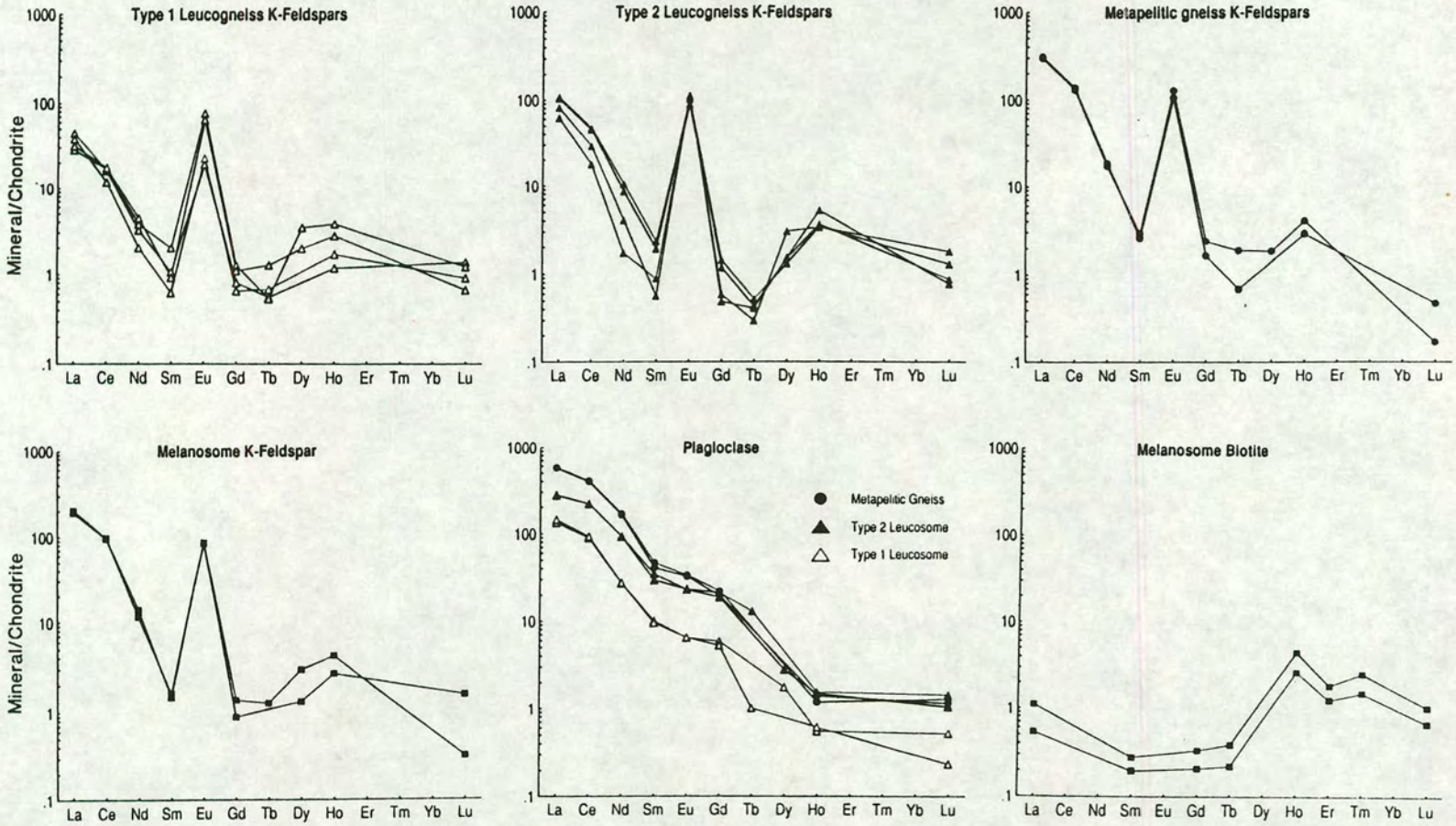

Figure 6.2. Chondrite normalised REE patterns for K-feldspar, plagioclase and biotite from Brattstrand Bluffs samples.

garnets precipitated from granitic melts could be distinguished from one another in leucogneiss lithologies. Garnet is rarer in Type 1 Leucogneisses than Type 2 Leucogneisses, but is the most important LG1 ferromagnesian phase. Two petrographic occurrences of garnet have been recorded in Type 1 Leucogneisses.

All garnets in the Type 1 Leucogneisses are almandine rich. FeO concentrations are relatively constant, and range from 33.77 to 34.19 wt %. Fe^{3+} contents are low (maximum Fe^{3+} (cations per 12 oxygens) = 0.24, compared with Fe^{2+} (cations per 12 oxygens) in the same analysis = 2.26). X_{alm}^{grt} varies from 0.62 to 0.72. X_{mg}^{grt} is relatively constant (0.23-0.24) and $X_{Mg^*}^{grt}$ similar due to low Fe^{3+} totals. Mn contents in both garnet types are low (maximum $X_{spess}^{grt} = 0.02$), and grossular contents are insignificant.

No major difference in X_{alm}^{grt} between Type A (containing small biotite and sillimanite inclusions, often aligned in trails) and Type B garnets (which are either inclusion free or poikiloblastic and contain large rounded quartz blebs). Type A garnets have slightly lower X_{Mg}^{grt} values than Type B garnets. This is most marked adjacent to small biotite inclusions. Low X_{Mg}^{grt} values in Type B garnets were recorded adjacent to cordierite overgrowths. Similar findings for Type A and Type B garnets in metapelitic gneisses were noted by Fitzsimons (1991).

Trace element concentrations in Type B garnet from Type 1 Leucogneisses are shown in Figure 6.3.d and are tabulated in Appendix D. REE curves show strongly enriched HREE totals (Lu mineral/chondrite values of 120), large negative Eu anomalies and low LREE concentrations. Sm concentrations are lower than in Type B garnets from melanosomes, metapelites and Type 2 Leucogneisses, probably reflecting lower bulk rock LREE concentrations.

The only other trace elements present in garnets from Type 1 Leucogneisses in any quantity are Y and Zr. Zr concentrations are very low (15 to 30ppm) relative to garnets from other Brattstrand Bluffs lithologies, reflecting low bulk-rock Zr concentrations in Type 1 Leucogneisses. Y concentrations are similar to Type B garnet in other lithologies.

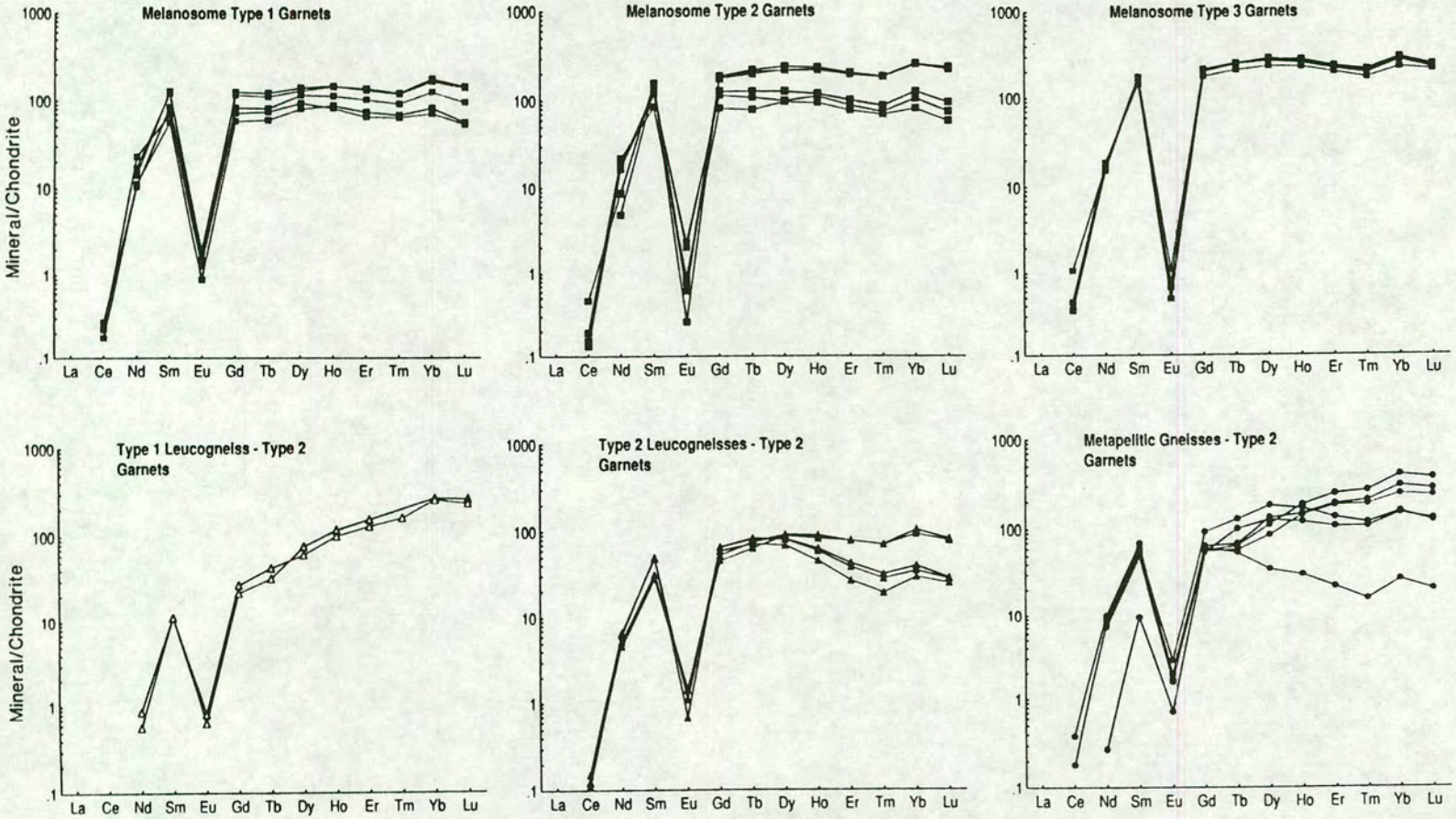

Figure 6.3. Chondrite normalised garnet REE patterns from Brattstrand Bluffs samples.

6.3. TYPE 2 LEUCOGNEISSES.

6.3.1. K-feldspar.

K-feldspar is more abundant than plagioclase in all Type 2 Leucogneisses. Representative analyses are shown in Appendix C, and plotted in Figure 6.1. Compositions are almost identical to those of K-feldspar in Type 1 Leucogneisses. X_{an}^{kfs} is invariably low (maximum = 0.07) reflecting low CaO contents. X_{or}^{kfs} ranges from 0.71 to 0.88. Lower orthoclase contents represent Na-rich stringlets in perthitic K-feldspar. These sodic patches are identical in composition to the perthitic K-feldspar of the Type 1 Leucogneisses. Although both petrographic types of K-feldspar have been recognised in LG2 samples, like Type 1 Leucogneiss K-feldspars these cannot be distinguished chemically.

K-feldspar REE patterns in Type 2 Leucogneisses are very similar in shape to those in Type 1 Leucogneisses. They have strongly fractionated LREE distributions, very large positive Eu anomalies and flat or hump-shaped HREE curves. La and Ce concentrations are slightly higher in LG2 K-feldspar relative to LG1 K-feldspar, while Sm concentrations are almost identical. Eu/Eu* values are larger than those LG1, ranging from 57 to over 200. Rb/Sr values range from 1.21 to 1.72, and are lower in Type 2 Leucogneiss K-feldspar than Type 1 Leucogneiss K-feldspar. Ba contents are, on average, almost double those of K-Feldspar from Type 1 Leucogneisses.

6.3.2. Plagioclase.

Although K-feldspar is more abundant than plagioclase in Type 2 Leucogneisses (LG2), plagioclase is more common in LG2 samples than in any of the other migmatite components. Both petrographic types of plagioclase are found in Type 2 Leucogneisses; subhedral tablets are more common in Type 2 Leucogneisses than in Type 1 Leucogneisses. Both subhedral plagioclase and late, anhedral plagioclase have compositions which classify them as andesine (X_{an}^{plag} varies from 0.32 to 0.45), but two distinct plagioclase compositions can be recognised. Subhedral, earlier

plagioclase is more calcic (X_{an}^{plag} ranges from 0.40 to 0.45) while anhedral plagioclase has X_{an}^{plag} values which vary between 0.32 and 0.35. No plagioclase compositions in the range X_{an}^{plag} 0.35-0.40 have been recorded in the Type 2 Leucogneisses. Metapelitic gneiss plagioclases show a similar compositional distribution (see Section 6.5.). X_{or}^{plag} is low for all samples, and Fe + Mg + Mn cation totals are always less than 0.01.

Ion-microprobe analysis of plagioclase in Type 2 Leucogneisses was restricted to anhedral, late plagioclase and no analyses were obtained from subhedral plagioclase. Plagioclase from Type 2 Leucogneisses has similar REE patterns to that found in Type 1 Leucogneisses, but both LREE and HREE abundances are greater. No positive Eu anomaly was recorded. Sr contents are approximately double those of plagioclase from LG1 samples, and Ba contents are similarly higher.

6.3.3. Garnet.

Garnet is very abundant in Type 2 Leucogneisses, comprising up to 20 % (by volume) in some samples. Two main petrographic occurrences of garnet have been recorded in Type 2 Leucogneisses -Type A (inclusion-rich) garnet cores are often overgrown by xenoblastic Type B garnet. Poikiloblastic-xenoblastic Type B garnet is the most abundant garnet type present in all leucogneiss samples. Type C garnet (small, euhedral garnet occurring as individual grains) was recorded in one sample.

Garnets in Type 2 Leucogneisses are relatively similar in composition to those from Type 1 Leucogneisses. They are Fe-rich almandine garnets, and, like the Type 1 Leucogneisses, no major differences between Type A and Type B garnets are apparent. FeO contents range from 30.83 to 32.59 and X_{alm}^{grt} varies from 0.58 to 0.64. The slightly more magnesian composition of garnets in Type 2 Leucogneisses is also reflected in higher X_{Mg}^{grt} values, which range from 0.23 to 0.30, but tend to exceed X_{Mg}^{grt} = 0.27. Fe3+ values are lower in Type 2 Leucogneiss than in Type 1 garnets due to the charge balance calculation procedure. A decrease in X_{Mg}^{grt} adjacent to cordierite rims and small biotite inclusions is recorded in garnet in Type 2 Leucogneisses.

Type C garnets in sample IF/88/119 are very similar in composition to both Type A and Type B garnets. They are Fe-rich almandine garnets, with FeO contents ranging between 31.1 and 31.3 wt % and X_{Mg}^{grt} values of 0.30. Mg and Fe contents are almost identical to those of Type A and B garnets. Both CaO (maximim CaO = 1.26 wt %) and MnO (maximum = 0.68 wt %) are low, and have similar values in all three garnet types.

Trace element concentrations in Type B garnet are given in Appendix D and REE curves are shown in Figure 6.3. LREE totals are slightly higher, giving larger negative Eu anomalies. The HREE portions of the REE curves have a characteristic flat or slightly depleted nature, similar to Type B garnets from melanosome and some metapelitic gneiss Type B garnets. HREE abundances are lower than in Type 1 Leucogneiss garnets. Zr contents are higher than garnet from Type 1 Leucogneisses, ranging from 35 ppm to 82 ppm, while Y contents are similar.

6.3.4. Biotite.

A limited amount of electron microprobe work was performed on biotites in Type 2 Leucogneisses, to determine whether there were compositional differences between biotite inclusions in Type B garnet and matrix biotite which overgrows the dominant foliation and is interpreted to have grown after melting.

Biotite inclusions are slightly richer in Al_2O_3, MgO and Na_2O, and have lower FeO contents than matrix biotite from the same sample. Titanium contents range between 0.64 and 0.76 cations per formula unit normalised to 14 octahedral and tetrahedral cations. A plot of FeO against TiO_2 for biotites from Type 2 Leucogneisses (Figure 6.4.) shows that biotite inclusions in Type B garnet have higher TiO_2 contents as well as consistently lower FeO. X_{Mg}^{Bt} values are relatively constant within each sample, and are higher in biotite inclusions than in matrix biotite.

Six ion-microprobe analyses of biotite were performed. REE contents of biotites were uniformly low in Type 2 Leucogneisses, melanosomes and metapelites,and chondrite-normalised plots show relatively flat curves with

little or no HREE enrichment in biotite inclusions in garnet or late matrix biotite. Rb contents range from 420 ppm to 1030 ppm, while Sr varies from 105 ppm to 430 ppm. Sr is lowest in Type 2 Leucogneiss.

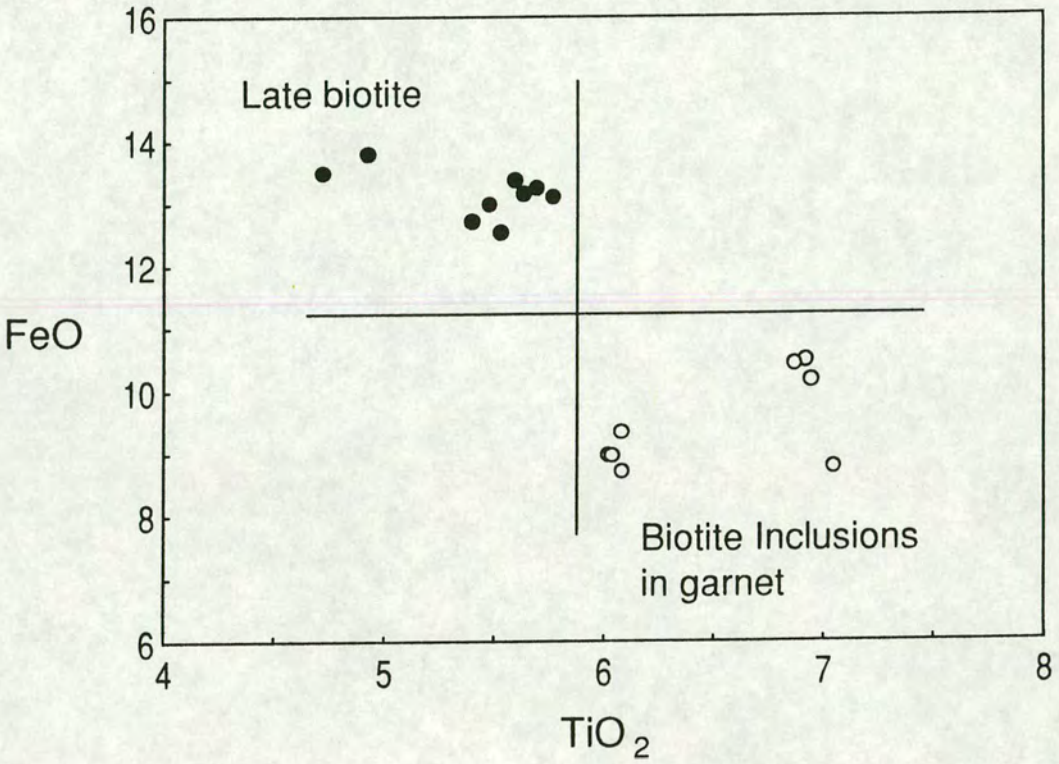

Figure 6.4. FeO against TiO_2 for biotite from LG2.

6.4. MELANOSOMES.

6.4.1. K-feldspar.

Large porphyroblastic K-feldspar is common in Melanosome samples from the migmatites of the Brattstrand Bluffs area, and anhedral K-feldspar has also been recorded. Plagioclase is much rarer than K-feldspar, and may be absent in the more restitic (less felsic) samples. K-feldspars in Melanosomes are typically orthoclase-rich, and sodic perthite stringlets are rarer than in K-feldspars from other lithologies. X_{or}^{Kfs} varies from 0.81 to 0.85, and CaO contents are low (maximum $X_{an}^{kfs} = 0.014$). K-feldspar in the Melanosomes is

compositionally very similar to the orthoclase rich K-feldspar of the Type 1 and Type 2 Leucogneisses.

K-feldspar REE curves are shown in Figure 6.2. They are almost identical to leucogneiss K-feldspar REE patterns, with large positive Eu anomalies (Eu/Eu* = 60-67) and steeply fractionated LREE concentrations. LREE contents are higher than K-feldspars from leucogneiss samples (mineral/chondrite values of 190-204), while HREE contents are similar. Ba contents are lower than those from Type 2 leucogneisses, while Rb/Sr values are similar (1.55 - 1.65).

6.4.2. Plagioclase.

Plagioclase in Melanosome lithologies is rare, and invariably occurs as tablet shaped subhedral grains or in plagioclase rich polygonal recrystallised aggregates formed in pressure shadows around large garnets. No anhedral plagioclase has been recorded in Melanosome lithologies.

X_{an}^{plag} in Melanosome samples varies from 0.39 to 0.43, and all plagioclase is therefore andesine in composition. Unlike the leucogneiss specimens, no plagioclase with X_{an}^{plag} values of approximately 0.30-0.33 has been recorded. X_{or}^{plag} contents are low in all anlyses (maximum $X_{or}^{plag} = 0.03$), and Fe + Mn + Mg cation totals (normalised to 8 oxygens) do not exceed 0.01.

6.4.3. Garnet.

Garnet is the most abundant ferromagnesian phase in the Brattstrand Bluffs Melanosome samples. It is much coarser grained than in the leucogneiss samples, and is often comprised of composite Type A garnet cores with Type B garnet rims. Rare Type C garnet has been recorded. Garnet end-member compositions are shown as X_{spess}^{grt} against X_{alm}^{grt} and X_{prp}^{grt} against X_{alm}^{grt} plots in Figure 6.5.

Type A garnets have X_{alm}^{grt} values ranging from 0.62 to 0.68, and X_{alm}^{grt} in Type B garnet ranges from 0.61 to 0.66. FeO and MgO concentrations in Type

A and Type B garnets are very similar, and X_{Mg}^{grt} values are in the range 0.25-0.30 for both types.

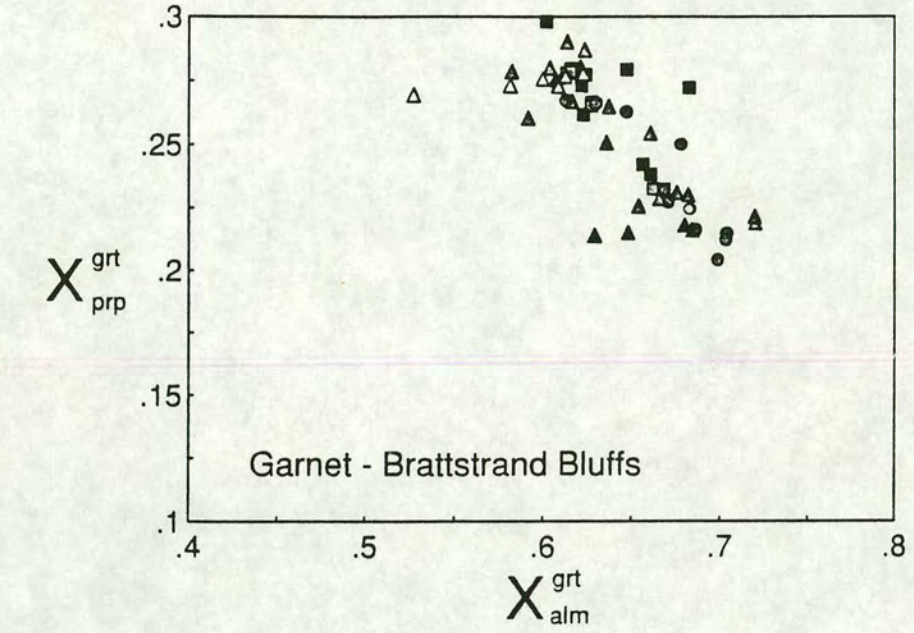

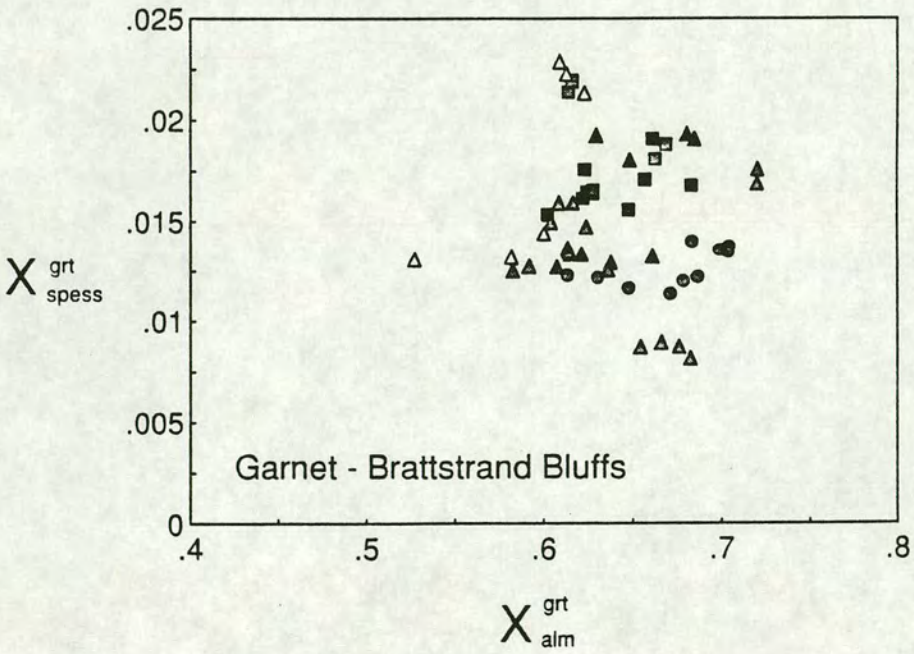

Figure 6.5.a. Xprp vs Xalm for garnets from Brattstrand Bluffs samples. Symbols: Type I Garnet; MEL - solid squares; MPG - solid black triangles. Type II Garnet; LG1 - open triangles; LG2 - shaded triangles; MPG, shaded circles.

Figure 6.5.b. Xspess vs Xalm for garnets from Brattstrand Bluffs samples. Symbols: Type I Garnet; MEL - solid squares; MPG - solid black triangles. Type II Garnet; LG1 - open triangles; LG2 - shaded triangles; MPG, shaded circles.

Type C garnets in IF/89/325 have X_{Mg}^{grt} = 0.30, and in terms of their Fe and Mg contents and low CaO concentrations are indistinguishable from Type A and B garnets. MnO in Melanosome garnets does not exceed 1.10 wt %, and is no higher in Type C (euhedral) garnet than in Types A or B. It is not, therefore, possible to distinguish Types A, B and C garnets in Melanosomes on the basis of their major element chemistry.

Ion-microprobe analysis of Type A, B and C garnet was performed for a number of melanosome samples. REE curves are shown in Figure 6.3. All three garnet types show similar patterns. LREE contents are similar or slightly higher than Type B garnet in Type 2 Leucogneisses, and Eu anomalies are large and negative. HREE patterns are flat and HREE abundances are relativey constant for all three garnet types. Zr concentrations are significantly higher in garnets from melanosomes than from leucogneiss lithologies. Zirconium in Type A garnet ranges from 81 to 164 ppm, in Type B garnet from 96 to 161ppm and in Type C garnet from 78 to 160ppm. One analysis of a Type C garnet gave a Zr content of 656 ppm, which probably represents a partial analysis of small zircon inclusion. Y contents in all garnet types are similar those recorded in Type B garnets from leucogneisses.

6.5. METAPELITIC GNEISSES.

As outlined in Section 6.1., the aim of the electron-microprobe work is to determine whether major element chemistry of phases interpreted as having restitic, peritectic and melt precipitated origins can be used to determine the important processes active during melt extraction and/or retention in a partial melting event. This Section aims to compare electron-microprobe data from variably migmatised metapelitic gneisses from the Brattstrand Bluffs area sampled and analysed by Fitzsimons (1991) with similar data from leucogneisses and Melanosome samples. Trace element data collected as part of this work will also be presented.

6.5.1. K-feldspar.

K-feldspar in the migmatitic metapelites is a common phase, typically more abundant than plagioclase. X_{or}^{kfs} ranges from 0.50 to 0.85, similar to the variation shown in Type 1 and Type 2 Leucogneiss K-feldspar. More sodic analyses again represent Na-rich patches in microperthitic K-feldspar. Figure 6.1. shows metapelite K-feldspar compositions plotted alongside K-feldspar compositions from other lithologies. The variation in composition in K-feldspar in metapelitic gneisses is greater than that exhibited in other lithologies.

K-feldspar from metapelites has near identical REE concentrations to those of K-feldspar from melanosomes. Eu anomalies are positive and large (Eu/Eu* = 47 - 49), and LREE abundances are higher than those found in leucogneiss K-feldspars. HREE contents are very low, while Ba contents are high and similar to Ba concentrations in K-feldspar from Type 2 Leucogneisses. Rb/Sr values are lower than those in Type 1 Leucogneisses (1.2 to 1.3), and similar to those of Type 2 Leucogneiss and melanosome plagioclase.

6.5.2. Plagioclase.

Plagioclase compositions from metapelitic gneisses show two distinct groupings, similar to the distribution of compositions in Type 2 Leucogneisses. Sodic plagioclase, with X_{an}^{plag} ranging from 0.28 to 0.34 (oligoclase - andesine) and more calcic (X_{an}^{plag} between 0.39-0.40) have both been recorded in metapelitic gneisses by Fitzsimons (1991). Oligoclase-rich plagioclase in metapelites is more sodic than plagioclase from the other lithologies studied.
REE patterns of late, anhedral plagioclase from metapelitic gneisses are shown in Figure 6.2. Again, LREE are strongly fractionated and there is no positive Eu anomaly. LREE concentrations are higher in metapelite plagioclase than in any of the other lithologies. Sr and Ba concentrations are also higher (360 - 370 ppm and 60 - 70 ppm respectively).

6.5.3. Garnet.

Garnet was present in all metapelitic gneiss samples studied by Fitzsimons (*op cit*). X_{alm}^{grt} values range from 0.67 to 0.81, with the majority around 0.73 to

0.75. These are slightly more iron-rich almandine garnets than those found in Type 1 Leucogneisses, Type 2 Leucogneisses and Melanosomes. X_{Mg}^{grt} varies from 0.10 to 0.30 and is lower in most metapelitic gneiss garnets than in garnets from the other lithologies. No compositional differences between Type A and Type B garnets were recorded.

Type B garnets from metapelitic gneiss samples show two different REE patterns. One suite of garnets shows similar patterns to Type B garnets in Type 1 Leucogneisses. HREE patterns show an increase from Gd to Lu, which contrasts with the relatively flat or depleted HREE patterns recorded in melanosome and Type 2 Leucogneiss Type B garnet. LREE concentrations (Ce, Nd) in metapelite garnets are relatively similar for both types of garnet. Zr contents are similar to those of garnets from Type 2 Leucogneisses, and range from 52 to 117 ppm. Y contents are similar to other garnet types.

6.6. ACCESSORY PHASES.

6.6.1. Monazite.

Monazite is the most abundant accessory phase in the leucogneisses, Melanosomes and metapelitic gneisses of the Brattstrand Bluffs migmatite complex. Monazite is a rare-earth phosphate with a Ce-selective structure. It exerts a major control on the behaviour of light rare-earth elements in peraluminous granitoids because these elements are strongly partitioned into monazite over other phases or the melt. The behaviour of monazite during crustal melting can be traced relatively easily: in effect it acts as a chemical spike since no other phase found in peraluminous granites has such high Th and LREE contents. Since the actual composition of monazite reflects the chemistry of the melt in which it is growing (Rapp & Watson, 1986), monazite chemistry can provide important constraints on the processes involved during melting. The low LREE contents of the Type 1 Leucogneisses and the unusual chemistry of the Type 3 Leucogneisses (high Th, LREE contents) are indications that monazite may have played an important part in determining the chemistry of the individual components of

the Brattstrand Bluffs granulite facies migmatites. The role of monazite in the melting process is considered fully in Chapter 8.

Monazite has the basic formula (Ce, La, Th)PO_4. Typical Th contents range from 4-12% ThO_2. The Th-rich variety of monazite is known as cheralite, and contains around 30% ThO_2. Thorium substitution occurs through the following reactions:

$$Th^{4+} + Si^{4+} \Leftrightarrow REE^{3+} + P^{5+}, \text{ and} \quad (6.1)$$

$$Th^{4+} + Ca^{2+} \Leftrightarrow 2REE^{3+} \quad (6.2)$$

In addition to Th, further substitution of LREE elements up to Gd or Tb into the (La,Ce) position means a wide range of compositions can occur depending on the activities of individual elements in the melt at the time of crystallisation.
Representative analyses of monazite compositions from Melanosomes (MEL), Type 3 Leucogneisses (LG3) and a metapelite from Brattstrand Bluffs are given in Appendix C. In addition, Table 6.1. shows a core and overgrowth pair from the metapelite IF/88/147 alongside several monazite compositions taken from the literature. Overgrowths (also referred to as rims) on rounded monazite cores suggest periods of igneous growth after resorption.

Monazite cores in all three lithologies studied (melanosome, metapelitic gneiss and leucogneiss) are relatively similar in composition to typical granitic monazites (Fig. 6.6.a).

Ce_2O_3 contents range from 28.09 wt % to 31.63 wt %, and Th concentrations are relatively low (minimum ThO2 = 5.17 wt %, maximum = 9.87 wt %). A plot of atomic wt % La/Nd against La + Ce + Pr (with each element normalised to La + Ce + Nd + Pr + Sm + Gd + Tb = 100%) shows that even the most LREE rich (Th poor) monazite cores have relatively unfractionated LREE concentrations (Figure 6.6.b). A strong negative correlation between Ca+Th cations (normalised to 16 oxygens) versus La + Ce + Nd cations (normalised to 16 oxygens) suggests that Th substitution for LREE was coupled with Ca (e.g. reaction 6.2.) (Figure 6.7.). Si contents are variable,

	1	2	3	4	5	6	7	8
La2O3	14.2	13.7	16.1	9.6	13.89	12.12	13.346	10.275
Ce2O3	28.1	21.7	31.3	19.6	16.31	5.19	28.201	23.116
Pr2O3	4.08	1.4	3.1	2.5	1.64	1.2	2.504	1.743
Nd2O3	15	3.6	10.6	4.5	2.34	5.91	10.387	8.579
Sm2O3	1.34	1.1	2.0	5.4	-	1.81	1.470	0.800
Eu2O3	<0.2	-	-	-	-	0.25	-	-
Gd2O3	<0.2	1.1	1.8	2.0	-	0.45	0.725	0.369
Tb2O3	-	-	-	-	-	0.05	0.000	0.024
Dy2O3	-	-	-	-	0.05	0.06	0.197	0.249
Ho2O3	-	-	-	-	-	0.01	-	-
Er2O3	-	-	-	-	-	0.03	-	-
Tm2O3	-	-	-	-	-	0.12	-	-
Y2O3	0.15	0.6	1.9	2.7	1.01	0.08	0.134	0.015
ThO2	2.10	22.50	0.9	19.5	11.34	31.64	9.608	21.410
UO2	0.18	1.2	0.1	1.6	15.64	4.33	1.859	3.165
CaO	<0.05	3.9	0.6	3.3	4.45	5.99	0.830	0.699
P2O5	24.9	28.4	30.5	30.0	31.02	27.10	27.850	25.489
SiO2	1.82	0.6	0.0	0.8	0.16	2.08	0.558	1.900

1. Monazite from the Murvey granite, Connemara. (Feeley et al, 1989).
2. Average of 8 pegmatite monazite analyses, Val Vigezzo. (Demartin et al, 1991).
3. Average of 7 fissure monazite analyses, Triolet. (Demartin et al, 1991).
4. Average of 7 pegmatite monazite analyses, Val Vigezzo. (Mannucci et al, 1986).
5. Rim of U rich monazite, Piona, Italy. (Gramaccioli & Segalstad, 1978).
6. Cheralite, (Type material MI 28881), India. (Bowles et al, 1980).
7. IF/88/147 MPG Monazite core.
8. IF/88/147 MPG Monazite overgrowth.

Table 6.1. Monzite rim-pair composition from IF/88/147, and selected monazite analyses from the literature.

although relatively high compared to literature values for pegmatitic monazites and are generally higher in overgrowths. Uranium contents are average for Th-rich monazites, ranging from 0.32 to 1.85 wt % UO_2. The similarity in monazite core compositions (e.g. Figure 6.7.) in the Melanosomes, leucogneisses and metapelitic gneisses suggests that the embayed and rounded monazite cores may have come from the same, probably granitic, precursor.

Monazite overgrowths show a greater range of compositions than the monazite cores do. They are unusually thorogenic; the most Th-rich monazite overgrowths are found in metapelitic gneisses and contain up to 21.41 wt % ThO_2. Monazite cores in the same sample contain only 9.60 wt% ThO_2. This strong enrichment of Th in overgrowths is seen in all monazite bearing lithologies, although the degree of enrichment is variable. Th contents are typically lower in overgrowths on monazite in leucogneisses than in Melanosome or metapelitic gneiss monazite rims. The increase in Th is accompanied by higher Ca and Si contents in the overgrowths, by slightly higher UO_2 concentrations (notably in the metapelitic gneisses) and by lower P and LREE concentrations as predicted by the substitution reactions above. Ce_2O_3 contents in overgrowths vary from 23.11 wt % to 30.27 wt %. LREE patterns in the overgrowths are even less fractionated, and plot closer to the cheralite composition given by Rapp and Watson (1986) and shown on Figure 6.6.

6.6.2. Zircon.

Zircon is both less abundant and petrographically simpler than monazite in the Brattstrand Bluffs migmatites. Two main occurrences of zircon were recorded. Large rounded grains with fine scale zoning and no magmatic overgrowths have HfO_2/ZrO_2 values of 0.25 to 0.28, typical of granitic zircons. Small, unzoned zircon needles have slightly higher Hf contents, with HFO_2 contents greater than 2.10 wt % and HfO_2/ZrO_2 values of 0.33-0.35. Yttrium, Thorium, Uranium and HREE contents are all very low. Zircon inclusions in Type II garnets were not analysed.

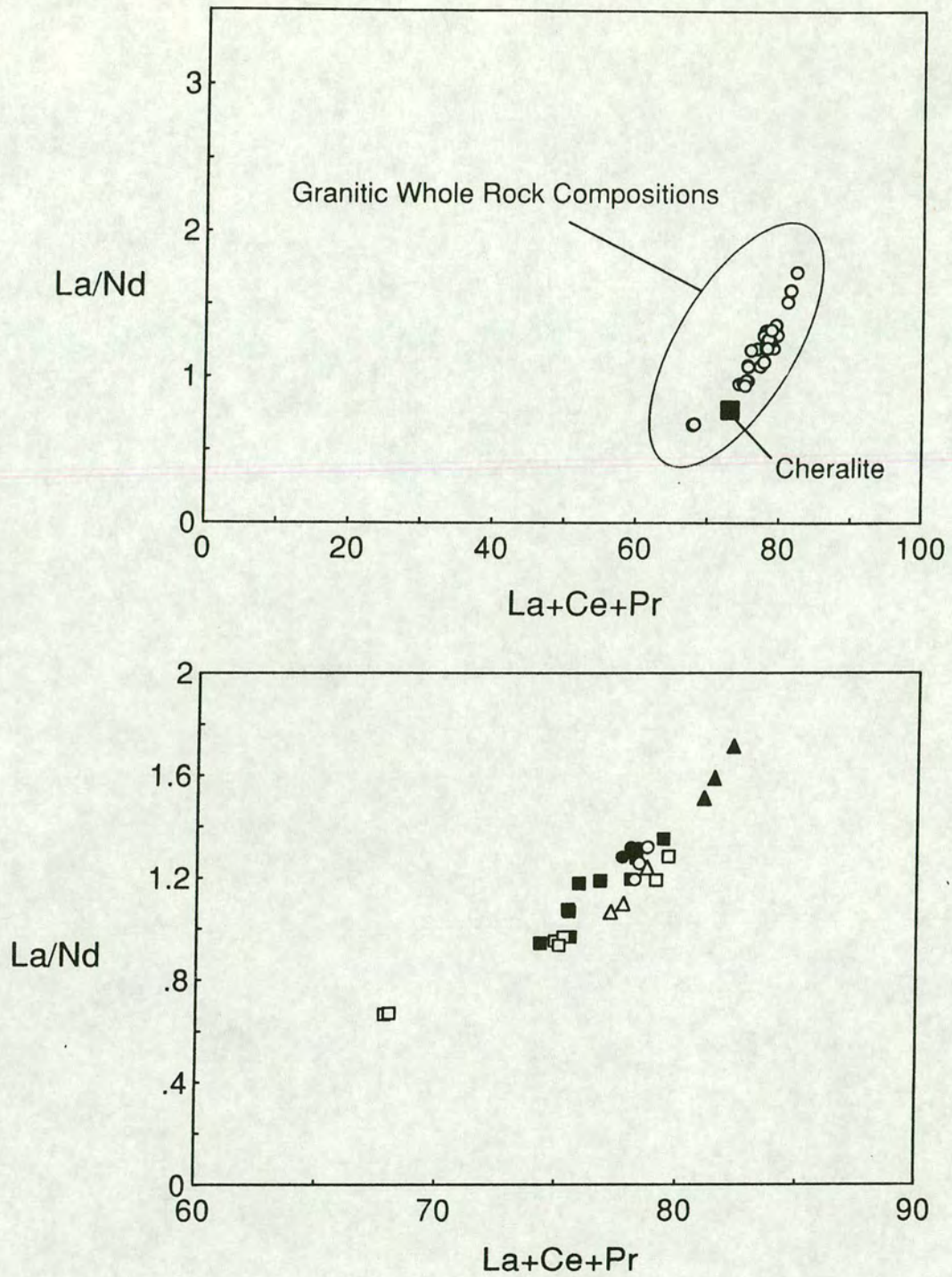

Figure 6.6.a. La/Nd against La+Ce+Nd for all monazite analyses.

Figure 6.6.b. La/Nd against La+Ce+Nd for all monazite analyses, showing lithologies. Symbols: Cores - solid, Rims - open. LG3 - triangles; MPG - circles; MEL - squares.

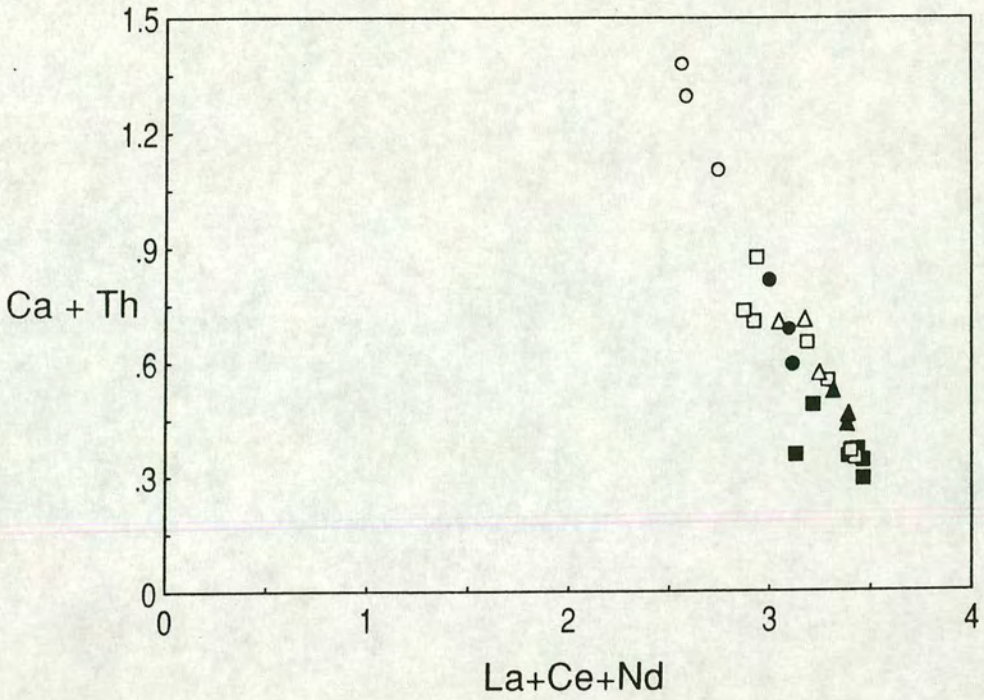

Figure 6.7. Ca+Th against La+Ce+Nd. Symbols as Figure 6.6.b.

Part 3.

Summary and Conclusions.

Chapter 7

Petrographic and geochemical constraints on processes involved during partial melting under granulite-facies conditions.

Chapter 7. Petrographic and geochemical constraints on processes involved during partial melting under granulite-facies conditions.

7.1. PETROGRAPHIC CONSTRAINTS ON THE MELTING PROCESS.

7.1.1. Introduction.

Migmatites are mixed-lithology rocks, found in high-grade metamorphic terranes, for which a number of very different origins have been proposed (see discussion in Ashworth, 1987). These have typically been categorised on the basis of open/closed system behaviour and whether melt is present or absent. This leads to a four-fold division for the origin of migmatites, summarised in Table 7.1.

	Open System	**Closed System**
Melt Present	Magmatic Injection	In-situ partial melting
Melt Absent	Metasomatism	Sub-solidus differentiation.

Table 7.1. Migmatite-forming Processes.

The aim of this work is to study the processes involved in a migmatite complex produced by partial melting, rather than to demonstrate that partial melting was responsible for the production of the Brattstrand Bluffs migmatites. While many migmatite terranes have been formed by melt absent processes (most notably stromatic migmatites by metamorphic differentiation e..g. Fitzsimons & Harley, 1991; Sawyer 1987; McLellan, 1989) the field and petrographic evidence presented by Fitzsimons (1991) for partial melting of metapelites in the Brattstrand Bluffs area is overwhelming. A review of melt-absent migmatite forming processes is therefore inappropriate in this work. What is interesting about the simplistic four-fold division of migmatite-forming processes given in Table 7.1. is that *in-situ*

partial melting is taken to be a closed-system phenomenon, which, in effect, rules out the extraction of melt from migmatite terranes. This has important consequences for any model which suggests that partial melting may produce granulite-facies conditions, since removal of the vapour phase (creating low aH_2O conditions neccessary for granulite-facies metamorphism) in a hygroscopic melt requires open system behaviour at some point in the melt formation and crystallisation history. The extent to which migmatite complexes are open to melt extraction and the processes operating as melts migrate from the complex are therefore important questions which must be addressed. The work of Fitzsimons (1991) has characterised the important melt-producing reaction(s) in the Brattstrand Bluffs migmatites, and a field estimate of total melt production (30-50 %) has been obtained from leucosome proportions (Fitzsimons & Harley, 1991). The aim of this chapter is to use petrographic and geochemical data summarised in Part 2 (Chapters 3, 4, 5 and 6) to ascertain the degree of melt-restite interaction (including the determination of geochemical signatures of incomplete melt segregation in a near-source environment), the evolution of melt proportion and of melt chemistry with increasing degrees of water undersaturation, and the importance of partial-melting under granulite facies conditions in preserving granulite-facies conditions. The main aspects to be addressed are as follows;

(i) Petrographic and geochemical evidence for restite and peritectic phases in the leucogneisses.

(ii) The influence of this material on the geochemistry of the leucogneiss suite.

(iii) Coupling and decoupling of major and trace element chemistry during partial melting under water-undersaturated conditions.

(iv) The development of a best-fit model for melt extraction, incorporating the effects of restite entrainment, unmixing and crystal fractionation, including the potential effects of aH_2O and other volatile components.

Summaries of the principal petrographic features of the three leucogneiss types, the migmatitic metapelitic gneisses and the melanosomes which are central to interpretations for their origin are presented in Sections 7.1.2.-7.1.6.

below. Mineral chemical data (presented in Chapter 6) is summarised in Section 7.2. and used to determine what the chemical differences between phases in the various lithologies tell us about about melt production and extraction. Having constrained the chemistry of individual minerals, the contrasting bulk-rock geochemical signatures of the leucogneiss types are then discussed in Section 7.3. The chemistry of the metapelitic gneisses and melanosomes are also interpreted in this section, to enable the development of a coherent model for the petrographic and geochemical processes active during melting for the whole migmatite complex. This model is presented in Section 7.4, and uses melt water content estimates to model the evolution of the migmatites under increasingly water-undersaturated conditions. Chapter 8 then goes on to use accessory phases, with their easily traced chemical "spikes" and characteristic behaviour under granulite-facies conditions, as geochemical markers to develop further the concepts introduced in this chapter.

7.1.2. Type 1 Leucogneisses.

Type 1 Leucogneisses are dominated by quartz and feldspar . The small size and isolation of leucosomes in stromatic migmatites suggests local derivation rather than injection, while subsolidus differentiation into leucosome and melanosome is unlikely because leucogneisses preserve only a localised, late metamorphic fabric (S4 in the scheme of Fitzsimons, 1991; Fitzsimons & Harley, 1991) compared to the pervasive foliation developed in the metapelitic gneisses (S3). Textures in the quartzofeldspathic leucogneisses consist dominantly of anhedral grains of heterogeneous grainsize with lobate feldspar-feldspar and feldspar-quartz intergrowths, indicative of an origin by crystallisation of a partial melt. Geochemical data which indicate very high normative quartz and high SiO_2 contents for some Type 1 Leucogneisses, suggests the presence of <u>restitic</u> quartz in some samples. Although restitic quartz is notoriously difficult to recognise from petrography (Wall *et al*, 1987), some large quartz grains which are cracked and rounded may represent clasts only partly dissolved in the melt. In this case, the cracking could be due to positive volume changes associated with partial melting (Rubie & Brearley, 1990), and veining by plagioclase in some samples suggests that at least some of the quartz was solid throughout the melting

episode. Most of the quartz recorded in the leucogneisses is anhedral, and only a small amount of restitic quartz has been recognised. Rounded quartz and quartz-K-feldspar blebs in garnet rims may represent liquidus material trapped in peritectic garnet. Table 7.2. shows the interpreted origin of phases found in the leucogneisses from the Brattstrand Bluffs area, while Table 7.3. shows the distribution of phases from different generations in the melanosomes, metapelitic gneisses and the three Leucogneiss types.

Interpreted origin of phases in Prydz Bay Leucogneisses.

	Primary Magmatic	Entrained from pre-melting assemblage	Entrained Peritectic	Secondary Restite
Quartz	XXX	Rare cracked grains		Rare in crd symplectites
K-Feldspar	XXX	Large inclusion rich grains	X	
Plagioclase	XXX			
Garnet	Rare euhedra	Large inclusion rich grains	Poikiloblastic grains	
Cordierite	Very rare euhedra		XX	As overgrowths on Grt
Sillimanite		Schlieren and large grains		
Biotite		In early garnet cores		Around garnet
Hercynitic Spinel				Intergrown with crd after garnet.
Ilmenite		??		??
Monazite	Overgrowths	Corroded cores		
Zircon	Small needles	Rare in early garnet Large rounded grains		
Graphite		??		

Table 7.2. Interpreted Origins of individual phases in the Brattstrand Bluffs Leucogneisses. (X - rare, XX - common, XXX - very abundant)

As K-feldspar is a peritectic phase produced during incongruent melting of biotite (Grant, 1985; Waters, 1988; Le Breton & Thompson, 1988), residual K-feldspar is likely to be found in the leucogneisses. S-Type granitoids and leucosomes from high-grade migmatite terranes are often K-Feldspar-rich. At least some of this, in the case of the Brattstrand Bluffs Leucogneisses, is likely to be of restitic origin. The presence of tiny sillimanite needles in the core of a K-feldspar grain indicates that not all the K-feldpar melted. However, peritectic K-feldspar and K-feldspar remaining from the pre-melting assemblage are much less abundant than crystals which have grown from the melt, especially in the Type 1 Leucogneisses.

Distribution of phases in Brattstrand Bluffs Migmatite Lithologies.

	Pre Melt Gt, Sill, Kfs	Peritectic Gt, Crd, Kfs	Hercynitic Spl (secondary rest.)	Embayed Mon cores	Rounded Zircon	Magmatic Zircon
MEL	----------	----------	----------	----------	----------	
MPG	----------	----------				
LG2	---------	---------	---------	---------	---------	---
LG3		---	---	----------	----------	---
LG1		---	---			---

Abundance

----------	Abundant
---------	Frequent
---	Rare

Table 7.3. Distribution of phases in the Brattstrand Bluffs Leucogneisses.

Two petrographically distinct plagioclase occurrences were recorded. Most plagioclase appears late in the melt crystallisation sequence, intruding cracked quartz grains as noted above. Earlier plagioclase, which is idiomorphic and often included in Kfs may be residual from the pre-melt assemblage. Although higher Ca-plagioclase has often been suggested as a restite phase, the low (to absent) concentrations of plagioclase in the metapelites would be more consistent with near exhaustion of plagioclase at source, rather than the extraction of unmelted plagioclase. While the exact timing of plagioclase growth is uncertain, several phases of growth may have occurred.

The mineralogy of the Type 1 Leucogneisses is consistent with precipitation from a melt. Of particular importance is the Type II Garnet they contain, which may represent either primary entrained garnet or garnet crystallised from the melt. This garnet is typically poikiloblastic and contains small rounded quartz grains - similar to garnets in metapelitic gneisses and melanosome. The low Mn content of Type II Garnet (see Section 7.3: *c.f.* Harrison, 1988; Miller & Stoddard, 1981) suggests they do not represent melt-

precipitated garnet and may therefore represent entrained material. Type II Garnet postdates the garnet which grew as part of the pre-melting assemblage (Type I Garnet), and occurs in the melt, so it must have formed during the melting event and must therefore be a solid product of the incongruent melting reaction which consumed biotite. Poikiloblastic garnet has been recognised as a residual phase by other authors, but it has always been thought to represent garnet from the original assemblage. The near ubiquitous presence of individual peritectic garnet porphyroblasts in Type 1 Leucogneisses, which contain little other obvious source material, suggests that even relatively cleanly extracted melts from migmatite terranes in the lower crust may contain restitic material. In the Type 1 Leucogneisses garnet contents rarely exceed 5%, suggesting fairly clean extraction. This is consistent with low modal abundances of any other phases which could be considered as restite, in contrast with Type 2 Leucogneisses (Section 7.1.3.).

7.1.3. Type 2 Leucogneisses.

Type 2 Leucogneisses contain higher abundances of mafic and aluminous material than the Type 1 Leucogneisses. As Fe_2O_3, MgO and Al_2O_3 all have low solubilities in felsic peraluminous melts (Chapter 2), the majority of this material is unlikely to have crystallised directly from the melt. In principle, garnet, cordierite, sillimanite and spinel in Type 2 Leucogneisses may represent material of the following derivation:

(i) True restite. i.e. phases entrained from the pre-melting assemblage which may or may not have equilibrated with the melt.

(ii) Peritectic restite. i.e. phases which grew during melting as solid products of incongruent melt producing reactions. Phases of types (i) and (ii) can be considered as "primary" restite.

(iii) Xenolithic material. (Phases from surrounding lithologies not involved in melting).

(iv) Enclaves of mafic melt trapped as a function of magma mixing.

(v) Secondary restite, formed by the breakdown of entrained primary restitic material as the melts cool or ascend.

Garnet, being modally the most important mafic phase and present in higher abundances (especially in Type 2 leucogneisses) than solubility constraints allow (Miller, 1985, Puziewicz & Johannes, 1988) is a very likely candidate for entrainment from source. Type I Garnet (early, sillimanite inclusions) in Type 2 and, more rarely, in Type 3 Leucogneisses is petrographically identical to most of the large garnets in the metapelites. The presence of Type I Garnet in leucogneiss samples shows that extraction was inefficient and that some source rock was entrained. The most abundant garnet is Type II Garnet, which occurs in all three leucogneiss types, as opposed to Type I Garnet which is only found in Type 2 Leucogneisses. It occurs as individual grains, and as rims on Type I Garnet in LG2 and MPG. This is important because it suggests that the most likely material to be entrained in a departing melt is peritectic in origin, rather than restitic.

Sillimanite is also very insoluble in granitic melts (see Chapter 2) and likely to be in excess, rather than having crystallised directly from the melt. It is more abundant in Type 2 Leucogneisses, which have high modal abundances of garnet and spinel. Spinel forms late, and most probably occurs as a result of the breakdown of entrained garnet. Spinel in the Type 2 Leucogneisses can therefore be considered as secondary restite, while garnet, sillimanite and cordierite (and to a lesser extent ilmenite, which is also most abundant in the Type 2 Leucogneisses) represent primary restite entrained as the melts left their source regions. It is notable that, with the exception of sillimanite, most of the primary restite formed as peritectic phases during melting. Although difficult to recognise petrographically, peritectic K-feldspar is therefore likely to be present in Type 2 Leucogneisses.

It is often difficult to distinguish restite-entrainment from magma mixing, especially in higher-level plutons (Vernon, 1984; Vernon, 1983). The advantage of leucogneisses from the Brattstrand Bluffs coastline is that interpreted transport distances are minimal, and it is unlikely that two melts of such dramatically different composition could have formed at the same time. Mineral assemblages developed in the leucogneisses and country rocks

(metapelites and melanosomes) show similarities which led Fitzsimons (1991) to suggest that the presence of garnet porphyroblasts in the leucogneisses identical to those in the host metapelites was evidence for local derivation and limited melt transport distances.

The composition of the "enclaves" (schlieren, pods and rafts of refractory material) is dominantly that of the melanosome - garnet, spinel and sillimanite - and is unlikely to represent a magma composition of any type (Chappell *et al*, 1987; Vernon, 1983). Fabrics are dominantly metamorphic, with large garnet porphyroblasts wrapped by sillimanite which defines a good foliation. Mafic material exists as clots, disaggregated clots and single grains in LG2. This is consistent with the view of Vernon & Wall (1983), who suggested that residual material should have a metamorphic fabric, with foliated, high temp fabrics and granoblastic grain shapes. If this restitic material is from the source area, however, then it should be actively melting at the time of entrainment, suggesting that textures will be modified by igneous rather than metamorphic fabrics (Chen et al, 1989). Small pockets of melt will enable clots of material to disaggregate more easily. This mechanism may explain the large amount of disaggregated, single grain restitic material present in the Type 2 Leucogneisses (e.g. Type II Garnet), and why individual grains (rather than clusters of several grains with a metamorphic fabric) are the most common restitic phase in the Type 1 Leucogneisses.

In summary, Type 1 and Type 2 Leucogneisses have different petrographic features which can be explained by incorporation/entrainment of variable amounts of aluminous and mafic phases (notably garnet (dominantly peritectic, but with rare garnet from the pre-melting assemblage), cordierite, sillimanite, hercynitic spinel and possibly K-Feldspar). This near-source entrainment indicates that partial melting under granulite facies conditions can give rise to varying degrees of melt segregation. Since efficient segregation of melts from the lower crust is important for crustal differentiation models and the preservation of granulite-facies conditions, the factors controlling the entrainment of major phases must be considered. In addition, the presence of restitic material in a granitic melt may have important consequences for bulk chemistry. For example, the addition of metamorphic garnet (typically almandine-rich) to a peraluminous magma

will increase the bulk Fe_2O_3, MgO, A/CNK and ΣHREE values, and decrease $La_{(n)}/Yb_{(n)}$ ratios. The role of mafic and aluminous material on the bulk chemistry of the leucogneisses is considered in Section 7.3., with an emphasis on the effects of restite entrainment/unmixing as modifiers of bulk magma chemistry.

7.1.4. Type 3 Leucogneisses.

Type 3 Leucogneisses have modal proportions which overlap with Type 1 Leucogneisses and Type 2 Leucogneisses. Assemblages are dominantly quartzofeldspathic, but peritectic garnet, cordierite, residual sillimanite and late hercynitic spinel are often present. While peritectic garnet is the most abundant mafic phase, restitic material is generally present in smaller quantities than in the Type 2 Leucogneisses.

Type 3 Leucogneisses were distinguished from the other leucogneisses in Chapter 4 on the basis of high LREE, Th and Zr contents, and not by their petrographic characteristics. Modal monazite and zircon contents, however, are higher than in Type 1 Leucogneiss and Type 2 Leucogneiss samples, and, as a consequence the unusual chemistry of the Type 3 Leucogneisses is likely to be controlled by their high accessory phase content. Since no monazite or large zircon grains have been recorded in early (pre-melting) garnet, it appears that accessory phases have been free in melt at least to some extent. If they were originally included in a phase which was breaking down during melting (e.g biotite consumption) then they would be free to interact with the melt at an early stage.

Accessory phases show distinctive behaviour in water undersaturated melts, since dissolution rates are very slow. This makes them good geochemical markers for tracing the fate of unmelted material in melts extracted from migmatite terranes. Chapter 8 compares Type 3 Leucogneisses with Type 1 Leucogneisses to determine why accessory phases have behaved differently in the two lithologies, and what consequences this may have for other granulite facies migmatites and for the generation of S-Type Granites.

7.1.5. Metapelitic Gneisses.

Metapelitic Gneisses show schollen and schlieren migmatitc structures, with melanosome, mesosome and leucosome components closely associated. Layering in migmatitic metapelites is occasionally cut by leucogneiss sheets and fingers, suggesting that some melt migration has occurred. Many metapelites, however, show stromatic fine scale layering suggesting melt retention rather than extraction.

The metapelitic gneisses are banded and comprised of quartz- and K-feldspar-rich bands alternating with garnet-, sillimanite-, cordierite- and hercynitic spinel-rich bands. Both Type I and Type II garnet is present, and plagioclase is absent in most samples. The most important feature of the metapelitic gneiss assemblage is that the phases present are those which make up the proposed restite component of the leucosomes. A spectrum of compositions, from stromatically banded metapelites to leucosomes containing abundant mafic material (i.e. Type 2 Leucogneisses) exists. Narrow leucogneiss bands containing as much as 30% modal Type II Garnet have been recorded (Fitzsimons, 1991). The similarity of the mesosome and leucosome assemblages limits the distance that melt movement has occurred, since restitic material entrained at depth will breakdown to assemblages stable at lower pressures if substantial upwards migration occurs (Wall *et al*, 1987).

7.1.6. Melanosomes.

Melanosome samples consist of coarse garnet, sillimanite and cordierite, with little or no feldspar. Quartz is absent in most samples. The interpreted origin of individual phases in melanosome samples is summarised in Table 7.4. The highly refractory, anhydrous mineralogy of the melanosome material is consistent with the removal of large volumes of melt, leaving a depleted residue. Mass balance constraints (Figure 7.1.) suggest that the removal of a typical peraluminous melt from a source with a metapelitic composition would require exceedingly large amounts of melting. Aluminous melanosome material does not form simple margins between mesosome and

Interpreted origin of phases in Prydz Bay Melanosomes.

	Metamorphic pre-melting assemblage	Peritectic	Post Peak	Primary Magmatic
Quartz				
K-Feldspar	Large inclusion rich grains	XX		
Plagioclase				
Garnet	Sillimanite-inclusion-rich large grains	Abundant poikiloblastic grains		Rare euhedra ?
Cordierite		XXX	As overgrowths on Grt	
Sillimanite	Schlieren and large grains			
Biotite	In early garnet cores		Around garnet	
Hercynitic Spinel			Intergrown with crd after garnet.	
Ilmenite	XX		??	
Monazite	Corroded cores			Overgrowths
Zircon	Rare in early garnet Large rounded grains			Small needles
Graphite				

Table 7.4. Interpreted origins of individual phases in the Brattstrand Bluffs Melanosomes.

between mesosome and leucosome, as has been recorded in small-degree melt fraction migmatite systems. While melanosome is often interlayered with metapelites, it also occurs as cross-cutting veins rich in garnet and cordierite, and as restitic schlieren in leucogneisses.

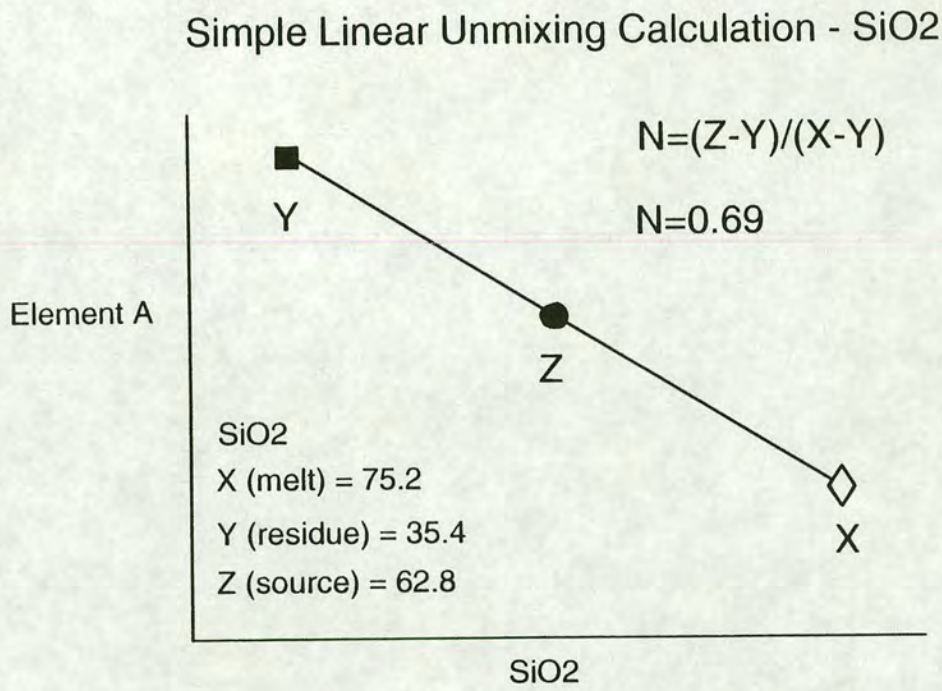

Figure 7.1. A simple mass-balance linear unmixing calculation carried out to determine N (degree of melting) to produce melt X from source Z, leaving residue X. Silica values represent typical LG1 (X), MPG (Z) and MEL (Y) values.

Although melanosomes have a mineralogy consistent with large degrees of melt extraction, restite-free melts retained in the complex have near minimum melt compositions, suggesting extremely high temperatures were not reached. Melanosomes are commonly found interbedded with pelites which show smaller degrees of partial melting.

Two main possibilities may explain these observations;

1. The melanosomes represent the residue after large degree melt extraction, but that these melts are no longer retained in the complex.

2. The melanosomes do not represent true restite reflecting the amount of melt extracted from a volume of source material as such, but

represent accumulated peritectic and residual phases entrained in smaller degree melts which have been left behind after the melt has been extracted.

Hypothesis 1 has several drawbacks. If such large degrees of melting have occurred, why have only certain layers been affected? Why do some melanosomes appear to cross cut the regional fabric if they represent pelites from which large amounts of melt have been removed? Such large amounts of melting (50-60%) may require the influx of water, yet the assemblages and mineralogy are consistent with the same melt reactions occurring in the pelites, which have <40% melting, and are interpreted as products of water-undersaturated melting. It is unlikely, therefore, that the melanosomes are the residues left behind after a large degree of partial melt was extracted.

Hypothesis 2 has several advantages. The most residual quartz-absent melanosomes appear to have undergone almost complete melt extraction. Only small amounts of melt has remained trapped in pressure shadows at the margins of large, Type I garnet. Most workers admit that there is a certain threshold, below which no more melt can be extracted (approx 5-10%). If the melanosomes represent an accumulation of small clumps of restite and individual crystals (including peritectic material) rather than the relict framework of the source rocks then there is no reason why any melt should remain trapped. Peritectic phases formed during incongruent melting grow at the interface between melt and source, and require the presence of melt to grow (Powell & Downes, 1990). Only a certain amount of peritectic garnet (or cordierite) will form, proportional to the amount of melt present. If melt-fluxing along structural pathways occurs, then much larger melt volumes can be attained at the site of melting, even for relatively small amounts of partial melting (10-20%). The presence of abundant coarse cordierite and garnet in cross-cutting veins may attest to this mechanism of formation. Similar cross-cutting cordierite-rich veins have been recorded in Australia (White & Chappell, 1990; Harley, 1992) and have been explained as peritectic phases left behind after melts are removed.

7.2. MINERAL CHEMISTRY CONSTRAINTS.

7.2.1. Introduction.

Major and trace element analysis of phases from leucogneiss, melanosome and metapelitic gneiss samples was performed to determine whether compositional differences existed between restite, peritectic and melt-precipitated phases. In particular, it was hoped that the chemistry of garnet, plagioclase and, to a lesser extent, K-feldspar from different parts of the migmatite would place important constraints on melt production and extraction. This Section aims to discuss the chemistry of the major phases found in the Brattstrand Bluffs lithologies. The chemistry of accessory phases is discussed briefly in Section 7.4.3., and more fully in Chapter 8.

7.2.2. K-Feldspar.

K-feldspar major element chemistry is almost identical for grains from leucogneiss, melanosome and metapelitic gneiss samples. X_{or}^{kfs} ranges from 0.77-0.88 for all grains (Figure 6.1), with small sodic stringers having higher X_{ab}^{kfs} (0.26-0.34). No zoning was recorded in any samples. Because K-feldspar compositions are essentially homogeneous, major element chemistry cannot be used to distinguish melt-precipitated and restitic K-feldspar, despite obvious petrographic differences. The apparent major element homeogeneity may be due either to post-melting homogenisation (intracrystalline diffusion or fluid circulation), or to rapid melting. Extreme disequilibrium melting occurs when melt is extracted before the melting assemblage can equilibrate, giving rise to melt phases with a similar composition to those of the source rocks.

Trace element compositions in K-feldspars from different components in the migmatite assemblage show small, but important, differences. Ba and Rb/Sr values are lowest in Type 1 Leucogneisses, and higher in Type 2 Leucogneisses and Metapelitic Gneisses. Ba contents of LG2 and MPG K-feldspar are almost double those of LG1. High resolution SIMS ion-microprobe analysis has failed to detect any zoning, suggesting internal homogenisation. While major element concentrations are similar for both types, LREE contents in Type 1 Leucogneiss K-feldspar are lower than those of Type 2 Leucogneiss K-feldspar. K-feldspar LREE contents strongly reflect

bulk-rock LREE concentrations (which are very low in LG1), suggesting that limited equilibration on a local outcrop (rather than complex) scale may be responsible for the lack of zoning and compositional heterogeneity.

7.2.3. Plagioclase.

The presence of complexly-zoned Ca-rich plagioclase cores in a granitic magma was used by White & Chappell (1977) as evidence for the presence of restite in a high-level S-Type granite pluton in S.E. Australia, and Scambos *et al* (1986) note a similar occurrence from the Center Pond Pluton in western U.S.A. It may therefore be possible to use plagioclase chemistry to distinguish between grains entrained from the pre-melting assemblage and those precipitated from the melt.

Plagioclase in samples from the Brattstrand Bluffs coast have oligoclase-andesine compositions, with X_{an} ranging from 0.27 to 0.45. Samples from metapelites and Type 2 leucogneisses show a slight bimodality in composition, with compositions in the ranges X_{an} = 0.27-0.35 and X_{an} =0.39-0.45. Petrographically earlier plagioclase in Type 2 leucogneisses is more calcic than later, anhedral plagioclase, while rare plagioclase recorded in pressure shadows around large garnet in IF/88/46B (a melanosome sample) is similar in composition to that of the Type 2 leucogneisses. Due to uncertainties in the timing of plagioclase growth (Chapter 3) it is difficult to determine whether the increase in X_{ab} in plagioclase appearing later in the crystallisation sequence, and in melts relative to source rocks, is a feature of restitic plagioclase entrainment or of evolution of the cooling melt. The near-absence of plagioclase in the metapelites suggests that initial plagioclase contents were low and/or that plagioclase exhaustion in the source occurred. If this is the case then entrainment of early plagioclase from the source is unlikely.

REE patterns in plagioclase from Type 1 and 2 Leucosomes and Metapelitic gneiss samples are unusual, in that no positive Eu anomaly is developed. This would occur if plagioclase formed under oxidising conditions. No evidence for oxidising conditions has been recorded from any lithology from the Brattstrands coastline. Petrographic evidence, including the presence of

graphite and ilmenite rather than magnetite suggests reducing rather than oxidising conditions. In addition, if oxidation during melt crystallisation occurred then K-feldspar should also show small or absent Eu anomalies. Although the crystallisation history of plagioclase is poorly constrained in the Brattstrand Bluffs leucogneisses, if early K-feldspar grew in a melt which became more oxidising with time then late crystallising plagioclase would have smaller positive Eu anomalies. Again, however, this does not provide an adequate explanation for the preservation of graphite (which definitely grew late in the paragenetic sequence) and ilmenite, and no other obvious process to explain the unusual REE patterns of the plagioclase from the Brattstrand Bluffs is obviously apparent.

7.2.4. Garnet.

Three types of garnet were distinguished petrographically. Early (Type I) garnets have aligned inclusion-rich cores (fine sillimanite and small rounded biotite) which probably represent the pre-melting assemblage. Type I garnets are most common in metapelites and melanosomes, but have also been recorded in leucogneisses. A second generation of poikiloblastic garnet (Type II), containing large rounded quartz blebs, forms individual grains in leucogneisses and overgrows Type I garnet in melanosomes and migmatitic metapelites. Rare euhedral Type III garnets are chemically indistinguishable from Type II Garnet, and are here interpreted as recrystallised Type II Garnet rather than melt precipitated grains. Igneous garnet typically has a much higher Mn content (du Bray, 1988; Harrison, 1988) which has not been witnessed in garnet from any migmatite lithology in the Brattstrand Bluffs area.

Type II garnets in leucogneisses with a depleted chemistry (low LREE, HREE, Zr and Th) have lower LREE, HREE and Zr than Type II garnets from metapelites and melanosomes. Zr contents in these peritectic garnets from depleted leucogneisses are also much lower than those in Type II garnets from the source and melanosome lithologies Since peritectic garnets grow at the site of melting (e.g. Powell & Downes, 1990), Type II garnet in the depleted Type 1 Leucogneisses must have grown in equilibrium with a melt which was **initially** depleted in Zr, LREE and HREE. The timing of the

depletion of these elements has important implications for melt producing processes (Section 7.3.1.). Later melts contain peritectic garnet indistinguishable from peritectic garnet in the source rocks. The low concentrations of Zr, LREE and HREE in the depleted leucogneisses have been ascribed to the limited dissolution of accessory phases in water-undersaturated melts, and may be characteristic of melts extracted from granulite-facies migmatite terranes.

7.3. BULK ROCK GEOCHEMICAL CONSTRAINTS.

7.3.1. Type 1 Leucogneisses.

Type 1 Leucogneisses are characterised by high SiO_2 values and weakly to moderately peraluminous A/CNK ratios. High SiO_2 contents are consistent with the movement of the quartz-feldspar cotectic towards quartz-rich compositions in peraluminous melts (Holtz *et al*, 1992), but, as noted from petrography, may also reflect the entrainment of excess quartz (especially in lithologies with SiO_2>76 wt %). K_2O contents are relatively high, and K_2O/Na_2O>1 in almost all samples. MgO, Fe_2O_3 MnO and TiO_2 contents are low, consistent with typical literature values for peraluminous magmas, suggesting that little entrained mafic material is present.

Type 1 Leucogneisses have typical crustal melt trace element patterns for most elements. Transition element concentrations are uniformly low. The most unusual geochemical feature of the Type 1 Leucogneisses is their very low concentrations of Zr, Th and LREE. Zr and LREE contents are well below those required to saturate a metapelite-derived peraluminous melt at appropriate temperatures using the equations of Watson (1988) and Montel (1992). The implications of low Zr, Th and LREE contents (elements typically hosted in accessory phases) are considered in the next chapter.

The geochemistry of the Type 1 Leucogneisses is consistent with their interpreted origin by partial melting of a metasedimentary source coupled with a minimal restite component (Miller, 1985). Both petrographic and geochemical data indicate that little restitic material is present, suggesting

melt segregation was efficient. They have almost identical geochemical signatures to the small melt fraction magmas described by Wickham (1987) from the Pyrenees (SiO_2 rich, mafic poor liquids with low concentrations of Mg, Fe, Ti, V, Ni, Zr, Hf, Th and LREE). The low restite component in Type 1 Leucogneiss samples means that they represent melt compositions relatively unaffected by unmixing or entrainment of source material. Whether they represent initial melt compositions depends upon the extent to which they have been altered by igneous fractionation and the possible loss of a late stage melt on cooling near their solidus.

One possible model which could explain the geochemical variations within the Type 1 Leucogneisses and between LG1 and the other suites is feldspar fractionation. This would provide an adequate explanation for the low Zr, Th and LREE concentrations characteristic of Type 1 Leucogneisses, since incompatible elements would become concentrated in residual liquids. The Th- and Zr- enriched Type 3 Leucogneisses could then represent fractionated melts left behind after precipitation of the felsic Type 1 Leucogneiss "cumulates". This model, and the role of fractionation, can be evaluated by plotting Th and Zr concentrations against an indicator of fractionation (e.g. Ba, Sr or K) the role of fractionation can be ascertained. Figure 7.2.a shows Th plotted against K for Type 1 and Type 3 Leucogneisses. Also indicated are the relative positions of melanosome and the orientation of the monazite-melt mixing line for monazite containing 10wt% ThO_2. While LG1 samples contain little Th, they exhibit a wide range of K (and Sr) concentrations. In contrast, Type 3 Leucogneisses have a very steep Th-K gradient. The relationships on this plot are clearly inconsistent with the derivation of Type 1 and 3 leucogneisses by fractional crystallisation of a feldspar-rich cumulate leaving a melt enriched in Th. A more plausible explanation may be that the Type 3 Leucogneisses are the product of the entrainment of a LREE enriched phase (and possibly a little K-feldspar to give the mixing line defined in Fig. 7.2.a), while Type 1 Leucogneisses represent melts containing variable amounts of entrained (peritectic) K-Feldspar but no LREE-rich accessory phase. Figure 7.2.b, however, shows a good correlation between Zr and Sr for Type 3 Leucogneisses. Type 1 Leucogneisses have Sr values which range (with one exception) to values as high as high as those of LG3. The simplest interpretation of this data is that, while fractionation of plagioclase or K-feldspar may be important for Zr variation **within** the Type 3 Leucogneiss

suite, it is not the mechanism responsible for the depletion of Zr in Type 1 Leucogneisses relative to Type 3 Leucogneisses, since no fractionation of elements other than those hosted in accessory phases has occurred between the two suites.

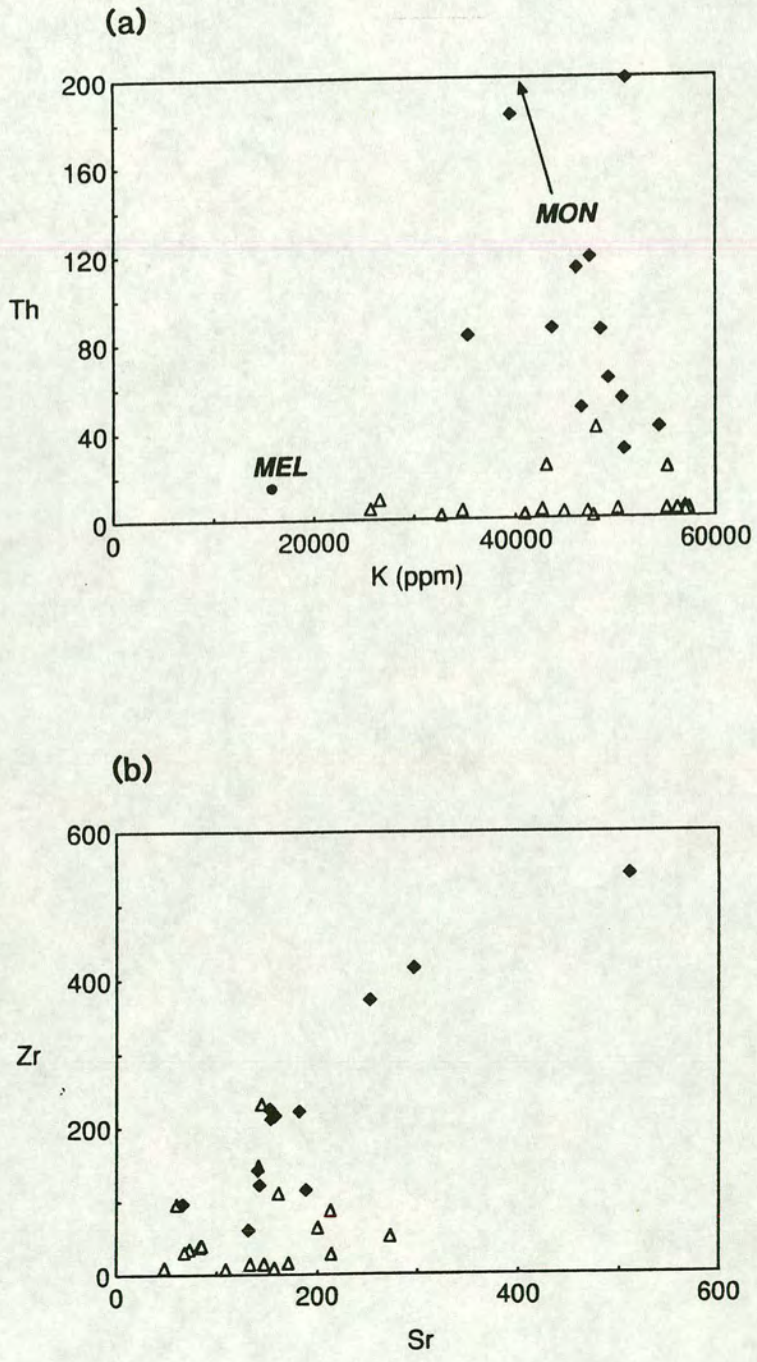

Figure 7.2.a. Th (ppm) vs K (ppm) Symbols as Figure 4.1.
Figure 7.2.b. Zr (ppm) vs Sr (ppm) Symbols as Figure 4.1.

Field relations and mineral chemistry place further constraints on the role of fractionation relative to entrainment. As noted above, trace element contents of peritectic garnet growing in equilibrium with the Type 1 Leucogneisses at the site of melting suggests that melts were depleted in Zr, Th and LREE at an early stage, rather than becoming depleted by fractionation once a certain melt fraction had formed. In addition, the small scale nature of many of the leucogneiss outcrops, the absence of any field evidence for igneous fractionation and similarities in major and trace element concentrations (other than those trace elements hosted in accessory phases) suggest it is it unlikely that the geochemical differences **between** the two suites are a result of fractional crystallisation.

7.3.2. Type 2 Leucogneisses.

Samples with high A/CNK ratios have high modal concentrations of aluminous phases, which may represent either restitic or xenolithic material. Melts comprised of feldspar will have an A/CNK ratio of 1.0, so A/CNK can be used as a measure of excess peraluminosity - this will increase as aluminous phases such as garnet and cordierite are entrained into the melt, and is unlikely to be too high if only resulting from phases precipitating due to the low solubility of Al_2O_3 in granitic melts. Exceptionally high A/CNK values in certain Type 2 Leucogneisses is especially indicative of contamination by pelitic or restitic material. These samples have high modal concentrations of garnet and cordierite (±spinel, sillimanite) petrographically identical to that seen in surrounding metapelites. High concentrations of Ni, Cr and other transition metals are typical of Type 2 Leucogneisses. Type 3 Leucogneisses have high La, Zr and Th contents, high LREE patterns. Chapter 8 deals with these elements - this chapter will concentrate on elements controlled dominantly by major, rather than accessory phases.

The presence of restitic material in a granitic melt may have important consequences for bulk chemistry, as discussed in Chapter 2. The restite-unmixing model suggests that a whole suite of melts will be produced during anatexis, ranging from near-minimum melt compositions to restite laden material. Restite unmixing produces a spectrum of bulk compositions which form a linear vector in compositional space. The ends of this unmixing

line are fixed by the compositions of the residue and the melt, while the gradient is controlled by the partitioning between the melt and the solid residue. In simple terms the residue can be considered as a single phase (e.g. Fig. 7.3.a). More realistically, the bulk composition of the residue is controlled by the individual phases present, and their relative proportions (Fig. 7.3.b). If two compositionally dissimilar assemblages or phases are entrained or unmixed then two mixing vectors may arise (Fig. 7.3.c). The precise orientation of the vectors again depends on the composition of the end-members. The presence of a second vector may indicate that an individual phase is becoming preferentially entrained.

The bulk composition of the entrained "member" that defines the end of the unmixing line will migrate with time as phases are consumed and the melt proportion increases, unless the melts are extreme disequilibrium melts or the melt-residue system remains closed. Curved restite-melt trends may therefore be possible. Elements which become concentrated in the refractory residue will unmix along vectors with a negative gradient. Figure 7.3.a shows that the melt composition evolves away from that of the residue with time as restite unmixes. If restite unmixing is considered unlikely (due to the difficulty of fractionating phases with only minimal density contrasts), then linear compositional trends can be interpreted using the restite entrainment mechanism. Sequential restite entrainment (Holtz & Barbey, 1991) displaces the bulk composition of the extracted melt-residue combination towards the residue composition with time. Restite unmixing essentially moves the composition of the magma to that of the true melt, while restite entrainment leads to a modification of the magma composition. The process(es) responsible for the linear compositional trends displayed by natural peraluminous melts (for many major and trace elements) must therefore be understood if we are to constrain initial melt composition.

One of the most important aspects of partial melting studies is to determine the composition of the original melt. The presence or absence of restitic material will alter the original melt chemistry, as will igneous processes such as crystal fractionation and the loss of late stage melt fractions, in essence leaving a "restitic" melt. Figure 7.4. shows the contrasting P-T grids derived for melts more aluminous and less aluminous than the garnet.

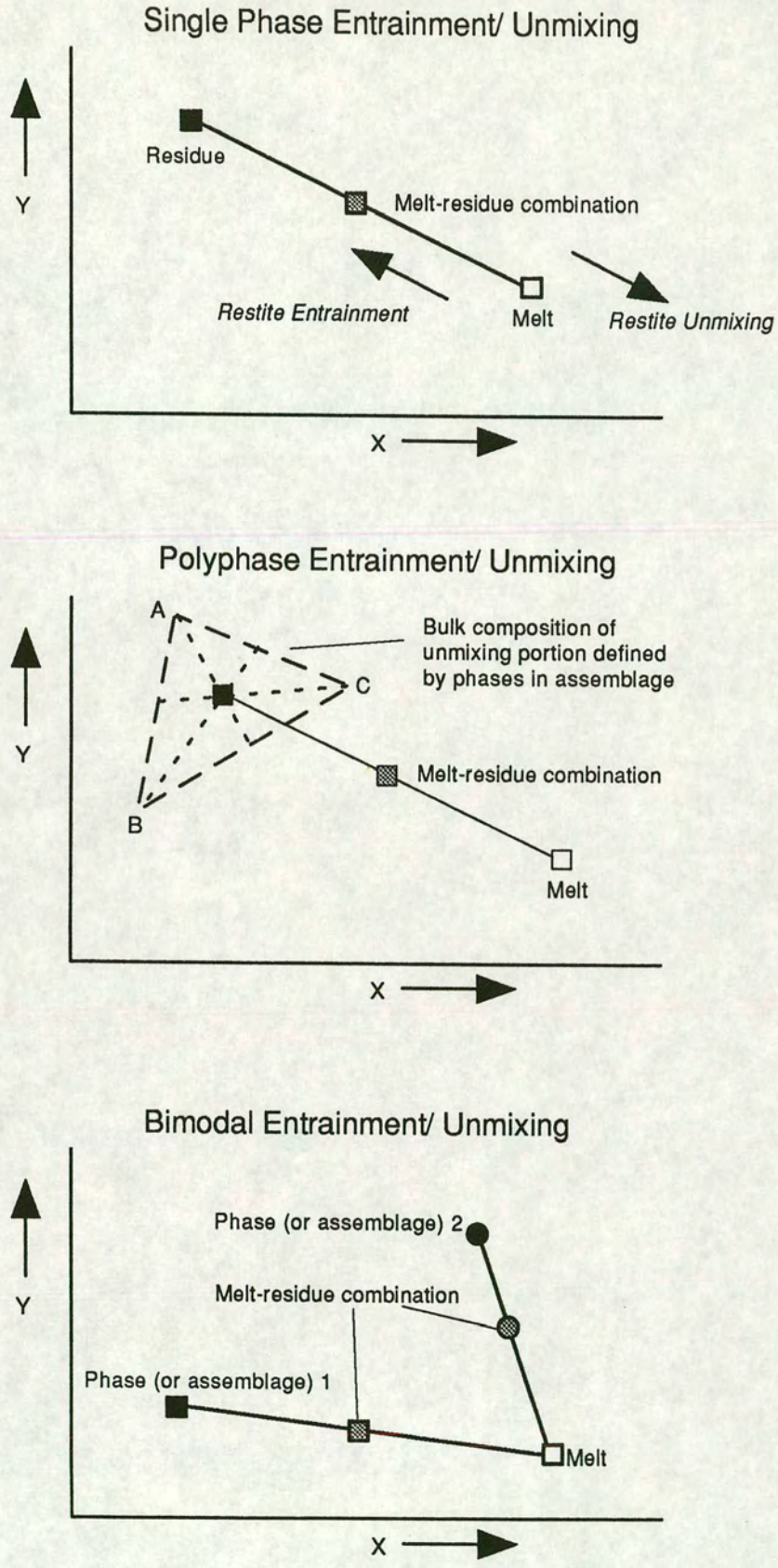

Figure 7.3. The geometry of restite unmmixing lines

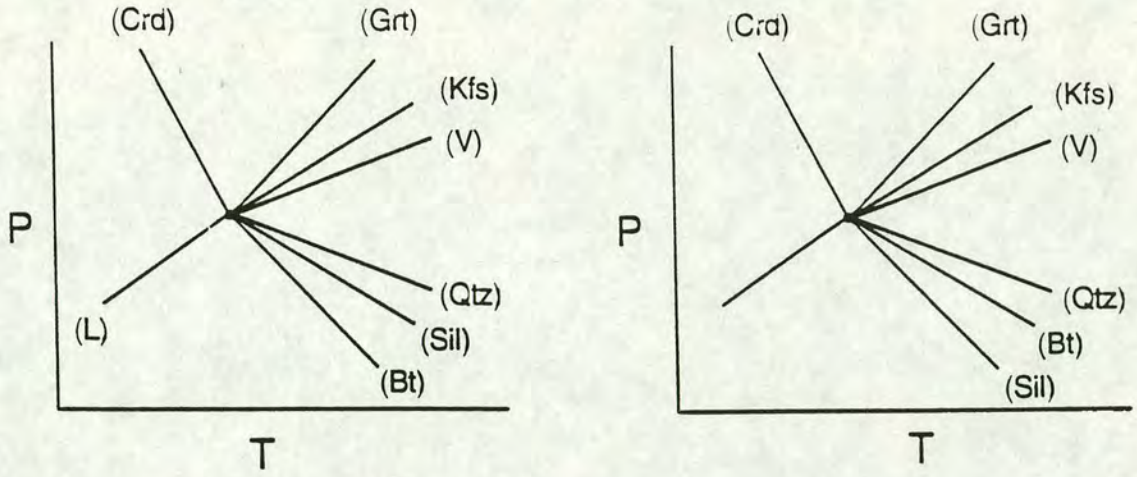

Grt + Sil + Bt + Qtz + Kfs + H2O = melt	(Crd)
Bt + Sil + Qtz + Kfs + H2O = Crd + melt	(Grt)
Bt + Sil + Qtz + H2O = Grt + Crd + melt	(Kfs)
Bt + Sil + Qtz = Grt + Crd + Kfs + melt	(V)
Grt + Crd + Kfs + H2O = Bt + Sil + melt	(Qtz)
Grt + Crd + Qtz + Kfs + H2O = Bi + melt	(Sil)
Grt + Sil + Crd + Qtz +Kfs + H2O = melt	(Bt)
Bt + Sil + Qtz = Grt + Crd + Kfs + H2O	(L)

Figure 7.4. Reaction topologies in KFMASH for melts with compositions (a) more Al-rich and (b) less Al-rich than the gt-crd tieline (After Fitzsimons, 1991).

To determine this, we must know from which end of the compositional spectrum the melt started. By distinguishing which direction melts have evolved along this spectrum (by entrainment, unmixing and/or fractionation) we can constrain the initial melt compositional fairly well. The remainder of this section is concerned with the interpretation of bulk-rock geochemical patterns shown by the leucogneisses with an aim to constraining their compositional evolution.

Linear geochemical trends are shown by several elements (major and minor) in inter-element plots for the Brattstrand Bluffs leucogneisses (Fig. 7.5.). Both single and bimodal mixing lines are seen. Single phase mixing/unmixing lines are described by Al_2O_3, MgO, Fe_2O_3 and TiO_2, and by V, Cr, and Zn When metapelite compositions are plotted on the same diagram, certain observations can be made. Figure 5.5.a shows a plot of Al_2O_3 against SiO_2 defining a broadly linear trend for metapelitic gneisses at the low Si end, through Type 2 & 3 Leucogneisses to Type 1 Leucogneisses at high SiO_2.

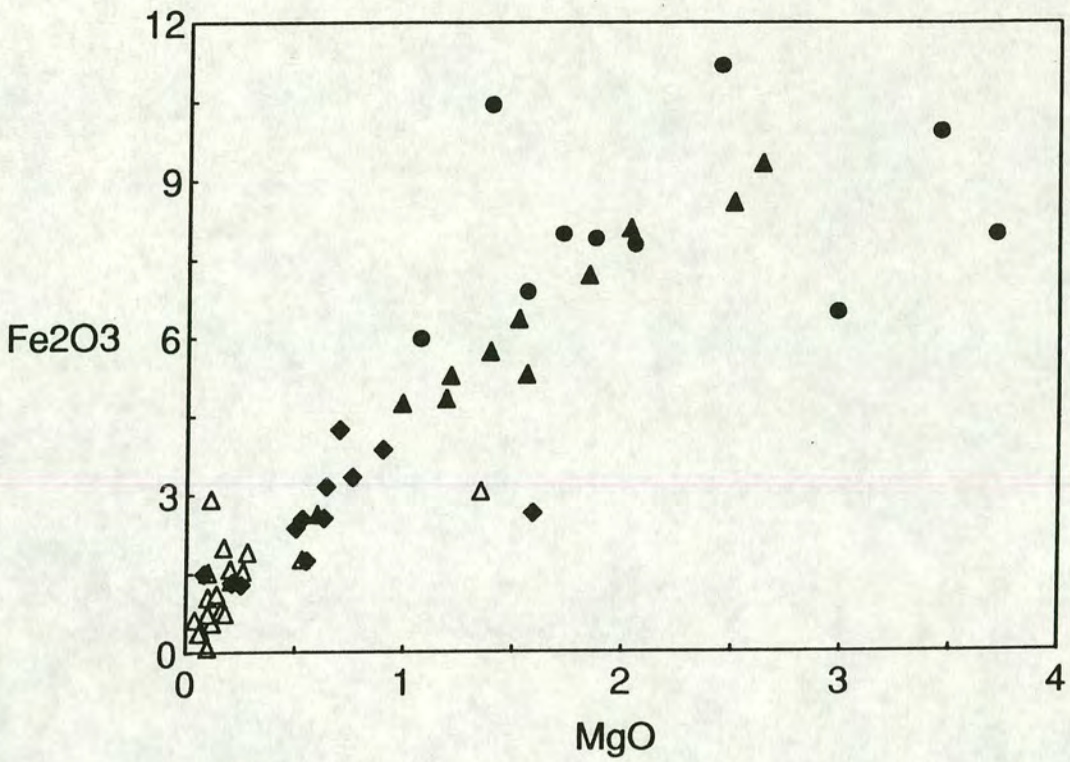

Figure 7.5. Fe_2O_3 vs MgO inter-element plot showing a single phase mixing/unmixing line.

This is a good example of single phase (represented by the metapelite bulk composition) mixing/unmixing which can be interpreted as modification of the broadly minimum melt compositions of Type 1 Leucogneisses by entrainment of varying amounts of pelitic material. A plot of Fe_2O_3 against MgO for the same samples emphasises the strongly linear correlation between these two elements (Fig. 7.5). Type 2 Leucogneisses have Fe_2O_3 contents much higher than peraluminous granitic melt solubilities predict. The increased Fe and Mg contents correlate with modal garnet and cordierite. The similarity of these phases with those of metapelites suggests that they do not represent precipitated phases from a more mafic (higher temperature) melt, but rather are entrained. One feature of this diagram is the decrease in heterogeneity from metapelites to Type 1 Leucogneisses, characteristic of partial melting.

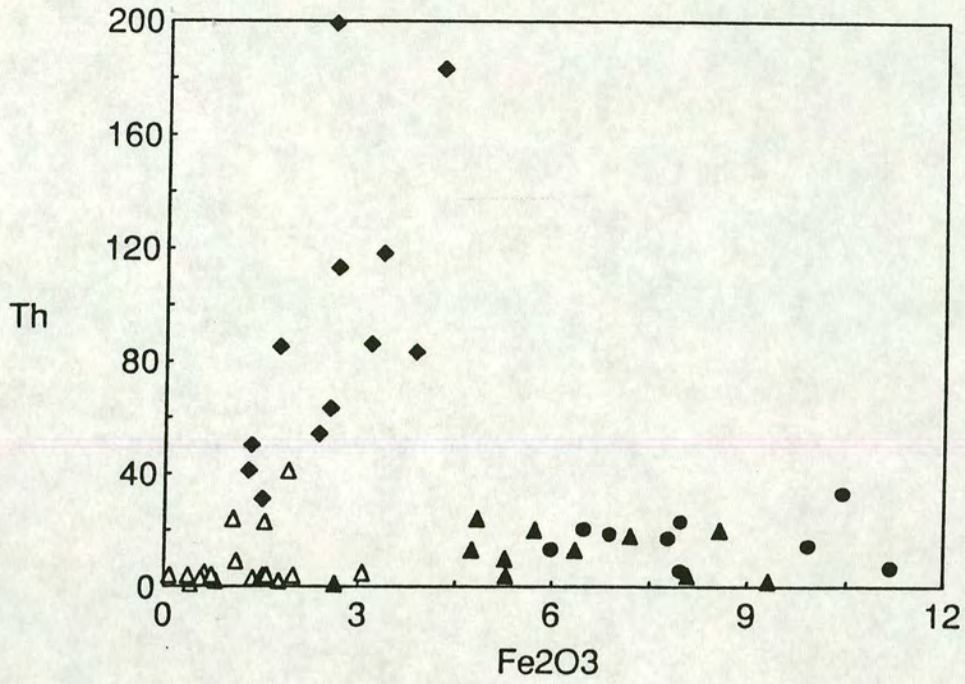

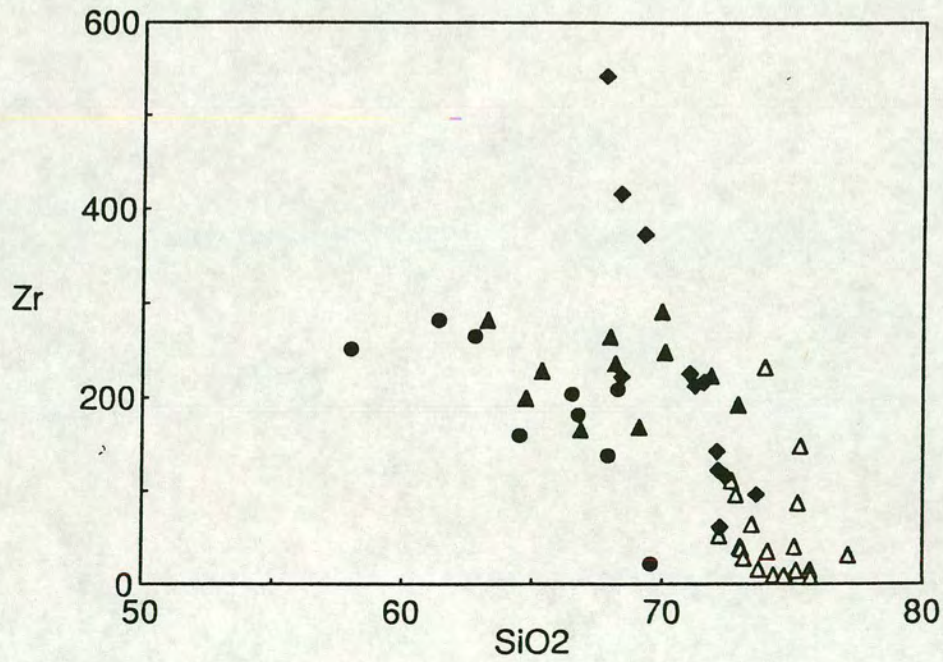

Figure 7.6.a. Th (ppm) vs Fe_2O_3 (wt%) plot showing bimodal pattern (Symbols as Figures 4.1 and 5.5)
Figure 7.6.b. Zr (ppm) vs SiO_2, showing bimodal pattern.

In contrast Figure 7.6.a and 7.6.b show bimodal plots. Again, the ends of one trend are represented by metapelite compositions and Type 1 Leucogneisses. Type 3 Leucogneisses form a second, steeper trend which is continuous with Type 1 Leucogneiss compositions. Type 3 Leucogneisses have much higher Th and Zr contents, so the mixing/unmixing lines have a phase (or assemblage) with very high Th contents. The direction of the trend if monazite or zircon were the phases entrained or unmixed is also depicted. The steep trends would intersect the Si content of monazite and zircon below the Y-axis (Zr or Th value), indicating that a small amount of some additional silicate phase or phases may be associated with the accessory phases. Obviously the steepest mixing/unmixing line for an element hosted exclusively (or dominantly in the case of Zr, since garnet in the metapelites contains some Zr) in one phase would occur when that phase is mixed on its own with melt, and shallower gradients would arise when that phase is diluted by other minerals of lesser trace element X content. In the Brattstrand Bluffs Leucogneisses, one branch of the bimodal plots can be ascribed to the mixing (entrainment) or unmixing of metapelite and the other represents accessory phase influence, acting independently of the principal restitic material. This is consistent with the release of the accessories into the melt at an early stage (most probably from a phase breaking down during melting).

Simple linear trends on two-element diagrams do not tell us whether restite entrainment or unmixing is responsible. It is reasonable to expect that the leucogneisses have retained some metapelitic residue when they were extracted. Migration distances were small, so fractionation and unmixing, although possible, are unlikely to be wholly responsible for the compositional trends developed. As melting proceeded, melt proportions would have increased and the coherence of the metapelitic gneisses decreased. Increased entrainment would therefore be expected with time or temperature. In this model, the bulk composition of the leucogneisses would evolve from Type 1 to Type 2 Leucogneiss compositions as more pelitic material was incorporated. Due to the low density contrasts between zircon and monazite and melt, and the small size of the accessory phases retained in Type 3 Leucogneisses, it is difficult to envisage a scenario where unmixing of accessories led to an evolution of melt composition from that of the Type 3 Leucogneisses to that of Type 1. A more reasonable interpretation is that

melts entrained accessory phases as they were extracted. This is developed further in the next chapter.

7.3.3. Metapelitic Gneisses (MPG).

Metapelitic gneisses from the Brattstrand Bluffs show a wide range of major and trace element compositions, reflecting the amount of melt retained and initial source heterogeneity. There is considerable compositional overlap between the more felsic metapelitic gneisses and Type 2 Leucogneisses, indicating that considerable melt retention may have occurred. Harker Type diagrams show straight lines for several elements (notably Al_2O_3, Fe_2O_3, MgO and several trace elements) from the most mafic MPG samples (SiO_2 = 57.98 wt %) to Type 1 Leucogneisses through Type 2 Leucogneisses. No MPG samples have been recorded with Th and Zr concentrations high enough to form the source end of the mixing line which links Type 1 and Type 3 Leucogneisses (Fig. 7.6.a,b), suggesting that preferential entrainment is responsible for this linear trend.

Trace element concentrations in metapelitic gneisses are similar to those of Type 2 Leucogneisses. Both are depleted in Sr and enriched in Ba and light and heavy rare-earth elements relative to PAAS (see below). Metapelites do not show the marked depletion in LREE, Th and Zr exhibited by Type 1 Leucogniesses, nor the extreme enrichment in Th and LREE shown by the Type 3 Leucogneisses. Both Type 1 and Type 3 Leucogneisses are depleted in HREE relative to PAAS, while the metapelites show enrichment. This is consistent with limited dissolution of refractory accessory phases in a departing water-undersaturated melt.

Since no true palaeosome is preserved in the complex, it is impossible to use trace element concentrations to determine degrees of partial melting. MPG samples show a slight enrichment in SiO_2 and depletion in Al_2O_3 relative to PAAS, but it is difficult to say whether this reflects an original feature of the source rocks or retention of melt. The compositional similarity between metapelitic gneisses and Type 2 Leucogneisses (REE patterns are almost identical for "average MPG and "average" LG2, Fig. 7.7.) suggests, however,

that melt extraction from the majority of metapelites was limited, most probably due to the viscosity of water-undersaturated melts produced under granulite facies conditions.

7.3.4. Melanosome.

Melanosome material from the Brattstrand Bluffs coastline have an extremely depleted, residual chemistry. SiO_2 Na_2O and CaO are very low (33-35 wt %) and Al_2O_3, Fe_2O_3, and MgO extremely high, consistent with an origin by extraction of large degrees of melt from a pelitic source. Trace element concentrations reflect the garnet-, spinel- and cordierite-rich assemblage - transition metals are high and Ba and Sr low, suggesting almost complete removal of the original feldspathic component. Both Zr and Th contents are much higher than in Type 1 Leucogneisses, and are high relative to the less restitic metapelitic gneisses. REE patterns are flat and characterised by a large Eu anomaly, and appear very similar to garnet REE patterns with the exception of high LREE contents. This is inconsistent with the near-total extraction of a melt component, and must be produced by accessory phases since none of the major phases in the melanosomes contain significant LREE.

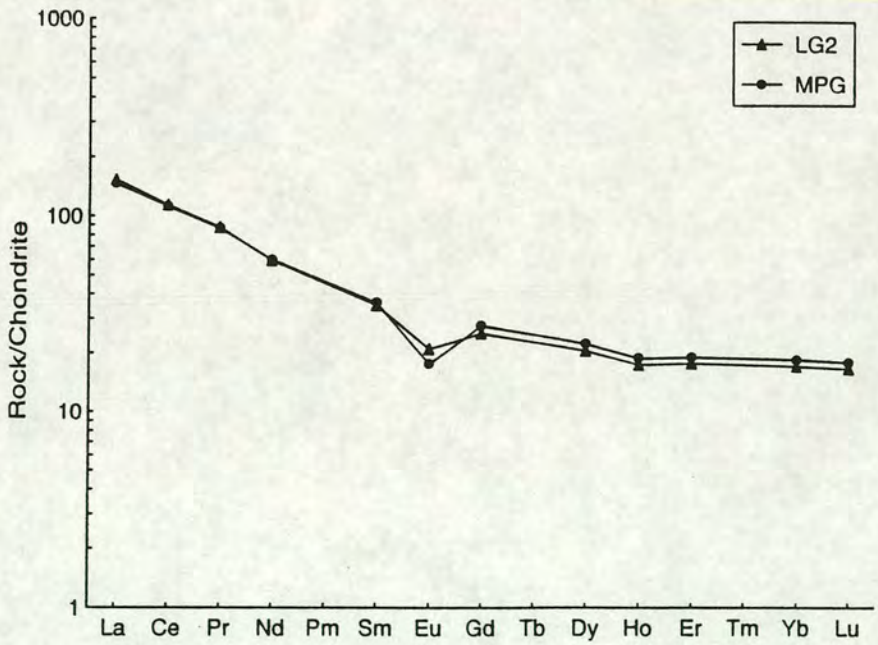

Figure 7.7. Chondrite normalised REE plot showing the similarity between average LG2 and average MPG.

In Section 7.1.6. it was suggested on petrographic grounds that instead of representing extremely depleted material which had lost large amounts of melt, the melanosomes may be either accumulations of mafic phases (dominantly garnet, but also cordierite) or the peritectic phases resulting from melt flushing. Accumulations of garnet would have low SiO_2 Na_2O and CaO, high Al_2O_3, Fe_2O_3, and MgO and associated trace elements. REE patterns from melanosome samples are very strongly controlled by the presence of garnet, and the HREE portion and large negative Eu anomaly of melanosome curves (Fig. 7.8.) would be similar to that of a garnet cumulate. Accumulation of garnet may therefore have occurred, especially in the schlieren-type melanosomes found in leucogneisses. Vein-type melanosomes (which are occasionally comprised almost entirely of garnet and/or cordierite) most probably represent peritectic material formed by melt flow along structurally-controlled pathways. Melanosome layers interbedded with metapelites again probably represent "flushed" metapelitic layers, rather than layers which have undergone extreme melting while adjacent layers show only moderate degrees of partial melting, and their more depleted chemistry results as a result of dynamic, rather than static, melting processes.

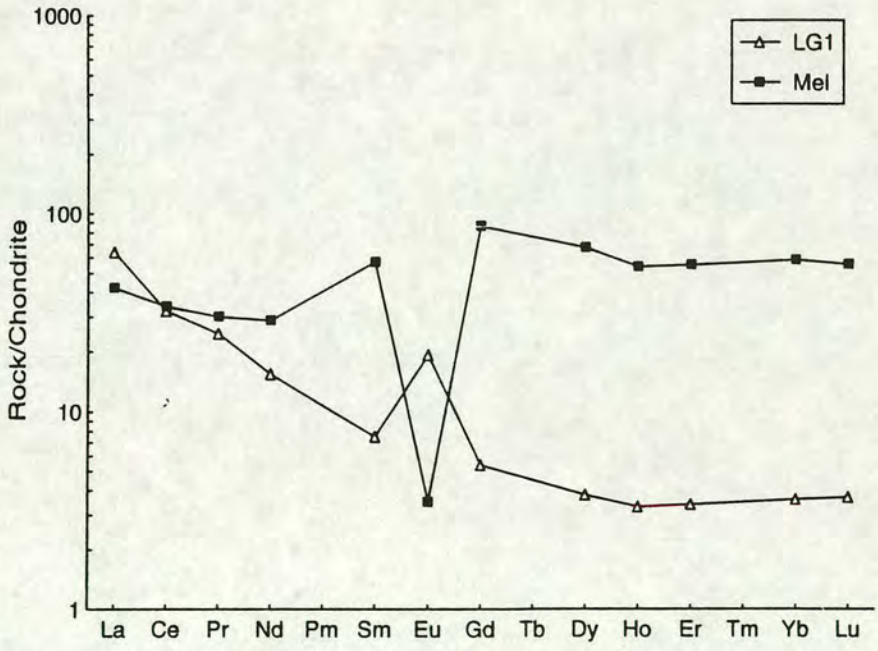

Figure 7.8. Chondrite normalised REE curves for average LG1 and MEL (sample IF/88/58). Note the relatively high LREE concentration of IF/88/58.

7.4. MODEL FOR MELT PRODUCTION AND EXTRACTION.

7.4.1. Estimates of Melt Water Content.

All granitic magmas, including those produced under water-undersaturated conditions, contain some H_2O. The amount of water present will have important consequences for the viscosity of the melt (and therefore how efficiently melt extraction can occur), liquidus phase relations, the dissolution of accessory phases (thus influencing trace element geochemistry) and the extent to which retrogression due to expulsion of water on crystallisation of the melt occurs. For a full understanding of the processes involved in the production of the Brattstrand Bluffs coastline migmatites it is therefore important that an estimate of the water content of the leucogneisses is obtained.

In the absence of externally derived aqueous fluids dehydration melting reactions in the source rock are buffered to lower aH_2O as melting proceeds, while the water content of the granitic liquid produced will decrease as melt volumes increase. There is therefore a direct relationship between water activities in melts and water activities in the melting source rock. Burnham (1976) noted a linear relationship between aH_2O and $X_{H_2O}^{Melt}$ for $X_{H_2O}^{Melt} < 0.5$. The mole fraction of H_2O can be calculated from the equation;

$$aH_2O = k(X_{H_2O}^{melt})^2 \qquad (7.1)$$

Fitzsimons (1991) estimated aH_2O in the Brattstrand Bluffs metapelites using the calibration curves of Edwards & Essene (1988) for the reaction biotite + sillimanite + quartz = garnet + K-feldspar + H_2O at 860°c and 6kbar. Since water will segregate preferentially into silicate melts, water contents will be lower in the pelites than the melt. Water activity is, however, fixed at the site of melting so at the time of melting, melt and pelite water contents are fixed using the above calculation. The low aH_2O values (equivalent to water contents of less than 2wt %) calculated for the metapelites by Fitzsimons (*op cit*) therefore represent an estimate of the minimum melt water content.

Calculated aH_2Ovalues range from 0.01 to 0.16 and are mostly less than 0.1. The results of the above calculation for a range of aH_2O values are shown in Figure 7.9. A melt coexisting with a pelite with $aH_2O = 0.1$ would have a minimum water content of 1.65 wt % H_2O if the aH_2O of the melt was the same as that of the metapelite.

Another estimation of melt water content can be obtained from Equation 7.1. if the activity used is the aH_2O of the melt itself. The aH_2O of a dehydration-melting reaction is defined by the P and T of the solidus for that reaction. Clemens & Vielzeuf (1987) constructed an isobaric T-aH_2O section for a fictive dehydration-melting reaction in the Qtz-Ab-Or-H_2O system at P=5 kbar, and showed that at T= 860°c $aH_2O = 0.25$. Solidus curves in the system Qtz-Ab-Or-H_2O-CO_2 constructed by Johannes & Holtz (1990) give similar aH_2O values of between 0.2 and 0.3. These activities correspond to melt water contents (calculated using Equation 7.1) in the Brattstrand Bluffs leucogneisses of 2.6-3.5 wt % H_2O. The majority of crustally derived silicic to intermediate magmas have water contents in the range 1-7 wt % H_2O and averaging 3.5 wt % H_2O (Clemens, 1984). Clemens & Vielzeuf (1987) calculated the water content of melts derived by anatexis of various lithologies containing hydrous phases and found that melts produced by breakdown of biotite contain 2.9 wt% H_2O at 5 Kb and 3.7 wt% H_2O at 10 Kb.

7.4.2. Evolution of Melt Water Content and Controls on Extraction.

The Type 1 Leucogneisses of the Brattstrand Bluffs coastline, with their high silica, low Mg, Fe, Ti, Cr, Ni, Zr, Th and LREE and apparently low restite component, have the geochemical and petrographic characteristics of low melt fraction anatectic liquids. They were almost certainly produced at melt fractions below the Rheologically Critical Melt Proportion (RCMP) (the melt fraction at which a partially molten solid loses coherence and begins to behave like a dense suspension). If the Type 1 Leucogneisses represent melt proportions of approximately 0.1-0.2 produced by partial melting of a typical pelite containing 1 wt% H_2O they would have contained approximately 3.5-4.5 wt% H_2O. Figure 7.9. shows that as the degree of melting increases the water content of the melt decreases (since the water content of the system is

fixed and increasing melt proportions simply "dilutes" the melt H_2O concentration). Initial melts formed in the Brattstrand Bluffs migmatite complex were probably water-saturated for a few degrees above the solidus. As melting proceeded aH_2O was buffered to lower values both in the metapelites and the melts, and the melt water contents decreased.

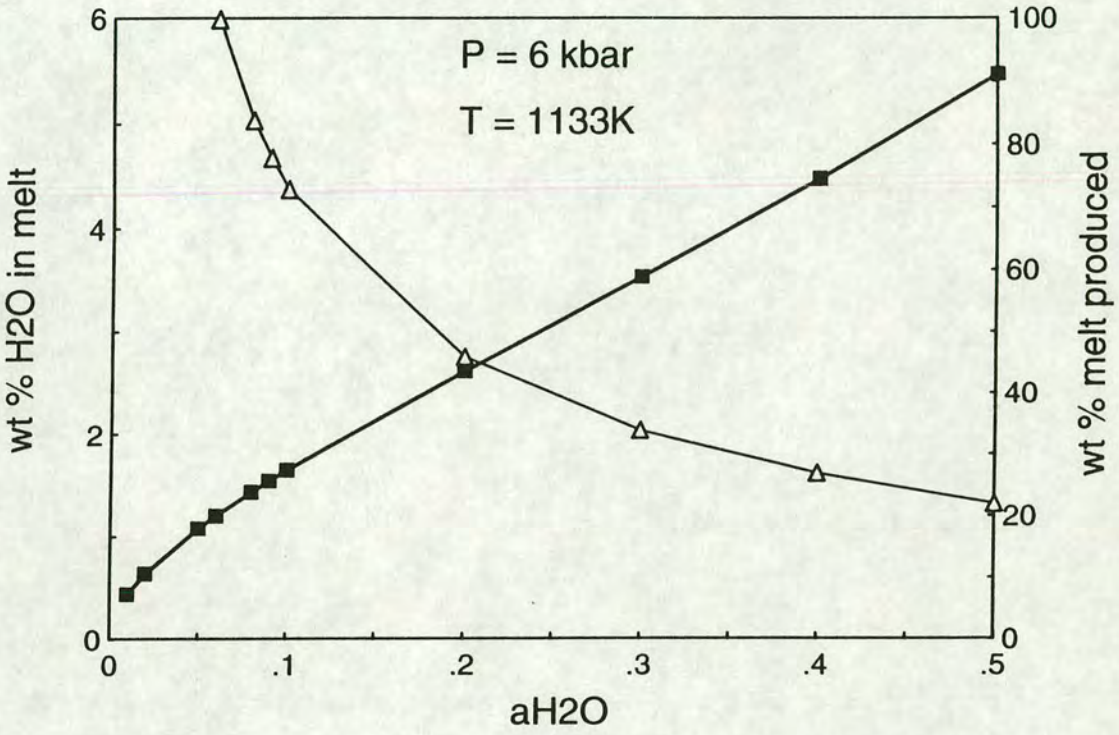

Figure 7.9. Graph showing Wt % H_2O against aH_2O (black squares, using the methods of Burnham (1976) and Clemens & Vielzeuf (1987). Also shown is wt% melt produced as a function of source H_2O content (white triangles) for a source containing 1.23 wt % H_2O (after Clemens & Vielzeuf, 1987).

Early low melt-fraction liquids, represented by the Type 1 Leucogneisses, were extracted efficiently but remained in the complex - migration distances of 500m or less. As melting proceeded, melt proportions increased and the R.C.M.P. was exceeded. At melt fractions of 0.4-0.5 melt water contents were lower (approximately 2 wt% H_2O) and consequently the melts were more viscous, less extractable and therefore more likely to entrain restitic and peritectic phases as the metapelites lost their coherence.

Water activities calculated for Type 1 Leucogneisses (0.3-0.4) are much higher than those calculated by Fitzsimons (1991) for the metapelites (0.02-0.16). Waters (1988) noted that gradients in aH_2O will develop in migmatites due to the diffusion of H_2O into melt segregations, but that these gradients could only be sustained by grain boundary diffusion over short distances. For the calculated activity gradients on a scale of metres to tens of metres recorded in the Brattstrand Bluffs migmatites, channelisation of aqueous fluids into melts must have occurred. These melts may have acted as a transfer medium for H_2O, removing water from the site of melting into shear zones. The anhydrous mineralogy of the leucogneisses (with mineral assemblages dominated by quartz-K-feldspar-plagioclase±garnet±cordierite) suggests that any aqueous fluid phase present was removed before the solidus was reached. It is therefore suggested that the leucogneiss sheets themselves lost a small amount of mobile, almost water-saturated residual melt (i.e. open-system behaviour at the final stages of melting).

7.4.3. Composition of Fluids dissolved in the melt.

The majority of fluids involved in crustal metamorphism are C-O-H-rich fluids. The breakdown of hydrous phases during partial melting produces an aqueous component, while organic matter in shales provides a source for carbon. An additional source of carbon from mantle derived fluids has been proposed for several granulite terranes (e.g. Touret, 1971; Newton, 1990; Newton *et al*, 1980). The water-undersaturated melts of the Brattstrand Bluffs coastline obviously contained carbon, since graphite is present as an accessory phase in both metapelitic gneisses and leucogneisses. The abundance of CO_2 is unlikely to have been very great, since the amount of graphite rarely exceeds 0.1 modal % (Fitzsimons, 1991). Furthermore, stable isotopic data (Fitzsimons, *pers comm*) suggests that this carbon has a dominantly biogenic source (δ13C = -15 to -25 per mil.), rather than a mantle origin. The addition of CO_2 before peak metamorphic conditions were attained would lower the aH_2O of the system (effectively increasing the temperature of the liquidus at any given P and T, see Fig. 2.6), inhibiting melting. The preservation of granulite facies conditions in the metapelitic gneisses by CO_2 flushing would therefore preclude melting as an origin for the leucogneisses. A better explanation for the increased carbon

concentrations leading to graphite precipitation is the model outlined in Section 7.3.2. By increasing aCO_2 by progressive dissolution and extraction of H_2O in a water-undersaturated melt small amounts of graphite could easily be precipiated during melting. This mechanism also provides an explanation for the presence of texturally-late graphite in the leucogneisses, since aCO_2 would increase progressively during melting until graphite was precipitated if water was preferentially extracted in melts, assuming that the anhydrous leucogneisses themselves lost a late stage, near water-saturated liquid (i.e. late graphite precipitation could have accompanied the loss of a hydrous fluid near the solidus).

Fluorine is an important species in many magmatic systems since HF will react with O^{2-} bridging ions, producing a dissociation analogous to the addition of H_2O (Burnham, 1979), resulting in lower viscosity. Substitution of F for OH in phlogopite stabilises phlogopite + quartz bearing assemblages to higher temperatures, and may be important in restricting vapour-absent melting in high-fluorine micas. In addition, Holtz et al (1993, *in prep.*) demonstrated that H_2O solubility in a melt increases with increasing melt F content at fixed P and T. At 2kbar an increase of 0.35wt% H_2O solubility was recorded by Holtz et al (op cit) for the addition of 1wt% F. It is important to note, however, that the decrease in melt viscosity because of higher H_2O solubility in F bearing melts will only be important for water saturated melts. The addition of F to the melt by the breakdown of biotite during dehydration melting will lower melt viscosity and aid extraction solely by the depolymerisation of the melt.

Fluorine partitions strongly into biotite over melt and volatile fluid. During incongruent partial melting of biotite, F is released and dissolved in the melt. If the system remains closed and no melt is extracted, then the retrograde biotite which grows will have the same F content as pre-melting biotite. If a water undersaturated but F-bearing melt is removed then, on cooling and recrystallisation, biotite will grow with a higher F content in the case where some aqueous fluid is lost. Fitzsimons (1991) used this mechanism to explain the F-enrichment of shear zone biotite relative to pre-melt biotite retained in the cores of early Type I Garnet.

Experimental work (Keppler & Wyllie, 1990, 1991) has shown that chemical fractionation of certain elements can occur in fluids containing C-O-H-F and Cl. Partition coefficients for Th and U are very low when H_2O is the only volatile species present. They increase strongly if F is present due to the production of fluoride complexes. Fluoride-rich solutions are able to extract some U and Th from a magma. U, but not Th, can be complexed to a lesser extent by Cl and carbonate (Keppler & Wyllie, 1991), while Th is not affected by CO_2-rich fluids, so a possible mechanism for fractionation of Th and U in magmatic systems involving CO_2 rich fluids exists.

In the Prydz Bay Leucogneisses, U is typically low, while Th shows variable enrichment in samples strongly dependant upon the modal abundance of monazite. U contents in Type 1 Leucogneisses are much higher than Type 2 Leucogneisses. Furthermore, U appears lower in monazite rims than monazite cores. During melting, the model for fluid evolution proposed above suggests that fluid compositions in the melt evolved from H_2O-rich to relatively CO_2 rich, as H_2O was preferentially extracted from the area of melting. Since CO_2 solubility is much lower than H_2O solubility in granitic melts, XH_2O will remain relatively high. As melting proceeded, the fluids extracted in the melt may become more CO_2-rich, allowing the removal of U (in the form of carbonate complexes) and the fractionation of U relative to Th. The extent to which CO_2 is enriched will depend on fO_2, since the precipitation of graphite may maintain a constant aH_2O despite the removal of H_2O-enriched melts. If CO_2 does increase, the Th/U ratio of monazite would increase as melts become more water undersaturated. In the model presented above, water activities decrease from early water undersaturated melts (LG1) to later melts (LG2), with MPG samples having the lowest aH_2O. Th/U should therefore be higher in monazite rims in metapelites than in Type 2 Leucogneisses. Table 8.3. (next chapter) shows this is the case. In addition, the earliest (high aH_2O, low aCO_2) melts have higher U contents than later melts (LG2) which contained dissolved fluids with a higher aCO_2.

Chapter 8.

Accessory phase controls on trace element behaviour.

Chapter 8. Accessory phase controls on trace element behaviour.

8.1. ACCESSORY PHASE BEHAVIOUR DURING ANATEXIS.

Incompatible elements such as Zr and LREE should preferentially partition into the melt during fusion. However, because they are essential structural components of accessory phases such as zircon and monazite they will be strongly partitioned into these phases in preference to any other phases or the melt (Miller & Mittelfehldt, 1982; Watson & Harrison, 1983). As a consequence, the concentrations of these elements in the melt are generally considered to be a good indication of the extent to which zircon and monazite are being consumed during melting. Accessory phases such as zircon have been the focus of several detailed studies on melt-mineral relationships (Montel, 1986; Bacon, 1989; Dirks & Hand, 1991) and the geochemical effects of entrainment and segregation (Miller, 1985; Miller and Mittelfehldt, 1982). They frequently exhibit petrographic characteristics (euhedral overgrowths, irregular embayments) related to growth and/or consumption through the crustal melting cycle. Crustal rocks which contain more than 60ppm Zr will yield melts saturated in zirconium (Watson, 1988). Similarly most of the continental crust has a high enough LREE concentration to saturate a peraluminous melt in a LREE bearing phase such as monazite (Miller & Mittelfehldt, 1982). Zircon and monazite are, therefore, likely to be present as accessory phases in most crustal melts, with important consequences for trace elements such as Th, Hf and U. As partial melting proceeds, easily fused components will melt first and a residue enriched in refractory phases such as zircon will be produced. Once the melt is saturated in Zr the level of Zr in the melt remains constant (Watson & Harrison, 1984), and the limited solubility of Zr and LREE in crustal melts (Weber & Barbey, 1987) ensures this concentration will be relatively low. Using empirical equations which take into account melt composition and temperature it is possible to calculate the saturation concentration (in ppm) for Zr and LREE (La-Gd) for a typical peraluminous melt of 73 wt% SiO_2 at a given temperature. These equations are;

$$ln C_{Zr} = 17.18 - 12900/T \text{ (for zircon) and}$$

$$ln\ C_{LREE} = 18.50 - 14160/T \text{ (for monazite)}$$

(Watson, 1988) and give saturation concentrations of 96.5ppm for Zr and 105.9ppm for LREE in a water saturated felsic melt (73 wt% SiO_2) at 750°c. A more refined empirical formula for REE saturation has been produced by Montel (1992). The model is derived from experimental data in the system $CePO_4$-SiO_2-$Al2O_3$-Na_2O-K_2O-excess H_2O at 800°C, and takes into account temperature, water content and melt chemistry. The solubility of the REE (considered as one element from La to Gd) is given by:

$$ln(REE_t) = 9.50 + 2.34D + 0.03879\sqrt{H_2O} - 13318/T$$

where

REE_t	=	La/139.91 + Ce/140.12 + Pr/140.90 + Nd/144.24 + Sm/150.40 + Gd/157.25. (REE in ppm, denominator is atomic weight).
D	=	(Na + K + 2Ca) / (Al.(Al + Si))
T	=	Kelvin
H_2O	=	wt %

Zr and LREE are essential structural constituents (ESC) in zircon and monazite respectively, so that the concentration of the ESC elements in an anatectic melt will be strongly controlled by the mineral phase behaviour and not by trace element partition coefficients (as would be the case for Rb, Sr, or the HREE in zircon). Four factors will affect the concentration of ESC elements in an anatectic melt. These are;

(i) The extent to which the accessory phase grain is in contact with the melt.
(ii) The solubility of the accessory phase containing the ESC.
(iii) Relative rates of solubility and extraction.
(iv) The initial concentration of the ESC in the parental lithology undergoing partial melting.

Anatectic melts may contain anomolously low Zr and/or LREE concentrations if the accesory phases in the protolith are shielded by preferential inclusion within coarse major phases which are either not being consumed in a melting reaction or are growing as a peritectic phase with melting. Accessory phases

hosted at grain-grain contacts or within phases actively contributing to the melting reaction will, in contrast, be continuously in contact with the melt and be able to contribute to the trace element budget controlled by solubility and rate of dissolution.

In general, the solubility of zircon is enhanced in wet melts, in higher temperature melts and in melts where SiO_2 concentration is low (Watson, 1988). Watson & Harrison (1983) state that at H_2O concentrations above the threshold of >1.5-2.0 wt.% zircon solubiliity in melts is independent of water content, whereas a water-undersaturated granitic melt containing only 0.2 wt.% H_2O dissolves 30-40% less zircon than a melt containing 2 wt.% H_2O at high temperatures (1200-1500°C). Since crustal melts formed through dehydration-melting under granulite facies conditions are water-undersaturated, residual zircon is likely to occur as a consequence of partial melting because the solubility of Zr in the melt is reduced (Fig 8.1).

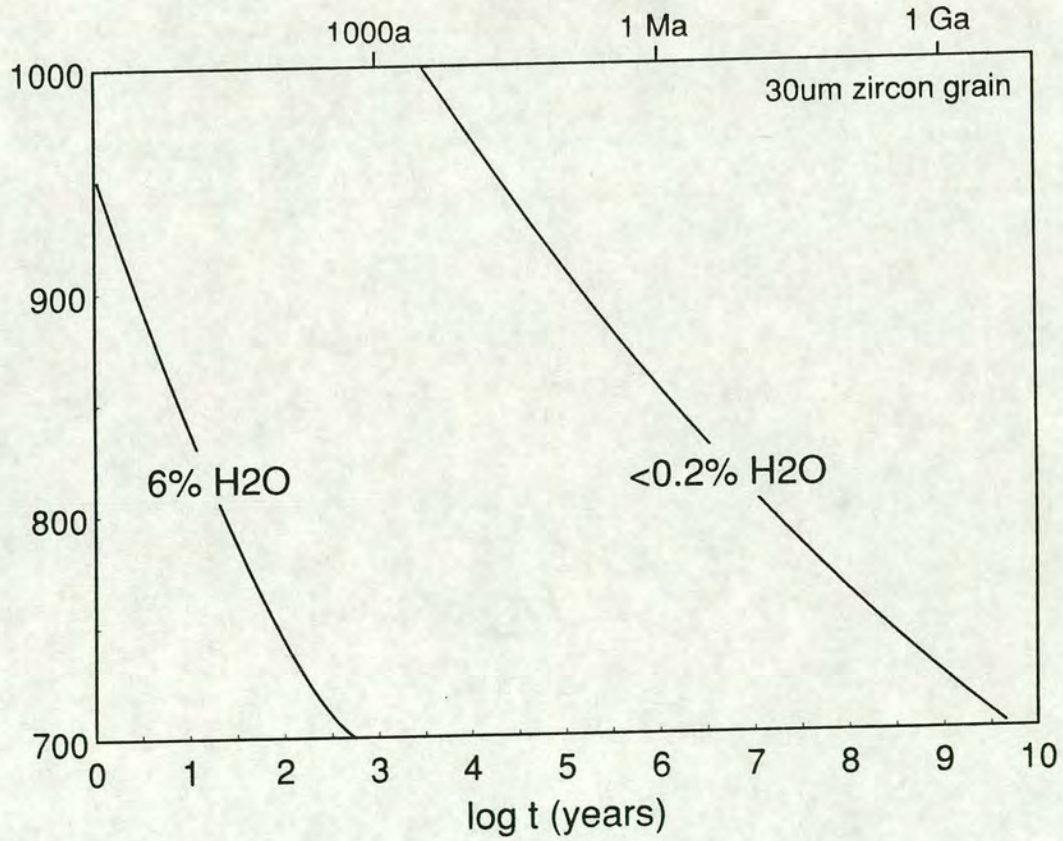

Figure 8.1. Zr solubility in haplogranitic melt as a function of T, time and H_2O (after Watson, 1988).

The solubility of monazite is dramatically reduced in drier and more peraluminous melts (Montel, 1986), and so monazite too is likely to exist as a residual phase under typical crustal melting conditions. With increasing differentiation in a rock suite LREE concentrations will increase until the monazite saturation curve is intercepted. At this point, monazite will start to precipitate, and if removed from the melt the total LREE concentration of the melt will fall (Fig 8.2.).

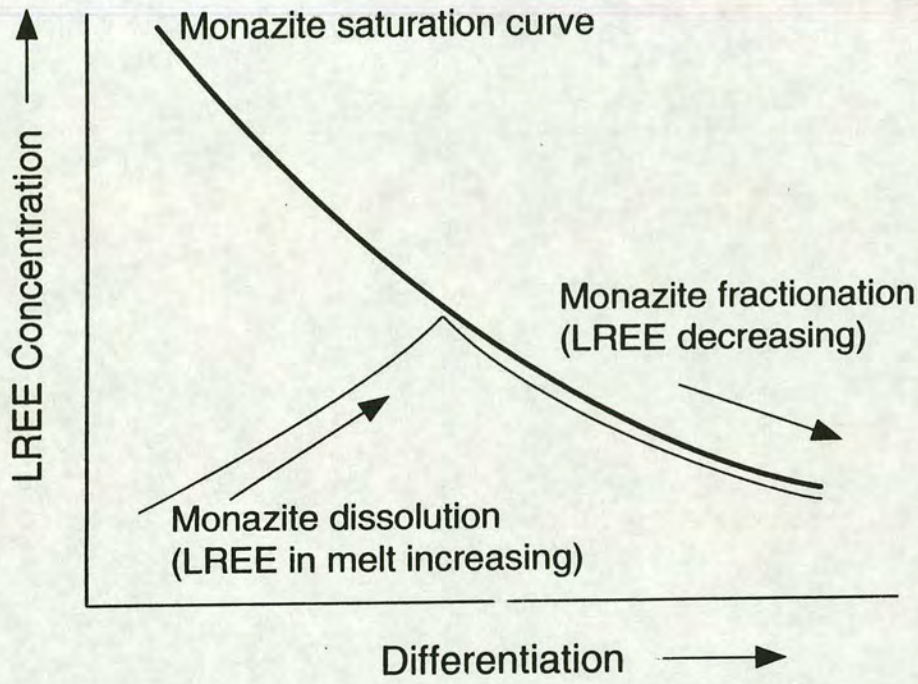

Figure 8.2. Variation of LREE content in a peraluminous magma with fractionation (after Miller & Mittelfehldt, 1982).

Fractionation of monazite has been proposed as a mechanism for LREE depletion with increased differentiation in peraluminous granites (Miller & Mittlefehldt, 1982).

The rate at which an accessory phase dissolves will also determine ESC element concentrations in the melt. Monazite dissolution is slow, and it may take up to 10^7 years to dissolve a large monazite crystal (Fig 8.3.) (Watson, 1988; Rapp &

Watson, 1986). Crystals larger than 30-100mm would be expected to survive over the duration of a crustal fusion event, whilst grains smaller than 30mm would probably be rapidly consumed (Rapp & Watson, 1986). Zircon solution is typically faster, although under water-undersaturated conditions it is still sluggish, and large original grains should survive the melting process as is shown by the extensive inheritance preserved in many S-Type granite zircons.

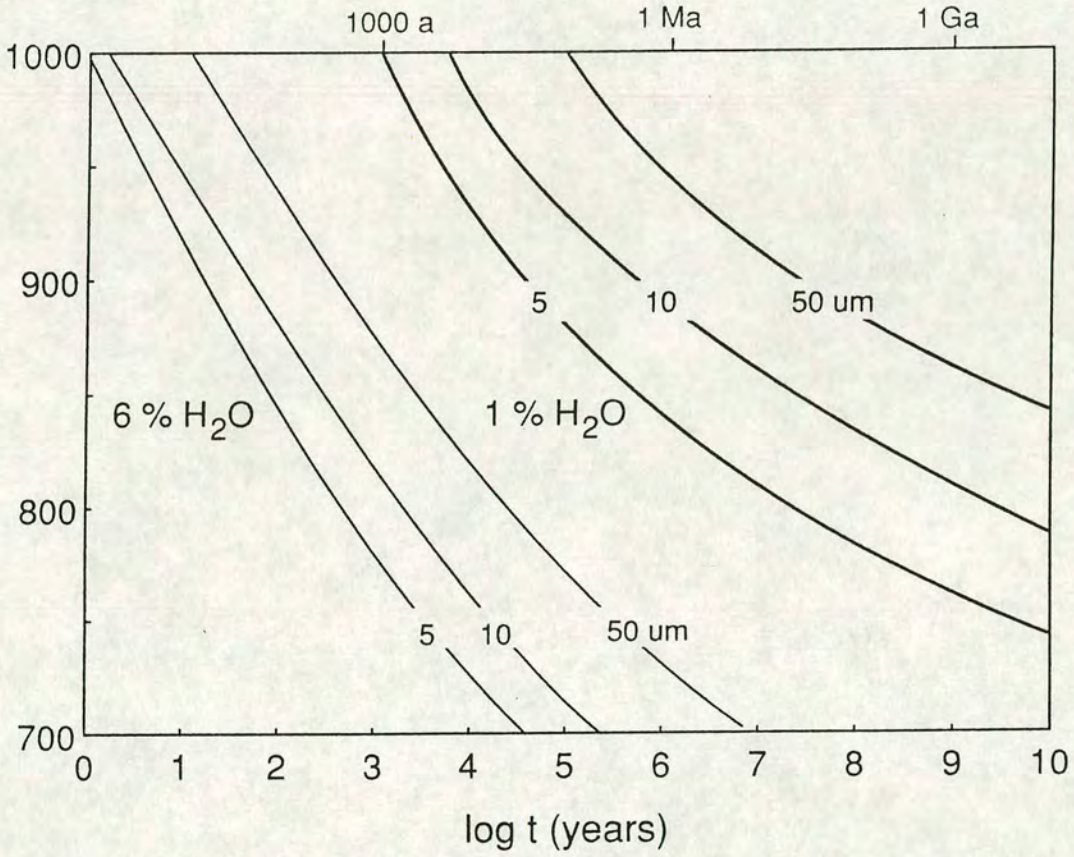

Figure 8.3. Monazite dissolution as a function of P, T and grainsize (after Rapp & Watson, 1986).

8.2. GEOCHEMICAL IMPORTANCE OF ACCESSORY PHASES IN THE PRYDZ BAY LEUCOGNEISSES.

8.2.1. Mass Balance.

The problem of accessory phase contribution to REE budgets in crustal melts has been recognised by many workers (e.g. Gromet & Silver, 1983). Accessory minerals are typically very small, but contain considerable amounts of rare-earth elements. The addition or removal of a REE-bearing phase to a melt may have important implications for the bulk REE pattern and subsequent petrological and geochemical interpretations. The role of accessory phases in determining REE chemistry can be addressed through mass balance calculations if the mineralogical compositions of the melts, restites and initial source rocks are known and, most importantly, if the REE and trace element compositions of the major mineral phases involved in the melting reactions are measured. In this study REE patterns for all important major phases have been obtained using SIMS analysis. In the mass balance calculations four lithologies have been considered:

(i) Type 1 Leucogneiss (garnet absent) (IF/88/276).
(ii) Type 1 Leucogneiss (garnet present) (IF/88/61).
(iii) Type 3 Leucogneiss (IF/88/122)
(iv) Melanosome (IF/88/58)

Modal values were obtained by point counting (500-600 points per sample) and converted to weight proportions using relevant densities, while SIMS REE data (Table 8.1) was used to generate REE plots for each rocktype using feldspar, garnet and biotite REE concentrations. SIMS analyses show that sillimanite, cordierite and spinel contributions to the REE budgets are negligible and can be ignored in the calculations. Although moderately high REE contents for cordierite have been recorded (F. Bea, *pers. comm.*) SIMS analysis of several cordierite grains showed that REE contents were extremely low.

Garnet and K-feldspar are the most important major phase contributors to the REE bulk rock patterns. K-feldspar shows a concave up, LREE-enriched pattern with a large positive Eu anomaly typical of those reported by other workers (Gromet & Silver, 1983; Reid, 1990). Garnet shows low LREE, high (but variable) HREE and a significant negative Eu anomaly ($Eu/Eu^* = 0.01$-0.10). Calculated results incorporating the modal data and major mineral phase REE data are shown as chondrite normalised plots (Fig. 8.4) with the observed bulk rock REE patterns for each sample shown for comparison.

The calculated pattern for sample the LG1 sample IF/88/276 correlates very well with the observed pattern for both LREE and HREE (Fig 8.4.a.), the most notable feature being the large calculated positive Eu anomaly. The modal proportions for this leucogranite are essentially similar to those of typical orthoclase-rich peraluminous crustal melts produced under vapour absent conditions (e.g. 50% K-feldspar, 30% quartz, 15% plagioclase and a small amount of biotite).

IF/88/61 is a Type 1 Leucogneiss which contains approximately 5% almandine garnet. Both the calculated and observed REE patterns for garnet-bearing leucosomes show a strongly positive Eu anomaly superimposed on a U-shaped pattern with depletion of MREE (Fig. 8.4.b.). The slight increase of HREE with respect to MREE reflects the contribution of small amounts of garnet to the REE budget. The similarities of the observed REE abundances with those calculated for these LG1 suggests that the majority of the REE are contained in major phases (feldspars, garnet) and that little or no contribution has been made by monazite or zircon.

Type 3 Leucogneisses typically have a modal mineralogy very similar to those of Type 1 Leucogneisses. As shown above, a rock consisting dominantly of two feldspars, quartz and a small amount of garnet should give rise to a pattern low in both LREE and HREE, with a characteristic large positive Eu anomaly. Figure 8.4.c. shows that Type 3 Leucogneisses have a REE pattern which does not correlate well with the REE contributions calculated from individual major phases. Type 3 Leucogneisses exhibit very high LREE totals, small negative Eu anomalies and low HREE totals (similar to LG1) giving rise to very steep REE curves. MREE are also higher in Type 3 Leucogneisses. Accessory phases such as monazite, which only occur in trace amounts, have not been included in the modal calculations and hence are not accounted for in the calculated REE patterns. As a consequence it is likely that the discrepancies between calculated and observed REE patterns reflect contributions from these accessories.

Based on the above it is suggested that the high LREE concentrations observed in Type 3 Leucogneisses reflect the entrainment of monazite. The correlation of high Th values with high La concentrations in Type 3 Leucogneisses (Fig. 8.5) is consistent with this interpretation, since monazites from the Brattstrand Bluffs coastline contain 8-23 wt % ThO_2. Type 3 Leucogneisses also exhibit

Table 8.1. Modal and SIMS REE compositions used for mass balance calculations.

Modal Composition (converted to weight fraction)

Sample no'	88/276	88/61	88/152	88/58
Qtz	0.32	0.32	0.38	0.00
Kfs	0.50	0.32	0.28	0.00
Plg	0.17	0.30	0.16	0.00
Grt (1)	0.00	0.00	0.00	0.35
Grt (2)	0.00	0.05	0.08	0.08

REE Concentration (ppm)

Sample no'	88/276	88/61	88/152	88/58
La	13.90	17.68	12.03	0.02
Ce	20.63	28.49	18.67	0.05
Nd	4.07	5.95	3.80	3.99
Sm	0.46	0.81	0.48	8.55
Eu	1.85	1.27	1.22	0.04
Gd	1.46	2.41	1.46	13.91
Dy	0.21	0.05	0.12	17.81
Ho	0.10	0.51	0.23	4.05
Er	0.03	0.16	0.05	10.56
Yb	0.02	3.05	1.14	12.63
Lu	0.02	0.46	0.18	1.56

Major phase REE concentrations (ppm)

Phase	Av Plag	Av Kfs	Av Grt (2)	Av Grt (1)	Av Grt (2)
	n=2	n=4	n=4	n=2	n=2
Lithology	LG1	LG1	LG1/2	MEL	MEL
La	45.9	11.8	0.0	0.1	0.0
Ce	79.4	13.5	0.0	0.1	0.2
Nd	17.3	2.1	0.4	9.6	8.2
Sm	2.0	0.2	2.3	18.7	26.2
Eu	0.5	3.5	0.1	0.1	0.1
Gd	5.5	1.0	7.9	28.8	50.1
Dy	-	0.4	23.5	38.6	56.2
Ho	0.0	0.2	8.2	8.8	12.5
Er	0.3	0.1	31.5	23.2	32.0
Yb	-	0.0	56.3	27.5	39.1
Lu	0.0	0.0	8.2	3.4	5.1

Note: Grt (1) and Grt (2) refer to early, inclusion rich garnet and later, peritectic garnet respectively.

Fig.8.4.. The results of mass balance calculations for 4 lithologies. **Fig. 8.4.a** - Type 1 Leucogneiss, garnet absent. **Fig. 8.4.b**. - Type 1 Leucogneiss containing 5 wt% garnet. **Fig. 8.4.c** - Type 2 Leucogneiss. **Fig. 8.4.d** - Quartz-absent Melanosome.

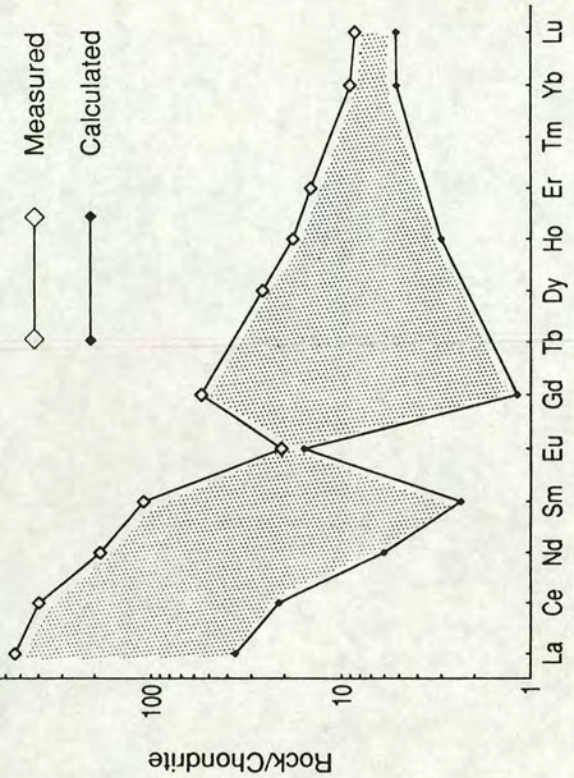

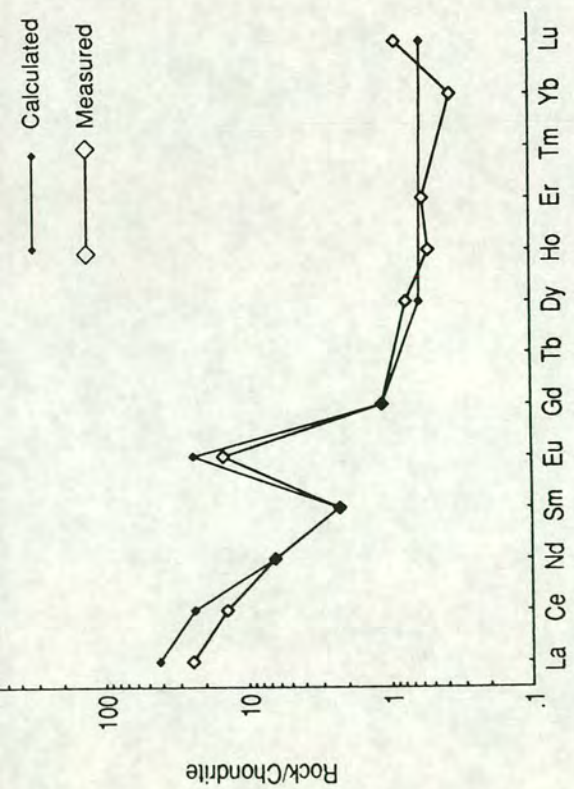

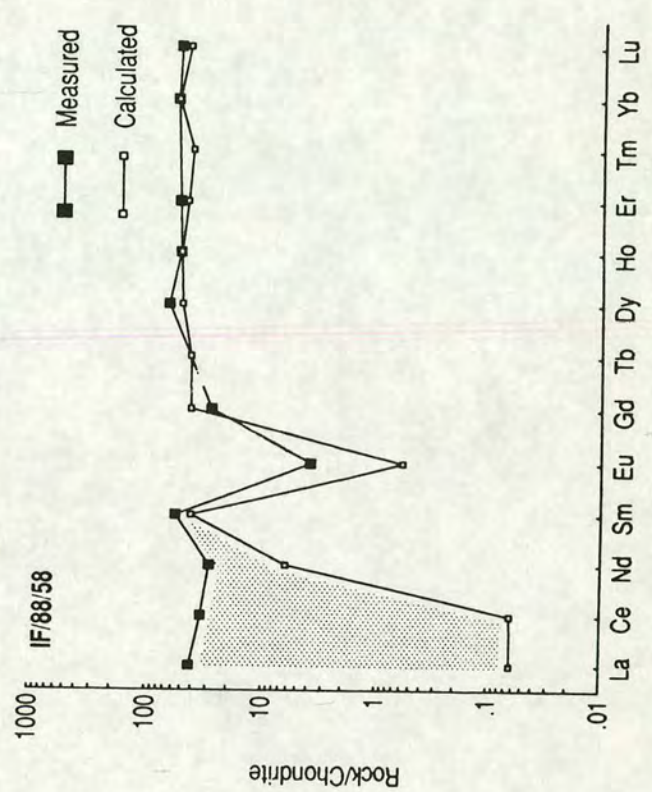

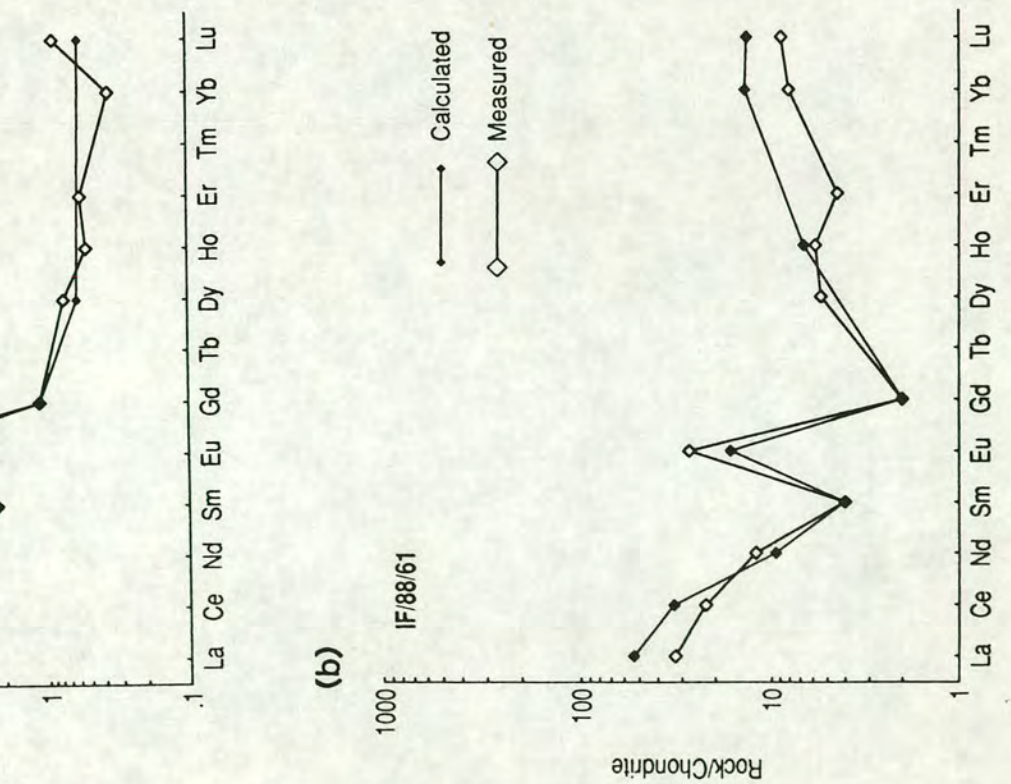

$LREE_t/LREE_t$* values greater than 1, indicating an excess of a LREE bearing phase above that required to saturate the melt. The Eu/Eu* features of the Type

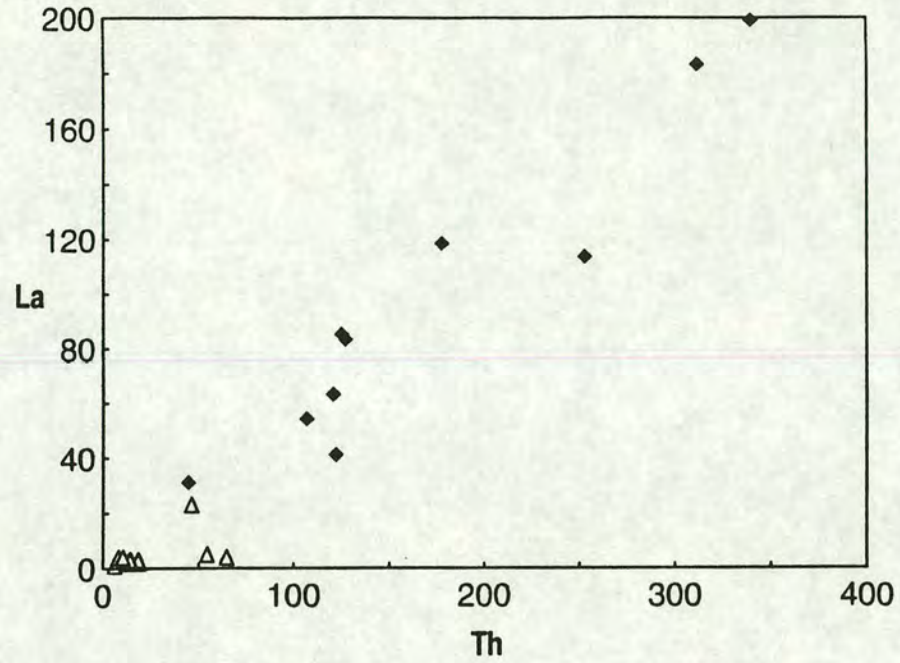

Figure 8.5. Plot of La (ppm) vs Th (ppm) for Type 1 and Type 3 Leucogneisses.

3 Leucogneisses can also be explained through monazite entrainment. Absolute Eu values are almost identical for LG1 and LG3. Since Eu* is calculated by interpolation between Sm and Gd, enhanced LREE and MREE values due to the entrainment of monazite will give rise to increased Eu* and hence decreased Eu/Eu* values as observed here. This is further emphasised by plots of La against Eu/Eu* (Fig. 8.6) which show a strong negative correlation as predicted if Eu/Eu* is a function of LREE concentration, dependent upon entrained monazite.

The final pattern calculated is for a quartz-absent melanosome IF/88/58 (Fig. 8.4.d.). The mineralogy of this sample is dominated by garnet (approximately 40%), while the remainder of the rock is comprised of sillimanite, cordierite, biotite and spinel. Garnet is the only major phase contributing to the REE budget, and the calculated pattern reflects this. An excellent correlation between measured bulk rock and calculated HREE values, controlled by garnet, contrasts strongly with a large discrepancy in LREE totals (shaded area). The enrichment of LREE relative to calculated values in IF/88/58 (observed LREE values are approximately 100 times greater than those calculated) can only be

ascribed to the presence of a LREE bearing accessory phase such as monazite. This concentration of monazite in the residue during vapour-absent partial

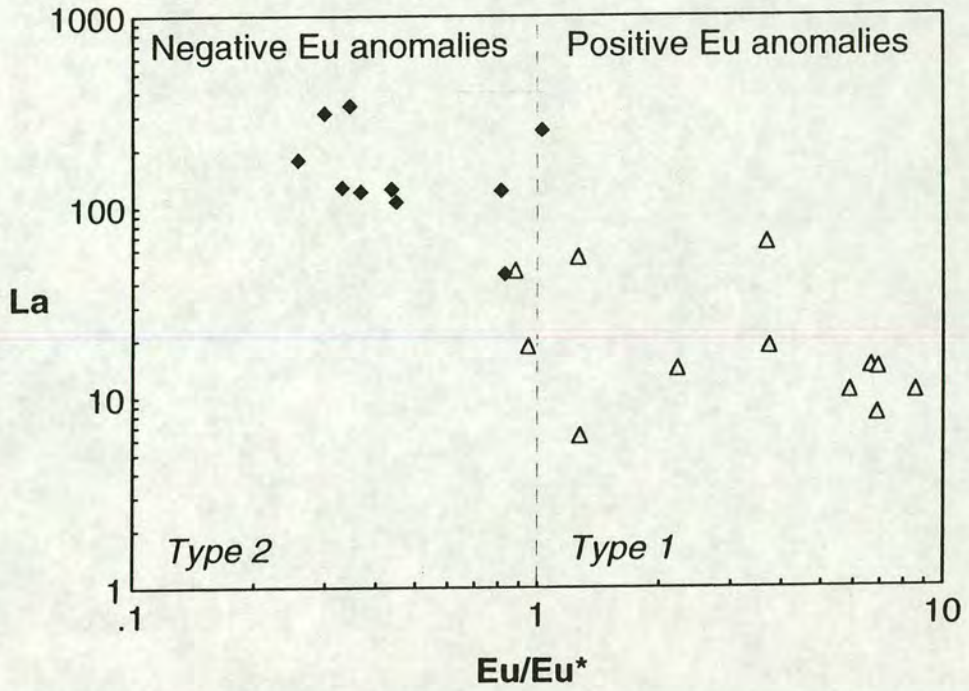

Figure 8.6. Plot of La (ppm) against Eu/Eu* for Type 1 and Type 3 Leucogneisses.

melting is predicted because of the limited solubility of monazite in dry melts. Recognition of monazite involvement in dehydration melting is, therefore, possible from LREE enriched REE patterns in melanosomes where large-scale melt extraction has occurred.

The limited solubility of pre-existing monazite in the relatively dry melts produced in dehydration-melting is demonstrated from the mass balance calculations on Type 1 Leucogneisses (LG1). Without entrainment of solid source material, as deduced for Type 3 Leucogneisses, the insoluble monazite will be concentrated in the residuum left after efficient melt extraction. This leads to the surprising result that, under vapour-absent conditions, refractory residues may become enriched in LREE (as shown by mass balance calculations on the K_2O and SiO_2 poor melanosome IF/88/58) while melts are depleted. Even though such melanosomes are restitic and highly residual in terms of major element charcteristics, they are not depleted in REE or those heat-producing elements hosted in accessory phases. From a trace element

perspective this material is still quite fertile, even though they have undergone considerable melt extraction.

The relative enrichment of residual material in REE, Th and U provides a striking example of decoupling of major and trace element behaviour in crustal anatexis and casts some doubt on previous general geochemical models relating to chemical depletion in high-grade terrains and deep-seated xenoliths. Trace element signatures will depend upon accessory phase distribution, which may be controlled by rates of processes including melting, mineral dissolution and melt extraction rather than by the gross amount of melting and scale of melt migration from the terrain.

8.2.2. Zirconium and Light Rare Earth Element saturation and implications for disequilibrium melting.

Most crustal lithologies contain a sufficient amount of zirconium (Zr) and light rare earth elements to saturate a melt in these components and allow precipitation of accessory phases such as zircon and monazite. Sawyer (1991(a)) noted that small-volume leucosomes derived from the partial melting of metabasic rocks contained very low concentrations of Zr, LREE and Th and in particular that Zr contents were lower than the equilibrium concentrations (Zr^*) required to saturate crustal melts according to the equations of Watson (1988). In a wider study Sawyer (1991(b)) collated leucosome compositions from many migmatite terrains and observed two geochemically distinct leucosome types. Small-volume melts with limited extraction distances and associated mafic selvedges were found to be depleted in Zr, Th, LREE and Hf relative to their proposed source lithologies, while large-volume vein-type leucosomes showed higher concentrations and more typical granitic trace-element geochemistry. Figure 8.7.a. is a plot which shows qualitatively the variation of melt extraction rate and the rate of chemical equilibration with temperature, as considered by Sawyer (1991(a)). Small-volume leucosomes with lower Zr than required to saturate the melt in zircon ($Zr/Zr^* < 1$) were interpreted by Sawyer (1991(a)) as lower temperature disequilibrium melts which failed to equilibrate with their source residue before extraction. A similar diagram showing the effect of variation in melt water content can be constructed (Fig. 8.7.b.), and indicates that disequilibrium melts can be produced at high temperatures if melts have

low water contents since accessory phase dissolution rates are dramatically lowered.

Type 1 Leucogneisses (LG1) from the Brattstrand Bluffs coastline have low concentrations of Th, LREE and Zr, and Zr/Zr* (using the equation of Watson, 1988) and $LREE_t/LREE_t^*$ significantly less than 1.0 (Fig. 8.8) suggesting that monazite and zircon both behave in a similar fashion and may be controlled by the same process(es).

Neglecting the possibility that the source rocks contain insufficient Zr and LREE to saturate the melt in zircon and monazite, which would be highly unusual for pelitic or semi-pelitic gneisses, LG1 melts may equate with the small-volume disequilibrium melts of Sawyer (1991, 1992). However, in this case field relations are more consistent with these leucogneisses being large-volume leucosome types. Both LG1 and Type 3 Leucogneisses form relatively large pods, veins and sheets which cross-cut layering in the host metapelites. They are not associated with mafic selvedges, suggesting that melt migration at least on the scale of tens of metres has occurred. This makes it rather unlikely that the non-equilibrium Zr and LREE concentrations in LG1 melts can be explained by small melt volume and limited extraction distance so another geochemical process is required to account for their unusual chemistry. We propose that the limited solubility of accessory phases in dry peraluminous crustal melts is the essential mechanism responsible for the marked depletion of LREE and HREE in LG1 leucogneisses and the production of a disequilibrium melt geochemistry for Zr, Th and LREE. The key factor in this model is that extraction must have occurred before extensive dissolution of zircon and monazite proceeded to allow Zr- and LREE-undersaturated melts to be produced.

The contrasting LG3 (Type 3 Leucogneisses) have high LREE, steep REE patterns and small negative Eu anomalies. Harris & Inger (1992) suggest these types of patterns represent equilibrium melt REE patterns based on major phase petrogenetic modelling. However, Zr/Zr* and $LREE_t/LREE_t^*$ values for Type 3 Leucogneisses leucogneisses are generally greater than unity (Fig. 8.8), suggesting that excess zircon and monazite entrainment may be important in these melts. The presence of relict monazite cores with embayed margins and

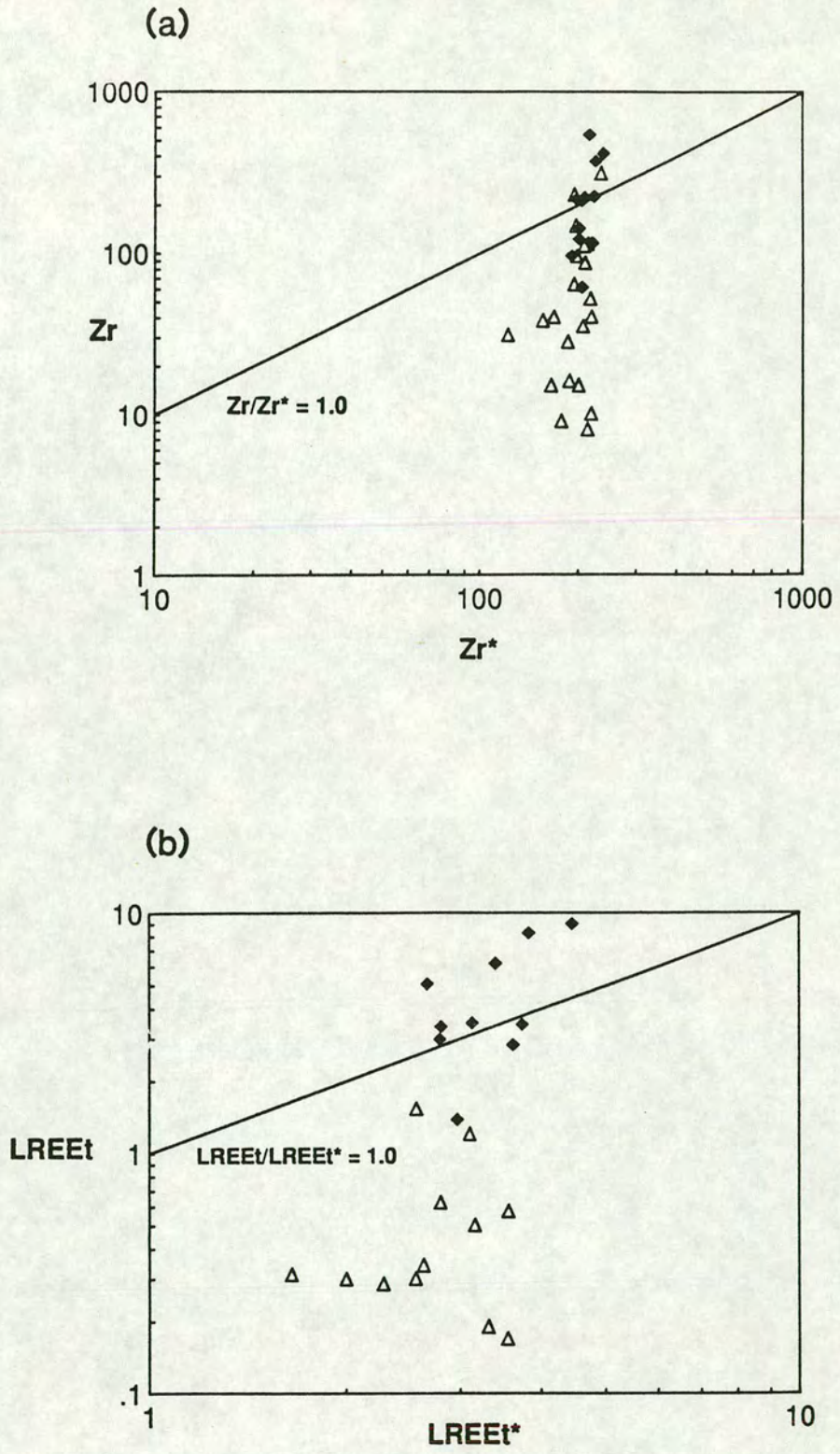

Fig. 8.7.a. Zr (observed) vs Zr* (the equilibrium concentration required to saturate a melt in Zr calculated using the equation of Watson, 1988). While Type 1 Leucogneisses typically have Zr/Zr* values <1.0, Type 2 Leucogneisses have Zr/Zr* ranging from less than 1.0 to 10. **Fig. 8.7.b.** shows a similar pattern for LREEt/LREEt* (calculated using the equation of Montel, 1992).

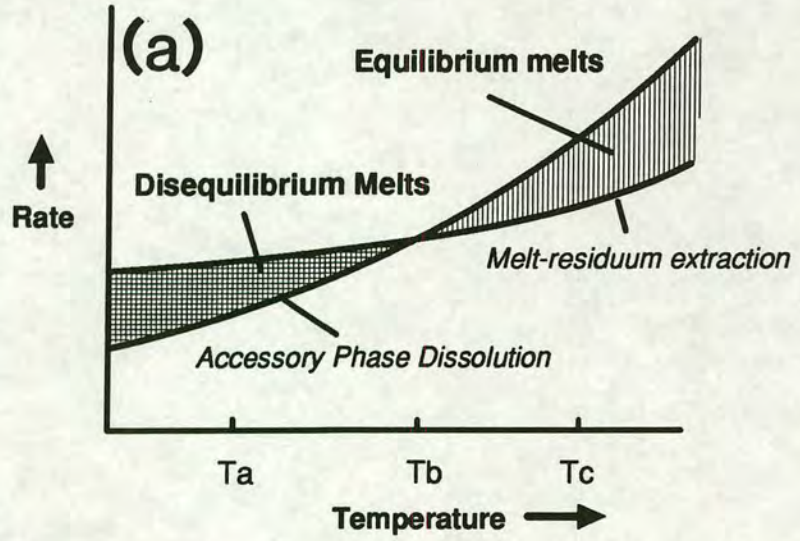

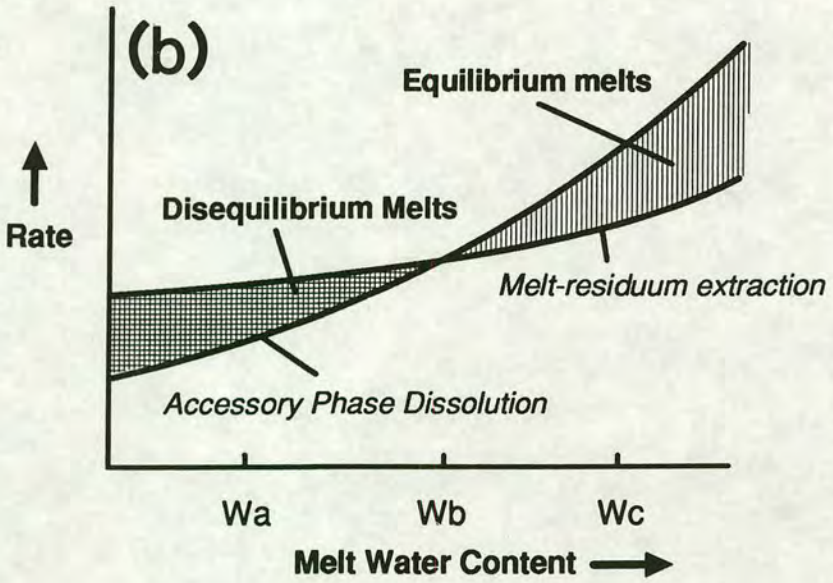

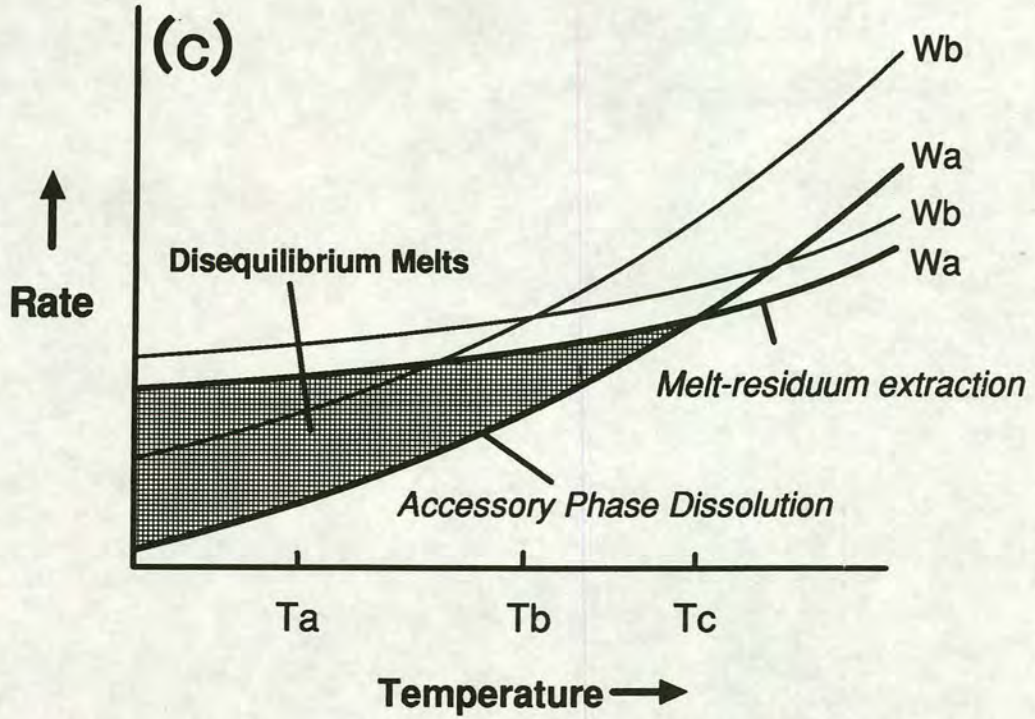

Fig. 8.8.a. A schematic plot showing rate vs temperature for accessory phase dissolution (steep curve) and the rate at which melt is extracted from the residue during partial melting (modified after Sawyer, 1991(b)) at a melt water content Wb. At Ta, rates of melt extraction exceed the rate at which accessory phases can dissolve into the melt, giving disequilibrium melt compositions (cross-hatched area) for elements which are ESC of accessory phases. Tb represents the minimum temperature required to saturate the melt, so that melts produced at Tc will be saturated with respect to ESC, giving equilibrium melts (ruled area). Since increased water contents in a melt will increase rates of accessory phase dissolution and melt extraction in exactly the same way as temperature (**Fig. 8.8.b**) we can draw a Rate vs Temperature diagram for melts formed at lower water contents (Wa, **Fig. 8.8.c.**). This diagram shows that the field of disequilibrium melting can extend to higher temperature (Tc) at lower melt water contents, which will have important consequences for melts produced under water-undersaturated conditions.

geochemically distinct rims indicates that monazite grains pre-dating partial melting are present in Type 3 Leucogneisses.

8.2.3. Constraints on the origin of monazite.

The model of Montel (1992) outlined in Section 8.1. allows us to calculate the equilibrium LREE concentration required to saturate a melt for a given temperature, water content and melt bulk composition. The calculation considers the LREE as one element from La to Gd. Results from this calculation in the previous section suggest that excess monazite is present in Type 3 Leucogneisses. If this monazite represents entrained material, then it may not be in equilibrium with the melt composition it is contained in. Using a modified version of the $LREE_t$ equation, (Montel, 1992) it is possible to calculate the composition of the melt in equilibrium with a monazite of known composition. In principle this allows us to determine whether a monazite is in equilibrium with the melt it is contained in, and, therefore, whether the monazite precipitated from that melt, or if the monazite has a non-primary origin (e.g. entrained). Montel (1992) applied this method to monazites in the Manaslu Granite and discovered that while monazite cores were in equilibrium with the granite LREE composition the rims were not. The rims were instead in equilibrium with a late-stage highly fractionated aplitic melt. In the Prydz Bay Leucogneisses, it should be possible to use this equation to determine whether the excess LREE in Type 3 Leucogneisses is caused by entrained monazite.

The modified version of Montel's equation leads to a monazite dissolution model which can predict individual REE contents for the melt corrected for non-ideal mixing in monazite. The fractionation of LREE relative to MREE by monazite is ascribed by Montel (1992) to non-ideal mixing rather than differential solubility of individual monazite end members. The correction for non-ideal mixing is given by the equation;

$$\mathbf{REE_i/(XREE_i.\gamma_i) = 9.50 + 2.34D + 0.03879\sqrt{H_2O} - 13318/T}$$

where

$\mathbf{REE_i}$ = melt content in ppm divided by atomic weight of REE "i".

$XREE_iPO4$	=	mole fraction of REE_iPO_4 in monazite.
γ_i	=	correction factor to account for non-ideal mixing in monazite.

Using monazite from the Macusani obsidian Montel (1992) calculates g_i from the empirical relationship:

$$T(°K) \ln \gamma_i = W_i$$

where

W_{Ce}=-37.24, W_{La}=74.80, W_{Pr}=163.3, W_{Nd}=288.33, W_{Sm}=767.11, W_{Gd}=1037.64.

These values are only strictly applicable to systems involving monazite of a similar composition to those in the Macusani Volcanics. Since monazite rims from the Brattstrand Bluffs area contain up to 23wt% ThO_2, the appropriateness of these W_i values may be limited. However, the cores of the monazite crystals from Brattstrand Bluffs are of a similar composition to the Macusani monazite, so accurate estimations of the composition of the melt from which they formed should be possible.

Results of the calculations are shown in Table 8.2. Calculations were carried out at various temperatures and water contents for a low ThO_2 (8.08 wt%) monazite core and a high ThO_2 (21.41 wt%) monazite rim from IF/88/147 (Table 8.3). The effect of varying temperature and water content on the predicted melt compositions is consistent with the increased solubility of monazite in hot, wet melts.

8.2.3.1. Monazite cores.

Low-Th monazite cores (with corresponding high LREE contents) are in equilibrium with melts which have much higher LREE contents than that of the postulated melt (given by LG1 in Table 8.1). Only the coolest, wettest melt (800°C, 4 wt% H_2O) gives a La value close to that of average LG1, while the remainder of the LREE are much too high. Fitzsimons (1991) gives a peak metamorphic temperature of 860°C for the Brattstrand Bluffs area. If melt generation and monazite crystallisation occurred within 25°C of this temperature, then the melt compositions predicted to be in equilibrium with the monazite cores are very different to those actually recorded. Since the non-ideal

Table 8.2. Melt Compositions with equilibrium cores and rims (compositions given in Table 8.3.)

.

Temp	**1108**	**1108**	**1108**	**1108**	**1073**	**1098**	**1123**	**LG1**
H2O	**8**	**4**	**2**	**0.01**	**4**	**4**	**4**	
Melt ppm								
La	29.8	28.8	28.2	26.8	19.5	25.8	33.8	21.1
Ce	56.2	54.4	53.2	50.5	36.8	48.8	63.8	27.9
Pr	6.1	5.9	5.8	5.5	4	5.3	7	3
Nd	25.8	25	24.4	23.2	17	22.4	29.2	9.7
Sm	5.3	5.1	5	4.8	3.5	4.6	6	1.5
Gd	6.8	6.5	6.4	6.1	4.6	5.9	7.6	1.5
Melt Normalised								
La	90.2	87.3	85.3	81.1	59.1	78.3	102.4	63.8
Ce	64.9	62.9	61.4	58.4	42.5	56.4	73.8	32.2
Pr	50.3	48.7	47.6	45.3	33.1	43.7	57.1	24.7
Nd	40.9	39.6	38.7	36.8	27	35.6	46.3	15.4
Sm	26.1	25.2	24.7	23.5	17.5	22.8	29.4	7.5
Gd	24.6	23.8	23.3	22.1	16.6	21.5	27.6	5.4

Melt compositions in equilibrium with monazite rims

Temp	**1108**	**1108**	**1108**	**1108**	**1073**	**1098**	**1123**	**LG1**
H2O	**8**	**4**	**2**	**0.01**	**4**	**4**	**4**	
Melt ppm								
La	21.3	20.6	20.1	19.1	13.9	18.5	24.1	21.1
Ce	43.8	42.4	41.5	39.4	28.7	38.1	49.8	27.9
Pr	4.6	4.5	4.4	4.1	3	4	5.2	3
Nd	20.6	20	19.5	18.5	13.6	17.9	23.4	9.7
Sm	2.6	2.6	2.5	2.4	1.8	2.3	3	1.5
Gd	3.4	3.3	3.2	3	2.3	3	3.8	1.5
Melt Normalised								
La	64.4	62.4	61	57.9	42.3	55.9	73.2	63.8
Ce	50.7	49.1	48	45.6	33.2	44	57.6	32.2
Pr	37.7	36.5	35.7	33.9	24.8	32.8	42.8	24.7
Nd	32.7	31.7	31	29.4	21.6	28.5	37.1	15.4
Sm	13	12.6	12.3	11.7	8.7	11.4	14.7	7.5
Gd	12.3	11.9	11.6	11.1	8.3	10.8	13.8	5.4

	Core	Rim
SiO2	0.570	1.899
Y2O3	0.476	0.015
P2O5	28.283	25.489
UO2	1.554	0.699
ThO2	8.076	21.410
CaO	1.698	3.166
La2O3	13.800	10.274
Ce2O3	28.500	23.116
Pr2O3	2.514	1.742
Dy2O3	0.180	0.249
Nd2O3	10.483	8.597
Sm2O3	1.406	.0.800
Gd2O3	0.717	0.369
Tb2O3	0.066	0.024
Total	98.338	97.849

Table 8.3. Monazite core and rim compositions from IF/88/147 used in the monazite-melt equilibrium calculations.

mixing corrections used in the calculation are based on a monazite composition not too dissimilar to that of the cores, errors introduced at this stage of the calculation will be minimal. It is unlikely, therefore, that the monazite cores precipitated from a melt of Type 1 Leucogneiss composition, and they probably represent entrained material rather than primary grains overgrown by monazite formed in a later event.

8.2.3.2. Monazite Rims.

As already pointed out, the non-ideal mixing corrections for the LREE in monazite will not be applicable to monazite compositions which depart markedly from those of the Macusani monazites. It is unlikely that the melt composition calculations for the rims will be as accurate as those for the cores, but the Montel (1992) model has been applied to test whether the ThO_2-rich rims could have precipitated from a melt of Type 1 Leucogneiss composition. Since Type 1 Leucogneisses have consistently low LREE contents they may be a likely source for the monazite rims. The calculated results reinforce this. The best-fit melt REE compositions are consistent with monazite rim growth at

approximately 800°C from a melt with 4wt% H_2O (the same conditions as best-fit results from the cores), and calculated LREE values are much closer to those of the average LG1 leucogneiss. At the higher temperatures thought to represent true monazite crystallisation conditions (835-850°C) the calculated melt compositions fit observed compositions less well. While the effect of increased Th and Si substitution into monazite on the non-ideal mixing corrections of Montel is uncertain, the calculations suggest that magmatic growth of Th-rich monazite rims from a melt similar in composition to the average Type 1 Leucogneiss is possible, while the cores are unlikely to have precipitated directly from these melts and probably represent entrained material as deduced in the earlier sections on the basis of geochemical arguments.

8.3. MONAZITE AND ZIRCON ENTRAINMENT MECHANISMS.

Chapter 7 discussed the entrainment of major phases and the effect these have on the bulk chemistry of the departing melts. Zircon and monazite may be entrained into the melt either as individual grains (if they were originally located at grain edges) or as inclusions in major phases. While both methods of entrainment would lead to greater LREE, Th and Zr contents in the extracted melt, it may be possible to distinguish which is responsible on the basis of geochemical correlations with other elements. Garnet (and/or cordierite) has been identified as the most likely restitic phase found in the leucogneiss suite. While Th shows a strong correlation with Fe_2O_3, high Th concentrations are not associated with high Fe_2O_3 contents (Figure 8.9.). In contrast, Zr contents (Fig. 8.10.a.) show a strong correlation with Fe_2O_3, especially in Type 2 Leucogneisses.

Figures 8.10.a. and 8.10.b. show the trends which may develop for various combinations of garnet, zircon and monazite entrainment. Zr shows a strong correlation with Fe_2O_3 in Type 2 Leucogneisses, suggesting that zircon inclusions in garnet may be, at least in part, responsible for the higher Zr concentrations in these samples than in Type 1 Leucogneisses. Type 3 Leucogneisses, on the other hand, show direct entrainment of monazite and zircon into the melt. The most likely explanation for this direct interaction of

melt and accessory phases is that zircon and monazite were hosted either at grain boundaries, or as inclusions in a phase which broke down during melting (e.g. biotite).

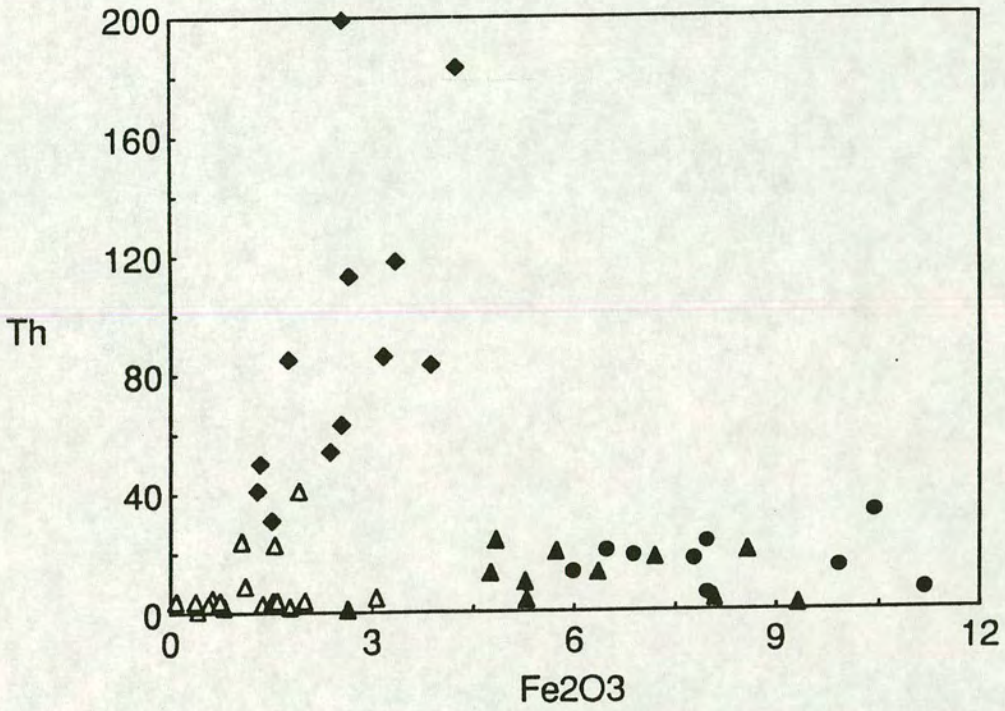

Figure 8.9. Th vs Fe_2O_3 for the Brattstrand Bluffs Leucogneisses.

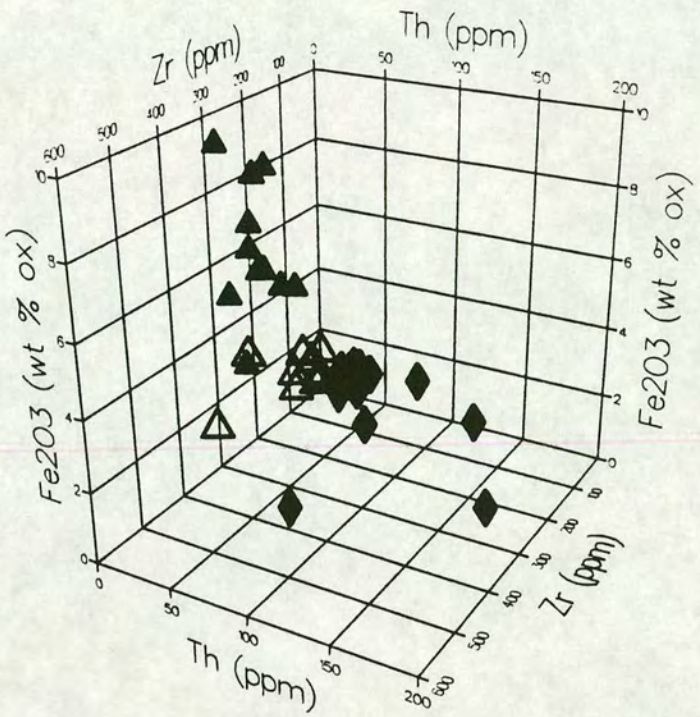

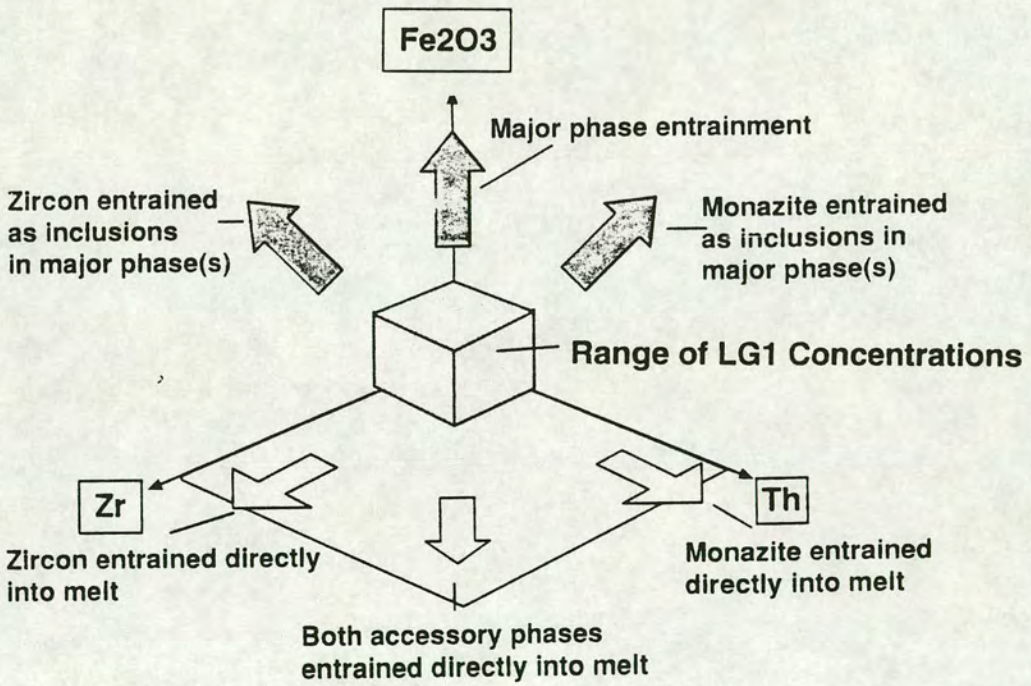

Figure 8.10.a. Zr vs Th vs Fe_2O_3 plot for Type 1, 2 and 3 Leucogneisses (Symbols as Figure 4.1.).
Figure 8.10.b. Interpreted summary of Figure 8.10.a.

Chapter 9

Conclusions & Summary.

Chapter 9. Conclusions & Summary.

9.1. INTRODUCTION.

The aim of this chapter is to summarise the role of partial melting in the formation of the Brattstrand Bluffs granulite-facies migmatite complex. Section 9.2. reiterates the findings of Chapter 7, which considered the extent and efficiency of melt extraction on the basis of petrographic and geochemical characteristics. Using this data, the model that granulite terranes may represent the residue left behind after extraction of a granitic melt fraction is considered. Section 9.3. considers the implications of disequilibrium melting and the entrainment source material, concentrating on the distinctive geochemical aspects of accessory phases, which represent easily recognised geochemical markers with which to trace source and restite entrainment in crustal melts. Section 9.4. of this chapter describes the post-melting processes important in the preservation of granulite facies conditions. Finally, a summary of the main findings of this work and some suggestions for final work are given.

9.2. MELT EXTRACTION FROM THE LOWER CRUST AND THE PRODUCTION OF GRANULITE FACIES TERRANES.

Any model for large scale granulite production involving removal of a water-bearing melt requires that the composition of the lower/middle crust is similar to that of a solid aggregate left after removal of a granitic liquid (Vielzeuf & Vidal, 1990). Although the upper crust has a broadly granodioritic composition (Arculus & Ruff, 1990, Taylor & McLellan, 1985), this material is metaluminous and contrasts with the peraluminous magmas produced by melting of recycled crustal material. In addition, while some granulite terranes (e.g. Ivrea) may have a broadly restitic character, many granulite terranes containing migmatite complexes (including the Brattstrand Bluffs coastline) show features consistent with the retention of melt rather than wholescale extraction. The bulk composition of the residue left behind is not solely controlled by the composition of the extracted melt, but by the composition of the whole extracted assemblage.

As Vielzeuf *et al* (1990) point out, the restite unmixing (or entrainment) model for the production of geochemical variation in granitoid suites is fundamentally incompatible with crustal differentiation through granite extraction from granulite terranes, since no efficient redistribution of chemical components would occur if restite-laden melts moved upwards in the crust (Clemens, 1987; Vielzeuf et al, 1990). The melt-removal model for the mechanism of crustal differentiation and the preservation of granulite facies conditions in the lower crust therefore requires the efficient extraction of restite free melts, yet in the the Brattstrand Bluffs migmatite complex (which preserves granulite facies assemblages over large areas) melt removal has been limited. Transport distances are small, and many melts contain a large amount of source material.

Large amounts of restitic and peritectic material can be recognised in many leucosomes, using both petrographic and geochemical criteria outlined in Chapter 2. Type 2 Leucogneisses contain higher abundances of entrained, pre-melting garnet and peritectic garnet formed at the melt-residue interface during melting. Other restitic phases, identified both by petrographic characteristics and geochemistry include cordierite, sillimanite, ilmenite, hercynitic spinel, monazite and zircon. The geochemical characteristics of Type 1 and Type 2 Leucogneisses are consistent with a model involving the progressive entrainment of more restitic material as the melts became more water undersaturated (and therefore more viscous and less easily extracted). Type 1 Leucogneisses have the mineralogy and geochemistry of low melt fraction partial melts, formed below the R.C.M.P. at melt fractions of approximately 0.1-0.2. Initial melt water contents of 3.5-4.5 wt% decreased as the degree of partial melting increased. The first formed, less viscous Type 1 Leucogneisses, although water-undersaturated, may have been able to migrate more rapidly from the melting region before extensive dissolution of accessory phases was possible (Chapter 8 and Section 9.3.). Extraction distances, however, were short (<500m), and Type 1 Leucogneisses appear to have been largely retained in the complex. As melting proceeded, the melts produced became more water-undersaturated, more viscous and less easily extracted. These melts (Type 2 Leucogneisses) entrained more restitic and peritectic phases.

The importance of the entrained restite component in the Brattstrand Bluffs coastline is that extraction of melt <u>without an entrained source component</u>

has occurred only on a limited scale across the structural section. The extraction of melt from a high grade metamorphic terrane is therefore not necessary for the preservation of granulite-facies conditions, and partial melting in the lower crust does not neccessarily lead to the removal of granitic melts and large scale crustal differentiation. The Brattstrand Bluffs example shows that there is no necessity for the removal of all, or even most of the melt portion from a granulite facies migmatite complex to preserve high-grade anhydrous mineral assemblages, even when melting is the mechanism by which aH_2O is lowered. Melt retention in the migmatitic metapelites is widespread - the near identical REE patterns of metapelitic gneisses (which contain small patches of melt as stromatic bands and veinlets) and Type 2 Leucogneisses (with their high entrained restitic and peritectic phase concentrations) suggest that partial melting occurred in an almost closed system on the scale of the exposed crustal section.

9.3. ACCESSORY PHASE CONTROLS ON MELT CHEMISTRY.

Three geochemically distinct leucogneiss suites have been identified in the Brattstrand Bluffs area. These have been derived by vapour-absent dehydration melting of a pelitic source under granulite-facies conditions (6Kb, 860°C), leaving a melanosome residue enriched in garnet and accessory phases. The three leucogneiss types have similar field relations and major element chemistry. Trace elements controlled by major phases (transition metals, Ba, Rb, Sr) are also comparable, whereas trace elements dominantly hosted in accessory phases (Zr, Th, LREE) show strong differences, and are markedly enriched in Type 3 Leucogneisses.

Contrasting accessory phase behaviour exerts a very strong control on apparent melt trace element and REE geochemistry, even in the case of well-segregated vein- and cross-cutting leucogranite types. Limited dissolution of slowly-reacting accessory phases which host REE and Th, U and Zr as essential structural components will produce depleted bulk-rock trace element signatures in melts if those melts are water-undersaturated and leave the sites of melting on timescales shorter than the dissolution rates. This behaviour is well demonstrated by the Type 1 Leucogneisses of this study, which preserve low Zr, Th and LREE compositions previously

considered (Sawyer, 1991(a), (b)) to be characteristic of small-volume disequilibrium melts (Zr/Zr^* and $LREE_t/LREE_t^*$ <1.0) despite having the field relations (melt volume estimates of 40-50%, no associated mafic selvedges, cross-cutting relationships) of larger volume partial melts. Mass balance calculations indicating that the REE budget of these leucogneisses is dominated by major phases are consistent with the conclusion that these melts have been extracted efficiently before significant dissolution of accessory phases. The removal of these melts before acheivement of saturation in Zr and LREE makes them disequilibrium melts (Sawyer, 1991 (a)) since rates of segregation have exceeded rates of equilibration for these elements.

Limited dissolution of accessories coupled with their entrainment, on the other hand, can lead to significant enrichments in the apparent bulk-rock REE, Th and Zr concentrations of melts. This behaviour is demonstrated by the Type 3 Leucogneisses of this study, which have strongly enriched LREE contents, high Th concentrations and Zr/Zr^* and $LREE_t/LREE_t^*$ values greater than 1.0 mainly as a consequence of monazite and zircon entrainment from the source. This inference is backed up by mineral mass-balance calculations which indicate that the bulk of the LREE reside in accessory phases, by LREEt/LREEt* values greater than 1.0, and by the presence of relict monazite grains with magmatic overgrowths. Zr/Zr^* and $LREE_t/LREE_t^*$ plots indicate that similar processes are affecting both LREE and Zr concentrations, controlled repectively by monazite and zircon. While Type 1 Leucogneisses representing disequilibrium melts are undersaturated in Zr and LREE due to efficient extraction before equilibration, the trace element chemistry of Type 3 Leucogneisses is consistent with production by this disequilibrium melting coupled with inefficient extraction and entrainment of monazite.

The majority of other crustal melts derived from pelitic sources described in the literature for which REE data are avaliable are large granite plutons (e.g. Manaslu Leucogranite (Vidal *et al*, 1982); Cooma Granodiorite, (White & Chappell, 1988)) which have moderately high LREE contents and negative Eu anomalies. Petrogenetic modelling calculations by Barbey *et al* (1989) and Harris & Inger (1992) indicate that equilibrium melts produced by melting of pelitic source rocks will have REE patterns similar to those of the majority of these S-Type granite plutons. Typical crustal melts, with moderate LREE

concentrations and negative Eu anomalies, may reflect the increased dissolution of monazite in a melt produced under wet-melting (vapour-saturated) conditions.

In contrast, partial melting under vapour-absent conditions in the lower crust gives rise to dry peraluminous melts, in which monazite and zircon are relatively insoluble. Melts derived by water-undersaturated melting of pelites containing monazite will be depleted in LREE as monazite is concentrated in the residuum, as illustrated by the high LREE present in the refractory residuum identified in this study. If melting takes place at a pressure high enough to allow garnet to remain stable as a residual phase then the corresponding depletion of HREE may produce a positive Eu anomaly in the melt. The size of this Eu anomaly will depend on the degree of extraction of the feldspar component of the source. Large positive Eu/Eu* values in Type 1 Leucogneisses correspond to virtually complete removal of plagioclase and K-feldspar from the residue due to moderately high degrees of partial melting (F = 0.4 - 0.5). While migmatite leucosomes with REE patterns identical to LG1 have been recorded in the literature (Barbey *et al*, 1989), peraluminous plutons have not. This would suggest that melts generated in granulite-facies migmatite terrains are unlikely to represent the precursors of S-Type granite plutons. Amphibolite terranes may therefore represent a more likely source for S-Type granites than granulite-facies migmatite complexes. However, Type 3 Leucogneisses from the Brattstrand Bluffs coastline, which do have REE patterns similar to the compositions of typical leucogranite plutons, were produced by a combination of disequilibrium melting and monazite entrainment. Indeed, the average REE pattern, Zr/Zr* and $LREE_t/LREE_t$* produced by mixing and averaging Type 1 and Type 3 Leucogneisses together is indistinguishable from those of equilibrium melts of large S-Type granite plutons.

Type 2 Leucogneisses contain large amounts of major phases entrained from both the pre-melting assemblage, and from the peritectic assemblage developed during incongruent melting of biotite, while Type 3 Leucogneisses have a geochemistry consistent with the preferential entrainment of accessory phases, with a limited major phase component. In Chapters 7 & 8 a model was developed which proposed that the Type 1 Leucogneisses represent the first-formed melts, which were extracted rapidly before equilibration with the melting assemblage occurred. Type 2 Leucogneisses

formed later, or in areas where more disaggregation of the source was able to occur, when melt proportions were greater and parts of the metapelite assemblage began to lose their coherence. The preferential release of accessory phases into Type 3 Leucogneisses may have occurred as the phases they were hosted in (e.g. biotite) broke down during melting. Major element chemistry and phase petrology suggests that the Type 3 leucogneisses represent an intermediate stage between LG1 (which are almost free of restitic material) and the restite-rich LG2, and may have formed at intermediate melt fractions, when biotite breakdown was well underway but before the RCMP was reached.

9.4. POST MELTING PROCESSES.

The preservation of granulite-facies anhydrous mineral assemblages in the leucogneisses and surrounding migmatitic metapelites indicates the removal of aqueous fluids released by the breakdown of hydrous phases, thus preventing complete or even partial retrogressive back-reaction. This may have occurred either by the removal of melts containing a dissolved aqueous component, or by removal of the fluids expelled as the melts crystallised.

The small transport distances proposed for the Brattstrand Bluffs migmatites mean that melts have essentially been retained in the complex. The leucogneisses and metapelites do not show the widespread retrogression as witnessed in the Lewisian Inverian event (Cartwright, 1990) and the regional biotite event in the Arunta Complex (Warren & Hensen, 1989). Instead, retrogression is restricted to narrow shear zones, suggesting focussed, rather than pervasive, flow of aqueous fluids expelled from cooling melts. Melts may have, in effect, acted as a transfer medium, dissolving water at the site of melting and moving it to retrogressive shear zones where it was expelled from the complex, without the requirement for major melt loss to provide a mechanism for crustal dessication. While there is no unambiguous field or geochemical evidence for the nature of this late, fluid rich, melt it may be responsible for some felsic pegmatites recorded in the Brattstrand Bluffs coastline by Fitzsimons (*pers comm*).

9.5. SUMMARY

The main findings of this thesis are as follows:

(i) Melts produced under granulite-facies conditions quickly become water-undersaturated. The earliest melts in the Brattstrand Bluffs migmatite terrane (Type 1 Leucogneisses) were removed from the melting zone before equilibration with the residual assemblage. These melts are depleted in Zr, Th and LREE due to the slow dissolution of accessory phases in water undersaturated melts.

(ii) As anatexis proceeds, melt water contents decrease and the granitic liquids produced become more viscous and less easily extractable. More source material becomes entrained. In the Type 2 Leucogneisses, major phases entrained from the pre-melting assemblage, and those formed as peritectic phases during the incongruent melting of biotite can be distinguished petrographically. In Type 3 Leucogneisses, the preferential entrainment of zircon and monazite has given rise to Zr, Th and LREE concentrations higher than those expected for melts equilibrating with a typical pelitic source.

(iii) Melts have essentially been retained in the complex, suggesting that the **removal** of melt from migmatite complexes in the middle to lower crust is not an essential mechanism for the production of granulite terranes, in contrast to models of granulite genesis and crustal generation which suggest that granulites represent the refractory assemblage left after extraction of a granitic liquid. The preservation of anhydrous mineral assemblages in both the migmatitic metapelites and the leucosomes indicates that aqueous fluids have been lost as the melts crystallised in-situ, rather than by the removal of melts containing a dissolved aqueous component. Melts may act as transfer mediums, dissolving water released at the melting site during the breakdown of biotite and transporting it to low pressure shear zones, where retrogression is concentrated as fluids move to higher structural levels. In this way, granulite terranes produced by vapour-absent partial melting can be produced which do not have the mineralogy and geochemistry of a residue left after the removal of a granitic melt.

9.6. FUTURE WORK.

This project represents a detailed petrographic and geochemical study to place further constraints on the processes involved during partial melting in a granulite terrane, following on from Fitzsimons (1991) original work in the Brattstrand Bluffs area. The following topics represent the most important questions arising from this thesis.

(i) The extension of experimental work on accessory phase dissolution rates into mafic bulk compositions, and perhaps to higher pressures. The importance of accessory phases in determining whether melts represent equilibrium or disequilibrium liquids has been demonstrated by this thesis, and by the work of Sawyer (1991). While monazite, apatite and zircon dissolution rates for haplogranitic and peraluminous melt compositions are relatively well constrained, dissolution rates for accessory phases of major geochemical importance in mafic migmatites (allanite, sphene, rutile) are less certain. If allanite dissolution rates are similar to those of monazite then LREE depletion in mafic migmatites may occur, analogous to that described in the Type 1 Leucogneisses in this thesis.

(ii) Experimental work on melt extraction rates is required to determine whether melts produced under water-undersaturated conditions are depleted in Zr, Th and LREE because melt is extracted rapidly or because accessory phase dissolution is slow. The composition of melts produced in contact aureoles, where melts are produced rapidly by rapid temperature increases overstepping melting reactions, may provide a useful example where melt production and extraction is much more rapid than equilibration.

(iii) Further detailed electron and ion-microprobe mineral chemistry in other migmatite terranes is neccessary to determine whether source and peritectic phases can be identified in higher-level crustal plutons. Work of this nature is essential if the role of restite entrainment and unmixing in the production of geochemical variation within granite suites is to be fully ascertained. Granites produced by melting under fluid present (e.g. upper-amphibolite-facies) conditions, where re-equilibration of

mineral trace element compositions is less likely, may prove more useful than melts produced under granulite facies conditions.

REFERENCES.

Abbey, S. 1980. Studies in the "standard samples" for use in the general analysis of silicate rocks and minerals. Part 6; 1979 edition of "usable" values. *Geol. Surv. Can. Spec. Paper*, **80**, 14.

Allegre, C. J. & Minster, J. F., 1978. Quantitative models of trace element behaviour in magmatic processes. *E.P.S.L.*, **38**, 1-25.

Allibone, A. H. & Norris, R. J. 1992. Segregation of leucogranite microplutons during syn-anatectic deformation: an example from the Taylor Valley, Antarctica. *J. Met. Geol.*, **10**, 589-600.

Arculus, R. J., 1988. Continental crustal evolution and the role of supra- and subcrustal granites. *Terra Cognita*, **8**, 257.

Arculus, R. J. & Ruff, L. J., 1990. Genesis of continental crust: evidence from island arcs, granulites, and exospheric processes. In: Vielzeuf, D. & Vidal, Ph. (eds), *Granulites and Crustal Evolution*. Dordrecht: Kluwer Academic Publishers, 7-23.

Arzi, A. A., 1978. Critical phenomena in the rheology of partially melted rocks. *Tectonophysics*, **44**, 173-184.

Ashworth, J. R., 1985. Introduction. In: Ashworth, J. R. (ed), *Migmatites*. Glasgow: Blackie & Son Ltd, 1-35.

Ashworth, J. R. & Brown, M., 1990. An overview of diverse responses to diverse processes at high crustal temperatures. In: Ashworth, J.R. & Brown, M. (eds) *High-temperature Metamorphism and Crustal Anatexis*. London: Unwin Hyman, 1-18.

Bacon, C. R., 1989. Crystallisation of accessory phases in magmas by local saturation adjacent to phenocrysts. *Geochimica et Cosmochimica Acta.*, **53**, 1055-1066.

Barbero, L. & Villaseca, C., 1992. The Layos Granite, Hercynian Complex of Toledo (Spain): an example of a parautochthonous restite-rich granite in a granulitic area. *Trans. Roy. Soc. Edin. Earth Sci.*, **83**, 127-138.

Barbey, P., Bertrand, J. M., Angoua, S., & Dautel, D. 1989. Petrology and U/Pb geochronology of the Telohat migmatites, Aleksod, Central Hoggar, Algeria. *Contrib. Mineral. Petrol.* **101**, 207-219.

van Bargen, N. & Waff, H. S., 1986. Permeabilities, interfacial areas and curvatures of partially molten systems. Results of numerical computations of equilibrium microstructures. *J. Geophys. Res.*, **91**, 9261-9276.

Battachyrya, A. & Sen, S. K., 1986. Granulite metamorphism, fluid buffering and dehydration melting in the Madras charnockites and metapelites. *Journal of Petrology*, **27**, 1119-1141.

Black, L.P., Kinny, P.D. & Sheraton, J.W., 1990. A revised chronology for the Vestfold Block based on ion-probe zircon ages. In *Gondwana: Terranes and Resources, Tenth Australian Geological Convention, Hobart 1990, Abstracts.* Sydney: Geological Society of Australia, 253.

Bottinga, Y. & Weill, D. F., 1972. The viscosity of magmatic silicate liquids: a model for calculation. *Amer. J. Sci.*, **272**, 438-75.

Bowen, N. L. & Tuttle, O. F., 1950. The system $NaAlSi_3O_8$-$KAlSi_2O_8$-SiO_2-H_2O. *J. Geol.*, **58**, 489-511.

Bowie, S. H. U. & Horne, J. E. T., 1953. Cheralite, a new mineral of the monazite group. *Min. Mag.*, **30**, 90-93.

Bowles, J. F. W., Jobbins, E. A., & Young, B. R., 1980. A re-examination of cheralite. *Min. Mag.*, **43**, 885-888.

du Bray, E., 1988. Garnet compositions and their use as indicators of peraluminous granitoid petrogenesis - southeastern Arabian Shield. *Contrib. Mineral. Petrol.*, **100**, 205-212.

Brouand, M., Banzet, G., & Barbey, P., 1990. Zircon behaviour during crustal anatexis. Evidence from the Tibetan Slab migmatites (Nepal). *J. Volc. Geothermal. Res.*, **44**, 143-161.

Brown, G. C. & Fyfe, W. S., 1970. The production of granitic melts during ultrametamorphism. *Contrib. Mineral. Petrol.*, **28**, 310-318.

Burnham, C. W., 1992. Calculated melt and restite compositions of some Australian granites. *Trans. Roy. Soc. Edin. Earth Sci.*, **83**, 387-397.

Burt, D. M., 1989. Compositional and phase relations among Rare Earth Elements Minerals. *in* B. R. Lipin & G. A. Mackay (eds), Geochemistry and Mineralogy of Rare Earth Elements. *Reviews in Mineralogy*, **21**, pp259-307.

Cartwright, I., 1990. Prograde metamorphism, anatexis, and retrogression of the Scourian Complex, north-west Scotland. In: Ashworth, J.R. & Brown, M. (eds) *High-temperature Metamorphism and Crustal Anatexis.* London: Unwin Hyman, 371-399.

Cawthorn, R. G., & Brown, P. A., 1976. A model for the formation and crystallisation of corundum normative calc-alkaline magmas through amphibole fractionation. *J. Geol.*, **84**, 467-76.

Chappell, B. W. & White, A. J. R. 1974., Two contrasting granite types. *Pac. Geol.*, **8**, 173-4.

Chappell, B. W., White, A. J. R. & Wyborn, D., 1987. The importance of residual source material (restite) in granite petrogenesis. *Journal of Petrology*, **28**, 1111-1138.

Chen, Y. D., Price, R. C. & White, A. J. R., 1989. Inclusions in three S-Type granites from S.E. Australia. *J. Pet.*, **30**, 1181-1218.

Clarke, G.L., 1988. Structural constraints on the Proterozoic reworking of Archaean crust in the Rayner Complex, MacRobertson and Kemp Land Coast, East Antarctica. *Precambrian Research* **40/41,** 137-156.

Clemens, J. D. 1990. The granulite-granite connexion. *in* Vielzeuf, D. & Vidal, Ph. (eds), *Granulites and Crustal Evolution.* Dordrecht: Kluwer Academic Publishers, 25-36.

Clemens, J. D. 1984. Water contents of intermediate to siliceous magmas. *Lithos*, **17**, 273-287.

Clemens, J. D. & Vielzeuf, D., 1987. Constraints on melting and magma production in the crust. *E.P.S.L.*, **86**, 287-306.

Clemens, J. D. & Wall, V. J., 1988. Controls on the mineralogy of S-Type volcanic and plutonic rocks. *Lithos*, **21**, 53-66.

Clemens, J. D. & Wall, V. J., 1981. Crystallisation & origin of some peraluminous (S-Type) granitic magmas. *Can. Mineral.* **19**, 111-132.

Coats, J. S. & Wilson, J. R., 1971. The eastern end of the Galway Granite. *Min. Mag.*, 38, 138-151.

Collins, W. J. & Vernon, R. H., 1992. Mid-crustal contamination of granitic magmas (Abstract). *Trans. Roy. Soc. Edin. Earth Sci.*, **83**, 488.

Copeland, P., Parrish, R. R., & Harrison, T. M., 1988. Identification of inherited radiogenic Pb in monazite and its implications for U-Pb systematics. *Nature*, **333**, 760-763.

Debon, F. & Le Fort, P., 1983. A chemical-mineralogical classification of common plutonic rocks and associations. *Trans. Roy. Soc. Edin. Earth Sci.*, **73**, 135-149.

Demartin, F., Pilati, T., Diella, V., Donzelli, S. & Grammaccioli, C. M., 1991. Alpine monazite: further data. *Can. Mineral.*, **29**, 61-67.

De Yoreo, J. J., Lux, D. R. & Guidotti, C. V., 1989. The role of crustal anatexis and magma migration in the thermal evolution of thickened continental crust. In Daly, J. S. et al (eds). Evolution of Metamorphic Belts. *Geol. Soc. Spec. Publ.*, **43**.

Dirks, P. & Hand, M., 1991. Structural and metamorphic controls on the distribution of zircon in an evolving quartzofeldspathic migmatite: an example from the Reynolds Range, central Australia. *J. Met. Geol.*, **9**, 191-201.

Dougan, T. W., 1979. Compositional and modal relationships and melting reactions in some migmatitic metapelites from New Hampshire and Maine. *Am. Jour. Sci.*, **279**, 897-935.

Edwards, R. L. & Essene, E. J., 1988. Pressure, Temperature and C-O-H fluid fugacities across the amphibolite-granulite transition, northwest Adirondack Mountains, New York. *Journal of Petrology* **29**, 39-72.

Ellis, D.J., 1986. Garnet-liquid Fe^{2+}-Mg equilibria and implications for the beginning of melting in the crust and subduction zones. *American Journal of Science* **286,** 765-791.

Ellis, D. J. & Obato, M., 1992. Migmatite and melt segregation at Cooma, New South Wales. *Trans. Roy. Soc. Edin. Earth Sci.*, **83,** 95-106.

Ellis, D. J., Sheraton, J. W., England, R. N. & Dallwitz, W. B., 1980. Osumilite-sapphirine-quartz granulites from Enderby Land, Antarctica - mineral assemblages and reactions. *Contrib. Mineral. Petrol.* **72,** 123-143.

Essene, E. J., 1988. Critical evaluation of the pervasive CO_2 flooding model for granulites (Abstr.). *Terra Cognita*, **8,** 254.

Exley, R. A., 1980. Microprobe studies of REE-rich accessory minerals; implications for Skye granite petrogenesis and REE mobility. *E.P.S.L..*, **48,** 97-110.

Feely, M., McCabe, E., & Williams, C. T., 1989. U-, Th- and REE-bearing accessory minerals in a high heat production leucogranite within the Galway granite, western Ireland. *Trans Inst . Min. Metall.*, **98,** 27-32.

Fitzsimons, I. C. W. 1991. *The Metamorphic Histories of some Proterozoic Granulites from East Antarctica.* PhD. thesis, University of Edinburgh, 375pp. (Unpublished).

Fitzsimons, I. C. W. & Harley, S. L. 1991. Geological relationships in high-grade gneisses of the Brattstrand Bluffs coastline, Prydz Bay, east Antarctica. *Australian Journal Earth Sciences*, **38,** 497-519.

Flood, R. H. & Vernon, R. H., 1978. The Cooma granodiorite, Australia: an example of *in-situ* crustal anatexis. *Geology*, **6,** 81-84.

France-Lanord, C. & le Fort, P., 1988. Crustal melting and granite genesis during the Himalayan collision orogenesis. *Trans. Roy. Soc. Edin. Earth Sci.*, **79,** 183-195.

Fyfe, W. S., 1973. The granulite facies, partial melting and the Archaean crust. *Phil. Trans. Roy. Soc. Lond.* **A 273,** 457-461.

Goodman, S., 1991. Melt segregation and migration. EOS, **52.**

Gramaccioli, C. M., & Segalstad, T. M., 1978. A uranium- and thorium-rich monazite from a south-Alpine pegmatite at Piona, Italy. *Am. Mineral.*, **63**, 757-761.

Grant, J. A., 1985. Phase equilibria in low-pressure partial melting of pelitic rocks. *American Journal of Science* **285,** 409-435.

Green, T. H., 1976. Experimental generation of cordierite- or garnet-bearing granitic liquids from a pelitic composition. *Geology*, **4**, 85-88.

Green, D. H. & Ringwood, A. E., 1967. An experimental investigation of the gabbro to eclogite transformation and its petrological applications. *Geochimica et Cosmochimica Acta* **31,** 767-833.

Grew, E.S., 1980. Sapphirine + quartz association from Archaean rocks in Enderby Land, Antarctica. *American Mineralogist* **65,** 821-836.

Gromet, L. P. & Silver, L. J., 1983. Rare earth element distributions among minerals in a granodiorite and their petrogenetic implications. *Geochimica et Cosmochimica Acta.*, **47**, 925-939.

Gupta, L. N. & Johannenes, W., 1985. Effect of metamorphism and partial melting of host rocks on zircons. *J. Met. Geol.*, **3**, 311-323.

Hansmann, W. & Oberli, F. 1991., Zircon inheritance in an igneous rock suite from the southern Adamello batholith (Italian Alps). Implications for petrogenesis. *Contrib. Mineral. Petrol.*, **107**, 501-518.

Harley, S. L., 1992. Proterozoic granulite terranes. In: Condie, K. C. (ed). *Proterozoic Crustal Evolution.* Amsterdam. Elsevier, 310-360.

Harley, S.L., 1987. Precambrian geological relationships in high-grade gneisses of the Rauer Islands, East Antarctica. *Australian Journal of Earth Sciences* **34,** 175-207.

Harley, S. L. & Fitzsimons, I. C. W. 1991. Pressure-temperature evolution of metapelitic granulites in a polymetamorphic terrane: the Rauer Group, east Antarctica. *J. Met. Geol.*, **9**, 231-243.

Harley, S.L. & Hensen, B.J., 1990. Archaean and Proterozoic high-grade terranes of East Antarctica (40-80°E): a case study of diversity in granulite facies metamorphism. In: Ashworth, J.R. & Brown, M. (eds) *High-temperature Metamorphism and Crustal Anatexis*. London: Unwin Hyman, 320-370.

Harris, N. B. W. & Inger, S. 1992. Trace element modelling of pelite-derived granites. *Contrib. Mineral. Petrol.*, **110**, 46-56.

Harris, N. B. W., Pearce, J. A. & Tindle, A. G., 1986. Geochemical characteristics of collision-zone magmatism. In: Coward, M. P. & Ries, A. C. (eds). Collision Tectonics. *Geol. Soc. Lond. Spec. Publ.*, **19**, 67-81.

Harrison, T. M. & Watson, E. B., 1983. Kinetics of zircon dissolution and zirconium diffusion in granitic melts of variable water content. *Contrib Mineral. Petrol.*, **84**, 66-72.

Harrison, T. M. & Watson, E. B., 1983. The behaviour of apatite during crustal anatexis. Equilibrium and kinetic considerations. *Geochimica et Cosmochimica Acta*, **48**, 1467-1477.

Harrison, T. M., 1987. The timescales of generation, transport and cooling of granite plutons. Abstract.

Harrison, T. N., 1988. Magmatic garnets in the Cairngorm granite, Scotland. *Min. Mag.*, **52**, 659-667.

Hinton, R. W. 1990. Ion microprobe analysis of silicates; Measurements of multi-element glasses. *Chem. Geol.*, **83**, 11-25.

Hinton, R. W. & Upton, B. G. J. 1991. The chemistry of zircon: Variations within and between large crystals from syenite and alkali basalt xenoliths. *Geochimica et Cosmochimica Acta*, **55**, 3287-3302.

Holtz, F., 1989. Importance of melt fraction and source rock composition in crustal genesis - the example of two granitic suites of northern Portugal. *Lithos*, **24**, 21-35.

Holtz, F. & Barbey, P., 1991. Genesis of Peraluminous Granites II. Mineralogy and chemistry of the Tourem Complex (North Portugal). Sequential melting vs restite unmixing. *J. Pet.*, **32**, 959-978.

Holtz, F., Johannes, W. & Pichavant, M., 1992. Peraluminous granites: the effect of alumina on melt composition and coexisting minerals. *Trans. Roy. Soc. Edin. Earth Sci.*, **83**, 409-416.

Huppert, H. E. & Sparks, R. S. J., 1988, The generation of granitic magmas by intrusion of basalt into continental crust. *J. Pet.*, **29**, 599-624.

James, P.R. & Tingey, R.J., 1983. The Precambrian geological evolution of the East Antarctic metamorphic shield - a review. In: Oliver, R.L., James, P.R. & Jago, J.B. (eds) *Antarctic Earth Science.* Canberra: Australian Academy of Science, 5-10.

Janardhan, A. S., Newton, R. C. & Hansen, E. C., 1982. The transformation of amphibolite facies gneiss to charnockite in southern Karnataka and northern Tamil Nadu, India. *Contrib. Mineral. Petrol.* **79,** 130-149.

Jeffrey, D. J. & Acrivos, A., 1976. The rheological properties of suspensions of rigid particles. *Am. Inst. Chem. Eng. J.*, **22**, 417-432.

Johannes, W. & Holtz, F., 1990. Formation and composition of H_2O-undersaturated granitic melts. In: Ashworth, J.R. & Brown, M. (eds) *High-temperature Metamorphism and Crustal Anatexis.* London: Unwin Hyman, 87-104.

Jurewicz, S. R. & Watson, E. B., 1985. Distribution of partial melt in a felsic system: importance of surface energy. *Contrib. Mineral. Petrol.*, **84**, 66-72.

Keppler, H. & Wyllie, P. J., 1991. Partitioning of Cu, Sn, Mo, W, U and Th between melt and aqueous fluid in the systems haplogranite-H_2O-HCl and haplogranite-H_2O-HF. *Contrib. Mineral. Petrol.*, **109**, 139-150.

Keppler, H. & Wyllie, P. J., 1990. Role of fluids in transport and fractionation of uranium and thorium in magmatic processes. *Nature*, **348**, 531-533.

Kinny, P.D. & Black, L.P., 1990. Zircon ages and the distribution of Archaean and Proterozoic rocks in the Rauer Islands. In: *Gondwana: Terranes and Resources, Tenth Australian Geological Convention, Hobart 1990, Abstracts.* Sydney: Geological Society of Australia, 251-252.

Kruhl, J. H., 1991. The structural history of the Calabrian lower crustal section. *Res Terrae. Ser. A.*, **5**, 40.

Lamb, W. M. & Valley, J. W., 1985. C-O-H fluid calculations and granulite genesis. In: Tobi, A.C. & Touret, J.L.R. (eds) *The Deep Proterozoic Crust in the North Atlantic Provinces.* Dordrecht: Reidel, 119-131.

Lamb, W. M., Valley, J. W. & Brown, P. E., 1987. Post-metamorphic CO_2-rich fluid inclusions in granulites. *Contrib. Mineral. Petrol.* **96,** 485-495.

Le Breton, N. & Thompson, A. B., 1988. Fluid-absent (dehydration) melting of biotite in metapelites in the early stages of crustal anatexis. *Contrib. Mineral. Petrol.* **99,** 226-237.

Lee, D. E., & Bastron, H., 1967. Fractionation of rare earth elements in monazite and allanite as related to the geology of the Mt Wheeler Mine area, Nevada. *Geochimica et Cosmochimica Acta*, **31**, 339-356.

Mannucci, G., Diella, V., Grammacioli, C. M. & Pilati, T., 1986. A comparative study of some pegmatitic and fissure monazite from the Alps. *Can. Mineral.*, **24**, 469-474.

Maillet, L. A. & Clarke, D. B., 1985. Cordierite in the peraluminous granites of the Meguma Zone, Nova Scotia, Canada. *Min. Mag.*, **49**, 695-702.

McKenzie, D., 1985. The extraction of magma from the crust and mantle. *E.P.S.L.*, **74**, 81-91.

McCarthy, T. S. 1976. Chemical interrelationships in a low-pressure ganulite terrain in Namaqualand, South Africa, and their bearing on granite genesis and the composition of the lower crust. *Geochimica et Cosmochimica Acta* , **40**, 1057-1068.

McLellan, E.L., 1988. Migmatite structures in the Central Gneiss Complex, Boca de Quadra, Alaska. *J. Met.. Geol.* **6,** 517-542.

Mehnert, K. R., 1968. *Migmatites & the origin of granitic rocks.* Amsterdam: Elsevier, 393pp.

Miller, C. F. 1985. Are strongly peraluminous magmas derived from pelitic sedimentary sources. *J. Geol.*, **93**, 673-689.

Miller, C. F., Hanchar, J. M., Harrison, T. M., Wark, D. A., Woden, J. L. & Bennet, V. C., 1991. The granite-source connection: narrowing the gap through study of lower crustal xenoliths and accessory minerals. Abstract, A.G.U. Conference, 1992.

Miller, C. F., Hanchar, J. M., Woden, J. L., Bennet, V. C., Harrison T. M., Wark, D. A. & Foster, D. A., 1991. Source regions of granitoid plutons: evidence from lower crustal xenoliths and inherited accessory minerals. Abstract, A.G.U. Conference, 1992.

Miller, C. F. & Mittlefehldt, D. W., 1982. Depletion of LREE in felsic magmas. *Geology*, **10**, 129-133.

Miller, C. F. & Stoddard, E. F., 1981. The role of manganese in the paragenesis of magmatic garnet: an example from the Old Woman-Piute Range, California. *J. Geol.*, **89**, 233-246.

Miller, C. F., Watson, E. B., & Harrison, T. M., 1988. Perspectives on the source, segregation and transport of granitoid magmas. *Trans. Roy. Soc. Edin.: Earth Sciences.*, **79**, 135-156.

Mittlefehldt, D. W. & Miller, C. F., 1983. Geochemistry of the Sweetwater Wash Pluton, California: Implications for "anomolous" trace element behaviour during differentiation of felsic magmas. *Geochimica et Cosmochimica Acta*, **47**, 109-124.

Mohr, D. W. 1984. Zoned porphyroblasts of metamorphic monazite in the Anakeesta Fmn. Great Smoky Mountains, North Carolina. *Am. Mineral.*, **69**, 98-103.

van der Molen, I. & Paterson, M. S., 1979. Experimental deformation of partially-melted granite. *Contrib. Mineral. Petrol.*, **70**, 299-318.

Montel, J. M. 1992. Monazite as petrogenetic indicator in granite genesis. (Abstract, Goldsmith Conference. (in press)).

Montel, J. M., 1986. Experimental determination of the solubility of Ce monazite in SiO_2-Al_2O_3-K_2O-Na_2O melts at 800°c, 2Kb under H_2O) saturated conditions. *Geology*, **14**, 659-662.

Nakamura, N., 1974. Determination of REE, Ba, Fe, Mg, Na and K in carbonaceous and ordinary chondrites. *Geochimica et Cosmochimica Acta*, **38**, 757-775.

Nesbitt, H. W. 1980. Genesis of the New Quebec and Adirondack granulites: evidence for their production by partial melting. *Contrib. Mineral. Petrol.*, **72**, 303-310.

Newton, R. C., 1990. Fluids and melting in the the Archaean deep crust of southern India. In: Ashworth, J. R. & Brown, M. (*eds*) *High Temperature metamorphism and Crustal Anatexis. London: Unwin Hyman Ltd.* 149-179.

Newton, R. C., Smith, J. V. & Windley, B. F., 1980. Carbonic metamorphism, granulites and crustal growth. *Nature* **288,** 45-50.

Nicholson, H. 1990. *The Magmatic Evolution of Krafla, N.E. Iceland.* PhD. thesis, University of Edinburgh. (Unpublished).

Oliver, R.L., James, P.R., Collerson, K.D. & Ryan, A.B., 1982. Precambrian geologic relationships in the Vestfold Hills, Antarctica. In: Craddock, C. (ed.) *Antarctic Geoscience.* Madison: University of Wisconsin Press, 435-444.

Patino-Douce A. E. & Johnston A. D. 1991. Phase equilibria and melt productivity in the pelitic system: implications for the origin of peraluminous granitoids and aluminous granulites. *Contrib. Mineral. Petrol.*, **107**, 202-218.

Phillips, G. N., 1980. Water activity changes across an amphibolite-granulite facies transition, Broken Hill, Australia. *Contrib. Mineral. Petrol.* **75,** 377-386.

Phillips, G. N., Wall, V. J. & Clemens, J. D., 1981. Petrology of the Strathbogie batholith: a cordierite-bearing granite. *Can. Mineral.*, **19**, 47-63.

Powell, R. & Downes, J., 1990. Garnet porphyroblast-bearing leucosomes in metapelites: mechanisms, phase diagrams, and an example from Broken Hill, Australia. In: Ashworth, J. R. & Brown, M. (*eds*) *High Temperature metamorphism and Crustal Anatexis.* London: Unwin Hyman Ltd. 105-123..

Presnall, D. C. & Bateman, P. C., 1973. Fusion relations in the system $NaAlSi_3O_8$-$CaAl_2Si_2O_8$-$KAlSi_3O_8$-H_2O and generation of granitic magmas in the Sierra Nevada Batholith. *Bull. Geol. Soc. Am.*, **84**, 3181-201.

Puziewicz, J. & Johannes, W., 1988. Phase equilibria and compositions of Fe-Mg-Al minerals and melts in water-undersaturated peraluminous granitic systems. *Contrib. Mineral. Petrol.*, **100**, 156-68.

Pupin, J. P., 1980. Zircon and granite petrology. *Contrib. Mineral. Petrol.*, **73**, 207-220.

Ragland, P. C., 1989. *Basic Analytical Petrology*. New York. Oxford University Press. 362pp.

Rapp, R. P. & Watson, E. B., 1986. Monazite solubility and dissolution kinetics: implications for the Th and LREE chemistry of felsic magmas. *Contrib. Mineral. Petrol.*, **94**, 304-316.

Reid, M. R., 1990. Ionprobe investigation of rare-earth element distributions and partial melting of metasedimentary granulites. In: Vielzeuf, D. & Vidal, Ph. (eds), *Granulites and Crustal Evolution*. Dordrecht: Kluwer Academic Publishers, 507-522.

Rudnick, R. L & Presper, T. 1990. Geochemistry of intermediate/- to high-pressure granulites. *in* Vielzeuf, D. & Vidal, Ph. (eds), *Granulites and Crustal evolution*. pp 523-550.

Rubie, D. C. & Brearley, A. J., 1990. A model for rates of disequilibrium melting during metamorphism. In: Ashworth, J.R. & Brown, M. (eds) *High-temperature Metamorphism and Crustal Anatexis*. London: Unwin Hyman, 57-85.

Sawyer, E. W., 1993. Structure and composition of migmatite leucosomes: implications for the melt-residuum separation process. (In Press, *Phys. Earth. Planet Int.*)

Sawyer E. W. 1991a. Disequilibrium melting and the rate of melt-residuum separation during migmatisation of mafic rocks from the Grenville Front, Quebec. *J. Pet.*, **32**, 701-738.

Sawyer E. W. 1991(b). Effects of temperature and segregation rate on the trace element concentrations of crustal melts. (Abstract). *Res Terrae Ser. A.*, **5**, 70.

Sawyer, E. W. & Bedard, P. L., 1991. Melt segregation and Migration. EOS. **52**

Sawka, W. N., Chappell, B. W. & Norrish, K., 1984. Light-rare-earth-element zoning in sphene and allanite during granitoid fractionation. *Geology*, **12**, 131-134.

Scambos, T. A. Loiselle, M. C. & Wones, D. R., 1986. The Center Pond pluton: the restite of the story (phase separation and melt evolution in granitoid genesis). *Am. Jour. Sci.*, **286**, 241-280.

Searle, M. P. & Fryer, B. J., 1986. Garnet, tourmaline and muscovite-bearing leucogranites, gneisses and migmatites of the Higher Himalaya from Zanskar, Kulu, Lahoul and Kashmir. In: Coward, M. P. & Ries, A. C. (eds). Collision Tectonics. *Geol. Soc. Lond. Spec. Publ.*, **19**, 185-201.

Sederholm, J. J. 1967. *Selected Works. Granites and Migmatites.* Oliver & Boyd, Edinburgh.

Shand, S. J., 1927. *Eruptive Rocks.* London. Murby.

Shaw, H. R., 1972. Viscosities of magmatic silicate liquids: an empirical method of prediction. *Am. J. Sci.*, **272**, 870-93.

Sheraton, J.W., Black, L.P. & McCulloch, M.T., 1984. Regional geochemical and isotopic characteristics of high-grade metamorphics of the Prydz Bay area: the extent of Proterozoic reworking of Archaean continental crust in East Antarctica. *Precambrian Research* **26,** 169-198.

Sorenson, S. S., 1991. Petrogenetic significance of zoned allanite in garnet amphibolites from a palaeo-subduction zone: Catalina Schist, southern California. *Am. Mineral.*, **76**, 589-601.

Sheraton, J.W., Offe, L.A., Tingey, R.J. & Ellis, D.J., 1980. Enderby Land, Antarctica - an unusual Precambrian high-grade metamorphic terrain. *Journal of the Geological Society of Australia* **27,** 1-18.

Stone, M. 1988. The significance of almandine garnets in the Lundy & Dartmoor granites. *Min. Mag.*, **52**, 651-658.

Streckeisen, A. L., 1973. Plutonic Rocks: Classification and nomenclature recommended by the I.U.G.S. subcommission on the systematics of igneous rocks. *Geotimes*, **18(10)**, 26-30.

Stüwe, K. & Powell, R., 1989. Low-pressure granulite facies metamorphism in the Larsemann Hills area, East Antarctica; petrology and tectonic implications for the evolution of the Prydz Bay area. *J. Met. Geol.*, **7**, 465-483.

Tait, R.E., 1989. *Local processes involved in the generation of mafic migmatites from the Rauer Islands, East Antarctica.* D.Phil. thesis, University of Oxford, 407 pp. (Unpublished).

Tarney, J. & Windley, B. F. 1977. Chemistry, thermal gradients and evolution of the lower crust. *J. Geol. Soc. Lond.*, **134**, 153-172.

Taylor, S. R. & McClennan, S. M., 1985. *The continental crust: it's composition and evolution.* Oxford, Blackwell. 312pp.

Thompson, A. B., 1990. Heat, fluids and melting in the granulite facies. *In* Vielzeuf, D. & Vidal, Ph. (eds), *Granulites and crustal evolution.* 37-58.

Toramaru, A. & Fujii, N., 1986. Connectivity of melt phase in a partially molten peridotite. *J. Geophys. Res.*, **91**, 9239-9252.

Touret, J., 1986. Fluid inclusions in rocks from the lower continental crust. In: Dawson, J. B., Carswell, D. A., Hall, J. & Wedepohl, K. H. (*eds*), *The Nature of the Lower Continental Crust. Geological Society Special Publication*, **24**, 161-172.

Touret, J., 1971. Le faciès granulite en Norvège méridionale I. Les associations minerales. *Lithos* **4**, 239-249.

Tuttle, O. F. & Bowen, N. L., 1958. Origin of granite in the light of experimental studies in the system $NaAlSi_3O_8$-$KAlSi_2O_8$-SiO_2-H_2O. *Geol. Soc. Am. Mem.* **74**.

Vavra, G., 1990. On the kinematics of zircon growth and its petrogenetic significance: a cathodoluminescence study. *Contrib. Mineral Petrol.*, **106**, 90-99.

Valley, J. W., 1986. Stable isotope geochemistry of metamorphic rocks. In: Valley, J. W., Taylor, H. P. & O'Neil, J. R. (eds). *Stable Isotopes in High Temperature Geological Processes: Reviews in Mineralogy*, **16**, 445-489.

Vidal, P., Cocherie, A. & Le Fort, P., 1982. Geochemical investigations of the origin of the Manaslu leucogranite (Himalaya, Nepal). *Geochimica et Cosmochimica Acta*, **46**, 2274-92.

Vernon, R. H., 1983. Restite, xenoliths and microgranitoid enclaves in granites. *Journal & Proceedings, Royal Society of New South Wales,* **116**, 77-103.

Vernon, R. H., 1984. Microgranitoid enclaves in granites; globules of hybrid magma quenched in a plutonic environment. *Nature,* **309**, 438-439.

Vernon, R. H. & Collins, W. J., 1988. Igneous microstructures in migmatites. *Geology,* **16**, 1126-1129.

Vielzeuf, D., Clemens, J. D., Pin, C., & Moinet, E., 1990. Granites, granulites and crustal differentiation. *In* Vielzeuf, D. & Vidal, Ph. (eds), *Granulites and crustal evolution.* 59-85.

Vielzeuf, D. & Holloway, J. R., 1988. Experimental determination of the fluid-absent melting relations in the pelitic system. *Contrib. Mineral. Petrol.* **98,** 257-276.

Vielzeuf, D. & Vidal, Ph., 1990. The NATO ARW granulite conference: a report. In: Vielzeuf, D. & Vidal, Ph. (eds), *Granulites and Crustal Evolution.* Dordrecht: Kluwer Academic Publishers, 1-6.

Wall, V. J., Clemens, J. D. & Clarke, D. B., 1987. Models for granitoid evolution and source composition. *J. Geol.*, **95,** 731-49.

Warren, R.G., 1983. Metamorphic and tectonic evolution of granulites, Arunta Block, central Australia. *Nature* **305,** 300-303.

Warren, R. G. & Hensen, B. J., 1989. The P-T evolution of the Proterozoic Arunta Block, central Australia, and implications for tectonic evolution. In: Daly, J. S., Cliff, R. A. & Yardley, B. W. D. (eds) Evolution of Metamorphic Belts, *Geological Society of London Special Publication No.* **43,** 349-355.

Waters, D. J., 1988. Partial melting and the formation of granulite facies assemblages in Namaqualand, South Africa. *Journal of Metamorphic Geology* **6,** 387-404.

Waters, D. J. & Whales, C. L., 1984. Dehydration melting and the granulite transition in metapelites from southern Namaqualand, S. Africa. *Contrib. Mineral. Petrol.* **88,** 269-275.

Watson, E. B. & Harrison, T. M., 1983. Zircon saturation revisited: temperature and compositional effects in a variety of crustal magma types. *E. P. S. L.*, **64**, 295-304.

Watson, E. B. & Harrison, T. M., 1984. Accessory minerals and the geochemical evolution of crustal magmatic systems: a summary and prospectus of experimental approaches. *Phys. Earth. Planet. Int.*, **35**, 19-30.

Watson, E. B., 1979. Zircon saturation in felsic liquids: experimental data and applications to trace element geochemistry. *Contrib. Mineral. Petrol.*, **70**, 407-419.

Watson, E. B., 1982. Melt infiltration and magma evolution. *Geology*, **10**, 236-240.

Watson, E. B. 1988. The role of accessory minerals in granitoid geochemistry. (Abstract). *The Origin of Granites*. The Royal Society of Edinburgh & The Royal Society of London Hutton Meeting, Edinburgh. pp 19-20.

Watson, E. B., Vicenzi, E. P. & Rapp, R. P., 1989. Inclusion/host relations involving accessory minerals in high-grade metamorphic and anatectic rocks. *Contrib. Mineral. Petrol.*, **101**, 220-231.

Watt, G. R. 1992. *Geology of the Mount Hay - Mount Chapple massif (Arunta Block, Hermannsburg 1:250,000 Sheet area, central Australia) Field report, 1990. Record 1992/22.* Bureau of Mineral Resources, Geology & Geophysics, Australia.

Watt, G. R. & Harley, S. L., 1993. Accessory phase controls on the geochemistry of crustal melts and restites produced by dehydration melting. (*Contrib. Mineral. Petrol.*, **114**, 550-566).

Weber, C., Barbey, P, Cuney, M. & Martin, H., 1985. Trace element behaviour during migmatisation. Evidence for a complex melt-residuum-fluid interaction in the St. Malo migmatitic dome (France). *Contrib. Mineral. Petrol.*, **90**, 52-62.

White, A. J. R. 1990. *A workshop on Crustal Protoliths of Granites*. Course Notes, Department of Geology, University of St Andrews, St Andrews, Scotland.

White, A. J. R. & Chappell, B. W., 1991. Per migma ad magma down under. *Geological Journal*, **25**, 221-225.

White, A. J. R. & Chappell, B. W., 1977. Ultrametamorphism and granitoid genesis. *Tectonophysics*, **43**, 7-22.

Wickham, S. M., 1987. The segregation and emplacement of granitic magmas. *J. Geol. Soc. Lond.*, **144**, 281-297.

Winkler, H. G. F., 1979. *Petrogenesis of metamorphic rocks*. New York. Springer Verlag.

Wood, B. J. & Fraser, D. G., 1986. *Elementary thermodynamics for geologists*. Oxford. Oxford University Press.

Wyllie, P. J., 1983. Experimental studies on Biotite- and Muscovite granites and some crustal magmatic sources. In: Atherton, M. P. & Gribble, C, D. (eds). *Migmatites, Melting and Metamorphism*. Nantwitch. Shiva. 127-139.

Wyllie, P. J., 1977. Crustal anatexis: An experimental Review. *Tectonophysics*, **43**, 41-71.

Zeck, H. P., 1970. An erupted migmatite from Cerro del Hoyazo, S.E. Spain. *Contrib. Mineral. Petrol.*, **26**, 225-46.

Zinner, E. & Crozaz, G. 1987. A method for the quantitative measurement of rare earth elements in the ion microprobe. *Intl. J. Mass Spectrom. Ion Processes*, **69**, 17-38.

Appendix A.

BULK ROCK CHEMISTRY.

Type 1 Leucogneisses

	88/47	88/55	88/61	88/108	88/109	88/116-2	88/136	88/138	88/170
SiO2	75.20	74.04	73.43	72.98	75.15	73.90	74.28	75.68	74.69
Al2O3	13.58	13.94	14.73	14.17	12.81	12.49	14.10	14.35	14.21
Fe2O3	0.80	0.63	1.78	1.37	1.53	3.06	0.41	0.75	0.57
MgO	0.16	0.04	0.53	0.21	0.10	1.35	0.07	0.18	0.12
CaO	1.65	0.60	2.22	1.20	0.45	2.21	0.89	1.02	0.47
Na2O	2.36	2.24	2.25	2.75	1.70	1.83	3.09	1.49	1.51
K2O	4.91	6.82	3.92	5.65	6.87	3.08	5.72	5.37	6.83
TiO2	0.06	0.02	0.03	0.14	0.02	0.81	0.04	0.03	0.04
MnO	0.01	0.03	0.03	0.01	0.07	0.03	0.02	0.01	0.01
P2O5	0.08	0.18	0.08	0.12	0.19	0.03	0.08	0.09	0.12
Total	98.81	98.53	99.00	98.60	98.89	98.79	98.68	98.97	98.57
K (ppm)	40917	56833	32667	47083	57250	25667	47667	44750	56917
Ni	9	9	11	8	8	50	8	9	10
Cr	1		8	3		48		2	3
V	4	1	5	9	2	101	1	20	18
Sc	2	3	5	3	7	2	1	1	
Cu						26	1		
Zn	7	4	12	16	0	76	2	7	2
Sr	213	73	200	84	133	144	48	147	157
Rb	208	304	139	277	318	130	203	217	289
Zr	87	35	64	40	15	232	10	15	9
Nb	2	1	1	4	1	9	2		1
Ba	829	121	855	234	486	716	102	679	813
Pb	58	71	47	60	87	42	63	51	59
Th	2	5	2	3	4	5	1	3	3
La	14	2	11	19	10	55	5	12	12
Ce	40	11	22	47	14	117	17	27	22
Nd	16	5	9	19	6	40	6	9	8
Y	6	9	12	12	16	7	11	6	6
A/CNK	1.11	1.15	1.23	1.11	1.16	1.21	1.09	1.42	1.32
Xmg	0.28	0.11	0.37	0.23	0.11	0.47	0.25	0.32	0.29
ppm									
La	18.53		10.72	18.58	65.06	54.66	6.29	14.43	14.17
Ce	33.47		19.44	38.74	14.68	105.69	11.16	20.89	19.11
Pr	3.59		2.72	4.43	1.45	11.06	1.33	1.91	1.99
Nd	12.30		7.60	15.00	4.90	36.50	3.90	5.80	5.80
Pm									
Sm	2.08		0.81	2.62	0.85	5.53	0.64	0.73	0.68
Eu	2.15		2.11	0.77	1.12	1.92	0.29	1.45	1.60
Gd	1.30		1.46	2.25	1.03	3.40	0.76	0.57	0.73
Tb									
Dy	0.74		1.85	1.76	1.82	1.42	1.17	0.59	0.53
Ho	0.12		0.44	0.31	0.41	0.21	0.25	0.12	0.09
Er	0.39		0.99	1.02	1.56	0.56	0.86	0.48	0.34
Tm									
Yb	0.29		1.77	0.91	2.46	0.39	0.93	0.63	0.36
Lu	0.05		0.30	0.13	0.39	0.08	0.13	0.10	0.07
La (N)/Yb(N)	42.6		4.0	13.6	17.6	93.4	4.5	15.3	26.2
Eu/Eu*	3.73		5.89	0.95	3.67	1.26	1.27	6.64	6.92

Type 1 Leucogneisses (continued)

	88/200	88/206	88/213	88/219	88/258	88/272	88/276	88/294	88/315	88/325
SiO2	75.29	72.63	73.04	72.82	75.08	73.71	75.73	72.18	77.15	73.13
Al2O3	12.37	14.43	15.64	14.55	14.49	14.03	13.51	15.07	15.02	15.26
Fe2O3	2.92	1.55	2.00	1.91	1.06	1.59	0.09	0.37	1.12	0.74
MgO	0.11	0.26	0.17	0.28	0.10	0.20	0.10	0.06	0.14	0.10
CaO	1.01	1.08	0.94	1.01	1.08	0.69	1.01	1.49	0.84	0.84
Na2O	2.01	2.01	2.25	2.35	1.72	2.04	3.02	2.11	1.18	1.91
K2O	4.97	6.61	4.17	5.75	5.16	6.01	5.11	6.73	3.19	6.60
TiO2	0.20	0.19	0.03	0.20	0.16	0.03	0.02	0.04	0.07	0.03
MnO	0.07	0.01	0.11	0.02	0.00	0.02	0.00	0.00	0.02	0.01
P2O5	0.02	0.07	0.12	0.13	0.07	0.21	0.20	0.13	0.08	0.16
Total	98.96	98.85	98.47	99.01	98.92	98.53	98.66	98.18	98.81	98.77
K (ppm)	41417	55083	34750	47917	43000	50083	42583	56083	26583	55000
Ni	9	15	9	10	12	9	8	10	8	9
Cr	1	1		2		1		0	0	8
V	1	9	3	7	4	7	2	2	4	12
Sc	7	2	11	5	0	8		1	3	1
Cu	4							12	1	
Zn	19	24	8	27	46	7	0	2	5	4
Sr	141	161	83	60	85	171	109	273	68	214
Rb	111	241	151	294	299	234	187	184	130	228
Zr	148	111	38	96	40	16	8	52	31	28
Nb	6	10	2	13	5	1	1	2	2	1
Ba	1748	647	258	237	239	853	412	1927	189	1249
Pb	16	72	54	61	60	62	68	58	35	60
Th		23	4	41	24	4	4	4	9	4
La	16	43	3	45	42	8	7	17	15	7
Ce	25	87	12	97	84	14	15	47	36	22
Nd	11	30	6	34	27	6	6	18	12	9
Y	12	19	22	22	7	14	3	7	12	6
A/CNK	1.18	1.16	1.58	1.22	1.40	1.26	1.10	1.12	2.17	1.29
Xmg	0.07	0.25	0.14	0.22	0.16	0.20	0.69	0.24	0.20	0.21
ppm										
La	14.16	46.47					8.15			10.62
Ce	21.09	80.50					12.24			18.65
Pr	2.03	8.25					1.44			2.30
Nd	7.40	26.70					4.10			7.20
Pm										
Sm	1.38	4.61					0.46			0.89
Eu	1.37	1.24					1.14			2.56
Gd	2.54	3.81					0.56			0.93
Tb										
Dy	2.46	3.27					0.26			0.67
Ho	0.38	0.56					0.04			0.14
Er	0.98	1.60					0.13			0.46
Tm										
Yb	0.79	1.27					0.08			0.49
Lu	0.12	0.19					0.03			0.08
La (N)/Yb(N)	11.9	24.4					67.9			14.4
Eu/Eu*	2.22	0.88					6.88			8.56

Type 2 Leucogneisses

	88/73	88/75	88/95	88/98	88/112	88/116-1	88/119	88/131	88/139
SiO2	66.85	69.09	63.25	64.73	65.34	69.93	72.87	70.07	67.96
Al2O3	16.52	15.58	16.09	15.60	17.37	14.51	13.18	15.04	16.47
Fe2O3	4.75	4.83	9.32	8.08	8.57	5.27	5.29	6.35	7.19
MgO	0.99	1.19	2.63	2.03	2.50	1.21	1.56	1.52	1.84
CaO	2.68	2.71	1.54	4.07	0.74	1.96	0.98	1.62	0.50
Na2O	2.78	2.42	1.38	2.11	0.63	1.82	0.73	1.06	0.69
K2O	3.69	3.14	4.51	1.07	2.73	3.82	3.20	1.39	3.85
TiO2	0.79	0.64	0.95	1.17	0.99	0.55	0.59	0.83	0.87
MnO	0.07	0.06	0.17	0.14	0.13	0.08	0.08	0.14	0.13
P2O5	0.08	0.08	0.03	0.28	0.05	0.04	0.04	0.04	0.05
Total	99.20	99.73	99.86	99.28	99.05	99.20	98.52	98.06	99.54
K (ppm)	30750	26167	37583	8917	22750	31833	26667	11583	32083
Ni	19	15	40	37	53	33	26	55	18
Cr	22	22	158	31	201	16	90	122	98
V	56	58	148	145	177	44	80	121	93
Sc	14	11	27	23	25	14	13	17	20
Cu	10	4	12	26	10	15	9	28	0
Zn	58	52	88	94	115	64	38	61	67
Sr	164	153	162	287	93	162	113	75	118
Rb	157	141	222	59	113	132	114	44	154
Zr	165	168	282	199	228	291	192	248	264
Nb	17	14	16	14	16	6	18	17	12
Ba	648	608	1096	607	640	821	844	323	909
Pb	46	38	40	19	24	53	31	21	34
Th	13	24	2	4	20	10	4	13	18
La	62	56	47	47	33	70	27	40	44
Ce	136	120	76	108	76	140	50	86	86
Nd	51	46	20	45	30	48	15	34	30
Y	27	27	55	21	51	33	32	41	48
A/CNK	1.23	1.27	1.62	1.30	3.26	1.36	2.05	2.43	2.65
Xmg	0.29	0.33	0.36	0.33	0.37	0.31	0.37	0.32	0.34
ppm									
La	62.88	58.78	45.44	48.90	38.19	68.93	27.56	40.92	46.96
Ce	126.93	119.52	69.41	99.10	76.56	129.17	48.07	85.87	87.27
Pr	13.94	13.28	6.45	11.72	8.96	12.97	4.94	9.97	9.11
Nd	48.60	46.90	20.10	42.90	32.40	43.80	16.10	35.80	32.40
Pm									
Sm	9.27	8.71	4.12	8.05	6.35	7.90	2.94	6.36	6.73
Eu	1.96	1.82	1.77	1.64	0.95	2.11	1.40	1.09	1.21
Gd	7.06	6.76	6.34	6.48	7.67	7.46	3.51	6.27	7.26
Tb									
Dy	5.41	5.63	9.56	4.74	9.79	6.54	5.35	7.71	8.72
Ho	0.95	0.97	1.91	0.83	1.83	1.22	1.17	1.50	1.71
Er	2.72	2.45	5.87	2.18	5.39	3.85	3.95	4.60	5.27
Tm									
Yb	2.23	1.95	5.64	1.79	5.24	4.00	4.01	4.56	5.12
Lu	0.33	0.29	0.85	0.28	0.78	0.64	0.59	0.69	0.74
La (N)/Yb(N)	18.8	20.1	5.4	18.2	4.9	11.5	4.6	6.0	6.1
Eu/Eu*	0.71	0.70	1.06	0.67	0.42	0.83	1.33	0 52	0.53

Type 2 Leucogneisses (continued)

	88/186	88/193
SiO2	71.83	68.17
Al2O3	14.14	15.11
Fe2O3	2.64	5.73
MgO	0.60	1.39
CaO	2.48	1.73
Na2O	2.78	1.56
K2O	3.84	4.99
TiO2	0.38	0.61
MnO	0.00	0.06
P2O5	0.06	0.07
Total	98.75	99.41
K (ppm)	32000	41583
Ni	9	17
Cr	2	61
V	25	71
Sc	3	14
Cu	11	7
Zn	56	68
Sr	221	188
Rb	166	183
Zr	223	236
Nb	8	11
Ba	1324	962
Pb	15	46
Th	1	20
La	15	56
Ce	36	121
Nd	13	45
Y	6	33
A/CNK	1.07	1.36
Xmg	0.31	0.32
ppm		
La		60.03
Ce		117.09
Pr		12.64
Nd		44.80
Pm		
Sm		8.57
Eu		2.08
Gd		8.04
Tb		
Dy		7.22
Ho		1.23
Er		3.54
Tm		
Yb		3.09
Lu		0.46
La (N)/Yb(N)		13.0
Eu/Eu*		0.76

Type 3 Leucogneisses

	88/103	88/105	88/107	88/122	88/152	88/161	88/164	88/225	88/230
SiO2	72.39	69.24	68.32	67.72	71.55	72.11	72.06	73.58	72.19
Al2O3	14.28	13.64	15.44	14.78	14.24	14.21	14.39	14.33	14.58
Fe2O3	1.29	4.24	2.56	2.65	3.34	2.37	2.54	1.33	1.50
MgO	0.25	0.70	0.63	1.59	0.76	0.50	0.53	0.21	0.08
CaO	1.02	2.09	1.83	1.66	1.28	1.15	1.24	0.81	0.73
Na2O	2.43	2.05	2.52	2.09	1.83	1.89	1.97	2.39	2.65
K2O	6.50	4.73	6.10	5.51	5.67	6.05	5.89	5.57	6.08
TiO2	0.27	0.64	0.57	1.17	0.40	0.26	0.26	0.26	0.17
MnO	0.00	0.02	0.01	0.00	0.03	0.02	0.02	0.00	0.01
P2O5	0.08	0.11	0.19	0.07	0.10	0.10	0.11	0.27	0.56
Total	98.51	97.46	98.17	97.24	99.20	98.67	99.02	98.75	98.56
K (ppm)	54167	39417	50833	45917	47250	50417	49083	46417	50667
Ni	8	10	11	16	11	12	12	10	12
Cr	1	11	8	1	8	4	4	4	11
V	11	39	31	137	19	12	13	10	13
Sc	1	6	4	0	5	8	8	3	2
Cu									1
Zn	17	210	47	51	23	10	14	53	22
Sr	188	252	296	510	157	142	140	66	131
Rb	408	249	363	175	269	285	275	376	315
Zr	115	373	416	542	216	122	142	96	61
Nb	7	13	13	6	9	5	5	10	4
Ba	696	1037	1230	3896	693	557	550	265	823
Pb	91	63	60	60	68	71	70	47	55
Th	41	183	199	113	118	54	63	50	31
La	114	294	305	227	161	100	111	53	42
Ce	200	587	603	405	334	205	230	131	97
Nd	52	175	187	124	108	65	74	58	39
Y	11	24	20	6	35	28	32	13	14
A/CNK	1.11	1.11	1.10	1.19	1.24	1.21	1.21	1.25	1.19
Xmg	0.28	0.25	0.33	0.54	0.31	0.29	0.29	0.24	0.10
ppm									
La	121.92	311.40	339.78	252.56	177.24	106.82	120.52		44.55
Ce	196.86	573.98	630.24	426.07	347.21	204.05	230.45		92.43
Pr	17.68	57.56	62.89	41.31	35.80	21.17	23.76		10.42
Nd	51.00	178.00	196.00	130.90	117.90	67.90	76.90		37.20
Pm									
Sm	6.82	28.43	27.58	12.98	22.32	12.04	14.16		6.66
Eu	1.43	2.07	2.36	3.11	1.60	1.53	1.47		1.52
Gd	3.35	11.18	11.68	4.07	14.33	8.14	9.55		4.06
Tb									
Dy	1.79	6.39	4.93	1.17	8.96	5.99	7.05		2.14
Ho	0.27	1.00	0.78	0.25	1.37	0.97	1.13		0.36
Er	0.68	1.70	1.91	0.64	3.27	2.54	2.96		0.99
Tm									
Yb	0.29	0.95	0.84	0.17	1.99	1.63	1.89		0.83
Lu	0.05	0.15	0.12	0.04	0.29	0.22	0.25		0.12
La (N)/Yb(N)	280.3	218.5	269.7	990.4	59.4	43.7	42.5		35.8
Eu/Eu*	0.81	0.30	0.34	1.03	0.26	0.45	0.37		0.83

Type 3 Leucogneisses (continued)

	88/278	88/279	88/336
SiO2	71.21	71.00	68.40
Al2O3	14.29	14.71	15.73
Fe2O3	3.16	1.75	3.86
MgO	0.64	0.55	0.90
CaO	1.28	1.51	2.01
Na2O	2.38	2.52	2.79
K2O	5.22	5.80	4.23
TiO2	0.41	0.47	0.41
MnO	0.01	0.00	0.06
P2O5	0.20	0.16	0.06
Total	98.81	98.47	98.45
K (ppm)	43500	48333	35250
Ni	11	19	11
Cr	3	6	6
V	22	30	31
Sc	4	1	10
Cu	6		0
Zn	53	55	45
Sr	153	152	181
Rb	232	275	101
Zr	212	225	222
Nb	9	8	6
Ba	846	815	765
Pb	67	74	66
Th	86	85	83
La	109	110	117
Ce	220	220	231
Nd	74	73	80
Y	13	11	35
A/CNK	1.20	1.12	1.23
Xmg	0.29	0.38	0.32
ppm			
La		124.83	126.92
Ce		234.77	235.34
Pr		24.34	24.18
Nd		80.50	81.60
Pm			
Sm		13.72	14.16
Eu		1.55	1.32
Gd		6.85	9.46
Tb			
Dy		2.25	7.42
Ho		0.33	1.40
Er		0.74	4.11
Tm			
Yb		0.36	3.27
Lu		0.07	0.46
La (N)/Yb(N)		231.2	25.9
Eu/Eu*		0.44	0.33

Metapelitic Gneisses

	88/35	88/56	88/62	88/74	88/82	88/83	88/146B	88/147	88/203	88/228
SiO2	69.55	66.50	66.95	66.74	68.27	64.49	57.98	61.34	62.77	67.89
TiO2	0.784	0.872	0.840	0.707	0.713	0.841	1.407	1.134	1.200	0.606
Al2O3	14.60	15.81	16.29	16.90	15.68	15.24	21.25	16.99	19.27	17.13
Fe2O3	6.47	7.77	7.88	7.97	6.87	10.43	9.92	7.96	11.18	5.98
MnO	0.055	0.167	0.105	0.091	0.084	0.390	0.113	0.088	0.111	0.060
MgO	2.98	2.05	1.87	1.72	1.56	1.39	3.45	3.71	2.44	1.07
CaO	0.98	0.83	0.63	0.57	0.85	0.75	3.23	3.77	0.44	0.69
Na2O	1.92	1.73	1.42	1.15	1.30	1.31	2.07	2.23	0.60	2.02
K2O	1.828	3.858	2.839	4.106	3.235	5.011	0.664	1.818	2.396	4.168
P2O5	0.056	0.080	0.034	0.057	0.064	0.111	0.048	0.262	0.034	0.133
LOI	0.92	0.28	1.05	0.19	1.08	0.00	0.21	0.12	-0.10	0.41
Total	100.14	99.95	99.91	100.20	99.71	99.96	100.34	99.42	100.34	100.16
Ba	268.0	1018.7		794.6	464.9	3187.2	282.5	905.2	580.3	502.6
Rb	145.4	191.0		209.5	218.3	237.6	44.8	142.5	98.3	225.9
Sr	81.5	117.7		127.3	70.8	95.1	175.1	193.8	93.7	81.4
Pb	15.3	42.5		36.7	37.5	54.9	22.9	24.3	22.3	39.6
Y	25.7	36.8		48.8	27.9	50.2	33.1	26.3	67.5	35.2
Th	20.1	17.0		5.5	18.5	32.8	14.3	22.9	6.5	13.0
U	2.4	3.8		2.0	3.5	3.0	0.8	1.8	1.0	2.1
Zr	20.9	202.6		180.7	208.0	158.3	250.7	281.2	264.6	137.1
Nb	12.6	14.6		13.5	15.8	10.5		19.6	21.2	13.7
Cr	226.3	161.7		164.0	135.9	126.4	217.4	186.0	279.9	84.9
V	134.6	134.3		125.1	126.9	137.5	239.3	181.3	212.0	78.7
Sc	17.4	18.8		32.2	19.9	28.4	21.6	23.5	32.5	15.9
Ni	25.9	57.2		43.3	69.1	52.0	86.2	23.1	116.8	22.5
Cu	17.1	30.8		15.0	115.4	42.7	22.0	18.8	35.9	11.3
Zn	94.0	98.9		106.6	140.0	97.5	126.6	144.6	180.1	94.4
A/CNK	2.11	1.85	2.49	2.29	2.18	1.70	2.13	1.36	4.40	1.89
Xmg	0.48	0.34	0.32	0.30	0.31	0.21	0.41	0.48	0.30	0.26
La	43.52	51.99		38.88	46.08	60.14	79.06		34.80	
Ce	87.27	100.96		70.55	94.43	129.51	158.77		57.90	
Pr	9.40	10.80		7.54	10.67	14.23	17.14		5.97	
Nd	33.80	38.10		25.60	38.70	52.10	61.60		22.00	
Pm										
Sm	6.18	7.32		5.48	7.88	10.11	11.42		5.63	
Eu	0.91	1.65		1.49	0.83	1.84	1.63		1.25	
Gd	5.05	7.34		6.96	7.04	9.42	9.80		8.44	
Tb										
Dy	4.98	7.52		8.76	5.81	9.54	6.98		12.00	
Ho	0.93	1.37		1.67	1.09	1.76	1.25		2.24	
Er	2.84	4.12		4.98	3.49	5.10	3.78		6.51	
Tm										
Yb	2.66	3.80		4.72	3.49	4.53	3.60		5.76	
Lu	0.41	0.57		0.69	0.54	0.66	0.54		0.83	
La(N)/Yb(N)	10.9	9.1		5.5	8.8	8.9	14.6		4.0	
Eu/Eu*	0.48	0.68		0.74	0.33	0.57	0.46		0.56	

Melanosomes

	IF/88/46A	IF/88/46C	IF/88/58
SiO2	33.48	53.26	35.40
TiO2	1.80	1.45	1.49
Al2O3	35.90	22.29	38.67
Fe2O3	21.65	14.98	20.15
MnO	0.32	0.23	0.37
MgO	7.05	4.20	4.32
CaO	0.43	0.62	0.38
Na2O	0.17	0.75	0.21
K2O	1.53	2.40	0.46
P2O5	0.02	0.05	0.03
LOI	-0.81	-0.25	-0.81
Total	102.35	100.24	101.48
Ba	905.9	40.0	76.9
Rb	226.3	125.1	44.2
Sr	8.9	96.6	12.1
Pb	3.9	25.6	3.0
Y	120.6	79.2	125.1
Th	17.8	11.2	8.7
U			2.1
Zr	241.2	246.7	199.1
Nb	35.8	24.9	30.3
Cr	406.2	311.6	364.8
V	431.6	240.5	367.4
Sc	54.0	40.0	89.3
Ni	249.1	92.4	160.1
Cu	19.7	16.8	25.5
Zn	464.8	187.4	195.0
A/CNK	13.19	4.49	25.21
XMg	0.39	0.36	0.30
La	31.83	34.6	13.91
Ce	65.31	61.86	29.33
Pr	7.72	6.71	3.67
Nd	30.89	25.55	18.20
Pm			
Sm	11.54	9.24	11.60
Eu	0.32	1.19	0.27
Gd	14.60	12.52	23.90
Tb			
Dy	23.19	15.91	23.13
Ho	4.66	3.12	4.10
Er	15.02	10.07	12.42
Tm			
Yb	16.54	10.54	12.84
Lu	2.36	1.54	1.89
La (N)/Yb(N)	1.3	2.2	0.7
Eu/Eu*	0.08	0.34	0.05

Appendix B.

CHONDRITE NORMALISING FACTORS.

APPENDIX B. CHONDRITE NORMALISING VALUES

La	0.330
Ce	0.865
Pr	0.122
Nd	0.630
Sm	0.203
Eu	0.077
Gd	0.275
Tb	0.058
Dy	0.342
Ho	0.076
Er	0.225
Tm	0.036
Yb	0.220
Lu	0.034

(Nakamura, 1974)

Appendix C.

MAJOR ELEMENT MINERAL CHEMISTRY.

Major Element Mineral Chemistry - Type 1 Leucogneisses

K-Feldspar

	207	207	325	325	325	325	170	170	170
SiO2	65.184	64.923	65.995	65.619	65.331	65.960	65.399	64.589	65.614
TiO2	0.057	0.050							
Al2O3	18.395	18.414	18.930	18.678	18.790	18.785	18.904	18.479	19.184
Cr2O3	0.020	0.019							
ZnO	0.031	0.017							
FeO	0.059	0.072	0.046	0.015	0.026	0.023	0.013	0.002	0.006
MnO	0.019	0.010	0.004	0.004	0.010	0.000	0.014	0.010	0.002
MgO	0.010	0.013	0.009	0.008	0.011	0.007	0.017	0.019	0.032
CaO	0.158	0.134	0.194	0.185	0.180	0.113	0.383	0.456	0.729
Na2O	2.238	1.965	2.160	1.850	1.676	1.763	2.073	1.844	2.540
K2O	13.049	13.632	13.351	13.703	13.896	13.802	12.983	14.279	11.921
Total	99.221	99.251	100.690	100.063	99.919	100.452	99.784	99.677	100.029
cations normalised for 8 oxygens									
Si	3.001	2.996	2.994	2.999	2.993	3.002	2.990	2.982	2.982
Ti	0.002	0.002							
Al	0.998	1.002	1.012	1.006	1.015	1.008	1.019	1.006	1.028
Cr	0.001	0.001							
Zn	0.001	0.001							
Fe	0.002	0.003	0.002	0.001	0.001	0.001	0.000	0.000	0.000
Mn	0.001	0.000	0.000	0.000	0.000	0.000	0.001	0.000	0.000
Mg	0.001	0.001	0.001	0.001	0.001	0.000	0.001	0.001	0.002
Ca	0.008	0.007	0.009	0.009	0.009	0.006	0.019	0.023	0.035
Na	0.200	0.176	0.190	0.164	0.149	0.156	0.184	0.165	0.224
K	0.766	0.803	0.773	0.799	0.812	0.801	0.757	0.841	0.691
Total	4.981	4.990	4.981	4.979	4.980	4.973	4.971	5.018	4.962
Xan	0.008	0.007	0.017	0.009	0.009	0.006	0.020	0.022	0.037
Xab	0.205	0.179	0.195	0.169	0.154	0.162	0.191	0.160	0.235
Xor	0.787	0.815	0.795	0.822	0.837	0.833	0.789	0.818	0.727

Plagioclase

	325	325	325	170	170	170	147 core	147 core	147 rim
SiO2	59.365	59.232	59.419	58.900	58.323	58.647	59.711	59.705	59.028
Al2O3	25.686	25.608	25.832	25.935	25.404	25.796	24.960	24.991	25.266
FeO	0.021	0.017	0.025	0.034	0.031	0.033	0.045	0.027	0.043
MnO	0.015	0.001	0.001	0.007	0.000	0.005	0.030	0.009	0.003
MgO	0.005	0.015	0.007	0.018	0.010	0.020	0.004	0.012	0.018
CaO	7.579	7.531	7.672	7.898	7.406	7.949	6.969	6.981	7.526
Na2O	6.848	6.518	6.668	6.504	7.331	6.870	7.722	7.636	7.555
K2O	0.277	0.236	0.195	0.154	0.956	0.172	0.228	0.249	0.211
Total	99.796	99.158	99.819	99.449	99.460	99.493	99.670	99.610	99.380
cations normalised for 8 oxygens									
Si	2.651	2.657	2.650	2.638	2.632	2.632	2.673	2.673	2.648
Al	1.352	1.354	1.358	1.370	1.352	1.365	1.317	1.319	1.336
Fe	0.001	0.001	0.001	0.001	0.001	0.001	0.002	0.001	0.002
Mn	0.001	0.000	0.000	0.000	0.000	0.000	0.001	0.000	0.000
Mg	0.000	0.001	0.000	0.001	0.001	0.001	0.000	0.001	0.001
Ca	0.363	0.362	0.367	0.379	0.358	0.382	0.334	0.335	0.362
Na	0.593	0.567	0.577	0.565	0.642	0.598	0.670	0.663	0.657
K	0.016	0.014	0.011	0.009	0.055	0.018	0.013	0.014	0.012
Total	4.977	4.956	4.964	4.964	5.040	4.989	5.010	5.006	5.018
Xan	0.373	0.384	0.384	0.398	0.340	0.386	0.328	0.331	0.351
Xab	0.610	0.602	0.604	0.593	0.608	0.604	0.659	0.655	0.637
Xor	0.016	0.014	0.012	0.009	0.052	0.019	0.013	0.014	0.012

Garnet

	315 Type 1	315 Type 1	315 Type 1	172 Type 2	172 Type 2	206 Type 2	206 Type 2	206 Type 2	206 Type 2
SiO2	37.078	37.162	37.164	37.771	37.738	37.142	37.301	37.277	37.277
TiO2	0.052	0.077	0.053	0.049	0.055	0.082	0.085	0.092	0.093
Al2O3	20.970	20.820	20.780	21.404	21.635	21.061	20.952	20.969	20.986
Cr2O3				0.011	0.015				
FeO	33.777	33.840	33.840	33.917	33.902	33.768	33.899	34.191	33.865
MnO	0.883	0.915	0.900	0.802	0.770	0.408	0.420	0.414	0.380
MgO	5.677	5.768	5.763	5.665	5.733	6.117	6.090	6.078	6.088
CaO	0.935	0.961	0.940	0.778	0.704	0.946	0.908	0.940	0.940
Na2O	0.015	0.001	0.000	0.007	0.008	0.003	0.023	0.016	0.000
K2O	0.002	0.012	0.012	0.003	0.000	0.006	0.011	0.000	0.012
F	0.000	0.155	0.000			0.000	0.036	0.059	0.000
Total	99.389	99.711	99.452	100.408	100.560	99.532	99.724	100.037	99.642
cations normalised for 12 oxygens									
Si	2.970	2.969	2.977	2.986	2.976	2.964	2.972	2.965	2.972
Ti	0.003	0.005	0.003	0.003	0.003	0.005	0.005	0.006	0.006
Al	1.981	1.961	1.962	1.995	2.012	1.981	1.968	1.966	1.972
Cr	0.000	0.000	0.000	0.001	0.001	0.000	0.000	0.000	0.000
Fe	2.263	2.261	2.267	2.242	2.236	2.254	2.259	2.274	2.258
Mn	0.060	0.062	0.061	0.054	0.051	0.028	0.028	0.028	0.026
Mg	0.678	0.687	0.688	0.667	0.674	0.727	0.723	0.720	0.723
Ca	0.080	0.082	0.081	0.066	0.059	0.081	0.078	0.080	0.080
Na	0.002	0.000	0.000	0.001	0.001	0.000	0.004	0.002	0.000
K	0.000	0.001	0.001	0.000	0.000	0.001	0.001	0.000	0.001
F	0.000	0.039	0.000			0.000	0.009	0.015	0.000
Total	8.038	8.066	8.040	8.014	8.015	8.041	8.046	8.056	8.037
Fe3+	0.115	0.238	0.120	0.045	0.045	0.123	0.151	0.183	0.113
Xmg	0.230	0.233	0.233	0.229	0.232	0.244	0.243	0.241	0.243
XMg*	0.240	0.254	0.243	0.233	0.235	0.255	0.256	0.256	0.252
Xalm	0.684	0.629	0.680	0.720	0.720	0.676	0.666	0.654	0.682
Xprp	0.216	0.214	0.218	0.219	0.221	0.231	0.229	0.225	0.230
Xuvr	0.000	0.000	0.000	0.000	0.000	0.000	0.000	0.000	0.000
Xsps	0.019	0.019	0.019	0.018	0.017	0.009	0.009	0.009	0.008
Xgrs	0.026	0.026	0.026	0.021	0.019	0.026	0.025	0.025	0.026
Xadr	0.055	0.112	0.057	0.022	0.022	0.059	0.072	0.087	0.054

Major Element Mineral Chemistry - Type 2 Leucogneisses

K-Feldspar

	105	172	172	139	139	139	193	193	193	130
SiO2	66.878	66.115	65.980	65.291	64.201	64.873	64.416	64.299	65.451	68.355
TiO2	0.060	0.044	0.018							0.107
Al2O3	18.800	19.358	19.240	18.913	18.200	18.595	18.523	19.588	19.295	19.267
Cr2O3		0.000	0.009							0.004
FeO	0.012	0.014	0.014	0.033	0.002	0.028	0.023	0.030	0.032	0.041
MnO	0.000	0.017	0.010	0.000	0.021	0.010	0.000	0.000	0.013	0.011
MgO	0.008	0.000	0.005	0.005	0.012	0.019	0.018	0.005	0.010	0.010
CaO	0.360	0.321	0.236	0.474	0.250	0.206	0.140	1.342	0.552	0.000
Na2O	1.441	2.985	2.807	1.999	2.290	1.851	1.273	2.277	1.706	1.440
K2O	13.083	11.534	12.014	13.434	14.540	14.045	14.663	11.817	13.541	9.871
F	0.283									0.000
Total	100.925	100.387	100.334	100.149	99.517	99.626	99.055	99.357	100.601	99.122
Cations normalised for 8 oxygens										
Si	3.011	2.986	2.987	2.983	2.979	2.988	2.990	2.949	2.976	3.060
Ti	0.002	0.001	0.001							0.004
Al	0.998	1.031	1.027	1.019	0.996	1.010	1.013	1.059	1.034	1.017
Cr		0.000	0.000							0.000
Fe	0.000	0.001	0.001	0.001	0.000	0.001	0.001	0.001	0.001	0.002
Mn	0.000	0.001	0.000	0.000	0.001	0.000	0.000	0.000	0.001	0.000
Mg	0.001	0.000	0.000	0.000	0.001	0.001	0.001	0.000	0.001	0.001
Ca	0.017	0.016	0.011	0.023	0.012	0.010	0.007	0.066	0.027	0.000
Na	0.126	0.261	0.246	0.177	0.206	0.165	0.115	0.202	0.150	0.125
K	0.751	0.665	0.694	0.783	0.861	0.825	0.868	0.691	0.785	0.564
F	0.040									0.000
Total	4.947	4.960	4.969	4.987	5.056	5.002	4.995	4.969	4.975	4.772
Xan	0.019	0.016	0.012	0.024	0.012	0.010	0.007	0.069	0.028	0.000
Xab	0.141	0.278	0.259	0.180	0.191	0.165	0.116	0.211	0.156	0.181
Xor	0.840	0.706	0.729	0.796	0.798	0.825	0.877	0.720	0.816	0.819

Plagioclase

	139	139	139	193	193	193	73	73	186	186	186
SiO2	58.604	58.624	57.968	57.284	57.024	57.190	60.213	60.156	59.306	59.149	59.335
Al2O3	26.359	26.479	26.515	27.264	27.225	27.191	24.974	24.963	25.407	25.567	25.311
FeO	0.010	0.032	0.044	0.052	0.030	0.030	0.044	0.063	0.070	0.074	0.056
MnO	0.009	0.000	0.130	0.000	0.005	0.000	0.000	0.036	0.000	0.000	0.003
MgO	0.009	0.015	0.007	0.012	0.005	0.015	0.014	0.020	0.023	0.000	0.023
CaO	8.382	8.552	8.634	9.334	9.397	9.193	6.706	6.788	7.363	7.397	7.221
Na2O	6.756	6.744	6.742	6.151	6.244	6.212	7.593	7.580	7.319	7.365	7.453
K2O	0.228	0.139	0.114	0.159	0.157	0.150	0.352	0.341	0.328	0.326	0.327
Total	100.357	100.584	100.037	100.256	100.086	99.982	99.897	99.946	99.815	99.878	99.728
cations normalised for 8 oxygens											
Si	2.611	2.607	2.593	2.561	2.556	2.563	2.685	2.682	2.653	2.646	2.657
Al	1.385	1.388	1.398	1.437	1.439	1.437	1.313	1.312	1.340	1.348	1.336
Fe	0.000	0.001	0.002	0.002	0.001	0.001	0.002	0.002	0.003	0.003	0.002
Mn	0.000	0.000	0.005	0.000	0.000	0.000	0.000	0.001	0.000	0.000	0.000
Mg	0.001	0.001	0.000	0.001	0.000	0.001	0.001	0.001	0.002	0.000	0.002
Ca	0.400	0.407	0.414	0.447	0.451	0.442	0.320	0.324	0.353	0.355	0.346
Na	0.584	0.581	0.585	0.533	0.543	0.540	0.656	0.655	0.635	0.639	0.647
K	0.013	0.008	0.007	0.009	0.009	0.009	0.020	0.019	0.019	0.019	0.019
Total	4.995	4.994	5.003	4.991	5.000	4.992	4.997	4.999	5.004	5.009	5.008
Xan	0.401	0.409	0.412	0.452	0.450	0.446	0.321	0.325	0.351	0.350	0.342
Xab	0.586	0.583	0.582	0.539	0.541	0.545	0.659	0.656	0.631	0.631	0.639
Xor	0.013	0.008	0.006	0.009	0.009	0.009	0.020	0.019	0.019	0.018	0.018

Garnet											
	119 Type 1	119 Type 1	119 Type 1	98 Type 2	98 Type 2	98 Type 2	119 Type 2	119 Type 2	119 Type 2	75-1 Type 2	75-1 Type 2
SiO2	37.669	37.801	37.694	37.600	37.555	37.673	37.365	37.356	37.489	37.722	37.530
TiO2	0.062	0.102	0.078	0.057	0.038	0.080	0.117	0.143	0.110	0.090	0.093
Al2O3	21.237	21.243	21.271	21.243	21.243	21.213	21.296	21.243	21.288	21.012	21.003
FeO	31.533	31.485	31.584	30.980	31.313	31.404	31.348	31.304	31.198	32.163	32.024
MnO	0.648	0.631	0.634	0.708	0.755	0.753	0.631	0.684	0.598	0.609	0.609
MgO	7.534	7.539	7.499	7.526	7.360	7.166	7.415	7.436	7.557	7.085	7.067
CaO	1.105	1.142	1.125	1.384	1.368	1.529	1.242	1.240	1.212	1.084	1.122
Na2O	0.018	0.000	0.021	0.020	0.011	0.008	0.000	0.001	0.016	0.023	0.004
K2O	0.000	0.001	0.000	0.008	0.005	0.016	0.018	0.001	0.013	0.001	0.006
F	0.000	0.000	0.000	0.000	0.000	0.000	0.097	0.036	0.085	0.000	0.144
Total	99.806	99.945	99.899	99.525	99.649	99.842	99.529	99.445	99.567	99.791	99.602
cations normalised to 12 oxygens											
Si	2.967	2.972	2.967	2.967	2.965	2.970	2.953	2.955	2.958	2.980	2.971
Ti	0.004	0.006	0.005	0.003	0.002	0.005	0.007	0.009	0.007	0.005	0.006
Al	1.972	1.969	1.974	1.976	1.977	1.972	1.984	1.981	1.980	1.957	1.960
Fe	2.077	2.070	2.079	2.044	2.067	2.071	2.072	2.071	2.058	2.125	2.120
Mn	0.043	0.042	0.042	0.047	0.050	0.050	0.042	0.046	0.040	0.041	0.041
Mg	0.884	0.883	0.880	0.885	0.866	0.842	0.873	0.877	0.889	0.834	0.834
Ca	0.093	0.096	0.095	0.117	0.116	0.129	0.105	0.105	0.102	0.092	0.095
Na	0.003	0.000	0.003	0.003	0.002	0.001	0.000	0.000	0.002	0.004	0.001
K	0.000	0.000	0.000	0.001	0.001	0.002	0.002	0.000	0.001	0.000	0.001
F	0.000	0.000	0.000	0.000	0.000	0.000	0.024	0.009	0.021	0.000	0.036
Total	8.044	8.038	8.044	8.044	8.046	8.041	8.062	8.051	8.058	8.038	8.063
Fe3+	0.135	0.114	0.133	0.134	0.138	0.125	0.209	0.162	0.199	0.117	0.223
Xmg	0.299	0.299	0.297	0.302	0.295	0.289	0.297	0.297	0.302	0.282	0.282
XMg*	0.313	0.311	0.311	0.317	0.310	0.302	0.319	0.315	0.323	0.294	0.306
Xalm	0.613	0.621	0.615	0.604	0.608	0.616	0.582	0.600	0.583	0.637	0.592
Xprp	0.279	0.281	0.278	0.280	0.273	0.267	0.273	0.276	0.279	0.265	0.260
Xuvr	0.000	0.000	0.000	0.000	0.000	0.000	0.000	0.000	0.000	0.000	0.000
Xsps	0.014	0.013	0.013	0.015	0.016	0.016	0.013	0.014	0.013	0.013	0.013
Xgrs	0.029	0.031	0.030	0.037	0.037	0.041	0.033	0.033	0.032	0.029	0.030
Xadr	0.064	0.054	0.064	0.064	0.066	0.060	0.099	0.077	0.094	0.056	0.105

Garnet (continued)

	75-2 Type 2	75-2 Type 2	112 Type 2	112 Type 2	130 Type 2	130 Type 2	130 Type 2
SiO2	37.788	37.722	37.840	37.627	37.221	37.091	37.230
TiO2	0.095	0.100	0.076	0.093	0.230	0.196	0.069
Al2O3	21.026	21.018	21.500	21.517	21.028	20.811	20.881
Cr2O3			0.190	0.117	0.061	0.069	0.237
ZnO						0.034	0.004
FeO	32.494	32.574	30.834	30.709	32.133	32.596	33.577
MnO	0.618	0.591	0.688	0.632	0.960	0.952	0.960
MgO	6.735	6.700	7.615	7.715	6.513	6.209	5.819
CaO	1.098	1.065	1.174	1.147	1.214	1.142	1.155
Na2O	0.000	0.034	0.007	0.019	0.009	0.025	0.007
K2O	0.012	0.007	0.001	0.001	0.016	0.000	0.007
F	0.000	0.065			0.083	0.040	0.266
Total	99.867	99.876	99.924	99.577	99.500	99.135	100.213
cations normalised to 12 oxygens							
Si	2.987	2.983	2.967	2.960	2.960	2.967	2.958
Ti	0.006	0.006	0.004	0.006	0.014	0.012	0.004
Al	1.959	1.959	1.988	1.995	1.972	1.963	1.956
Cr			0.012	0.007	0.004	0.004	0.015
Zn						0.002	0.000
Fe	2.148	2.154	2.022	2.020	2.137	2.181	2.231
Mn	0.041	0.040	0.046	0.042	0.065	0.065	0.065
Mg	0.793	0.789	0.890	0.904	0.772	0.740	0.689
Ca	0.093	0.090	0.099	0.097	0.103	0.098	0.098
Na	0.000	0.005	0.001	0.003	0.001	0.004	0.001
K	0.001	0.001	0.000	0.000	0.002	0.000	0.001
F	0.000	0.016			0.021	0.010	0.067
Total	8.029	8.043	8.029	8.035	8.050	8.045	8.086
Fe3+	0.087	0.150	0.088	0.107	0.174	0.152	0.324
Xmg	0.270	0.268	0.306	0.309	0.265	0.253	0.236
XMg*	0.278	0.283	0.315	0.321	0.282	0.267	0.266
Xalm	0.661	0.636	0.624	0.614	0.620	0.642	0.586
Xprp	0.254	0.251	0.287	0.290	0.244	0.234	0.212
Xuvr	0.000	0.000	0.006	0.004	0.002	0.002	0.007
Xsps	0.013	0.013	0.015	0.014	0.020	0.020	0.020
Xgrs	0.030	0.029	0.026	0.028	0.031	0.029	0.023
Xadr	0.042	0.072	0.043	0.052	0.083	0.072	0.151

Biotite

	98 Incl	98 Incl	75 Incl	75 Incl	98 Late	98 Late	75 Late	75 Late
SiO2	36.474	36.941	38.090	38.201	37.162	36.721	37.342	37.164
TiO2	6.945	6.922	6.024	6.041	4.721	4.926	5.768	5.636
Al2O3	13.276	13.378	13.330	13.482	12.902	13.112	12.866	13.055
FeO	10.167	10.479	8.968	8.959	13.493	13.791	13.105	13.157
MnO	0.017	0.008	0.006	0.014	0.018	0.041	0.043	0.044
MgO	15.783	15.942	17.411	17.439	15.204	14.881	14.331	14.304
CaO	0.014	0.000	0.011	0.009	0.029	0.000	0.015	0.040
Na2O	0.354	0.382	0.458	0.441	0.061	0.081	0.094	0.149
K2O	8.907	8.922	9.488	9.552	8.918	9.376	9.909	9.677
F	4.272	4.010	4.832	5.208	3.688	4.097	3.452	4.386
Total	96.209	96.984	98.619	99.346	96.197	97.025	96.925	97.612
cations normalised to (Si+Ti+Al+Cr+Fe+Mn+Mg)=14								
Si	5.289	5.316	5.357	5.333	5.457	5.374	5.464	5.395
Ti	0.757	0.749	0.637	0.634	0.521	0.542	0.635	0.615
Al	2.270	2.270	2.210	2.219	2.234	2.262	2.219	2.234
Fe	1.233	1.261	1.055	1.046	1.657	1.688	1.604	1.597
Mn	0.002	0.001	0.001	0.002	0.002	0.005	0.005	0.005
Mg	3.411	3.419	3.650	3.628	3.328	3.246	3.125	3.095
Ca	0.002	0.000	0.002	0.001	0.005	0.000	0.002	0.006
Na	0.100	0.107	0.125	0.119	0.017	0.023	0.027	0.042
K	1.648	1.638	1.703	1.701	1.671	1.751	1.850	1.792
F	1.959	1.825	2.149	2.299	1.713	1.896	1.597	2.014
OH	0.284	0.524	0.000	0.000	0.970	0.631	0.834	0.187
O	21.600	21.513	21.688	21.770	21.213	21.346	21.452	21.635
Total	16.672	16.585	16.889	16.983	16.605	16.787	16.529	16.796
XMg	0.734	0.731	0.776	0.776	0.668	0.658	0.661	0.660
Xk	0.943	0.939	0.932	0.934	0.990	0.987	0.986	0.977
XFevi	0.222	0.226	0.191	0.190	0.293	0.300	0.287	0.288
XOH	0.118	0.211	0.000	0.000	0.348	0.238	0.327	0.079

Major Element Mineral Chemistry - Melanosomes

K-Feldspar

	60	60	46A	46A	46C	46C
SiO2	64.696	64.632	64.482	64.579	65.279	65.394
TiO2	0.080	0.090	0.053	0.055		
Al2O3	18.904	18.962	18.968	18.890	18.657	18.652
Cr2O3	0.000	0.000	0.012	0.000		
FeO	0.014	0.021	0.171	0.124	0.005	0.030
MnO	0.009	0.000	0.000	0.000	0.009	0.027
MgO	0.008	0.000	0.017	0.008	0.013	0.018
CaO	0.294	0.336	0.316	0.269	0.159	0.238
Na2O	1.371	1.320	1.937	1.624	1.553	1.737
K2O	13.956	13.829	13.456	13.815	13.471	13.463
F	0.274	0.305	0.000	0.000		
Total	99.607	99.518	99.423	99.375	99.146	99.590
cations normalised for 8 oxygens						
Si	2.975	2.973	2.972	2.979	3.004	3.000
Ti	0.003	0.003	0.002	0.002	0.000	0.000
Al	1.025	1.028	1.031	1.027	1.012	1.009
Cr	0.000	0.000	0.000	0.000	0.000	0.000
Fe	0.001	0.001	0.007	0.005	0.000	0.001
Mn	0.000	0.000	0.000	0.000	0.000	0.001
Mg	0.001	0.000	0.001	0.001	0.001	0.001
Ca	0.014	0.017	0.016	0.013	0.008	0.012
Na	0.122	0.118	0.173	0.145	0.139	0.155
K	0.819	0.812	0.791	0.813	0.791	0.788
F	0.040	0.044	0.000	0.000		
Total	5.000	4.996	4.993	4.985	4.955	4.967
Xan	0.015	0.018	0.016	0.014	0.008	0.012
Xab	0.128	0.124	0.177	0.150	0.148	0.162
Xor	0.857	0.858	0.807	0.837	0.844	0.826

Plagioclase						
	60	60	60	46C	46C	46C
SiO2	57.943	57.964	58.084	56.886	56.556	56.959
TiO2	0.037	0.032	0.060			
Al2O3	25.919	26.323	25.910	26.475	27.133	26.873
Cr2O3	0.006	0.006	0.000			
FeO	0.055	0.040	0.062	0.046	0.042	0.110
MnO	0.000	0.000	0.009	0.003	0.012	0.000
MgO	0.003	0.000	0.005	0.020	0.015	0.010
CaO	8.203	8.419	8.139	9.132	9.468	9.152
Na2O	6.385	6.304	6.686	6.621	6.857	7.712
K2O	0.569	0.376	0.210	0.112	0.107	0.208
F	0.311	0.134	0.000			
Total	99.431	99.598	99.201	99.295	100.190	100.483
cations normalised for 8 oxygens						
Si	2.609	2.603	2.618	2.572	2.542	2.546
Ti	0.001	0.001	0.002			
Al	1.376	1.394	1.377	1.411	1.437	1.416
Cr	0.000	0.000	0.000			
Fe	0.002	0.002	0.002	0.002	0.002	0.004
Mn	0.000	0.000	0.000	0.000	0.000	0.000
Mg	0.000	0.000	0.000	0.001	0.001	0.001
Ca	0.396	0.405	0.393	0.442	0.456	0.438
Na	0.557	0.549	0.584	0.580	0.598	0.668
K	0.033	0.022	0.012	0.006	0.006	0.012
F	0.044	0.019	0.000			
Total	5.019	4.994	4.990	5.016	5.042	5.086
Xan	0.401	0.415	0.397	0.430	0.430	0.392
Xab	0.565	0.563	0.591	0.564	0.564	0.598
Xor	0.033	0.022	0.012	0.006	0.006	0.011

Garnet

	318	318	46	46	46	46	46A	46A
	Type 1	Type 1	Type 1	Type 1	Type 1	Type 1	Type 1	Type 1
SiO2	37.144	37.112	37.790	37.981	37.562	37.776	37.451	37.334
TiO2	0.078	0.082	0.078	0.065	0.088	0.103	0.066	0.085
Al2O3	21.072	21.027	21.041	21.037	21.162	20.941	21.305	21.426
Cr2O3	0.032	0.028	0.026	0.000	0.016	0.026	0.026	0.026
ZnO			0.016	0.020	0.015	0.005		
FeO	32.750	32.672	31.207	30.448	31.834	31.420	31.499	31.280
MnO	0.795	0.883	0.718	0.719	0.826	0.763	0.759	0.769
MgO	6.403	6.256	7.312	7.942	6.989	7.027	7.291	7.358
CaO	1.017	0.999	0.942	0.975	1.104	1.023	1.101	0.988
Na2O	0.000	0.020	0.005	0.028	0.012	0.000	0.004	0.000
K2O	0.000	0.006	0.000	0.000	0.000	0.004	0.007	0.006
F			0.000	0.044	0.044	0.265		
Total	99.290	99.086	99.136	99.260	99.562	99.591	99.419	99.271
cations normalised for 12 oxygens								
Si	2.964	2.968	2.992	2.992	2.971	2.988	2.962	2.956
Ti	0.005	0.005	0.005	0.004	0.005	0.006	0.004	0.005
Al	1.982	1.982	1.964	1.954	1.973	1.953	1.986	2.000
Cr	0.002	0.002	0.002	0.000	0.001	0.002	0.002	0.002
Zn	0.000	0.000	0.001	0.001	0.001	0.000	0.000	0.000
Fe	2.185	2.185	2.066	2.006	2.106	2.079	2.083	2.071
Mn	0.054	0.060	0.048	0.048	0.055	0.051	0.051	0.052
Mg	0.761	0.746	0.863	0.932	0.824	0.828	0.859	0.868
Ca	0.087	0.086	0.080	0.082	0.094	0.087	0.093	0.084
Na	0.000	0.003	0.001	0.004	0.002	0.000	0.001	0.000
K	0.000	0.001	0.000	0.000	0.000	0.000	0.001	0.001
F	0.000	0.000	0.000	0.011	0.011	0.066	0.000	0.000
Total	8.040	8.037	8.021	8.035	8.043	8.061	8.041	8.038
Fe3+	0.119	0.114	0.066	0.122	0.143	0.000	0.124	0.115
Xmg	0.258	0.254	0.295	0.317	0.281	0.285	0.292	0.295
XMg*	0.269	0.265	0.301	0.331	0.296	0.285	0.305	0.307
Xalm	0.657	0.661	0.647	0.602	0.623	0.683	0.622	0.624
Xprp	0.242	0.238	0.279	0.298	0.262	0.272	0.273	0.277
Xuvr	0.001	0.001	0.001	0.000	0.000	0.001	0.001	0.001
Xsps	0.017	0.019	0.016	0.015	0.018	0.017	0.016	0.016
Xgrs	0.027	0.026	0.025	0.026	0.029	0.028	0.029	0.026
Xadr	0.057	0.055	0.032	0.058	0.068	0.000	0.060	0.055

Garnet (continued)							
	46A	46A	325-1	325-1	325-1	318	318
	Type 2	Type 2	Type 2	Type 2	Type 2	Type 2	Type 2
SiO2	37.173	37.127	37.501	37.529	37.482	37.099	37.014
TiO2	0.111	0.094	0.080	0.076	0.088	0.047	0.082
Al2O3	21.286	21.189	21.313	21.296	21.451	20.993	21.074
Cr2O3	0.029	0.015	0.046	0.035	0.030	0.031	0.054
FeO	31.748	31.785	30.781	30.589	30.499	32.946	32.888
MnO	0.767	0.775	1.001	1.023	1.018	0.870	0.838
MgO	7.088	7.051	7.386	7.406	7.359	6.097	6.110
CaO	0.974	0.973	1.224	1.257	1.336	1.005	1.040
Na2O	0.021	0.018	0.013	0.005	0.000	0.010	0.029
K2O	0.000	0.003	0.000	0.000	0.006	0.003	0.003
Total	99.197	99.030	99.345	99.216	99.269	99.102	99.130
cations normalised for 12 oxygens							
Na	0.003	0.003	0.002	0.001	0.000	0.002	0.005
Mg	0.839	0.837	0.870	0.873	0.867	0.727	0.729
Al	1.994	1.989	1.986	1.986	1.999	1.981	1.988
Si	2.954	2.957	2.965	2.968	2.962	2.970	2.962
K	0.000	0.000	0.000	0.000	0.001	0.000	0.000
Ca	0.083	0.083	0.104	0.107	0.113	0.086	0.089
Ti	0.007	0.006	0.005	0.005	0.005	0.003	0.005
Cr	0.002	0.001	0.003	0.002	0.002	0.002	0.003
Mn	0.052	0.052	0.067	0.069	0.068	0.059	0.057
Fe	2.110	2.117	2.035	2.024	2.016	2.206	2.201
Zn	0.000	0.000	0.000	0.000	0.000	0.000	0.000
Total	8.043	8.044	8.037	8.033	8.033	8.036	8.039
Fe3+	0.132	0.135	0.112	0.101	0.098	0.111	0.123
Xmg	0.285	0.283	0.300	0.301	0.301	0.248	0.249
XMg*	0.298	0.297	0.312	0.312	0.311	0.258	0.260
Xalm	0.627	0.627	0.614	0.616	0.616	0.668	0.662
Xprp	0.266	0.265	0.278	0.280	0.278	0.232	0.232
Xuvr	0.001	0.000	0.001	0.001	0.001	0.001	0.002
Xsps	0.016	0.017	0.021	0.022	0.022	0.019	0.018
Xgrs	0.025	0.026	0.032	0.033	0.035	0.027	0.027
Xadr	0.063	0.065	0.054	0.048	0.047	0.053	0.059

Type 3 Garnet

Sample No.	325 Type 3	325 Type 3	325 Type 3	119 Type 3	119 Type 3	119 Type 3
SiO2	37.659	37.342	37.603	37.609	37.365	37.356
TiO2	0.099	0.124	0.097	0.130	0.117	0.143
Al2O3	21.239	21.183	21.362	21.313	21.296	21.243
Cr2O3	0.000	0.014	0.018			
FeO	30.656	30.749	30.584	31.112	31.348	31.304
MnO	0.991	1.071	1.041	0.637	0.631	0.684
MgO	7.326	7.256	7.343	7.441	7.415	7.436
CaO	1.264	1.308	1.377	1.259	1.242	1.240
Na2O	0.019	0.031	0.020	0.005	0.000	0.001
K2O	0.005	0.000	0.006	0.001	0.018	0.001
F				0.316	0.097	0.036
Total	99.257	99.078	99.452	99.824	99.529	99.445
Si	2.977	2.963	2.968	2.957	2.953	2.955
Ti	0.006	0.007	0.006	0.008	0.007	0.009
Al	1.979	1.982	1.988	1.976	1.984	1.981
Cr	0.000	0.001	0.001			
Fe	2.027	2.041	2.019	2.046	2.072	2.071
Mn	0.066	0.072	0.070	0.042	0.042	0.046
Mg	0.863	0.858	0.864	0.872	0.873	0.877
Ca	0.107	0.111	0.116	0.106	0.105	0.105
Na	0.003	0.005	0.003	0.001	0.000	0.000
K	0.001	0.000	0.001	0.000	0.002	0.000
F				0.079	0.024	0.009
Total	8.029	8.040	8.034	8.087	8.062	8.051
Fe3+	0.090	0.125	0.105	0.336	0.209	0.162
Xmg	0.299	0.296	0.300	0.299	0.297	0.297
XMg*	0.308	0.309	0.311	0.338	0.319	0.315
Xalm	0.623	0.609	0.613	0.527	0.582	0.600
Xprp	0.278	0.273	0.277	0.269	0.273	0.276
Xuvr	0.000	0.000	0.001	0.000	0.000	0.000
Xsps	0.021	0.023	0.022	0.013	0.013	0.014
Xgrs	0.034	0.035	0.037	0.033	0.033	0.033
Xadr	0.044	0.060	0.051	0.158	0.099	0.077

Accessory Phase Chemistry

Zircon

	112 LG3 rounded	112 LG3 rounded	112 LG3 rounded	112 LG3 needle	122 LG3 rounded	122 LG3 rounded
SiO2	32.350	32.462	32.410	31.963	31.799	32.173
Y2O3	0.190	0.000	0.000	0.000	0.006	0.000
ZrO2	64.951	64.925	65.443	64.687	66.221	66.212
ThO2	0.046	0.102	0.046	0.000	0.074	0.000
UO2	0.079	0.112	0.000	0.025	0.074	0.074
Yb2O3	0.126	0.000	0.050	0.000	0.118	0.000
HfO2	1.643	1.850	1.738	2.110	1.585	1.568
Er2O3	0.058	0.043	0.025	0.015	0.000	0.000
Dy2O3	0.028	0.048	0.000	0.000	0.000	0.000
Total	99.472	99.543	99.712	98.801	99.857	100.027
Cations normalised for 10 O						
Si	2.502	2.508	2.499	2.493	2.460	2.478
Y	0.008	0.000	0.000	0.000	0.000	0.000
Zr	2.450	2.446	2.461	2.460	2.500	2.486
Th	0.001	0.002	0.001	0.000	0.001	0.000
U	0.001	0.002	0.000	0.000	0.001	0.001
Yb	0.003	0.000	0.001	0.000	0.003	0.000
Hf	0.036	0.041	0.038	0.047	0.035	0.034
Er	0.001	0.001	0.001	0.000	0.000	0.000
Dy	0.001	0.001	0.000	0.000	0.000	0.000
Total	5.003	5.001	5.001	5.000	5.001	5.000

Accessory Phase Chemistry

Monazite

	58 MEL core	58 MEL core	58 MEL core	58 MEL core	60 MEL core	60 MEL core	46A MEL core	46A MEL core
SiO2	0.986	1.089	1.202	1.587	0.389	0.603	1.388	1.433
Y2O3	0.005	0.000	0.069	0.000	0.044	1.459	0.559	0.368
P2O5	27.224	27.041	27.375	26.175	28.773	28.565	26.919	26.798
CaO	0.662	0.534	0.376	0.381	1.374	0.947	0.379	0.397
UO2	0.341	0.340	0.372	0.322	0.496	1.771	0.417	0.440
ThO2	6.699	6.579	6.126	7.961	6.740	5.172	7.552	7.462
La2O3	13.805	13.938	13.231	12.918	13.731	13.520	15.240	15.334
Ce2O3	30.451	30.991	31.635	30.383	29.380	28.092	29.516	30.302
Pr2O3	3.046	2.839	3.270	2.838	2.823	2.530	2.816	2.844
Dy2O3	0.048	0.114	0.054	0.133	0.207	0.505	0.250	0.140
Nd2O3	12.784	13.004	13.615	13.641	11.505	11.427	11.876	11.298
Sm2O3	1.764	1.697	1.397	1.658	1.584	1.517	0.937	0.909
Gd2O3	0.753	0.713	0.492	0.565	0.732	0.992	0.340	0.337
Tb2O3	0.000	0.000	0.007	0.012	0.071	0.031	0.005	0.000
Total	98.568	98.880	99.223	98.574	97.850	97.131	98.196	98.063
cations normalised for 16 oxygens								
Si	0.162	0.178	0.195	0.263	0.063	0.098	0.228	0.236
Y	0.000	0.000	0.006	0.000	0.004	0.126	0.049	0.032
P	3.775	3.750	3.763	3.668	3.928	3.911	3.738	3.729
Ca	0.116	0.094	0.065	0.068	0.237	0.164	0.067	0.070
U	0.012	0.012	0.013	0.012	0.018	0.064	0.015	0.016
Th	0.250	0.245	0.226	0.300	0.247	0.190	0.282	0.279
La	0.834	0.842	0.792	0.789	0.817	0.806	0.922	0.930
Ce	1.826	1.859	1.881	1.841	1.734	1.663	1.772	1.824
Pr	0.182	0.169	0.193	0.171	0.166	0.149	0.168	0.170
Dy	0.003	0.006	0.003	0.007	0.011	0.026	0.013	0.007
Nd	0.748	0.761	0.790	0.806	0.663	0.660	0.696	0.663
Sm	0.100	0.096	0.078	0.095	0.088	0.085	0.053	0.052
Gd	0.041	0.039	0.026	0.031	0.039	0.053	0.018	0.018
Tb	0.000	0.000	0.000	0.001	0.004	0.002	0.000	0.000
Total	8.047	8.052	8.034	8.051	8.017	7.996	8.021	8.026

Monazite (continued)

	122 LG3 core	122 LG3 core	112 LG3 core	112 LG3 og	122 LG3 og	112 LG3 og	147 MPG core	147 MPG core
SiO2	1.209	1.249	1.417	1.911	3.492	2.833	0.712	0.570
Y2O3	0.000	0.000	0.004	0.000	0.000	0.000	0.000	0.476
P2O5	27.292	27.620	26.811	26.095	24.604	23.900	27.762	28.283
CaO	0.279	0.258	0.485	0.306	0.444	0.498	0.728	1.554
UO2	0.798	0.737	0.879	0.810	0.834	0.640	2.208	1.698
ThO2	8.670	8.334	9.866	11.315	14.695	15.308	11.465	8.076
La2O3	16.810	16.471	15.322	13.790	11.913	12.396	13.124	13.800
Ce2O3	30.384	30.543	29.979	28.942	27.273	27.578	27.259	28.560
Pr2O3	2.545	2.593	2.588	2.684	2.573	2.454	2.562	2.514
Dy2O3	0.006	0.155	0.091	0.133	0.101	0.075	0.073	0.180
Nd2O3	9.756	10.310	10.095	11.064	11.110	11.228	9.960	10.438
Sm2O3	0.722	0.731	0.783	0.976	0.925	0.849	1.257	1.406
Gd2O3	0.210	0.194	0.269	0.185	0.223	0.019	0.597	0.717
Tb2O3	0.000	0.000	0.076	0.000	0.000	0.000	0.084	0.066
Total	98.680	99.195	98.666	98.209	98.187	98.092	97.792	98.334
cations normalised for 16 oxygens								
Si	0.197	0.202	0.232	0.316	0.580	0.482	0.116	0.092
Y	0.000	0.000	0.000	0.000	0.000	0.000	0.000	0.041
P	3.765	3.778	3.721	3.652	3.457	3.439	3.834	3.868
Ca	0.139	0.128	0.154	0.143	0.148	0.117	0.386	0.294
U	0.010	0.009	0.018	0.011	0.016	0.019	0.026	0.056
Th	0.321	0.306	0.368	0.426	0.555	0.592	0.426	0.297
La	1.010	0.982	0.926	0.841	0.729	0.777	0.790	0.822
Ce	1.813	1.807	1.799	1.752	1.657	1.716	1.628	1.689
Pr	0.151	0.153	0.155	0.162	0.156	0.152	0.152	0.148
Dy	0.000	0.008	0.005	0.007	0.005	0.004	0.004	0.009
Nd	0.568	0.595	0.591	0.653	0.659	0.682	0.580	0.602
Sm	0.041	0.041	0.044	0.056	0.053	0.050	0.071	0.078
Gd	0.011	0.010	0.015	0.010	0.012	0.019	0.032	0.038
Tb	0.000	0.000	0.004	0.000	0.000	0.000	0.004	0.003
Total	8.027	8.018	8.032	8.029	8.028	8.048	8.050	8.038

Monazite (continued)

	46A MEL core	58 MEL og	58 MEL og	60 MEL og	60 MEL og	60 MEL og	46A MEL og	46A MEL og
SiO2	1.583	1.442	1.510	2.492	1.179	1.326	3.303	2.781
Y2O3	0.053	0.044	0.014	0.005	0.517	0.437	0.000	0.000
P2O5	26.454	26.596	26.479	25.274	27.584	27.501	24.057	24.633
CaO	0.402	0.343	0.357	1.321	1.584	1.615	0.290	0.304
UO2	0.703	0.356	0.382	0.377	0.526	0.799	0.220	0.271
ThO2	7.518	7.544	7.965	16.782	11.568	12.213	15.559	12.939
La2O3	14.601	13.034	12.895	10.951	9.817	9.591	13.619	13.517
Ce2O3	29.895	30.079	30.275	25.659	24.867	24.736	27.675	28.860
Pr2O3	2.953	2.905	3.084	2.281	2.784	2.761	2.421	2.935
Dy2O3	0.106	0.054	0.100	0.141	0.233	0.232	0.083	0.000
Nd2O3	12.174	13.634	13.267	11.664	14.693	14.247	10.567	11.298
Sm2O3	0.969	1.228	1.266	1.078	2.340	2.199	0.598	0.565
Gd2O3	0.153	0.461	0.577	0.093	0.619	0.864	0.000	0.063
Tb2O3	0.012	0.000	0.000	0.000	0.000	0.005	0.000	0.000
Total	97.576	97.721	98.172	98.119	98.312	98.526	98.393	98.166
cations normalised for 16 oxygens								
Si	0.262	0.239	0.250	0.415	0.192	0.215	0.556	0.467
Y	0.005	0.004	0.001	0.000	0.045	0.038	0.000	0.000
P	3.708	3.726	3.705	3.565	3.795	3.779	3.427	3.499
Ca	0.071	0.061	0.063	0.236	0.276	0.281	0.052	0.055
U	0.026	0.013	0.014	0.014	0.019	0.029	0.008	0.010
Th	0.283	0.284	0.300	0.636	0.428	0.451	0.596	0.494
La	0.892	0.796	0.786	0.673	0.588	0.574	0.845	0.837
Ce	1.812	1.822	1.832	1.565	1.479	1.470	1.705	1.773
Pr	0.178	0.175	0.186	0.138	0.165	0.163	0.148	0.179
Dy	0.006	0.003	0.005	0.008	0.012	0.012	0.004	0.000
Nd	0.720	0.806	0.783	0.694	0.853	0.826	0.635	0.677
Sm	0.055	0.070	0.072	0.062	0.131	0.123	0.035	0.033
Gd	0.008	0.025	0.032	0.005	0.033	0.047	0.000	0.004
Tb	0.001	0.000	0.000	0.000	0.000	0.000	0.000	0.000
Total	8.027	8.024	8.029	8.013	8.015	8.008	8.012	8.028

Monazite (continued)

	147 MPG core	147 MPG og	147 MPG og	147 MPG og
SiO2	0.558	1.722	1.900	1.262
Y2O3	0.134	0.000	0.015	0.013
P2O5	27.850	26.167	25.489	27.310
CaO	0.830	0.725	0.699	0.760
UO2	1.859	3.042	3.165	2.734
ThO2	9.608	20.132	21.410	16.979
La2O3	13.346	10.898	10.275	12.197
Ce2O3	28.201	23.226	23.116	24.833
Pr2O3	2.504	1.987	1.743	2.277
Dy2O3	0.197	0.217	0.249	0.044
Nd2O3	10.387	8.638	8.579	9.212
Sm2O3	1.470	0.952	0.800	0.985
Gd2O3	0.725	0.310	0.369	0.369
Tb2O3	0.000	0.000	0.024	0.000
Total	97.669	98.017	97.850	98.974
cations normalised for 16 oxygens				
Si	0.091	0.285	0.317	0.205
Y	0.012	0.000	0.001	0.001
P	3.853	3.661	3.601	3.752
Ca	0.325	0.539	0.566	0.475
U	0.030	0.027	0.026	0.027
Th	0.357	0.757	0.813	0.627
La	0.804	0.664	0.632	0.730
Ce	1.687	1.405	1.412	1.475
Pr	0.149	0.120	0.106	0.135
Dy	0.010	0.012	0.013	0.002
Nd	0.606	0.510	0.512	0.534
Sm	0.083	0.054	0.046	0.055
Gd	0.039	0.017	0.020	0.020
Tb	0.000	0.000	0.001	0.000
Total	8.047	8.049	8.069	8.038

Appendix D.

TRACE ELEMENT MINERAL CHEMISTRY.

Trace Element Mineral Chemistry

K-feldspar

	357 LG1	357 LG1	172 LG1	172 LG1	112 LG2	112 LG2	75 LG2	75 LG2	53 MPG
Si	309000	308000	308000	309000	299000	299000	299000	299000	308000
Rb	465.0	514.0	432.0	391.0	391.0	397.0	494.0	499.0	447.0
Sr	119.0	138.0	274.0	242.0	322.0	322.0	287.0	290.0	343.0
Y	0.02	0.02	0.03	0.03	0.05	0.08	0.02	0.02	0.07
Zr	0.03	0.03	0.47	0.76	0.05	0.06	0.09	0.10	0.06
Nb	0.01			0.04	0.01		0.03		
Ba	668.0	796.0	1830.0	1680.0	2660.0	2730.0	2440.0	2450.0	2280.0
La	14.80	12.60	9.32	10.40	20.40	26.90	35.80	34.30	103.00
Ce	14.00	10.30	14.60	15.20	15.40	25.10	40.90	39.10	119.00
Nd	2.02	1.27	2.37	2.81	1.09	2.57	6.61	5.43	11.80
Sm	0.22	0.13	0.41	0.19	0.18	0.12	0.47	0.39	0.53
Eu	1.47	1.74	5.90	4.97	8.38	8.81	7.91	6.88	8.11
Gd	0.85	0.93	1.14	1.15	0.71	1.20	2.58	2.46	5.80
Tb	0.03	0.04	0.03	0.07	0.02	0.02	0.03	0.03	0.04
Dy	0.02		1.17	0.67	1.04	0.53	0.45	0.52	
Ho	0.09	0.13	0.29	0.21	0.26	0.40	0.26	0.28	0.22
Er	0.03	0.10	0.15						0.02
Tm									
Yb		0.12	0.06	0.02	0.06				
Lu	0.05	0.03	0.04	0.02	0.06	0.03	0.04	0.03	0.02
Th	0.03	0.03	0.07	0.07	0.01	0.06	0.08	0.04	0.01
Chondrite normalised REE									
La	44.8	38.2	28.2	31.5	61.8	81.5	108.5	103.9	312.1
Ce	16.2	11.9	16.9	17.6	17.8	29.0	47.3	45.2	137.6
Nd	3.2	2.0	3.8	4.5	1.7	4.1	10.5	8.6	18.7
Sm	1.1	0.6	2.0	0.9	0.9	0.6	2.3	1.9	2.6
Eu	19.1	22.6	76.6	64.5	108.8	114.4	102.7	89.4	105.3
Gd	0.8	0.7	1.3	1.1	0.6	0.5	1.4	1.2	1.7
Tb	0.6	0.7	0.5	1.3	0.3	0.4	0.5	0.4	0.7
Dy			3.4	2.0	3.0	1.6	1.3	1.5	
Ho	1.2	1.7	3.8	2.8	3.4	5.2	3.5	3.7	2.9
Er									
Tm									
Yb									
Lu	1.4	0.9	1.2	0.7	1.8	0.8	1.3	0.9	0.5
Eu*	0.94	0.64	1.63	1.01	0.74	0.53	1.88	1.55	2.13
Eu/Eu*	20.31	35.29	46.88	63.66	146.42	215.23	54.54	57.49	49.48

K-feldspar (continued)

53 MPG	91-360 MEL	91-360 MEL
308000	302000	300000
436.0	488.0	477.0
354.0	296.0	306.0
0.04	0.02	0.02
0.06	0.07	0.04
	0.01	0.01
2370.0	1840.0	1940.0
98.50	63.30	67.50
113.00	83.40	85.10
10.90	8.83	7.29
0.59	0.30	0.33
9.82	6.62	6.50
5.50	4.68	4.73
0.11	0.07	0.01
0.64	1.02	0.45
0.31	0.32	0.21
0.07		0.07
0.01	0.01	0.05
0.03		
298.5	191.8	204.5
130.6	96.4	98.4
17.3	14.0	11.6
2.9	1.5	1.6
127.5	86.0	84.4
2.4	1.4	0.9
1.9	1.3	0.2
1.9	3.0	1.3
4.1	4.3	2.7
0.2	0.3	1.6
2.66	1.43	1.26
47.92	60.29	67.15

Trace Element Mineral Chemistry

Plagioclase

	357 LG1	357 LG1	75 LG2	75 LG2	146B MPG	146B MPG
Si	288000	288000	273000	274000	263000	266000
Rb	0.4	0.6	0.5	50.4	0.1	0.0
Sr	117.0	121.0	218.0	212.0	360.0	372.0
Y	0.28	0.30	0.25	0.24	0.16	0.17
Zr	0.04	0.03	0.04	0.04	0.14	0.20
Nb		0.02				
Ba	12.0	13.0	53.3	49.8	57.3	67.0
La	44.10	47.70	92.20	90.10	191.00	189.00
Ce	78.00	80.80	192.00	189.00	351.00	343.00
Nd	17.20	17.40	59.30	58.40	106.00	102.00
Sm	2.05	1.94	7.07	6.01	9.59	8.32
Eu	0.50	0.51	1.78	1.80	2.60	2.51
Gd	5.47	5.43	15.40	14.60	27.40	27.60
Tb		0.06		0.75		
Dy	0.61		0.96	0.07		
Ho	0.04	0.05	0.11	0.12	0.09	0.11
Er	0.28	0.24	0.43	0.68	0.87	0.68
Tm	0.04	0.01	0.03	0.10	0.05	0.01
Yb						
Lu	0.02	0.01	0.04	0.05	0.04	0.04
Th	0.06	0.07	0.06	0.08	0.01	0.02

Chondrite normalised REE

La	133.6	144.5	279.4	273.0	578.8	572.7
Ce	90.2	93.4	222.0	218.5	405.8	396.5
Nd	27.3	27.6	94.1	92.7	168.3	161.9
Sm	10.1	9.6	34.8	29.6	47.2	41.0
Eu	6.5	6.6	23.1	23.4	33.8	32.6
Gd	5.9	5.3	18.8	21.3	23.6	20.5
Tb	0.0	1.0	0.0	13.0	0.0	0.0
Dy	1.8	0.0	2.8	0.2	0.0	0.0
Ho	0.6	0.6	1.5	1.6	1.2	1.4
Er						
Tm						
Yb						
Lu	0.5	0.2	1.1	1.5	1.3	1.2
Eu*	8.02	7.42	26.82	25.45	35.43	30.74
Eu/Eu*	0.81	0.89	0.86	0.92	0.95	1.06

Trace Element Mineral Chemistry

Type 1 Garnet

	46 MEL	46 MEL	46a MEL	318 MEL	318 MEL
Si	174000	174000	175000	174000	174000
Rb					
Sr	0.128	0.235	0.199	0.0547	0.0627
Y	186	240	188	314	297
Zr	132	160	80.8	162	164
Nb		0.12	0.01		0.01
Ba	0.06	0.06	0.19	0.04	0.05
La	0.01	0.21	0.03	0.01	0.01
Ce	0.19	0.24	0.15	0.01	0.03
Nd	14.50	6.61	7.07	10.70	8.99
Sm	14.10	17.20	11.50	24.70	26.00
Eu	0.11	0.12	0.07	0.15	0.10
Gd	22.10	23.40	16.40	37.70	44.30
Tb	4.34	4.75	3.49	6.48	7.16
Dy	32.30	39.90	27.60	44.60	48.40
Ho	6.27	8.67	6.72	11.10	11.30
Er	14.70	23.30	16.90	31.10	29.80
Tm	2.32	3.34	2.48	4.42	4.34
Yb	15.70	27.70	18.20	39.30	36.70
Lu	1.83	3.27	1.92	4.96	4.80
Th		0.03	0.03	0.01	0.02
Chondrite normalised					
La	0.02	0.63	0.08	0.04	0.04
Ce	0.22	0.27	0.17	0.01	0.03
Nd	23.02	10.49	11.22	16.98	14.27
Sm	69.46	84.73	56.65	121.67	128.08
Eu	1.36	1.57	0.89	1.95	1.30
Gd	72.14	83.31	58.41	116.70	125.76
Tb	74.83	81.90	60.17	111.72	123.45
Dy	94.44	116.67	80.70	130.41	141.52
Ho	82.50	114.08	88.42	146.05	148.68
Er	65.33	103.56	75.11	138.22	132.44
Tm	64.44	92.78	68.89	122.78	120.56
Yb	71.36	125.91	82.73	178.64	166.82
Lu	53.82	96.18	56.47	145.88	141.18
Eu*	70.80	84.02	57.53	119.19	126.92
Eu/Eu*	0.019	0.019	0.015	0.016	0.010

Trace Element Mineral Chemistry

Type 2 Garnet

	325 MEL	325 MEL	325 MEL	46 MEL	318 MEL	318 MEL	172 LG1
Si	175000	175000	175000	174000	173000	174000	177000
Rb							
Sr	0.12	0.161	0.11	0.137	0.0458	0.0671	0.083
Y	447	423	409	214	252	229	226
Zr	146	96.9	95.6	128	161	157	15.3
Nb					0.03		
Ba	0.08	0.03	0.05	0.04	0.03	0.03	0.03
La	0.01	0.01	0.10	0.02	0.01	0.00	0.03
Ce	0.06	0.04	0.40	0.17	0.13	0.11	0.03
Nd	5.34	3.07	5.54	13.80	11.40	10.30	0.54
Sm	30.90	27.80	31.70	17.10	25.60	24.10	2.31
Eu	0.02	0.05	0.06	0.07	0.15	0.18	0.05
Gd	69.60	66.50	60.80	22.80	43.20	37.80	7.12
Tb	12.70	12.10	11.30	4.52	7.30	6.23	1.87
Dy	81.20	73.00	73.90	32.70	42.90	33.60	26.10
Ho	17.70	16.30	16.80	7.07	8.93	8.42	8.83
Er	45.40	44.10	43.20	17.20	22.50	19.70	34.30
Tm	6.56	6.58	6.53	2.49	3.11	2.66	64.30
Yb	55.10	56.50	54.90	17.70	27.40	22.90	57.70
Lu	7.42	7.45	7.93	1.98	3.20	2.52	8.66
Th				0.01	0.03	0.01	0.02
Chondrite normalised							
La	0.03	0.02	0.29	0.05	0.02	0.01	0.08
Ce	0.07	0.05	0.46	0.19	0.15	0.13	0.03
Nd	8.48	4.87	8.79	21.90	18.10	16.35	0.86
Sm	152.22	136.95	156.16	84.24	126.11	118.72	11.38
Eu	0.26	0.61	0.75	0.91	1.97	2.32	0.63
Gd	185.59	172.78	175.49	81.08	125.99	113.07	21.81
Tb	218.97	208.62	194.83	77.93	125.86	107.41	32.24
Dy	237.43	213.45	216.08	95.61	125.44	98.25	76.32
Ho	232.89	214.47	221.05	93.03	117.50	110.79	116.18
Er	201.78	196.00	192.00	76.44	100.00	87.56	152.44
Tm	182.22	182.78	181.39	69.17	86.39	73.89	1786.11
Yb	250.45	256.82	249.55	80.45	124.55	104.09	262.27
Lu	218.24	219.12	233.24	58.24	94.12	74.12	254.71
Eu*	168.90	154.86	165.83	82.66	126.05	115.89	16.59
Eu/Eu*	0.002	0.004	0.005	0.011	0.016	0.020	0.038

Type 2 Garnet (cont.)

172 LG1	112 LG2	112 LG2	75 LG2	75 LG2	75 LG2	146 MPG	35 MPG
176000	176000	177000	176000	176000	174000	175000	177000
0.0687	0.0433	0.151	0.0427	0.0328	0.0277	0.0453	0.085
219	194	229	150	116	138	68.1	289
31.2	76.2	35.4	63.1	82.8	55.3	117	64.3
0.04	0.04	0.46	0.02	0.01	0.00	0.02	0.03
0.04	0.01	0.01	0.01	0.01	0.01	0.03	0.01
0.03	0.03	0.10	0.13	0.11	0.11	0.33	0.03
0.36	2.89	3.28	3.92	4.20	4.06	6.31	0.17
2.31	5.60	6.31	10.20	9.62	9.79	14.10	1.94
0.06	0.11	0.11	0.05	0.08	0.09	0.12	0.06
8.72	12.30	13.70	22.90	21.10	26.20	26.50	20.80
2.49	3.67	4.32	4.69	4.11	4.78	3.15	5.85
20.90	30.40	31.00	27.80	23.50	27.60	12.00	43.20
7.55	6.27	6.79	4.79	3.44	4.52	2.30	9.15
28.60	17.50	17.40	9.60	5.92	8.59	4.95	24.10
5.70	2.51	2.53	1.13	0.69	1.00	0.57	3.85
54.90	20.40	22.90	8.64	6.40	7.62	5.83	33.00
7.70	2.64	2.78	0.96	0.84	0.94	0.69	4.37
0.05	0.03	0.02	0.05	0.02	0.00	0.04	0.01
0.12	0.04	0.04	0.02	0.03	0.04	0.08	0.04
0.03	0.03	0.11	0.15	0.13	0.12	0.38	0.03
0.57	4.59	5.21	6.22	6.67	6.44	10.02	0.27
11.38	27.59	31.08	50.25	47.39	48.23	69.46	9.56
0.80	1.43	1.45	0.68	1.10	1.13	1.56	0.72
27.16	45.43	52.78	65.55	59.13	65.32	61.88	55.21
42.93	63.28	74.48	80.86	70.86	82.41	54.31	100.86
61.11	88.89	90.64	81.29	68.71	80.70	35.09	126.32
99.34	82.50	89.34	63.03	45.26	59.47	30.26	120.39
127.11	77.78	77.33	42.67	26.31	38.18	22.00	107.11
158.33	69.72	70.28	31.39	19.17	27.72	15.72	106.94
249.55	92.73	104.09	39.27	29.09	34.64	26.50	150.00
226.47	77.65	81.76	28.32	24.71	27.59	20.41	128.53
19.27	36.51	41.93	57.90	53.26	56.77	65.67	32.38
0.042	0.039	0.035	0.012	0.021	0.020	0.024	0.022

Type 2 Garnet (cont.)

35 MPG	35 MPG	53 MPG	53 MPG
177000	173000	173000	173000
0.0773	0.138	0.073	0.0768
223	340	279	290
58.4	96.4	52.2	74.4
0.05	0.06	0.03	0.03
0.01	0.01	0.02	0.02
0.01	0.02	0.02	0.05
0.00	4.53	5.49	5.81
1.92	9.99	11.00	12.40
0.05	0.12	0.13	0.15
22.00	14.00	14.10	16.70
5.51	3.78	3.42	3.97
33.50	38.40	29.30	45.70
7.66	14.10	10.90	11.20
20.00	55.70	41.00	42.80
2.87	9.65	6.79	7.46
24.00	88.40	54.00	67.00
3.07	12.60	7.97	9.50
0.05	0.01	0.04	0.02
0.02	0.03	0.07	0.05
0.02	0.02	0.03	0.06
0.00	7.19	8.71	9.22
9.46	49.21	54.19	61.08
0.59	1.61	1.69	1.94
52.23	57.19	56.58	64.77
95.00	65.17	58.97	68.45
97.95	112.28	85.67	133.63
100.79	185.53	143.42	147.37
88.89	247.56	182.22	190.22
79.72	268.06	188.61	207.22
109.09	401.82	245.45	304.55
90.29	370.59	234.41	279.41
30.84	53.20	55.38	62.92
0.019	0.030	0.030	0.031

Trace Element Mineral Chemistry

Type 3 Garnet

	325 MEL	325 MEL	325 MEL	325 MEL	357 LG1	357 LG1	357 LG1
Si	176000	176000	176000	176000	176000	177000	176000
Rb							
Sr	0.187	0.209	0.228	0.215	0.0789	0.0896	0.0886
Y	444	500	507	529	729	700	729
Zr	78.8	6560	139	160	24.5	23.5	18.8
Nb	0.00	0.07					
Ba	0.03	0.12	0.07	0.03	4.39	0.21	0.04
La	0.03	0.17	0.02	0.02	0.01	0.03	0.03
Ce	0.38	0.92	0.31	0.30	0.57	0.43	0.24
Nd	11.70	10.60	11.00	9.75	11.10	8.47	6.52
Sm	29.10	35.00	31.70	35.20	31.20	24.60	23.30
Eu	0.06	0.09	0.04	0.05	0.29	0.23	0.17
Gd	62.80	71.10	70.80	75.40	61.40	61.10	62.00
Tb	12.10	14.30	14.20	14.50	14.00	13.70	14.70
Dy	78.90	91.20	97.30	94.50	110.00	104.00	102.00
Ho	17.20	19.10	20.20	20.90	26.10	24.40	25.80
Er	44.20	48.70	51.20	51.90	82.80	72.30	78.70
Tm	6.13	6.85	7.17	7.59	13.60	12.40	13.40
Yb	48.80	59.00	62.90	63.80	114.00	114.00	114.00
Lu	7.08	7.43	7.48	8.05	15.70	15.40	15.80
Th					0.03	0.03	0.01
Chondrite normalised							
La	0.08		0.05	0.05	0.04	0.09	0.10
Ce	0.44	1.07	0.36	0.35	0.66	0.50	0.28
Nd	18.57	16.83	17.46	15.48	17.62	13.44	10.35
Sm	143.35	172.41	156.16	173.40	153.69	121.18	114.78
Eu	0.77	1.12	0.49	0.67	3.75	2.96	2.17
Gd	175.99	209.48	200.49	211.70	197.54	178.69	184.11
Tb	208.62	246.55	244.83	250.00	241.38	236.21	253.45
Dy	230.70	266.67	284.50	276.32	321.64	304.09	298.25
Ho	226.32	251.32	265.79	275.00	343.42	321.05	339.47
Er	196.44	216.44	227.56	230.67	368.00	321.33	349.78
Tm	170.28	190.28	199.17	210.83	377.78	344.44	372.22
Yb	221.82	268.18	285.91	290.00	518.18	518.18	518.18
Lu	208.24	218.53	220.00	236.76	461.76	452.94	464.71
Eu*	159.67	190.95	178.33	192.55	175.62	149.94	149.45
Eu/Eu*	0.005	0.006	0.003	0.003	0.021	0.020	0.015

Trace Element Mineral Chemistry

Biotite

	75 Incl LG2	75 Late LG2	146B Incl MPG	146B Late MPG	318 Incl MEL	318 Late MEL
Si	177000	178000	173000	172000	176000	175000
Rb	1030	1010	792	421	853	761
Sr	10.6	11.7	43	19	34.6	21.7
Y	0.05	0.06	0.06	0.06	0.02	0.03
Zr	7.08	1.56	12.60	12.70	12.90	5.30
Nb	88.50	82.00	58.70	51.80	44.80	44.60
Ba	387	2200	3130	4110	2070	3430
La	0.03	0.23	0.61	0.44	0.18	0.37
Ce	0.05	0.05	0.06	0.23	0.04	0.06
Nd	0.00	0.09	0.03	0.07	-0.02	0.04
Sm	0.09	0.08	0.06	0.03	0.04	0.06
Eu						
Gd	12.30	67.20	91.10	133.00	66.90	122.00
Tb	0.01	0.01	0.01	0.01	0.01	0.02
Dy	0.35					
Ho	0.06	0.25	0.25	0.33	0.20	0.35
Er	0.16	0.41	0.35	0.38	0.28	0.42
Tm	0.04	0.06	0.10	0.09	0.05	0.09
Yb						
Lu	0.01	0.03	0.04	0.03	0.02	0.04
Th	0.02	0.06	0.06	0.03	0.00	0.00

Chondrite normalised

La	0.1	0.7	1.9	1.3	0.5	1.1
Ce	0.1	0.1	0.1	0.3	0.0	0.1
Nd	0.0	0.1	0.0	0.1	0.0	0.1
Sm	0.5	0.4	0.3	0.2	0.2	0.3
Eu						
Gd	0.3	0.3	0.3	0.1	0.2	0.3
Tb	0.2	0.2	0.2	0.1	0.2	0.4
Dy						
Ho	0.8	3.3	3.3	4.3	2.7	4.6
Er	0.7	1.8	1.6	1.7	1.3	1.8
Tm	1.0	1.8	2.9	2.6	1.5	2.5
Yb						
Lu	0.4	1.0	1.1	0.9	0.7	1.0

Appendix E.

ANALYTICAL PROCEDURES.

APPENDIX E. ANALYTICAL PROCEDURES.

E.1. BULK ROCK CHEMISTRY.

Aliquots were selected by cone and quarter reduction of an original sample of between approximately 0.5 and 1.0Kg in weight. Major and trace element analyses were carried out at Edinburgh using a Phillips PW1450 automatic X-ray spectrometer. Major elements were determined on glass disks prepared by fusing powdered samples with Spectroflux 105. Trace elements were determined on pressed-powder samples. Both major and trace element concentrations were calibrated against a range of international rock standards (Abbey, 1980). REE analyses were performed on the Phillips PV8210 1.5-m ICP-atomic emission spectrometer at Royal Holloway and Bedford New College (RHBNC), University of London, Egham. Chromatographic REE separation was accomplished using resin cation exchange columns using the method detailed in Nicholson (1990). A blank and an internal RHBNC standard were included with every six samples analysed, and after every tenth analysis a synthetic standard containing all the REE and Y was run to check for instrument drift.

E.2. MAJOR ELEMENT MINERAL CHEMISTRY.

E.2.1. Instrument, Operating Conditions and Correction Procedures.

Major element concentrations of phases discussed in this thesis were obtained by wavelength dispersive electron probe microanalysis using a Cameca Camebax Microbeam microprobe at the Department of Geology & Geophysics, University of Edinburgh. Analyses were performed at an accelerating voltage of 20kV and a beam current of approximately 20nA. Absolute abundances for each element were determined by comparison of X-ray count data with the standard for that element. These standards are given below. Correction for matrix effects was by an on-line PAP correction program. Counting times at peak and background spectrometerpositions were thirty seconds and fifteen seconds respectively.

Element Symbol	Atomic Number	Standard
F	9	Magnesium Fluoride
Na	11	Jadeite
Mg	12	Periclase
Al	13	Corundum
Si	14	Wollastonite
P	15	Apatite
K	19	Orthoclase
Ca	20	Wollastonite
Ti	22	Rutile
Cr	24	Metal
Mn	25	Metal
Fe	26	Metal
Zn	30	Metal
Y	39	Synthetic Glass
La, Ce, Pr, Nd, Sm, Gd, Tb	Various	Synthetic Glasses
Th	90	Metal
U	92	Metal

E.2.2. Normalisation procedures and chemical parameters.

Selected representative microprobe analyses for K-feldspar, plagioclase, garnet, biotite, monazite and zircon from the Brattstrand Bluffs Leucogneisses, melanosomes and some metapelitic gneisses are presented in Appendix B. Analyses are given both as weight per cent oxide and as cations per formula unit. Cations per formula unit have been calculated using 8 and 12 oxygens for the feldspars and garnet respectively. Biotite has been normalised to a total of 14 octahedral and tetrahedral cations, assuming 22 O (20 formula O units plus 4OH, equivalent in charge to 2 more O) because of uncertainties in H_2O and halogen contents. Full details of the methods used to define mineral parameters are given below.

K-Feldspar and Plagioclase.

Mole fractions of albite, anorthite and orthoclase were calculated using the following equations.

$$X_{an} = Ca/(Ca+Na+K)$$
$$X_{ab} = Na/(Ca+Na+K)$$
$$X_{or} = K/(Ca+Na+K)$$

where Ca, Na and K have been calculated on the basis of 8 oxygens.

Garnet.

Ferric iron contents in garnet have calculated using the charge balance equation;

$$Fe^{3+} = 2[12-(2Si + 2Ti + 1.5Al + 1.5Cr + Fe^{total} + Mn + Mg + Ca)]$$

after re-normalisation to 8 cations (rather than 12 O). The use of the PAP on-line correction programme produces a higher value for that calculated using the ZAF software which was used by Fitzsimons (1991). The PAP correction software is thought to produce more accurate analyses.

X_{Mg} and X_{Mg}^* were calculated using the following equations.

$$X_{Mg} = Mg/(Mg+Fe^{total}) \text{ and } X_{Mg}^* = Mg/(Mg+Fe^{total}-Fe3+).$$

Mole fractions of almandine, pyrope, uvarovite, spessartine, grossular and andradite were calculated using the following equations.

$$X_{alm} = (Fe^{(total)}-Fe^{3+})/3$$
$$X_{prp} = Mg/3$$
$$X_{uvr} = Cr/2$$
$$X_{sps} = Mn/3$$
$$X_{grs} = (Ca/3)-(Cr/2)-(Fe^{3+}/2)$$
$$X_{adr} = Fe^{3+}/2$$

Biotite.

Biotite formula units were normalised to 14 octahedral and tetrahedral cations, and O and OH contents calculated as follows:

O = 20 x (normalisation factor), and

OH = 24 - O - F

The following compositional parameters were then calculated.

$X_K = K/(Na+K)$

$X^{Fevi} = Fe/6$

$X_{OH} = OH/(OH+F)$.

Accessory phases.

Zircon cations were calculated on the basis of 10 oxygens, and monazite on the basis of 16.

E.2.3. Detection Limits and Accuracy.

The optimum analytical precision (which, multiplied by the analysis value, gives the 1 σ confidence level for this analysis) and the statistical lower limit of detection (based on 3σ confidence limits) were calculated using the following equations (after Wall, 1993).

$$\text{Detection Limit} = \frac{6}{m}\left(\frac{R_b}{T_b}\right)^{-\frac{1}{2}}$$

and

$$\text{Relative Precision} = \frac{1}{T_p^{1/2}\left(R_p^{1/2} - R_b^{1/2}\right)}$$

Where:

m	counts above background (counts sec^{-1} per nA) as measured on standard.
Rb	Background count rate for element on unknown.
Rp	Peak count rate for element on unknown.
Tb	Background count time (15 seconds in all analyses)
Tp	Peak count time (30 seconds in all analyses).

K-feldspar	Wt % Ox.	3σ	Detect Lim.
Si	65.62	0.28	0.017
Al	18.93	0.15	0.006
Fe	0.02	0.04	0.007
Mg	0.01	0.02	0.005
Ca	0.19	0.03	0.012
Na	1.85	0.08	0.047
K	13.70	0.15	0.037

Plagioclase	Wt % Ox.	3σ	Detect Lim.
Si	59.37	0.28	0.014
Al	25.69	0.18	0.006
Fe	0.02	0.04	0.006
Mg	0.01	0.02	0.005
Ca	7.58	0.11	0.013
Na	6.85	0.14	0.051
K	0.28	0.03	0.033

Garnet	Wt % Ox.	3σ	Detect Lim.
Si	37.74	0.28	0.016
Ti	0.06	0.03	0.008
Al	21.64	0.21	0.007
Cr	0.02	0.05	0.008
Fe	33.90	0.37	0.009
Mn	0.77	0.08	0.008
Mg	5.73	0.13	0.005
Ca	0.70	0.05	0.014
Na	0.01	0.04	0.049
K	0.00		0.042

Biotite	Wt % Ox.	3σ	Detect Lim.
Si	38.89	0.26	0.018
Ti	3.92	0.09	0.007
Al	12.78	0.15	0.006
Fe	7.29	0.18	0.008
Mn	0.03	0.04	0.006
Mg	20.01	0.19	0.005
Ca	0.00		0.013
Na	0.30	0.05	0.050
K	9.75	0.13	0.040
F	5.07	1.20	0.069

Zircon	Wt % Ox.	3σ	Detect Lim.
Si	31.78	0.21	0.025
Y	0.01		0.086
Zr	66.22	28.90	0.211
Th	0.07		0.075
U	0.07	0.32	0.117
Yb	0.12	0.12	0.088
Hf	1.58	0.09	0.034
Er	0.00		0.155
Dy	0.00		0.098

Monazite	Wt % Ox.	3σ	Detect Lim.
Si	2.66	0.094	0.018
Y	0.00		0.057
P	23.64	1.193	0.096
U	0.58	0.218	0.079
Th	14.43		0.131
Ca	0.61	0.327	0.014
La	12.02	0.349	0.454
Ce	28.32		0.613
Pr	2.78	0.129	0.470
Nd	11.49	2.096	0.409
Sm	0.86		0.422
Gd	0.08	0.003	0.282
Tb	0.00		0.201
Dy	0.13	0.012	0.213

Note: 3σ values refer to the wt % oxide value in the first column, detection limits refer to wt % element and not wt % oxide.

E.3. TRACE ELEMENTS.

E.3.1. Instrument, Operating Conditions and Correction Procedures.

Trace element concentrations in garnet, feldspar and biotite were determined on the Cameca ims-4f ion microprobe at the University of Edinburgh. An O^- primary beam with an accelerating voltage of -10 KeV was produced by a duoplasmatron gun giving a net impact energy at the sample (held at +4.5 KeV) of 14.5 KeV. Primary beam current was 8 nA producing a spot size of approximately 20-30 μm. An energy window of ±19 eV and an energy offset of 100 eV were used. Molecular species were reduced using energy filtering methods as described in Zinner & Crozaz (1987) and Hinton (1990). Analyses of the following isotopes were carried out; ^{30}Si, ^{85}Rb, ^{88}Sr, ^{89}Y, ^{90}Zr, ^{93}Nb, ^{138}Ba, ^{139}La, ^{140}Ce, ^{143}Nd, ^{147}Sm, ^{151}Eu, ^{157}Gd, ^{159}Tb, ^{161}Dy, ^{165}Ho, ^{167}Er, ^{169}Tm, ^{172}Yb and ^{175}Lu. Rb was corrected for the molecular FeSi peak at mass 84. Nb was corrected for the presence of $^{92}ZrH^+$ by measurement of the $^{94}ZrH^+$ peak at mass 95 (Hinton, 1990, Hinton & Upton, 1991). Determination of both LREE and HREE concentrations required correction for BaO, while HREE abundances were corrected for LREE oxides. Trace element abundances were calculated relative to Si (determined by electron microprobe analysis) and calibrated against glass standard NBS610.

E.3.1. Analytical Accuracy.

Standard counting errors (at 1σ confidence level) are used below to calculate errors for typical K-feldspar, Plagioclase, Garnet and Biotite analyses (all values - ppm).

	Kfs	± (1σ)	Plag	± (1σ)	Gt	± (1σ)	Bi	± (1σ)
Si	3.02E+05	204	2.73E+05	173	1.76E+05	165.44	1.76E+05	169.84
Rb	4.88E+02	15.9	5.35E-01	0.05	0	0	8.53E+02	2.90
Sr	2.96E+02	1.23	2.18E-01	0.65	7.28E-02	0.01	3.46E+01	0.33
Y	1.95E-02	5.62E-05	2.48E-1	0.02	3.45E+02	0.81	2.11E-02	0.01
Zr	7.37E-02	0.02	4.37E-02	0.01	9.71E+1	0.77	1.29E+01	0.29
Nb	5.30E-03	0.003	4.21e-03	0.002	0	0	4.48E+01	0.52
Ba	1.84E+03	3.51	5.33E+01	0.53	5.56E-02	0.02	2.07E+03	4.06
La	6.33E+01	0.53	9.22E+01	0.57	1.67E-02	0.01	1.78E-01	0.03
Ce	8.34E+01	0.66	1.92E+02	0.89	7.16E-02	0.02	3.91E-02	0.01
Nd	8.83E+00	0.55	5.93E+01	1.26	4.27E+00	0.40	0	0
Sm	3.00E-01	0.08	7.07E+00	0.37	1.45E+01	0.63	4.01E-2	0.03
Eu	6.62E+00	0.15	1.78E+00	0.10	9.81E-02	0.03	0	0
Gd	4.68E+00	0.35	1.54E+01	0.57	2.68E+01	0.88	6.69E+01	1.44
Tb	7.37E-02	0.011	0	0	6.58E+00	0.18	1.29E-02	0.01
Dy	1.02E+00	0.15	9.55E-01	0.07	4.26E+01	1.00	0	0
Ho	3.24E-01	0.04	1.14E-1	0.02	1.07E+01	0.23	2.04E-01	0.03
Er	0	0	4.29E-01	0.07	2.50E+01	0.76	2.84E-01	0.13
Tm	0	0	2.74E-02	0.01	3.70E+00	0.14	5.46E-02	0.04
Yb	0	0	0	0	3.12E+01	0.88	0	0
Lu	1.09E-02	0.1	3.61E-02	0.01	3.98E+00	0.15	2.30E-02	0.01
Th	4.16E-03	0.1	5.79E-02	0.02	5.13E-02	0.02	0	0